

ALESSANDRO LA CHIOMA

A CYCLOPEAN PERSPECTIVE
ON MOUSE VISUAL CORTEX:
ORIGIN OF DIRECTION SELECTIVITY AND
BINOCULAR DISPARITY PROCESSING



Dissertation
zur Erlangung des Doktorgrades der Naturwissenschaften
Doctor rerum naturalium (Dr. rer. nat.)

an der Fakultät für Biologie der
Ludwig-Maximilians-Universität München

Eingereicht am
17. Juli 2018

ALESSANDRO LA CHIOMA
A CYCLOPEAN PERSPECTIVE
ON MOUSE VISUAL CORTEX:
ORIGIN OF DIRECTION SELECTIVITY AND
BINOCULAR DISPARITY PROCESSING

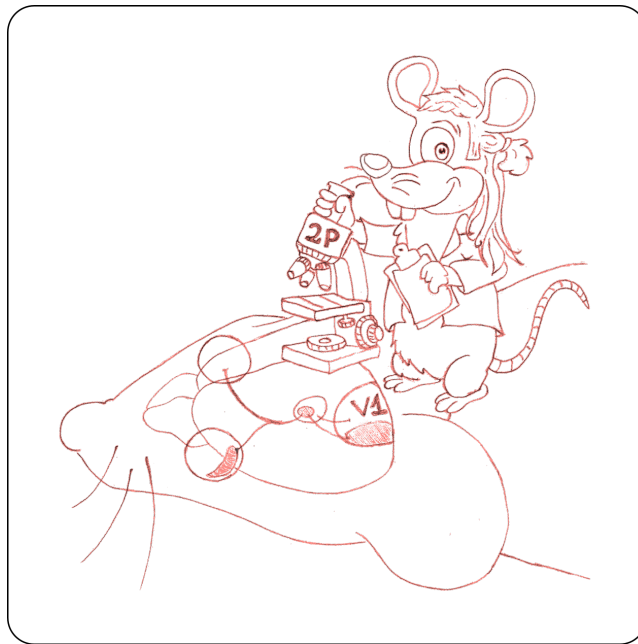
SUPERVISOR:

Prof. Dr. Mark Hübener
Max Planck Institute of Neurobiology
Am Klopferspitz 18
D-82152 Martinsried, Germany

Erstgutachter:	Prof. Dr. Mark Hübener
Zweitgutachter:	Prof. Dr. Laura Busse
Promotionsgesuch eingereicht am:	17.07.2018
Tag der mündlichen Prüfung:	11.10.2018

ALESSANDRO LA CHIOMA

A CYCLOPEAN PERSPECTIVE
ON MOUSE VISUAL CORTEX:
ORIGIN OF DIRECTION SELECTIVITY AND
BINOCULAR DISPARITY PROCESSING



The term "cyclopean" comes from the mythical one-eyed Cyclops of Homer's *Odyssey*. Béla Julesz in his influential work 'Foundations of Cyclopean Perception' (1971) defined a cyclopean stimulus as one whose features are hidden to each individual eye, but are evident to an hypothetical cyclopean eye – located inside the brain – that combines signals from both eyes' retinae. It thus can be said that the perception of a cyclopean image bypasses retinal processing, requiring cortical processing at a level where inputs from both eyes are combined.

CONTENTS

LIST OF FIGURES	vii
ACRONYMS	ix
SUMMARY	ix
1 INTRODUCTION	1
1.1 Organization of the visual system	1
1.1.1 The retina	1
1.1.2 Photoreceptors	3
1.1.3 Retinal ganglion cells	3
1.1.4 Visual pathways into the brain	4
1.1.5 Superior colliculus	5
1.1.6 Dorsal lateral geniculate nucleus	5
1.1.7 The primary visual cortex	6
1.1.8 Higher-order visual cortical areas	13
1.1.9 Binocularity	15
1.1.10 Measuring binocular disparity tuning	21
1.2 Direction selectivity	21
1.2.1 Direction-selective retinal ganglion cells	23
1.2.2 How can visual motion be detected in principle?	23
1.2.3 Asymmetric inhibition underlies retinal direction selectivity	24
1.2.4 Mechanisms underlying cortical direction selectivity	24
1.2.5 Retina-dependent cortical direction selectivity	27
1.2.6 Retina-independent cortical direction selectivity	27
1.2.7 Apparent motion illusion	29
1.3 Binocular disparity processing	32
1.3.1 Visual depth cues and binocular disparity	32
1.3.2 Demonstrating stereoscopic perception	34
1.3.3 Binocular disparity processing	34
1.3.4 Stereopsis and disparity processing in the mouse	38
1.4 <i>In vivo</i> two-photon calcium imaging	41
2 MATERIALS AND METHODS	46
2.1 Ethics	46
2.2 Virus injection and cranial window implantation	46
2.3 Intrinsic signal imaging	47
2.4 <i>In vivo</i> two-photon imaging	47
2.5 Eye tracking	48
2.6 Visual stimulation	48
2.6.1 Retinotopic mapping with intrinsic signal imaging	48
2.6.2 Mapping higher visual areas	49
2.6.3 Dichoptic apparatus	49
2.6.4 Retinotopic mapping	51
2.6.5 Monocular drifting gratings	52
2.6.6 Apparent motion stimuli	53
2.6.7 Dichoptic drifting gratings	55
2.6.8 Random dot stereograms	55
2.7 Image analysis	56
2.8 Data analysis	56
2.8.1 Retinotopic mapping of V1	56
2.8.2 Retinotopic mapping of higher visual areas	57

2.8.3	Retinotopic mapping online analysis	57
2.8.4	Eye rotation offset online analysis	58
2.8.5	Responsive cells	58
2.8.6	Ocular dominance index	59
2.8.7	Direction selectivity index	59
2.8.8	Direction tuning curve fit	59
2.8.9	Disparity selectivity index	60
2.8.10	Disparity tuning curve fit	60
2.8.11	Noise correlations	61
2.8.12	Population decoding with SVM	61
2.9	Statistics	64
3	RESULTS	65
3.1	Origin of direction selectivity in mouse visual cortex	65
3.1.1	Identification of DS and binocular neurons in V ₁	65
3.1.2	Neuronal responses to monocular apparent motion	66
3.1.3	Neuronal responses to dichoptic apparent motion	69
3.1.4	Population decoding of apparent motion	74
3.1.5	Apparent motion stimuli based on gratings	76
3.2	Binocular disparity processing in mouse visual cortex	82
3.2.1	Identification and targeting of areas V ₁ , LM, and RL for two-photon imaging	82
3.2.2	Binocular disparity is encoded by large fractions of neurons in areas V ₁ , LM, and RL	84
3.2.3	Ocular dominance is similar across areas	86
3.2.4	Disparity-dependent facilitation and suppression	87
3.2.5	No large-scale spatial organization for disparity tuning in the visual cortex	89
3.2.6	Non-uniform distribution of disparity preferences in individual experiments	91
3.2.7	Subsets of neurons in areas V ₁ and LM have asymmetric disparity tuning curves	92
3.2.8	Noise correlations are higher between neurons with similar disparity preference	94
3.2.9	Neuronal populations across visual areas effectively discriminate between grating disparities	94
3.2.10	Characterization of disparity tuning using random dot stereograms	96
3.2.11	Area RL contains more near-tuned cells compared to V ₁ and LM	98
3.2.12	Near disparity tuning of RL also revealed by gratings	100
3.2.13	Is disparity tuning related to elevation in visual field?	101
3.2.14	Imaging and dichoptic stimulation in the awake mouse	102
4	DISCUSSION	105
4.1	Origin of direction selectivity in mouse visual cortex	105
4.1.1	Complexity of responses to apparent motion	105
4.1.2	Are retina-dependent and -independent mechanisms for direction selectivity functionally specific?	108
4.1.3	Are retina-dependent and -independent mechanisms for direction selectivity differentially distributed across cortical layers?	110
4.1.4	Is anesthesia a major confounder?	111
4.1.5	Dichoptic apparent motion in the zebrafish	112
4.1.6	Outlook and future experiments	112
4.2	Binocular disparity processing in mouse visual cortex	115

4.2.1	How do rodents use binocular vision?	115
4.2.2	Wide distribution of disparity selectivity in mouse visual areas V ₁ , LM, and RL	116
4.2.3	Tuning characteristics of disparity-tuned neurons	118
4.2.4	Potential area correspondences between mouse and primate visual cortex	120
4.2.5	Most binocular disparity information is contained in low and middle spatial frequencies	122
4.2.6	Area RL encodes visual objects located in close proximity to the mouse	124
4.2.7	Does RL contain a visuo-tactile representation of nearby space?	125
4.2.8	Is disparity tuning related to visual field elevation?	128
4.2.9	Outlook and future experiments	130
4.2.10	Concluding remarks	131
	BIBLIOGRAPHY	132
	CURRICULUM VITAE	170
	ACKNOWLEDGEMENTS	172

LIST OF FIGURES

Figure 1.1	Visual system organization and binocularity in the mouse	2
Figure 1.2	Receptive fields of neurons at early stages of the visual pathway.	4
Figure 1.3	Mapping the retinotopic organization of mouse visual cortex using intrinsic signal imaging.	9
Figure 1.4	Retinotopic organization of primary and higher-order visual areas in the mouse.	15
Figure 1.5	Basic geometry of binocular disparity.	20
Figure 1.6	Motion blindness impairs everyday life activity.	22
Figure 1.7	The two models for visual motion detection.	25
Figure 1.8	Apparent motion illusion as a window into the origin of cortical direction selectivity.	30
Figure 1.9	Needle threading task to compare binocular and monocular depth perception.	33
Figure 1.10	Demonstrating stereopsis requires dichoptic presentation of stimuli.	35
Figure 1.11	Tuning curves and possible mechanisms for binocular disparity.	37
Figure 1.12	Behavioral assessment of visual depth perception in mice.	39
Figure 1.13	Basic optical design of a two-photon laser scanning microscope.	43
Figure 2.1	The two imaging protocols for experiments on binocular disparity.	50
Figure 3.1	Two-photon calcium imaging of direction-selective and binocular neurons in mouse V1	66
Figure 3.2	Retinotopic mapping and positioning of bars for apparent motion.	67
Figure 3.3	Direction tuning for drifting gratings and apparent motion.	68
Figure 3.4	Comparison of direction preferences between drifting gratings and apparent motion bars.	69
Figure 3.5	Different types of responses to dichoptic apparent motion.	71
Figure 3.6	Population decoding of drifting gratings and apparent motion stimuli.	74
Figure 3.7	Apparent motion stimuli based on gratings.	76
Figure 3.8	Comparison of direction preferences between drifting gratings and two-grating apparent motion.	77
Figure 3.9	Complexity of neuronal responses to contrast-modulated apparent motion.	81
Figure 3.10	Identification and targeting of areas V1, LM, and RL for two-photon calcium imaging.	83
Figure 3.11	Functional characterization of disparity-tuned neurons in areas V1, LM, and RL.	85

Figure 3.12	Ocular dominance and binocular interaction of individual neurons across visual areas. 88
Figure 3.13	Spatial and functional organization of disparity-tuned neurons. 90
Figure 3.14	Analysis of disparity tuning curves. 92
Figure 3.15	Noise correlations are higher between neurons with similar disparity preference. 93
Figure 3.16	Population decoding of binocular disparity. 95
Figure 3.17	Characterization of disparity tuning of mouse visual areas using random dot stereograms. 97
Figure 3.18	Area RL contains more near-tuned cells compared to V1 and LM. 99
Figure 3.19	Relation between retinotopic representation in elevation and disparity tuning. 102
Figure 3.20	Imaging in the awake mouse reveals strong disparity-tuned responses to RDS and near disparity tuning in RL. 104
Figure 4.1	The variability of left and right eye receptive fields of individual neurons. 106
Figure 4.2	Estimation of object distances encoded by disparity-tuned neurons. 125

ACRONYMS

AAV	adeno-associated virus
AM	apparent motion
cpd	cycles per degree
DI	disparity selectivity index
dLGN	dorsal lateral geniculate nucleus
DS	direction-selective
DSGC	direction-selective retinal ganglion cell
DSI	direction selectivity index
DT	disparity-tuned
FI	facilitation index
GECI	genetically encoded calcium indicator
LM	latero-medial area of mouse visual cortex
MT	middle temporal area of primate visual cortex
OD	ocular dominance
ODI	ocular dominance index
OGB	Oregon Green BAPTA
OS	orientation-selective
RDS	random dot stereogram
RF	receptive field
RGC	retinal ganglion cell
RL	rostro-lateral area of mouse visual cortex
ROI	region of interest
SAC	starburst amacrine cell
SC	superior colliculus
SEM	standard error of the mean
SF	spatial frequency
SI	suppression index
SVM	support vector machine
TF	temporal frequency
V1	primary visual cortex

SUMMARY

A major challenge for neuroscience is uncovering how the brain carries out specific neural computations. Mammals view the world through a pair of eyes, and this sensory input must be processed by binocular neural circuits in the visual system to ultimately generate a behavioral output. In this Thesis, I explore two fundamental computations carried out by neurons in the mammalian visual cortex: the extraction of visual motion direction and the integration of signals from both eyes for depth perception.

First, I investigated direction selectivity of neurons in mouse primary visual cortex (V_1). Although this property was first described more than half a century ago, how neurons in V_1 become sensitive to the direction of motion remains elusive. Here, I examined to which degree cortical direction selectivity is inherited from the retina, where it is first computed, and to which extent it is computed *de novo* in V_1 . To detect motion, at least two visual inputs separated in both space and time need to be compared. Thus, I designed a repertoire of visual stimuli, based on apparent motion, that distribute these two inputs over both eyes, with each retina used as a separate source of only one of the two inputs. As such, each retina alone was not able to detect any motion, while still allowing computation of motion direction in the cortex, where inputs from both eyes are integrated. *In vivo* two-photon calcium imaging was used for monitoring the activity of neurons in the visual cortex. V_1 neurons exhibited a large complexity of responses to apparent motion stimuli that did not allow making definitive statements on the actual contribution of visual motion computation in V_1 . Yet, the results are compatible with both an inheritance mechanism from the retina and a *de novo* generation for direction selectivity in V_1 .

Second, I investigated binocularity in the mouse visual cortex – the integration of inputs from both eyes in V_1 neurons. The small differences between the left and right eye images, called binocular disparities, provide the visual system with critical information for depth perception. In primates, binocular disparity is differentially processed across visual cortical areas. To test whether such specializations also exist in rodents, I characterized disparity selectivity in V_1 and in two higher-order visual areas, LM and RL, of the mouse. I employed a dichoptic stimulation protocol, using gratings at varying interocular phases as well as random dot stereograms. I found that disparity processing is highly distributed across neurons in areas V_1 , LM, and RL, but with clear differences in preferred disparities: area RL contains a higher fraction of neurons selective to near disparities compared to V_1 and LM, indicating that RL is specialized for processing visual objects at close distance to the mouse. Preference for near disparities in RL was evident using both gratings and random dot stereograms for stimulation, and it was also observed in the awake animal. Since recent data show that most neurons in mouse RL respond to both visual and whisker stimulation, I speculate that this area might contain a multimodal representation of the immediate space in front of the animal.

1

INTRODUCTION

"Can the brain understand the brain? Is it a giant computer, or some other kind of giant machine, or something more? The brain is a tissue. It is a complicated, intricately woven tissue, like nothing else we know of in the universe, but it is composed of cells, as any tissue is. They are, to be sure, highly specialized cells, but they function according to the laws that govern any other cells. Their electrical and chemical signals can be detected, recorded and interpreted and their chemicals can be identified; the connections that constitute the brain's woven feltwork can be mapped. In short, the brain can be studied, just as the kidney can."

David H. Hubel
Scientific American 1979

1.1 ORGANIZATION OF THE VISUAL SYSTEM

We view the world around us through a pair of eyes, whereby the three-dimensional structure of space is collapsed onto a two-dimensional image formed on each retina. From the eyes, retinal signals are transmitted to more than 40 structures in the mammalian brain (Morin and Studholme, 2014), taking part in a multitude of functionally distinct pathways. The two main pathways transmit retinal information in parallel to the superior colliculus (SC) in the midbrain, and to the dorsal lateral geniculate nucleus (dLGN) of the thalamus in the diencephalon. The dLGN in turn connects directly to the primary visual cortex (V1) in the dorsal telencephalon, forming the pathway retina-dLGN-V1 (Fig. 1.1a; Kandel et al., 2013).

This Thesis focuses on the mouse visual cortex. Thus, in the following introductory sections, I will first briefly review the flow of visual information from the retina to the SC and dLGN. Next, I will describe in more detail the fundamental features of the visual cortex and the neural architecture of binocular vision, which will be important for understanding the experiments described in this Thesis. The introduction will focus on the rodent visual system, while highlighting the most relevant similarities and dissimilarities to carnivorans and primates.

1.1.1 The retina

In the vertebrate visual system, the optical apparatus of each eye projects a two-dimensional image of the visual world onto the retina. Here, photoreceptor cells convert incoming photons to neuronal signals, a process termed phototransduction. These signals are then transmitted to retinal ganglion cells (RGCs) after undergoing substantial processing by a complex circuitry comprising several classes of interneurons – horizontal, bipolar and amacrine

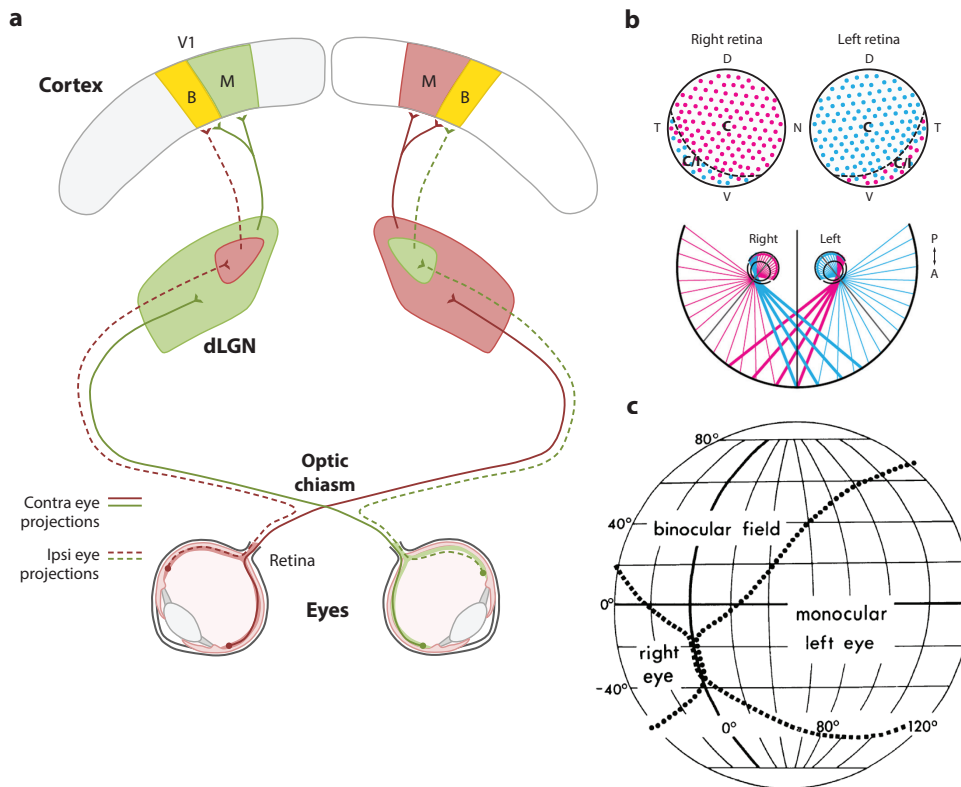


Figure 1.1 | Visual system organization and binocularity in the mouse. **a** | Schematic of eye-specific projections along the retina-dLGN-V1 visual pathway. Most RGCs axons cross the midline at the optic chiasm and project to the contralateral dLGN. A small fraction (5–10%) of RGCs from the most ventro-temporal part of retina send axons to the ipsilateral dLGN, within an eye-specific domain. Neurons in the dLGN project to two regions of V1: the monocular region (M) receives projections only from the contralateral eye; the binocular region (B), in the lateral third of V1, receives projections from both eyes. Adapted with permission from [Seabrook et al., 2017](#). **b** | Organization of contralateral- and ipsilateral-projecting RGCs. Top, the most ventro-temporal part of the retina contains a mixed population of contralateral- and ipsilateral-projecting RGCs. C, contralateral-projecting; I, ipsilateral-projecting; N, nasal; T, temporal; D, dorsal; V, ventral. Bottom, schematic illustrating the field of view of each eye. The central part of the visual field (~40 deg), subtended by the ventro-temporal crescent of the retina, is viewed by both eyes and processed by the dLGN and visual cortex in both hemispheres. Bottom schematic adapted from [Sterratt et al., 2013](#). **c** | Schematic outlining the approximate monocular and binocular fields of view, with the mouse head located in the center of the sphere. Grid spacing is 20 deg. Reprinted with permission from [Dräger, 1978](#).

cells. RGCs are the output neurons of each eye, and their axons, which bundle in the optic nerve, convey visual information to the brain in the form of action potentials. Therefore, the optical apparatus and the retina of each eye set fundamental limits on what can be seen, determining the quality and quantity of the information about the visual scene that the brain has access to ([Kandel et al., 2013](#)).

THE CONCEPT OF THE RECEPTIVE FIELD Before going further, I will introduce the concept of the “receptive field” (RF) that is essential for every neuron in the visual system, from photoreceptors and RGCs in the retina to neurons in the cerebral cortex. The RF of any given visual neuron can be defined as a confined region of visual space, in which light stimuli can alter the activity of that neuron. As such, the RF can be determined by measuring the response of the neuron in response to light stimuli displayed at

different locations in visual space. Moreover, this basic definition of the RF can be made more specific by including the particular characteristics that a light stimulus must have to alter the activity of that neuron, e.g. luminance, orientation, or direction of motion.

1.1.2 Photoreceptors

There are two types of photoreceptors in the mammalian retina – rods and cones – that are distinct in terms of their photopigments (the light-absorbing molecules that initiate phototransduction), cell morphology, distribution across the retina, and synaptic connectivity: collectively, these properties determine rods and cones as forming two functionally distinct systems. Rods are specialized for vision under dim light, at the expense of spatial resolution. In contrast, cones are less sensitive to light but support high acuity and also color vision.

The retina of the mouse contains both rods and cones in a ratio of roughly 35:1, thereby being specialized for low light vision. The average density of rods is higher than in the primate's retina and, surprisingly, the cone density in the mouse retina is on average similar to the primate's retina. However, the mouse eye (diameter of ~3 mm; [Tkatchenko et al., 2010](#)) is far smaller than that of most primates, resulting in much fewer photoreceptors that sample a given portion of the field of view ([Jeon et al., 1998](#)).

An important feature of the retina of several groups of mammals is the presence of a specialized region with a higher density of cones, crucial for high-acuity, high-contrast vision, which is absent in the mouse eye. In some primate species including humans, this retinal specialization – termed the fovea – is particularly developed and contains 99% of all cones in only 1% of retinal surface. Yet, most mammalian species do not have such an elaborate fovea; cats, for example, have a less developed retinal specialization termed area centralis ([Rapaport and Stone, 1984](#)). The mouse eye lacks a fovea or area centralis altogether; nonetheless, the density of photoreceptors is not homogeneous, but higher in the central part of the retina ([Jeon et al., 1998](#); [Volland et al., 2015](#)).

1.1.3 Retinal ganglion cells

The electrical signals generated by the photoreceptors, after processing by the retinal circuitry, are passed to a large variety of RGCs, comprising more than 30 types ([Baden et al., 2016](#)). Several “classic” RGC types have a so-called center-surround RFs ([Fig. 1.2a](#)). This typical RF consists of two concentric subregions, a central disk and a surrounding ring, with opposite responsiveness to stimulus luminance. For example, a cell with an ON-center RF will be activated by a bright stimulus appearing within the ON center, or by a dark stimulus illuminating the OFF surround; conversely, the same cell will be suppressed by a dark stimulus in the ON center or by a bright stimulus in the OFF surround ([Kandel et al., 2013](#)).

In addition to classic RGC types with center-surround RFs, which mostly encode luminance changes, many RGC types respond to more complex aspects of visual stimuli, such as specific edges, orientations, directions of motion or looming ([Baden et al., 2016](#)). Therefore, each RGC type extracts distinct features from the visual scene, delivering to the downstream visual

system a rich set of parallel information channels (Dhande and Huberman, 2014; Roska and Meister, 2014; Sanes and Masland, 2014; Dhande et al., 2015; Liang et al., 2018; Román Rosón et al., 2018). One prominent channel, for example, comprises a specialized class of direction-selective RGCs that extract visual motion information. These cells respond more vigorously to stimulus motion in one specific direction than any other. Direction-selective RGCs will be described in more detail in section 1.2.1.

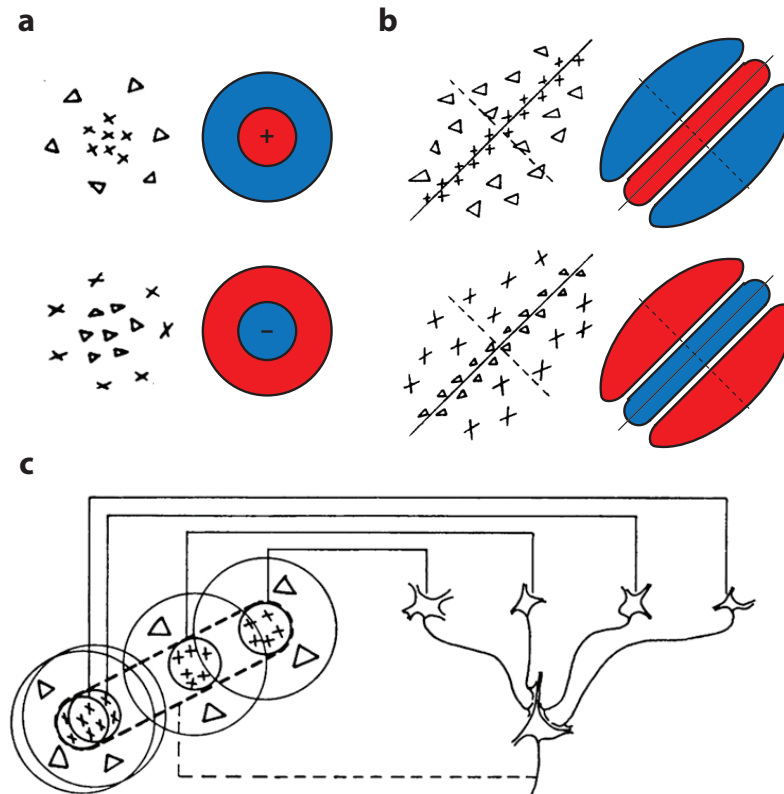


Figure 1.2 | Receptive fields of neurons at early stages of the visual pathway. **a** | Receptive field (RF) maps of center-surround RFs. Top left, hand mapping of an ON-center RF of a neuron in the cat dLGN by Hubel and Wiesel (1962). Top right, schematic of an ON-center RF. Bottom, OFF-center RF. **b** | RFs of cortical simple cells. ON subregions are shown in red, OFF subregions in blue. Left, hand mapping of RFs of simple cell from cat primary visual cortex by Hubel and Wiesel (1962). **c** | Original model for the generation of orientation selectivity of simple cells in V1 (Hubel and Wiesel, 1962). The orientation of the simple cell RF results from input convergence of presynaptic cells in the dLGN with center-surround RFs, which are aligned along one axis in visual space. Hand mappings in (a,b) and model in (c) reprinted with permission from Hubel and Wiesel (1962).

1.1.4 Visual pathways into the brain

After undergoing substantial processing at this early stage, retinal signals are transmitted to the next stations in the visual system via RGC axonal projections. In the mouse, as in other species with laterally positioned eyes, the majority of RGC axons decussate at the optic chiasm and target downstream structures in the contralateral hemisphere (Fig. 1.1a; Jeffery, 2001; Larsson, 2015).

1.1.5 Superior colliculus

The superior colliculus (SC) is the main retinorecipient subcortical structure in the mouse, receiving input from 85-90% of all RGCs (Ellis et al., 2016). In contrast, in primates only about 10% of RGCs target the SC (Perry and Cowey, 1984). Interestingly, around 80% of RGCs that innervate the mouse dLGN also project to the SC. This indicates that the SC has access to most retinal information provided to the dLGN (Ellis et al., 2016).

The SC is a highly organized structure for visual information processing that mediates several behaviors, also independently of the cortex. In primates, the SC is involved in spatial attention and visual target selection, especially for directing head and eye movements (Crapse et al., 2017; Seabrook et al., 2017). In several species, including the mouse, the SC mediates predator avoidance behaviors (Shang et al., 2015; Almada et al., 2018; Evans et al., 2018; Li et al., 2018).

The response properties of mouse SC neurons are surprisingly diverse. On the one hand, many SC neurons show feature selectivities that resemble in many respects the ones in retina, dLGN and visual cortex, including surround suppression and preference for orientation, direction and speed. On the other hand, a substantial fraction of SC neurons exhibits specific responses to more unusual stimuli, e.g. looming stimuli or very small, slowly moving stimuli (Gale and Murphy, 2014; Ahmadlou and Heimel, 2015; Feinberg and Meister, 2015; Seabrook et al., 2017; Shi et al., 2017). Although the SC is a crucial node in the mammalian visual system, its role in visual processing is only beginning to emerge.

1.1.6 Dorsal lateral geniculate nucleus

The dorsal lateral geniculate nucleus (dLGN) is the primary source of input from the eyes to the cortex, thereby representing a key gateway for visual perception. In the mouse, the dLGN receives input from 30-40% of all RGCs (Morin and Studholme, 2014; Ellis et al., 2016). In primates, by contrast, 90% of RGCs project to the dLGN, indicating that the retina-dLGN-V1 pathway is the most prominent in this species (Perry and Cowey, 1984).

Across most rodents and higher mammals (Larsson, 2015), the dLGN receives RGC input mostly from the contralateral eye and to a lesser degree from the ipsilateral eye, terminating in distinct eye-specific territories. According to the classical view, which has been recently challenged (see below), eye-specific input remains by and large segregated in the dLGN, and only in V1 signals from the two eyes converge (eye-specific input and binocularity of the dLGN will be described in more detail in paragraph 1.1.9.3).

Often, the dLGN is considered a simple relay nucleus interposed between retina and visual cortex, with limited contribution to visual processing. New data show, however, that the dLGN contains more complex visual representations than previously thought (for reviews see Usrey and Alitto, 2015; Denman et al., 2016; Ghodrati et al., 2017; Monavarfeshani et al., 2017). In the mouse, while about half of the dLGN neurons have typical center-surround RFs, ~10% of dLGN neurons are orientation-selective (OS), of which one fourth are also direction-selective (DS) (Grubb and Thompson, 2003; Marshel et al., 2012; Cheong et al., 2013; Piscopo et al., 2013; Sun et al., 2016). Interestingly, similarly to V1 neurons (Ayaz et al., 2013; Saleem et al., 2013), vi-

sual responses of dLGN neurons are strongly modulated by locomotion in a speed-dependent manner, indicating that the dLGN is involved in the interplay of cortical and neuromodulatory regions mediating the locomotion-related effects in visual processing (Erisken et al., 2014). Moreover, the dLGN receives substantial feedback projections from visual cortex that are implicated in regulating visual processing based on behavioral context (Vélez-Fort et al., 2014; Roth et al., 2015; Sherman, 2016). Therefore, the dLGN has emerged as an important node for visual information transmission with computationally relevant functions.

The dLGN of carnivorans and primates is subdivided into discrete eye-specific laminae connected by qualitatively different RGCs and populated by morphologically and functionally distinct dLGN cells. Despite lacking a clear cytoarchitectural lamination, mouse dLGN consists of a core region and a dorsolateral outer region referred to as the “shell” (Usrey and Alitto, 2015; Monavarfeshani et al., 2017; Guido, 2018). The core region receives input predominantly from center-surround and non-DS retinal ganglion cells, whereas the shell is preferentially targeted by DS retinal ganglion cells (Huberman et al., 2009; Kay et al., 2011; Rivlin-Etzion et al., 2011; Dhande and Huberman, 2014; Ray and Kay, 2015; Monavarfeshani et al., 2017; Seabrook et al., 2017). Furthermore, also the mouse dLGN contains eye-specific territories: a ventromedial zone in the core region of the dLGN receives RGC projections from the ipsilateral eye, while the remaining dLGN receives retinal input from the contralateral eye (Fig. 1.1a; see also paragraph 1.1.9.3 [Binocularity and the dLGN](#); Morin and Studholme, 2014; Monavarfeshani et al., 2017).

This functional organization of retinal inputs to the dLGN is mirrored by the presence of different classes of dLGN cells. The core region mostly contains neurons with center-surround RFs. By contrast, the shell region is rich in OS and DS neurons, whose projections target the superficial layers of V₁ (Marshel et al., 2012; Piscopo et al., 2013; Zhao et al., 2013; Cruz-Martín et al., 2014; Kondo and Ohki, 2015). The shell region of the mouse dLGN has notable homology to the so-called koniocellular layers of primate dLGN, based on its higher prevalence of OS and DS cells, its targeting of superficial layers of V₁, as well as the presence of afferent inputs from the SC (Ghodrati et al., 2017).

1.1.7 The primary visual cortex

The primary visual cortex (V₁) is the first stage of visual information processing in the neocortex. It consists of the so-called grey matter, which has a six-layered architecture, reflecting input and output connectivity of its neurons. The cellular and laminar organization of the visual cortex is largely similar not only to other cortical areas in the same species, but also across mammalian species (Harris and Shepherd, 2015; Miller, 2016).

THALAMOCORTICAL CONNECTIONS Visual input reaches the visual cortex by way of thalamocortical connections. In cats and primates, V₁ receives direct projections from the dLGN mostly in layer 4, and, less strongly, layer 6. In contrast, mouse V₁ receives thalamic input across all cortical layers: nearly all excitatory neurons in L₄ and L₅ as well as ~75% of cells in L_{2/3} and L₆ are directly targeted by dLGN projections, although the strongest

thalamocortical innervation occurs in L₄, as in higher mammals (Harris and Shepherd, 2015; Ji et al., 2016).

LOCAL AND LONG-RANGE PROJECTIONS Once visual input has reached the visual cortex, the signals are processed and redistributed through cortical circuits, which can be divided into two main types: local and long-range. Local circuits remain confined within a given cortical area and interconnect neurons that reside in the same layer, or across layers of a same vertical segment of cortex perpendicular to the surface (columnar connections). Long-range circuits interconnect local circuits across different cortical areas and parts of the brain (Harris and Mrsic-Flogel, 2013; Harris and Shepherd, 2015; D'Souza and Burkhalter, 2017)

EXCITATORY AND INHIBITORY NEURONS Cortical neurons are the basic circuit components and comprise two broad classes: excitatory and inhibitory neurons. (1) Excitatory cells, also referred to as principal cells, constitute ~80% of cortical neurons (Harris and Shepherd, 2015). These cells propagate signals within and among brain regions by making synaptic contacts with downstream (postsynaptic) neurons through excitatory synapses. The majority of excitatory cells display a typical morphology characterized by a pyramidal shaped soma and two distinct types of dendrites: a basal dendritic tree extending from the base of the soma with multiple branches, and an apical dendrite emerging from the apex of the soma and stretching towards the cortical surface. In terms of axonal projections, excitatory cells can range from targeting only local postsynaptic partners to reaching out to brain regions several millimeters away (Kandel et al., 2013; Harris and Shepherd, 2015; Zeng and Sanes, 2017).

(2) Inhibitory neurons, or interneurons, constitute the remaining ~20% of cortical neurons. Despite making up a minority of the total neuronal population, inhibitory cells play a crucial role in sculpting signal dynamics through neuronal circuits (Priebe and Ferster, 2008; Isaacson and Scanziani, 2011; Priebe and Ferster, 2012; Wilson et al., 2012; Haider et al., 2013). One of their key functions is to antagonize the generation of action potentials in the postsynaptic cell, i.e. to suppress its activation, by releasing the neurotransmitter γ -aminobutyric acid (GABA). Inhibitory cells mostly take part in local circuits, making contact to postsynaptic elements within or across layers (Kätzel et al., 2011; Tremblay et al., 2016). Inhibitory neurons include many morphological and electrophysiological types, which can be grouped into three genetically defined classes, present in roughly the same proportions: parvalbumin-expressing, somatostatin-expressing, and vasoactive intestinal peptide-expressing interneurons (Harris and Shepherd, 2015; Jiang et al., 2015; Tremblay et al., 2016; Zeng and Sanes, 2017).

CORTICAL LAYERS The experimental work presented throughout the Thesis focuses on neurons in layer 2/3 of mouse visual cortex. In the following paragraph, a brief description of the organization of the various layers is given.

The most superficial cortical layer (L₁) contains few neurons that are mostly inhibitory, but is rich of dendrites of excitatory neurons located in deeper layers as well as axons arriving from the thalamus and from various cortical and subcortical regions (Ibrahim et al., 2016).

Layer 2/3 has a high density of neurons that are considered to be particularly implicated in visual information processing and integration (Niell, 2015). L2/3 neurons locally receive considerable input from L4 neurons and project predominantly to L5, while their long-range connections target other cortical areas (Harris and Mrsic-Flogel, 2013; D'Souza and Burkhalter, 2017). L4 excitatory cells connect to all layers, though most densely to L2/3, and receive little columnar excitatory input in return.

L5 pyramidal neurons have dendrites spanning throughout the cortical column and a large dendritic tuft in L1, with which they integrate inputs coming from both local and long-range afferents. Locally, L5 receives input from and projects to layer L2/3. In terms of long-range connectivity, L5 neurons consist of two classes that project to other cortical areas and to subcortical regions, respectively.

L6, similar to L5, comprises two distinct classes of excitatory neurons, referred to as corticocortical and corticothalamic cells. The former class shows extensive horizontal connections to other cortical areas, including higher visual areas, located in both the same and the opposite hemisphere; the latter class provides input to thalamic structures (Vélez-Fort et al., 2014). Locally, L6 neurons preferentially target inhibitory cells in L2/3 and L4.

1.1.7.1 *Retinotopic organization of V1*

A key feature of many parts of the mammalian visual system is their retinotopic organization. V1 too, contains a retinotopic map: an ordered map of visual space that parallels the topological organization of the RFs in the retina (Fig. 1.3). In other words, two neighboring locations in visual space project onto two neighboring locations in the retina and are then connected to neighboring locations in the visual cortex. Although neighboring neurons in mouse V1 have RFs that, on average, cover nearby retinotopic positions, a smooth retinotopic progression is evident only at a scale of 50-100 μm . Indeed, RFs of neurons located within few tens of micrometers are often locally disorganized and scatter by about half the RF size (Smith and Häusser, 2010; Bonin et al., 2011).

Furthermore, the spatial relationships of visual inputs are not mapped isotropically throughout V1. The mapping between the distance across two points in visual space and its cortical representation is described by the cortical magnification factor, expressed as the cortical distance corresponding to one degree of visual angle (mm/deg). The cortical magnification factor decreases with eccentricity in the visual field. In other words, a visual stimulus of a given size located in the central visual field is processed by a larger cortical area, and hence by a higher number of neurons, compared to the same stimulus located in the peripheral visual field.

This is particularly evident in carnivorans and primates where the cortical magnification factor is much higher in the central visual field, which corresponds to the region of the fovea or area centralis of the retina, respectively. In the mouse, the retina lacks a fovea or area centralis and the cortical magnification factor ($\sim 10 \mu\text{m}/\text{deg}$) varies less as a function of visual field eccentricity. Nonetheless, a central portion, about 40 deg wide, of the visual field in front of the mouse has a disproportionately larger representation in the cortex than more peripheral parts of the visual field. Specifically, the central visual field, which roughly spans one fourth of the field of view of one eye,

is mapped onto one third of V1 (see also section 1.1.9.1 [Neural architecture of binocularity in the mouse](#); Wagor et al., 1980; Schuett et al., 2002).

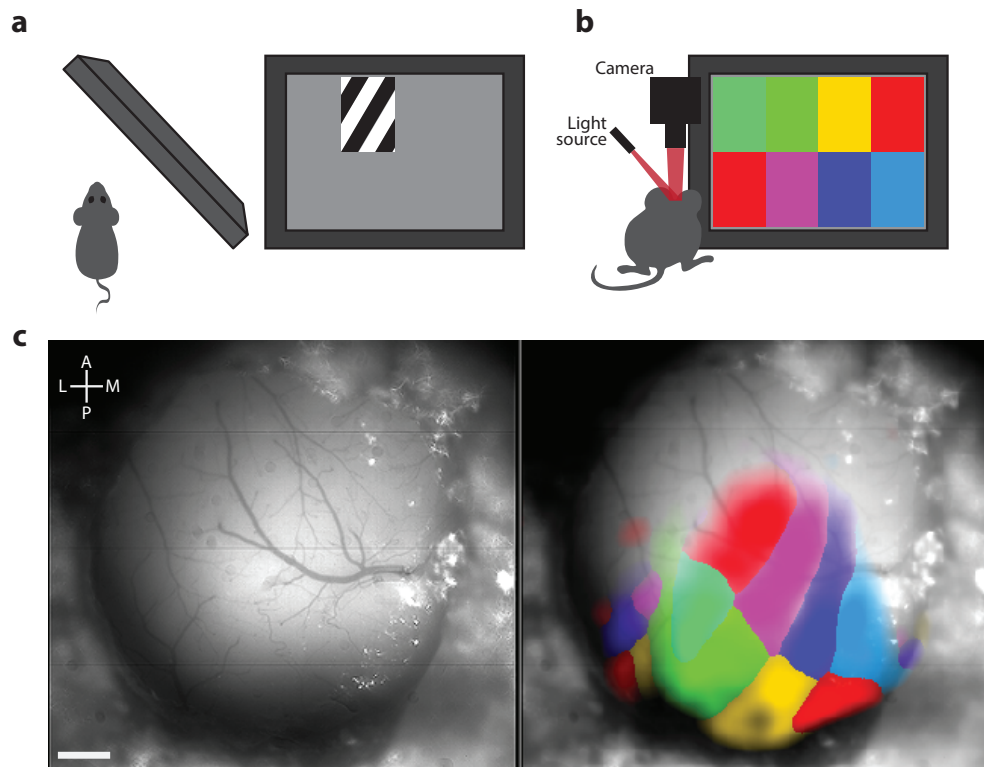


Figure 1.3 | Mapping the retinotopic organization of mouse visual cortex using intrinsic signal imaging. **a** | Small visual stimuli, like patches of drifting gratings, are displayed at several distinct locations on a stimulus monitor. Left, top view of the mouse presented with visual stimuli. Right, screenshot of a grating stimulus presented at a given location on the monitor. **b** | During stimulus presentation, the cortical surface on the contralateral hemisphere is illuminated by red light and the reflected light is detected by a camera. The color code representing stimulus location is used to generate color-coded retinotopic maps. **c** | Example of retinotopic mapping of V1. Left, image of the brain surface and blood vessel pattern through a cranial window implant, illuminated with green light to enhance the blood vessel contrast. Right, retinotopic map, color-coded for stimulus location. Cortical regions activated by a visual stimulus show a decrease reflected red light. A map of retinotopy is then generated by assigning a color to each pixel, based on the stimulus location that evoked the strongest activation. Scale bar, 500 μm .

1.1.7.2 Fundamental receptive field properties of visual cortical neurons

Many of the fundamental RF properties of V1 neurons were established in seminal experiments conducted in cats and monkeys in the late 1950s and early 1960s by David Hubel and Torsten Wiesel, who were awarded the Nobel Prize in 1981.

1.1.7.3 Orientation selectivity

In V1, the majority of neurons respond vigorously to elongated stimuli, like bars or edges, of a specific orientation in space. For this reason, they are referred to as orientation-tuned or orientation-selective (OS). By systematically presenting a bar within the neuron's RF across the full range of orientations, it is possible to characterize the neuron's "tuning curve" for orientation, i.e. the neuron's response as a function of stimulus orientation. The peak of the tuning curve (the orientation to which the neuron is maximally responsive)

describes the preferred orientation of the neuron, while the curve width, typically at half height, describes how selective the response is (Hubel and Wiesel, 1959; Hubel and Wiesel, 1962).

1.1.7.4 *Direction selectivity*

A large fraction of OS neurons are in addition direction-selective (DS), as they respond better to stimulus motion in one specific direction than any other (Hubel and Wiesel, 1959; Hubel and Wiesel, 1962).

1.1.7.5 *Simple and complex cells*

Following Hubel's and Wiesel's initial description of RFs in V_1 , neurons can be subdivided into two broad classes: simple cells and complex cells. Simple cells have RFs composed of spatially segregated ON and OFF subfields (Fig. 1.2b). Within ON subfields, the cell responds to increases in luminance, whereas within OFF subfields the cell responds to decreases in luminance. The subfields are often elongated in one orientation, such that a simple cell typically responds selectively to a bright oriented bar presented along its ON subfield, or to a dark bar presented along the OFF subfield. Often, even stronger neuronal responses can be elicited by presenting light and dark bands together in form of a grating, with optimal position and bar width (termed spatial frequency of the grating) that best match the specific RF structure of the cell. Conversely, oriented stimuli presented perpendicularly to the elongation axis of the cell's RF elicit no or only small responses. In addition, simple cells are generally considered to operate as linear filters, as they appear to compute a weighted sum of the light intensities in the stimulus. For example, when presented with a grating drifting at a certain temporal frequency, the response of a simple cell shows a periodic modulation at the same frequency as the stimulus (Mechler and Ringach, 2002).

Complex cells are similar to simple cells in that both are typically OS. Unlike simple cells, though, complex cells are generally characterized by nonlinear responses (Mechler and Ringach, 2002). The RF of complex cells is not elongated along one axis and is not structured in separate ON and OFF subfields, such that mixed ON and OFF responses can be elicited throughout their RF.

1.1.7.6 *Ocular dominance*

Many V_1 neurons in cats and primates have binocular RFs, as their activity can be driven by presenting stimuli to either eye. The ocularity of a neuron can be quantified by measuring its response to visual stimuli presented monocularly to each eye. This RF property is called ocular dominance (OD), as cortical neurons are typically dominated by either the contralateral or the ipsilateral eye. Since dLGN cells with binocular RFs have been rarely, if at all, reported in early studies, V_1 has been widely considered the first stage of the visual pathway where the inputs from the two eyes are integrated at the level of individual neurons. More recently, however, it has been under debate whether binocular integration takes place already in the dLGN, since binocular neurons have been observed in rodents (Grieve, 2005; Howarth et al., 2014; Jaepel et al., 2017; Rompani et al., 2017) and marmoset monkeys (Zeater et al., 2015; see paragraph 1.1.9.3 *Binocularity and the dLGN*).

1.1.7.7 *The concept of cortical computation*

All these fundamental RF properties of cortical neurons, since Hubel and Wiesel's pioneering studies and for many years thereon, have been considered to arise *de novo* in V₁, contributing to the concept of "cortical computation", in which cortical neurons would receive simple center-surround input from retinal and thalamic cells and transform it into a novel, more complex representation of visual information. Accordingly, the selective signals already computed in the retina, such as the direction selectivity found by Barlow and coworkers in the rabbit (Barlow and Hill, 1963; Barlow et al., 1964; Barlow and Levick, 1965), were assumed to serve only subcortical and reflexive responses, without reaching the cortex.

A canonical example of a cortical computation is the generation of orientation selectivity, for which a simple scheme was already proposed by Hubel and Wiesel (Fig. 1.2c; Hubel and Wiesel, 1962): a simple cell in V₁ becomes OS by integrating convergent inputs from dLGN cells with RFs aligned in visual space. The ON and OFF centers of the circular RFs of dLGN inputs are arranged in parallel bands, thereby resulting in the elongated RF of the post-synaptic simple cell. This circuit model for orientation selectivity has found substantial support (Chapman et al., 1991; Reid and Alonso, 1995; Chung and Ferster, 1998; Alonso et al., 2001; Jin et al., 2011), even though a conclusive proof is still missing, and complementary circuit mechanisms have been suggested (Ringach et al., 1997; Reinhold et al., 2015; Kremkow et al., 2016; Lee et al., 2016).

For generating orientation selectivity of complex cells, Hubel and Wiesel proposed a hierarchical circuit, in which a given complex cell receives convergent input from multiple simple cells with the same orientation preference, but offset RF positions (Fig. 1.2c; Hubel and Wiesel, 1962). Another classic example of a canonical computation is the generation of direction selectivity of simple cells, which will be described in detail in section 1.2.4).

However, it is now established that complex response properties, such as orientation and direction selectivity are not exclusive to the visual cortex, rather they can already be found in the retina and dLGN across mammalian species; in the mouse, RGCs and dLGN cells have been demonstrated to be part of a parallel pathway that conveys DS signals generated in the retina to neurons in superficial V₁ (Cruz-Martín et al., 2014; for details see section 1.2.4). Thus, the concept of a purely cortical computation of certain response properties might need to be revisited to encompass the possibility that part of the complex response properties present in V₁ are inherited from subcortical structures. Investigating this possibility for a specific RF property, direction selectivity, will be one aim of this Thesis.

1.1.7.8 *Mouse primary visual cortex*

The fundamental response properties that are hallmarks of carnivoran and primate V₁ are also found in mouse visual cortex. Separate ON and OFF subfields, orientation and direction selectivity have been quantitatively confirmed for mouse V₁ neurons, though manifesting at a much larger spatial scale, as mouse vision operates at a resolution that is one to two orders of magnitude lower than that in primates (Dräger, 1975; Wong and Brown, 2006; Niell and Stryker, 2008; Huberman and Niell, 2011; Niell, 2015). While having a lower acuity, it is important to consider that the behavioral world of

the mouse occurs at a much smaller scale compared with monkeys and humans, with most relevant visual information contained within a few dozens of centimeters.

Crucially, despite the relatively low visual acuity of mice, and their skillful use of olfaction and whisking, a number of mouse behaviors are strongly driven by vision (Carandini and Churchland, 2013; Juavinett et al., 2018). Vision plays a key role in navigation (Morris et al., 1982; Harvey et al., 2012; Chen et al., 2013a; Saleem et al., 2013; Marcos and Harvey, 2016), social interaction (Langford et al., 2006), predator avoidance (Yilmaz and Meister, 2013; Shang et al., 2015; De Franceschi et al., 2016; Vale et al., 2017; Almada et al., 2018; Evans et al., 2018; Li et al., 2018), prey capture (Hoy et al., 2016; Han et al., 2017; Park et al., 2018), and depth perception (Waugh, 1910; Fox, 1965; Leamey et al., 2007; Mazziotti et al., 2017). In addition, mice have been shown to be able to visually recognize two-dimensional images (Robinson et al., 2001; Lee et al., 2012; Glickfeld et al., 2013a; Gavornik and Bear, 2014; Cooke et al., 2015; Goard et al., 2016; Yu et al., 2017) and three-dimensional objects (Beer et al., 2013; Park et al., 2018).

1.1.7.9 *Salt-and-pepper organization*

A notable difference of the mouse visual cortex compared to that in most higher mammals is the lack of any type of large-scale spatial organization other than retinotopy. In cats and primates, response properties like orientation selectivity and OD are orderly organized into a columnar architecture. In V1 of these species, neurons within the same “column” (i.e. within a vertical segment spanning across the cortical layers) share orientation preference; by gradually moving tangentially across the cortical surface, the orientation preference of neurons in adjacent columns shifts systematically (Hubel and Wiesel, 1977), often forming a stereotypical pattern of “pinwheels” (Bonhoeffer and Grinvald, 1991; Ohki et al., 2006). In addition, neurons with similar OD are systematically arranged into alternating bands or patches dominated by either eye (Hubel and Wiesel, 1962; Hubel and Wiesel, 1969; Wiesel et al., 1974; Hubel and Wiesel, 1977; Shatz et al., 1977).

Neurons in mouse V1 do not show any obvious large-scale spatial layout, but they are rather intermingled in a so-called “salt-and-pepper” organization (Hübener, 2003; Mrsic-Flogel et al., 2007; Ohki and Reid, 2007; Zariwala et al., 2011; Kondo et al., 2016; Ringach et al., 2016; Jimenez et al., 2017; Maruoka et al., 2017), thereby proving that large-scale maps are dispensable for achieving sharp tuning of individual neurons (Ohki and Reid, 2007; Kaschube, 2014; Weigand et al., 2017).

While the salt-and-pepper organization of mouse visual cortex is broadly accepted, it is worth mentioning that recent experiments have shown that neurons in mouse V1 do show a spatial organization at a fine-scale, in the range of a few tens of micrometers: distinct types of excitatory and inhibitory neurons in L5 are arranged into microcolumns, to form hexagonal modules that tessellate not just the visual cortex but a large extent of the mouse neocortex – an organizing logic likely conserved across mammalian species (Maruoka et al., 2017; see also Ji et al., 2015; Kondo et al., 2016; Ringach et al., 2016; Scholl et al., 2017b).

1.1.8 Higher-order visual cortical areas

The visual cortex of primates beyond V₁ (also referred to as striate cortex in these species) comprises many distinct higher-order visual areas, collectively referred to as extrastriate areas. Each of the higher visual areas performs different and advanced analyses of the visual input and is specifically interconnected to other sensory, limbic and motor areas. The primate visual cortex is thus an intricate network with multiple specialized areas, engaged in parallel and hierarchical streams to support different aspects of perception and behavior.

Visual information processing is generally considered to be distributed into two anatomically and functionally distinct pathways, known as the ventral and dorsal streams, sometimes also referred to as the “what” and “where” pathways, respectively (Ungerleider and Mishkin, 1982). (1) The temporal or ventral stream, extending from V₁ into the inferior part of the temporal lobe (areas V₂, V₃, V₄, IT, etc.), is thought to be primarily involved in object recognition and high-resolution form vision. (2) The parietal or dorsal stream, extending into the parietal lobe (areas V₂, MT, MST, etc.), is thought to be primarily involved in spatial aspects of vision, such as motion perception and spatial representation of the visual scene (Maunsell and Newsome, 1987; Orban, 2008; Nassi and Callaway, 2009; Kravitz et al., 2011; Kandel et al., 2013).

It is now established that also the mouse visual cortex boasts a sophisticated organization of several distinct areas, each with specific functional properties and interconnections (Glickfeld et al., 2014; Glickfeld and Olsen, 2017; Gămănuț et al., 2018; Han et al., 2018).

An early cytoarchitectonic study in the mouse visual cortex distinguished five extrastriate areas surrounding V₁ (Rose, 1929). More recently, Wang and Burkhalter (2007) employed multicolor anterograde tracers injected at multiple separate sites in V₁ and provided compelling evidence for the existence of at least nine distinct and retinotopically organized areas in the mouse visual cortex. (Glickfeld et al., 2014; Glickfeld and Olsen, 2017; Gămănuț et al., 2018; Han et al., 2018).

In addition to anatomical methods, functional approaches based on several imaging methods have been successfully used to map visual cortical areas (Schuett et al., 2002; Kalatsky and Stryker, 2003; Mrsic-Flogel et al., 2003; Husson et al., 2007; Tohmi et al., 2009; Bonhoeffer and Hübener, 2016). By presenting visual stimuli at different locations in the animal’s visual field and imaging the responsive regions of the cortex, it is possible to define continuous retinotopic maps of the entire visual cortex, allowing to delineate its distinct areas (Fig. 1.4a,b). Using intrinsic signal imaging, a method that does not need any exogenous sensors, about a dozen distinct visual areas were identified (Andermann et al., 2011; Marshel et al., 2011; Garrett et al., 2014; Juavinett et al., 2016). Using more sensitive, genetically encoded calcium indicators, a few additional areas could be mapped, with the current count adding to 16 retinotopically organized areas (Wekselblatt et al., 2016; Zhuang et al., 2017).

Although these visual cortical areas in the mouse are believed to contribute differentially to perception and behavior, our understanding of their role in visual processing is still elusive. Despite some discrepancy across studies, it is emerging that primary and higher visual areas have somewhat

distinct tuning properties for spatial frequency, temporal frequency, orientation and motion direction of visual stimuli (Andermann et al., 2011; Marshel et al., 2011; Roth et al., 2012; Tohmi et al., 2014; Murakami et al., 2017).

According to these basic stimulus selectivities, higher visual areas appear to be subdivided into two functionally distinct groups (Murakami et al., 2017; Smith et al., 2017). In one group, areas LM, LI, POR, and P, located lateral to V₁, prefer slower grating stimuli, with high spatial frequency and low temporal frequency. In the other group, areas AL, RL, A, AM, and PM, located more on the anterior and medial sides of V₁, show more heterogeneous spatiotemporal selectivities: neurons in areas AL and, especially, RL and A prefer faster grating stimuli, with low spatial frequency and high temporal frequency, while areas AM and especially PM are tuned for slower grating stimuli. Notably, this functional subdivision of higher visual areas largely matches anatomical classifications based on corticocortical connectivity: the two groups of visual areas are overall distinct in their projection patterns to other cortices, and visual areas within each group are more densely interconnected (Wang et al., 2011, 2012). Thus, these findings support the view that also the rodent visual cortex is organized into two subnetworks, which may share similarities with the ventral and dorsal streams of primates. Although encouraged by anatomical data, the existence of such distinct processing streams in rodents is still quite speculative, as functional evidence to support this concept is presently scant compared to primates (Wang and Burkhalter, 2013; Glickfeld et al., 2014; Laramée and Boire, 2014; Glickfeld and Olsen, 2017).

An important mechanism to establish distinct functional specializations of higher visual areas is through specific connectivity. Interestingly, it has been recently shown that areas AL, PM, and LM are targeted by functionally distinct axons from V₁ that match the different response properties shown by each target area (Glickfeld et al., 2013b; Matsui and Ohki, 2013; Kim et al., 2017). Such a high degree of specificity seems to exist also for connections from higher visual areas back to V₁, since inputs from AL, PM, and LM to V₁ show specific tuning-and retinotopic-dependent projections (Huh et al., 2018; Nguyen et al., 2018). Furthermore, a very recent study, using a newly developed method for axonal tracing, performed a high-throughput analysis of long-range projection patterns of individual V₁ neurons. It was found that most neurons project to multiple higher visual areas with a non-random connection logic, thereby suggesting that specific subpopulations of V₁ neurons provide input to subsets of target areas and hence differentially contribute to their functional specialization (Han et al., 2018).

The overall advanced level in the processing hierarchy of higher visual areas compared to V₁, along with their rich connections to other sensory and non-sensory regions, suggest a role in integrating visual inputs with other sensory modalities as well as with motor and cognitive signals, to ultimately drive a behavioral output. In particular, area RL of mouse visual cortex represents an interesting case of multimodal integration. Area RL, anatomically located between V₁ and the barrel cortex (the cortical area that processes somatosensory input from the whiskers), contains small numbers of unimodal neurons, which respond to either visual or whisker stimulation, and in addition a large fraction of bimodal neurons (Olcese et al., 2013). These data raise the possibility that RL may integrate visual and tactile information for spatial navigation or visuo-tactile object interaction.

Finally, the mouse visual cortex is endowed with virtually all the key features and cell types typically found in higher mammals. The elaborate yet simpler organization of the mouse visual cortex, combined with its experimental tractability, offers a powerful model for studying the cellular and circuit mechanisms underlying the multiple stages of visual processing up to higher-order perception and behavior (Niell, 2011; Glickfeld et al., 2014; Zoccolan, 2015; Glickfeld and Olsen, 2017; Luo et al., 2018).

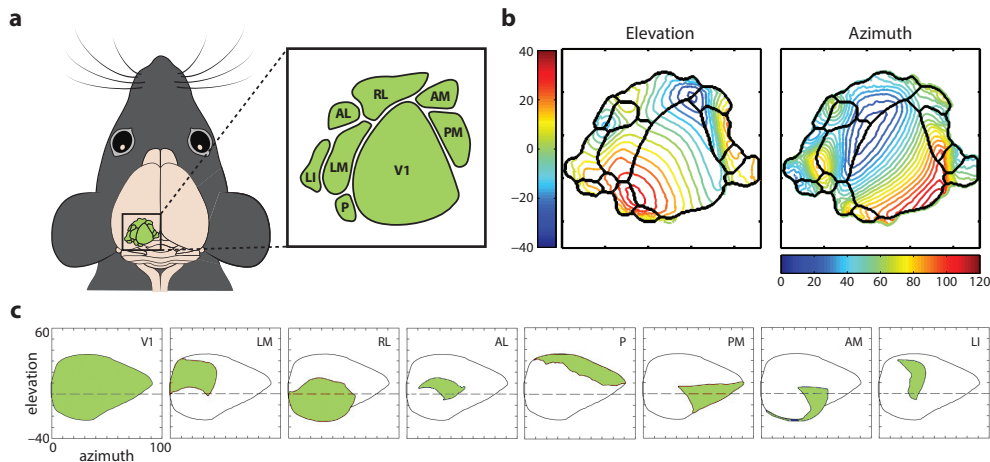


Figure 1.4 | Retinotopic organization of primary and higher-order visual areas in the mouse. **a** | Schematic illustrating the cortical location of V1 and several higher-order visual areas in the left hemisphere. **b** | Vertical and horizontal retinotopy of different visual areas shown as elevation and azimuth contour plots, respectively. Contour lines depict equally spaced, iso-elevation and iso-azimuth lines. Scale is indicated by tick marks, 1 mm. Reprinted with permission from Garrett et al. (2014). **c** | Visual field coverage of different visual cortical areas. Each panel illustrates the extent of the visual field covered by each area, depicted in green. Note that the visual field representations of higher areas are often incomplete or biased in space. Adapted from Zhuang et al. (2017).

1.1.9 Binocularity

In the following, I will elaborate on one particular aspect of visual processing in the neocortex – binocularity – since it is at the basis of the experimental work described in this Thesis.

Virtually all vertebrates and many invertebrates view the world through a pair of eyes. Indeed, for many animals including mammals, birds, amphibians and insects, a fundamental ability of the visual system is to combine information from the left and the right eye, which permits binocular vision whenever both eyes view a common segment of visual space. Entertaining two eyes, instead of just one, is resource demanding for any organism; still it has evolved across phyla, implying a vital role for the fitness of diverse species (Read, 2015; Nityananda and Read, 2017).

Probably, the most striking benefit of binocular vision is enhanced depth perception via stereopsis. Because the two eyes are spatially displaced on the head, their fields of view are slightly different from each other. As a result, the images formed by the two eyes have small dissimilarities – termed binocular disparities – that can be exploited by the visual system to triangulate the distance of objects from the observer, and also generate a vivid three dimensional perception of depth, as anyone can best appreciate when using a virtual reality headset or when viewing a 3D film in a movie theater as com-

pared to a normal movie. Although depth perception based on binocular disparities is undoubtedly advantageous in many conditions, depth information can also be extracted by using only one eye, through “monocular cues” like motion parallax, perspective, relative size, occlusion, shading and lighting, and several others (for more explanations, see section 1.3.1 [Visual depth cues and binocular disparity](#)).

The presence of two eyes with a binocular overlap of the monocular visual fields does not necessarily imply that a given species has also evolved stereoscopic depth perception. In fact, having two eyes offers several evolutionary advantages other than stereopsis.

The simplest benefit is that, similarly to other paired organs of the body, a spare eye is crucial in case one gets damaged and becomes critical for the survival of an animal that relies on vision.

Another important benefit is that two eyes can parse a wider portion of an animal’s surrounding at any given moment. This advantage is often particularly exploited by prey species to efficiently monitor their surroundings for predators. In these species, the two eyes tend to be lateral on the head and oriented at opposite sides, providing a more panoramic view at the expense of a narrower segment of binocular overlap necessary for stereopsis. An extreme example is the rabbit, which features an additional narrow portion of binocular overlap above and behind the animal ([Hughes, 1971](#)). Conversely, predator species generally adopt the opposite strategy in this trade-off, by evolving forward facing eyes with a wider binocular overlap for stereopsis at the expense of a more limited overall visual field.

Furthermore, vision at the binocular overlap employs two separate detectors, i.e. the two eyes, to sample the same visual scene, thereby improving the signal-to-noise ideally by a factor of $\sqrt{2}$ according to simple signal statistics.

1.1.g.1 *Neural architecture of binocularity in the mouse*

In the following paragraphs, I will describe the features of the mouse visual system serving binocular vision. I will then introduce binocular disparity processing, which will be important throughout the rest of this Thesis.

The mouse visual system features the essential components for binocular vision. Despite the fact that the eyes are laterally placed an angle of about 60 deg from the central azimuth, there is a binocular overlap of about 40 deg in front of the mouse. Relative to the head, the binocular visual field starts about 15 deg below the horizon, reaches its greatest width at about 20 deg above the horizon, and gradually becomes narrower toward the upper part continuing even slightly behind the animal’s head ([Fig. 1.1c](#); [Dräger, 1978](#); [Coleman et al., 2009](#); [Sterratt et al., 2013](#)). This region of binocular overlap is mapped onto roughly a third cortical territory of V1 and about half of the higher visual areas LM and RL ([Fig. 1.4](#); [Garrett et al., 2014](#); [Zhuang et al., 2017](#)).

1.1.g.2 *Contralateral- and ipsilateral-projecting retinal ganglion cells*

In the mouse, most RGCs (90-95%) of each eye cross the midline at the optic chiasm and project to visual structures located in the contralateral hemisphere, whereas a minority (5-10%) of RGCs do not decussate and project to the ipsilateral hemisphere ([Fig. 1.1a](#); [Dräger and Olsen, 1980](#); [Coleman et al., 2009](#)). Compared to the mouse, a larger fraction of RGCs project ipsilat-

erally in most carnivorans (10-30%) and primates (30-45%). Ipsilateral-projecting RGCs are located in the temporal retina, which, in these species, does not contain any contralateral-projecting RGCs (Jeffery, 2001; Larsson, 2015). In contrast, in the mouse, the crossed (contralateral) RGC projection originates from the entire retina, whereas the uncrossed (ipsilateral) RGC axons originate from the ventro-temporal part of the retina, often referred to as ventro-temporal crescent, which contains a mixed population of contralateral-and ipsilateral-projecting RGCs (Fig. 1.1b; Dräger and Olsen, 1980; Coleman et al., 2009; Sterratt et al., 2013). As a result, the field of view of each eye is processed by the dLGN and visual cortex located in the contralateral hemisphere, even though a separation of left hemifield/right hemisphere and right hemifield/left hemisphere does not occur at the vertical meridian. In fact, the very central part of the field of view, subtended by the ventro-temporal crescent of the retina, is processed by the dLGN and visual cortex in both hemispheres. Therefore, ipsilateral-projecting RGCs are crucial for binocular vision, as a binocular neuron in a given hemisphere receives visual signals from these cells as well. In addition, binocular signals are provided by another indirect pathway, the corpus callosum (see below paragraph 1.1.9.6).

Whether the population of ipsilateral-projecting RGCs comprises specific types still remains to be elucidated. Interestingly, one type of RGC (alpha cells) shows a steep gradient along the nasal-temporal axis of the mouse retina. In the temporal retina, corresponding to the central visual field, these cells are much denser, resulting in a higher number and overlap of RFs that support an enhanced sampling of the central part of the visual field (Bleckert et al., 2014; Dhande and Huberman, 2014).

1.1.9.3 *Binocularity and the dLGN*

In carnivorans and primates, the dLGN of each hemisphere receives RGC axons from the ipsilateral and contralateral eye within anatomically segregated, eye-specific laminae separated by so-called interlaminar zones.

In the mouse, too, the dLGN receives retinal projections from the ipsi- and contralateral eye in distinct eye-specific territories: RGC axon terminals from the ipsilateral retina are confined to a ventromedial zone in the core region of the dLGN (Fig. 1.1a) (Morin and Studholme, 2014; Monavarfeshani et al., 2017). There is mounting evidence, however, that a substantial fraction of neurons in the rodent dLGN are binocular. Electrophysiological recordings of the mouse dLGN found no evidence for a functional segregation of ipsilateral input, rather suggesting that dLGN cells located in the termination zone for ipsilateral RGCs are actually all binocular (Howarth et al., 2014). A recent study, using rabies virus trans-synaptic tracing, demonstrated that 40-50% of dLGN cells with RFs in the binocular visual field receive RGC input from both eyes. Interestingly, at least two kinds of binocular dLGN cells seem to exist: one kind dominated by contralateral inputs originating from various RGC types; another kind, vice versa, dominated by ipsilateral inputs originating from only few, selected RGC types (Rompani et al., 2017).

Such a prominence of binocular responses in the mouse dLGN might be due to a less definite anatomical segregation of the eye-specific territories compared to carnivorans and primates, which would more easily result in a crossover of RGC terminations and/or dendritic arbors of dLGN cells across these territories. Nevertheless, binocular responses have also been reported

in the dLGN of cats and marmoset monkeys (Erulkar and Fillenz, 1960; Cheong et al., 2013; Zeater et al., 2015; see also Wallace 2016; Dougherty et al., 2018), but the segregation of both eyes' inputs is certainly more pronounced in the thalamus of these species compared with the mouse. Thus, the more extensive binocular integration in the dLGN seems to be a distinctive feature of the rodent visual system, the functional implications of which need to be elucidated.

1.1.9.4 *Binocularity in the primary visual cortex*

In many carnivoran and primate species, including cats, macaques and humans, neurons in V₁ are clustered according to their eye preference to form OD columns – alternating cortical regions dominated by one eye or the other, vertically running across all cortical layers (Kandel et al., 2013). In cats and macaques, OD columns are highly segregated in L₄, the major thalamorecipient layer, such that L₄ neurons are monocular or strongly dominated by either eye, while most neurons in the other layers, albeit still dominated by either eye, exhibit at least some degree of binocularity (Hubel and Wiesel, 1968; Shatz et al., 1977; Shatz and Stryker, 1978).

In mouse V₁, two regions can be distinguished: a larger, strictly monocular region, driven exclusively by the contralateral eye, and a binocular region, occupying roughly one third of V₁ on its anterolateral aspect, receiving mixed input from both the contra- and the ipsilateral eye (Fig. 1.1a). While the binocular region is, on average, dominated by the contralateral eye, most neurons therein can be activated by stimuli presented to either eye, whereas only a small fraction of them can be driven exclusively via one eye (Dräger, 1975; Gordon and Stryker, 1996; Hübener, 2003; Kameyama et al., 2010). Neurons in the binocular region do not show any obvious large-scale spatial organization for OD, but are rather intermingled in a salt-and-pepper fashion (Mrsic-Flogel et al., 2007; Maruoka et al., 2017; see also paragraph 1.1.7.9). The anatomical organization of OD in the mouse, compared with cats and primates, might reflect the relatively low number of connections coming from the ipsilateral eye and/or an overall lower absolute number of neurons in V₁, even though the connectivity principles leading to a spatial organization for OD (as well as for other features like orientation selectivity) rather than a salt-and-pepper arrangement are under debate (Kaschube, 2014; Weigand et al., 2017).

1.1.9.5 *Binocularity in the visual cortical areas*

The largest, continuous representation of the binocular visual field in the visual cortex is located at the intersection of area V₁ with the higher-order areas LM and RL. Here, the horizontal representation of the binocular visual field in V₁ is mirrored and continues more laterally into areas LM and RL, such that the reversal meridian determines the boundary between V₁ on one side and LM and RL on the other side.

Also in the mouse, like in carnivorans and primates and as pointed out already in paragraph 1.1.7.1, the cortical representation of the binocular part of the visual field is expanded relative to the monocular visual field (Fig. 1.4). The cortical magnification factor increases substantially with eccentricity, by more than two-fold in areas LM and RL (Garrett et al., 2014). This indicates that visual information from the binocular field of view is transmitted

by twice the number of inputs per degree of space, and encoded by twice as many neurons in the binocular region of mouse visual cortex. Intriguingly, the partial and strongly biased representation of the central visual field present in areas LM and RL suggests that these extrastriate areas might support specific behaviors that rely on visual input from both eyes.

1.1.9.6 *Callosal projections*

Visual cortical areas in the two hemispheres are connected by interhemispheric projections that pass through the corpus callosum, the major fiber bundle in the brain. Across mammalian species, including rodents, callosal terminals are strongly enriched in the cortical regions that map the most central portion of the visual field (Hübener and Bolz, 1988; White et al., 1999; Mizuno et al., 2007; Wang et al., 2007; Pietrasanta et al., 2012; Bocci et al., 2014), thereby pointing towards an important role of these projections in generating binocularity. The entire visual field, as viewed by both eyes, is perceived as a single coherent image, even though it is split into two distinct representations in the visual cortex of each hemisphere. The callosal connections might be crucial for fusing the two partial representations into a single, coherent view of the world – the so-called cyclopean perception.

In cats and primates, the visual callosal pathway has been implicated in the developmental maturation of the visual cortex, in shaping neuronal responses to binocular stimuli, in neuronal disparity tuning as well as depth perception (Pietrasanta et al., 2012). In rodents, it seems that a considerable fraction of the ipsilateral eye input is indirectly conveyed via the callosal pathway from the opposite hemisphere, rather than coming from ipsilateral-projecting RGCs within the same hemisphere (Restani et al., 2009; Cerri et al., 2010). This marked impact of callosal connections on binocular responses might be the consequence of the prominent decussation of RGC projections in this species, with only a minority of eye-specific inputs projecting ipsilaterally (Pietrasanta et al., 2012). Nonetheless, the contribution of callosal connections to visual processing in rodents is still largely unexplored.

1.1.9.7 *Binocular disparity: basic geometry*

An object simultaneously seen by both eyes is viewed, by each eye, from a slightly different vantage point. For example, as depicted in Figure 1.5, when fixating a green dot, the image of the dot will form on the fovea of each retina, i.e. at the same relative position for the two eyes. A given fixation point defines a “fixation plane” called horopter: any point along the horopter will be projected such that, on both retinæ, its image will have the same distance to the image of the green dot. These points of projections, which fall on the same relative positions on the two retinæ, are defined as “corresponding points”. The arrowhead, instead, will form images at two non-corresponding retinal locations, with different distances to the fovea (the retinal distance FH in the left eye is different from F'H' in the right eye). Crucially, the magnitude of that retinal difference – termed retinal or binocular disparity – is a function of the object's distance from the observer and from the fixation point.

Binocular disparities are typically expressed as difference in angular position between eye projections ($\alpha - \beta$ in Fig. 1.5). For an object located nearer

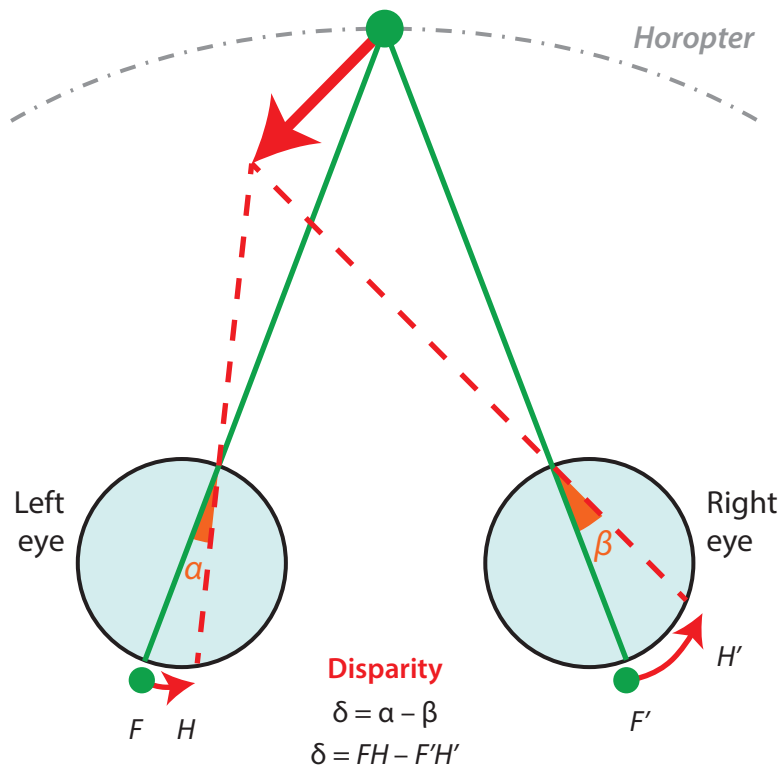


Figure 1.5 | Basic geometry of binocular disparity. When both eyes fixate on the origin of the arrow, the image of the green dot forms on the fovea of each retina (F). The images of objects located along the horopter (gray line) are formed at corresponding points on the two retinæ. The image of objects located in front of the fixation plane (red arrowhead) or behind it, are formed at non-corresponding points on the two retinæ, at different retinal distances from the fovea of each retina (distance FH is different from $F'H'$). This retinal difference ($FH - F'H'$, or $\alpha - \beta$) is termed retinal or binocular disparity. Note that the magnitude of binocular disparity, for a given fixation point, changes with object's distance from the observer.

than the fixation point (the arrowhead), the projection lines cross in front of the fixation point, generating a “crossed” disparity (by convention assigned with negative values); vice versa, objects farther away than the fixation point generate “uncrossed” (positive) disparities, since the projection lines cross beyond the fixation point.

1.1.9.8 Binocular disparity and eye movements

Fixating the green dot, as depicted in [Figure 1.5](#), typically involves a coordinated movement of the eyes to bring the dot on the fovea. Retinal disparities can thus be measured taking the fovea as a reference point. In fact, any other common retinal landmark could as well be used as a reference point for determining disparities, such that the presence of a fovea (that mice lack) is in principle not necessary. Eye movements are *per se* not necessary for enabling stereoscopic viewing. For instance, all non-mammalian species that were reported to be capable of stereopsis have eyes with very limited or no mobility, such as owls, falcons, toads and praying mantises ([Collett, 1977](#); [Fox et al., 1977](#); [Wagner and Frost, 1993](#); [van der Willigen, 2011](#); [Read, 2015](#); [Nityananda et al., 2016, 2018](#)). In fact, eye movements add considerable complexity to the problem of computing object distance from binocular disparities. Retinal disparities are indeed determined not only by the depth of the objects in visual space, but also by the position of the eyes:

as the eyes are moved, the projection of an object on the retina moves too. Consequently, the mapping between object distance and retinal disparities is not one-to-one, but changes all the time with eye position. For this reason, triangulating the absolute distance of an object requires the visual system of an animal with mobile eyes to take into account eye position.

On the other hand, for an organism with fixed eyes, triangulating the absolute depth of an object is a less demanding task for the visual system, because the mapping between object distance and retinal disparities is fixed, too (for more details, see also Discussion, paragraph [4.2.4.1 Absolute and relative disparity](#)).

1.1.10 Measuring binocular disparity tuning of individual neurons

Binocular disparities are the building blocks from which the visual system constructs stereoscopic depth perception. This implies that, at a certain stage in the visual system, binocular disparities must be encoded by neurons, by comparing visual stimuli between the two eyes. That is, for a neuron to be sensitive to disparities, it must receive input from both eyes (i.e. it must be binocular), having one RF for the left eye and one RF for the right eye, and its activity must depend on the specific position of a stimulus within its left and right eye RFs.

Consequently, the disparity tuning of a neuron can be assessed by systematically presenting a visual stimulus at varying relative positions between the two eyes. For example, a bar can be presented always at the same location to the left eye and systematically shifted when presented to the right eye, causing systematic changes in binocular disparity. The visually evoked responses of a given neuron can be measured as a function of the stimulus disparity, generating the neuron's tuning curve for disparity, similarly to what is typically done for orientation selectivity (see paragraph [1.1.7.3 Orientation selectivity](#)). A neuron that shows a response modulation upon binocular disparity, i.e. it responds more vigorously to some disparities than to others, is thus disparity-tuned or disparity-selective (see [Fig. 3.11a](#) for example tuning curves of disparity-tuned neurons).

The independent stimulation of each eye necessary for measuring disparity tuning, called *dichoptic* stimulation, can be achieved by e.g. using a pair of mirrors (a so-called haploscope) to redirect the field of view of each eye onto two independent stimulus monitors. Another option is by using eye goggles that, by means of e.g. polarized lenses, allow a single screen to present different stimuli to each eye.

1.2 DIRECTION SELECTIVITY

Imagine being suddenly unable to perceive visual motion. Although you probably do not need to hunt a flying bird for survival, daily activities like crossing a road, pouring a coffee or playing goalie in soccer would be extremely difficult, as evidenced by people affected by motion blindness ([Fig. 1.6](#)). For most animals, perceiving motion speed and direction of features in the visual scene is a crucial requirement, because it underlies vital behaviors such as fleeing from predators, catching prey, and finding a mating partner. In addition, motion vision plays a critical role for navigation

and course control: in fact, as an animal moves through its environment, the images of the visual scene shift across its eyes in function of the specific self-motion maneuvers.

The task of extracting motion direction from the visual scene requires the comparison of luminance across both space and time – a computation performed by specific neuronal circuits in the visual system. Neurons sensitive to the direction of visual motion were first described in cat primary visual cortex (V₁) in seminal work by David Hubel and Torsten Wiesel (Hubel, 1959; Hubel and Wiesel, 1959). In mammals, V₁ is the first cortical area to receive visual signals from the retina via the dorsal lateral geniculate nucleus (dLGN) in the thalamus, thereby forming a fundamental stage of visual information processing. In V₁, the majority of neurons (more than 3/4 of all cells in mouse V₁; Niell and Stryker, 2008) are orientation-selective (OS), i.e. they respond to bars and edges of only one orientation. A large fraction of these neurons (around a third of all cells in mouse V₁; Niell and Stryker, 2008) are in addition direction-selective (DS), as they respond more vigorously to stimulus motion in one direction than any other. Although DS neurons have been first described in cat V₁ half a century ago (Hubel, 1959; Hubel and Wiesel, 1959), the question of how direction selectivity of cortical neurons emerges is still largely unsolved.

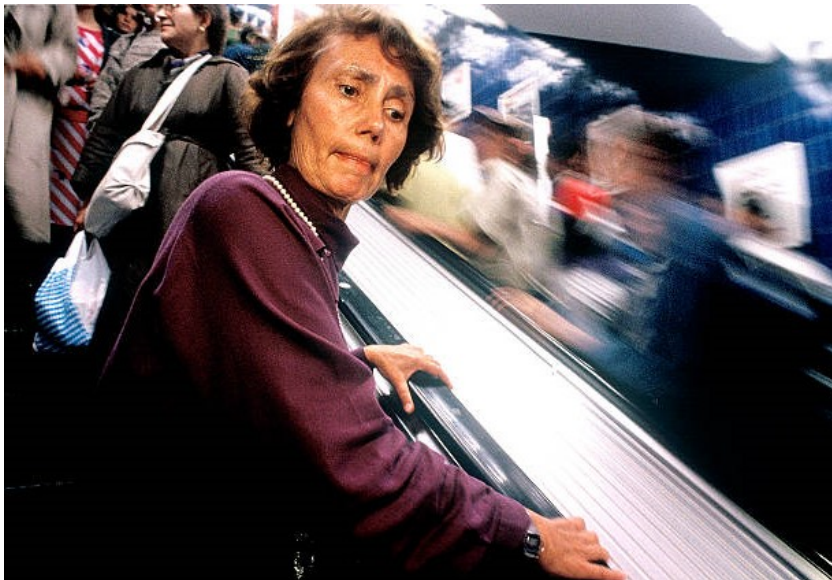


Figure 1.6 | Motion blindness impairs everyday life activity. In the photograph (by Joe McNally / Getty Images), Gisela Leibold, affected by motion blindness, feels anxious as she rides down an escalator in a subway in Munich (1982). Motion blindness, or akinetopsia, is a rare disorder characterized by the selective impairment of visual motion perception, while visual acuity and perception of other features like color or shape is unaffected. It is generally caused by bilateral lesion of area V₅, which plays a key role in visual motion perception. Much of what is known about motion blindness was learnt by studying Gisela Leibold (known as patient LM), which also had a great impact in visual motion research in general (Zihl and Heywood, 2015).¹

¹ Following is an excerpt by Zihl and Heywood (2015). < A rather shy lady presented herself at the Max Planck Institute of Psychiatry [in Munich]. When asked for her major problems, she reported that since her brain hemorrhage she could no longer see movements. “People, dogs, and cars appear restless, are suddenly here and then there, but disappear in between. Very often I don’t even know where they have left, because they move too fast, so I lose them quite often.” Fluids appeared frozen, like a glacier, which caused great difficulty, for example, with pouring tea or coffee into a cup. Most events were much too fast for her and

1.2.1 Direction-selective retinal ganglion cells

Already in the 1960s the pioneering studies of Barlow and coworkers in the rabbit retina reported the existence of direction-selective retinal ganglion cells (DSGCs), making up for about one fourth of all RGCs (Barlow and Hill, 1963; Barlow et al., 1964; Barlow and Levick, 1965; Oyster and Barlow, 1967). In the mouse retina, roughly a third of all ganglion cells are direction selective, consisting of more than eight subtypes (Baden et al., 2016). Such a prominence of retinal direction selectivity has been often considered a peculiar feature of the retina of these species, since only a minority of DSGCs were reported in an early study in the cat retina (Cleland and Levick, 1974). A later publication, though, observed a tenth of DSGCs in the cat retina (Shou et al., 1995), and, very recently, a major class of RGCs (the magnocellular-projecting parasol cells) in the primate retina has been demonstrated to be motion sensitive (Manookin et al., 2018).

The early work on the rabbit retina demonstrated that direction selectivity is not an exclusive feature of V₁, but it can also be found much earlier in the visual pathway, just 2-3 synapses downstream of photoreceptors. Since then, DSGCs have been under intense investigation in rabbit and mouse retinæ. The experimental accessibility of the retina and the large proportion of this class of ganglion cells in these species have made DSGCs an ideal substrate for studying the cellular mechanisms underlying visual motion computation.

1.2.2 How can visual motion be detected in principle?

An object moving across space consists of a luminance pattern that changes position over time. Thus, two luminance receptors that are spatially offset will be sequentially activated by a moving stimulus. To extract motion information, a detector must perform a computation by comparing the signals from at least two receptors, across both space and time (Fig. 1.7a,b).

Two distinct circuit schemes have been proposed to carry out such space-time signal correlations, each requiring an asymmetry with respect to input distribution and timing, as well as a nonlinear interaction. In the asymmetric excitation model, introduced by Hassenstein and Reichardt (Hassenstein and Reichardt, 1956), a stimulus moving in the preferred direction triggers an excitatory signal from the first receptor that, appropriately delayed, combines with the signal from the other receptor. The resulting coincidence of signals at the level of the detector is nonlinearly enhanced to generate an output response that is larger than the sum of the individual signals (Fig. 1.7a). Conversely, the asymmetric inhibition model, first proposed by Barlow and Levick (Barlow and Levick, 1965), relies on inhibitory signals that suppress the response to non-preferred directions. In this case, the coincidence of sig-

she needed a considerable time to perform even simple routine activities, such as cutting bread or using the vacuum cleaner. She reported that reading took more time than before, writing had become somehow difficult. She could no longer use the tube, bus or tram. She also found it very irritating to meet friends because she could not respond in time to their handshake and [...] she had to avoid watching their (changing) facial expressions while speaking, in particular, their lips seem to “jump rapidly up and down, and I am very often unable to listen to what they were saying.” In contrast, when people, faces, objects and cars were stationary, she had no difficulty in seeing them “clearly” and could recognize them immediately and accurately. >

nals at the level of the detector results in a nonlinear suppression of the output response (Fig. 1.7b).

1.2.3 Asymmetric inhibition underlies direction selectivity of retinal ganglion cells

Barlow and Levick, based on their observations in the rabbit retina, suggested that the selective responses of DSGCs arise primarily by asymmetric inhibition (Barlow and Hill, 1963; Barlow et al., 1964; Barlow and Levick, 1965).

In the mouse retina, which is probably the best understood circuit of the vertebrate brain to date, asymmetric inhibitory input from starburst amacrine cells (SACs) has been largely shown to be a major mechanism underlying the direction selectivity of DSGCs (Fried et al., 2002; Briggman et al., 2011; Wei et al., 2011; Yonehara et al., 2011; for a review see Vaney et al., 2012; Mauss et al., 2017). Compelling evidence for a specific asymmetric connectivity between DSGCs and SACs was provided by using two-photon population calcium imaging in combination with neuronal reconstruction of a small patch of mouse retina by serial block-face scanning electron microscopy (Briggman et al., 2011). Crucially, a DSGC of a given preferred direction receives a much larger number of synaptic contacts (11:1) from SACs whose somata are located on the “anti-preferred” side of the DSGC, i.e. opposite to where the preferred direction originates.

In this way – given the tight relation between location of a cell in the retina and the position of its RF in visual space – a stimulus moving in the anti-preferred direction recruits the SAC with the appropriate timing to suppress the activation of the DSGC. Conversely, a stimulus moving in the preferred direction escapes inhibition and succeeds in activating the DSGC, because the asymmetric inhibitory input from the SAC arrives too late to suppress the DSGC (Fig. 1.7b).

Nonetheless, asymmetric inhibition is not the only determinant of the direction selectivity of DSGCs, but other complementary mechanisms play a role in sharpening tuning, including asymmetric excitatory input and intrinsic properties of DSGCs. Remarkably, evidence shows that the excitatory and inhibitory inputs to DSGCs are themselves already biased for motion direction, moving the initial source of direction selectivity one synapse upstream of DSGCs, at the level of SACs (Euler et al., 2002; Mauss et al., 2017).

The computation of motion direction has been extensively investigated in the insect visual system as well. The first neurons in the visual pathway of the fruit fly exhibiting DS responses – the T₄ and T₅ cells in the lobula plate – generate direction selectivity by combining both asymmetric excitation and asymmetric inhibition (Borst and Helmstaedter, 2015; Mauss et al., 2017).

1.2.4 Potential mechanisms underlying cortical direction selectivity

Thus, while we have an advanced understanding on how direction selectivity is generated in these two model systems, the mammalian retina and the fly visual system, the generation of cortical direction selectivity is far less clear. In principle, one could imagine two scenarios: cortical direction selectivity might be simply inherited from the retina, at least in such mammals that have substantial direction selectivity among retinal cells (retina-depen-

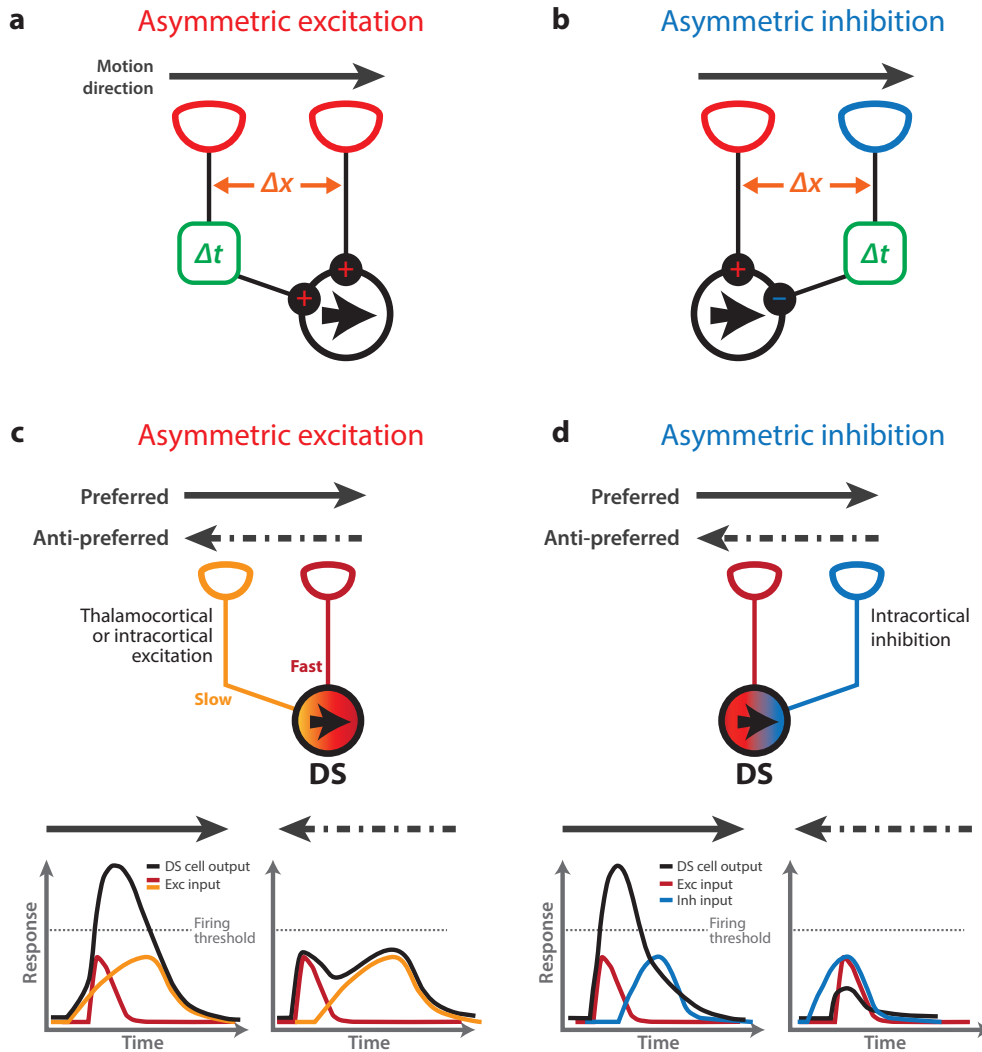


Figure 1.7 | The two models for visual motion detection. (a–b) A motion detector (black circle) with preferred direction from left to right (black arrow) receives signals from two receptors with a spatial offset Δx . **a** | In the asymmetric excitation model, a stimulus moving in the preferred direction (from left to right) activates first the left receptor, whose signal is delayed by a temporal filter (Δt) and is combined with the direct signal from the right receptor. The excitatory non-linearity generates a response that is greater than the sum of the responses elicited by each receptor input individually. **b** | In the asymmetric inhibition model, a stimulus moving in the non-preferred direction (from right to left) triggers an inhibitory signal from the right receptor (blue) that is delayed with appropriate timing (Δt) to suppress the direct signal from the left receptor. (c–d) Models for cortical computation of direction selectivity. A direction-selective cell (black circle) with preferred direction from left to right is depicted. **c** | In the asymmetric excitation model, the cortical DS cell receives asymmetric excitatory input from the dLGN or other cortical cells. Top, the RFs of presynaptic inputs are ordered according to their respective visual space location from left to right and response latency from slow (orange) to fast (red). The orange–red gradient of the DS cell represents the spatial gradient of response latencies of its RF. Bottom left, a stimulus moving from left to right leads to synchronous and therefore maximal excitation of the postsynaptic cell, which passes the threshold for action potential firing to produce the DS output (black line). Bottom right, when a stimulus moves from right to left (anti-preferred direction), the excitatory inputs are not temporally synchronous and do not effectively coincide in the postsynaptic cell. The weaker response in the postsynaptic cell is not sufficient to pass the firing threshold, such that no DS output is produced. **d** | In the asymmetric inhibition model, the cortical DS cell receives intracortical inhibitory input with spatially asymmetric RFs (blue). Bottom left, a stimulus moving in the preferred direction (from left to right) elicits DS responses because the asymmetric inhibitory input arrives too late to suppress the excitatory input (red). Bottom right, a stimulus moving from right to left (anti-preferred direction) recruits the inhibitory input with the appropriate timing to suppress the excitatory drive of the postsynaptic cell.

dent computation). Alternatively, direction selectivity could be generated *de novo* in the cortex (retina-independent computation). Of course, it is also well conceivable that both mechanisms are at play. Until recently, it has been rejected that in the mammalian visual system DS signals computed in the retina might be transmitted to V1 to contribute to cortical direction selectivity. The main reason behind this assumption was that DSGCs were thought to supply input only to subcortical circuits, without reaching the cortex. DSGCs could hence not influence cortical direction selectivity, but rather be involved in purely reflexive responses related to vestibular control and eye movements (Simpson, 1984; Yoshida et al., 2001; Pushchin, 2013; Sun et al., 2015; Sabbah et al., 2017; Shi et al., 2017).

Consequently, direction selectivity in the visual cortex has been considered a cortical computation, arising *de novo* in V1 from non-DS inputs and independently of retinal direction selectivity. Under this assumption, several circuit models for cortical direction selectivity have been put forward, which can be grouped within the framework of the two fundamental circuits for motion detection described above (Fig. 1.7c,d).

1.2.4.1 *Asymmetric excitation model for cortical direction selectivity*

In the asymmetric excitation model, a DS neuron in V1 has a RF with a spatial gradient of response latencies, generated by the integration of excitatory inputs with incremental timing and spatially shifted in the visual field (Fig. 1.7c). Accordingly, a DS neuron will receive simultaneous and therefore maximal excitation only when a stimulus moves along the RF in the preferred direction, from the longest to the shortest latency region of its RF (Reid et al., 1987, 1991). In one specific incarnation of this model, the temporal diversity of excitatory inputs to DS neurons arises from dLGN cells with different response latencies (Saul and Humphrey, 1992; Ferster et al., 1996; Saul et al., 2005). Strong evidence in favor of this model has been obtained by a very recent study in the mouse, showing that the integration of thalamic inputs with the appropriate spatiotemporal offset is the primary source of direction selectivity in L4 neurons (Lien and Scanziani, 2018). In another incarnation of the asymmetric excitation model, the temporal and spatial diversity of excitatory inputs to cortical DS neurons arises intracortically, i.e. from other V1 cells rather than from dLGN cells, as some evidence indicated (Emerson and Gerstein, 1977; Suarez et al., 1995; Maex and Orban, 1996; Livingstone, 1998; Peterson et al., 2004).

1.2.4.2 *Asymmetric inhibition model for cortical direction selectivity*

Alternatively, in the asymmetric inhibition model, the emergence of direction selectivity requires the interaction between excitatory inputs and the cortical inhibitory system that asymmetrically suppresses responses to non-preferred directions, with circuit mechanisms analogous to the ones identified for retinal direction selectivity (Fig. 1.7d; Barlow and Levick, 1965; Torre and Poggio, 1978; Grama and Engert, 2012). However, the evidence that inhibition of the non-preferred direction contributes to the computation of cortical direction selectivity is somewhat controversial. For instance, in cat V1 both excitation and inhibition are tuned to the same direction of motion, but rather differ in relative timing (Priebe and Ferster, 2005). By contrast, a very recent study in the ferret V1 demonstrated that intracortical inhibition

has a major influence on the degree of direction selectivity by suppressing responses to the non-preferred directions (Wilson et al., 2018a). In addition, optogenetic activation of parvalbumin-expressing inhibitory cells enhanced both orientation and direction selectivity in mouse V1 and improved perceptual discrimination in awake mice, thereby supporting inhibition-based models (Lee et al., 2012).

1.2.5 Retina-dependent computation of cortical direction selectivity

In the mouse, several recent studies support the hypothesis that retinal direction selectivity does contribute to direction selectivity in the cortex, challenging the view of a *de novo* cortical computation.

Using transgenic mouse lines, specific classes of DSGCs have been shown to project to the dLGN, predominantly in the shell region, which is located in dorsolateral outer part (Huberman et al., 2009; Kay et al., 2011; Rivlin-Etzion et al., 2011). A new study performed two-photon imaging of retinothalamic axons in the dLGN and observed that RGCs provide OS and DS input to the dLGN with a fine-scale organization (Liang et al., 2018; see also Marques et al., 2018; Román Rosón et al., 2018). The shell region of the dLGN contains neurons that are highly tuned to stimulus direction (Marshel et al., 2012; Piscopo et al., 2013; Scholl et al., 2013b; Zhao et al., 2013). Importantly, these cells also project to V1, since a subset of dLGN thalamocortical axons, measured by two-photon imaging in V1, are in fact DS. In addition, the direction preferences shown by the dLGN thalamocortical axons were overall biased for the cardinal directions, similarly to RGCs in the retina (Cruz-Martín et al., 2014; Kondo and Ohki, 2015; Sun et al., 2016; Jaepel et al., 2017). This bias appears to propagate to the cortex, as V1 neurons tend to be more frequently tuned to cardinal directions, especially early in development (Rochefort et al., 2011; Hagihara et al., 2015; Hoy and Niell, 2015). Direct evidence that DSGCs contribute to cortical direction selectivity came from trans-synaptic tracing based on rabies virus (Cruz-Martín et al., 2014). By using this approach, Cruz-Martín et al. demonstrated that, along the retino-geniculo-cortical pathway, there exists a specific di-synaptic circuit dedicated to routing DS signals from DSGCs in the retina to superficial layers of V1 (L1 and upper L2/3; Cruz-Martín et al., 2014). The layer specificity of the DS di-synaptic circuit is paralleled by a dependence of response properties of V1 neurons on cortical depth (Hoy and Niell, 2015; Sun et al., 2016; O'Herron et al., 2018). For example, neurons in upper L2/3 were found to be more biased for the horizontal axis than in lower L2/3 (Kreile et al., 2011).

1.2.6 Retina-independent computation of cortical direction selectivity

On the other hand, it is unlikely that direction selectivity present in V1 is entirely due to inheritance from DSGCs. Importantly, only a minority of dLGN cells were found to be DS (<5%, compared to a minimum of 30% in V1). Furthermore, DS neurons in the dLGN respond more continuously to a periodic grating stimulus, indicating a nonlinear, "complex-like" RF (Piscopo et al., 2013; Zhao et al., 2013; Hei et al., 2014); by contrast, the majority of V1 DS cells in L2/3 and L4 have a linear/simple RF (Niell and Stryker, 2008; Hei et al., 2014; Li et al., 2015) and, as such, it is unlikely that these cells may inherit direction selectivity from nonlinear DS cells in the dLGN.

Finally, the di-synaptic pathway linking DSGCs to V₁, identified by [Cruz-Martín et al. \(2014\)](#), is confined to the superficial layers of V₁ (mostly L₁), passing through to the shell region (dorsolateral outer part) of the dLGN. By contrast, the retino-geniculo-cortical pathway carrying untuned signals from non-DS retinal ganglion cells projects to deeper layers of V₁ (L₄) passing through the core region of the dLGN. Thus, the pathway transmitting DS-signals is not only functionally distinct, but also at least partially anatomically separated, indicating that it is parallel to the classic retino-geniculo-cortical pathway.

Together, these findings suggest the existence of two parallel mechanisms underlying cortical direction selectivity in the mouse: one relying on direct inheritance of DS information generated in the retina; and another one relying on retina-independent, *de novo* generation of direction selectivity by thalamocortical and/or intracortical circuits.

Indeed, a very recent study by [Hillier et al. \(2017\)](#) provides compelling evidence for the existence of both forms of DS computations in mouse V₁. Two different genetic approaches were used to selectively disrupt retinal direction selectivity and analyze the effect on cortical direction selectivity. One manipulation was based on the ablation of starburst amacrine cells (SACs) through cell-specific expression of the diphtheria toxin receptor, resulting in the loss of direction selectivity along all axes in most DSGCs. The other manipulation disrupted retinal direction selectivity only along the horizontal directions, by deleting the gene for FRMD7, which is specifically expressed in SACs. Upon deletion of this gene, SACs transition from supplying asymmetric to symmetric inhibitory input to RGCs only along the horizontal axis, via an unknown mechanism ([Yonehara et al., 2016](#)). After disruption of retinal direction selectivity induced by either manipulation, the overall degree of direction selectivity in V₁ remained surprisingly unaffected, but the distribution of direction preferences shown by V₁ cells was dramatically changed: the strong over-representation of cells tuned to the posterior direction present in control mice disappeared completely, unbalancing the distribution toward vertical directions.

Although this work convincingly demonstrated the existence of both a retina-dependent and retina-independent mechanism for the generation of cortical direction selectivity, several issues remain unsolved. For example, the functional significance and the quantitative contribution of each of the two computations under physiological conditions, as well as how they emerge during development, are still open questions that could not be fully addressed by the genetic approaches in the study by [Hillier et al. \(2017\)](#). The diphtheria toxin approach did not entirely abolish retinal direction selectivity, such that cortical direction selectivity might still be influenced by residual retinal DS signals. Moreover, the RGCs affected by either manipulation lost their direction tuning through increased activation to non-preferred directions, such that they became equally responsive to any direction of motion. On the one hand, this permitted analyzing the influence of RGCs attributable to their specific DS activity – and not just to their activity in general. On the other hand, the overall firing of the manipulated RGCs increased by over two-fold, possibly leading to homeostatic synaptic modifications at the level of the dLGN or in V₁ ([Turrigiano, 2011, 2017](#)). Compensatory mechanisms are also suggested by the observation that the fraction of DS neurons in V₁ did not drop after disruption of retinal direction selectivity.

Altogether, several open questions on the relationship between retinal and cortical direction selectivity require further investigation, ideally with acute or reversible manipulations, e.g. by means of optogenetic or chemogenetic inactivation.

1.2.7 Apparent motion illusion as a window into the origin of cortical direction selectivity

Therefore, I developed an approach for blocking retinal direction selectivity based simply on visual stimulus manipulation, hence in an acute and non-invasive fashion. The aims of this study were to clarify (1) to which extent cortical direction selectivity is generated via retina-independent computation, and (2) which functional and spatial properties neurons in V1 with retina-dependent and -independent computations have.

To this end, it is crucial to disentangle the retina-dependent from the retina-independent computation of direction selectivity, which take place at two distinct stages of the visual pathway. The approach I chose was inspired by classic psychophysical studies of the visual system, in which psychophysicists and physiologists have developed and exploited specifically tailored visual stimuli to decipher the complexity of the system (Eagleman, 2001). Examining the perceptual effects of particular optical illusions can provide insights into where in the visual pathway a certain phenomenon arises and thereby also into the underlying mechanisms. To give a specific example: Figure 1.8a depicts an image that can evoke a classical optical illusion, namely an “afterimage”. Fixating on it for a certain amount of time (say 30 sec) and then looking elsewhere, lets the image with inverse contrast persist for several seconds. Importantly, when fixating on it with just one eye and then looking elsewhere with the other eye, there will be no afterimage whatsoever. This perceptual effect indicates that the mechanism underlying the afterimage illusion is eye-specific, arising from monocular neurons at a stage before inputs from both eyes converge. Indeed, the mechanism underlying this particular optical illusion takes place at the level of the retina, due to desensitization of photoreceptors (rods and cones exposed to the same stimulus exhaust the supply of available photopigment necessary for phototransduction) or neural adaptation in the local retinal region (Shimojo et al., 2001).

Analogously, in this study I employed the trivial fact that mice have two eyes, and that properties of a binocular percept cannot arise in the retina, but only at a stage of the visual system where inputs from both eyes converge, namely at the level of binocular neurons in the dLGN or, more likely, in V1. Since a fundamental prerequisite for extracting motion direction is the presence of at least two visual signals that are distinct in both position and time, I used the two retinae as the source of those very signals for binocular neurons.

To do so, I took advantage of an optical illusion called apparent motion (AM), which allows perceiving continuous motion from a series of static images displayed in rapid succession, as it occurs, for example, when watching a movie in the cinema or on TV (Fig. 1.8b). Accordingly, the perceived motion of a bar can be perfectly mimicked by using just two static bars displayed with a small offset in space and time: instead of presenting a fluidly drifting bar, a static bar is first flashed in one position and, immediately thereafter in the

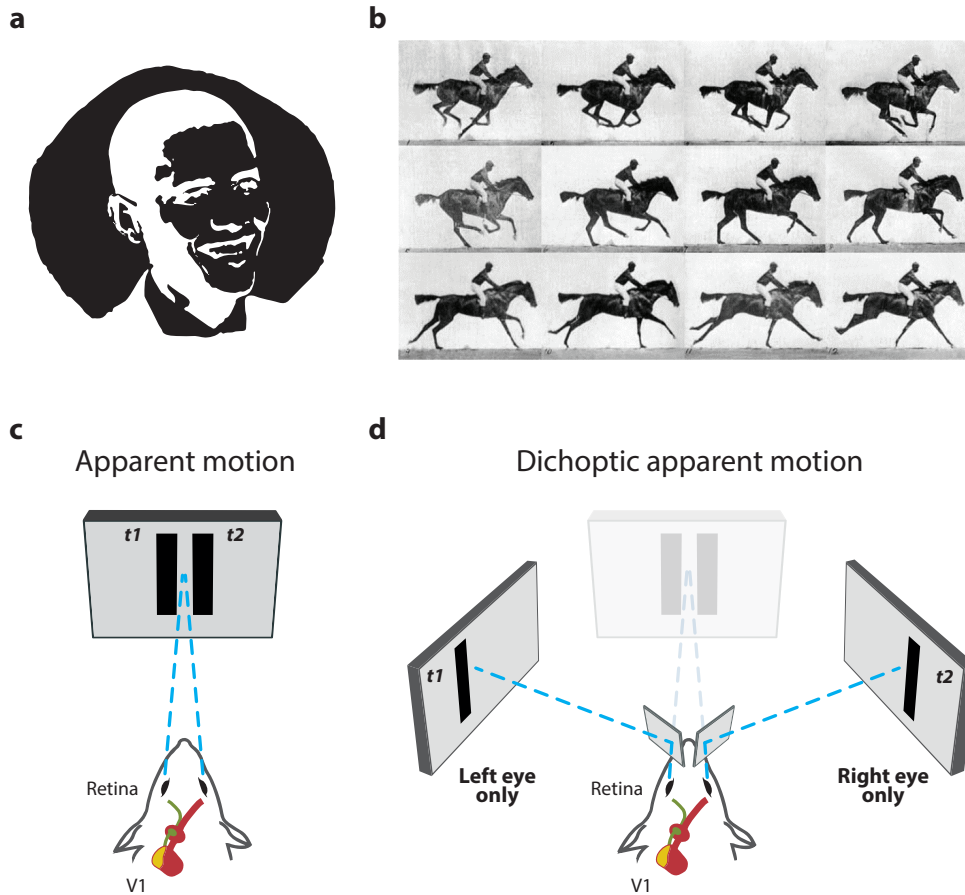


Figure 1.8 | Apparent motion illusion as a window into the origin of cortical direction selectivity. Optical illusions are powerful tools for studying how and where in the visual pathway a certain aspect of visual processing takes place. **a** | The drawing illustrates a negative afterimage. When the viewer looks at Barack Obama's face for 30–60 seconds and then looks at a white surface, the image of Obama will still be present with inverted contrast for several seconds. However, exposing only one eye to the image and then looking elsewhere with the other eye does not induce any afterimage. **b** | The optical illusion of apparent motion occurs when a series of static images is displayed in rapid succession and is perceived as fluidly moving, as demonstrated by the photograph series "Horse in Motion" by Eadweard Muybridge (1878). This photograph series, considered the first movie ever, was created by positioning 24 cameras in parallel along a track which were triggered by trip wire as the horse passed. The animation was played on a zoopraxiscope, a device of his invention and a precursor to the movie projector. The photograph series also demonstrated that a galloping horse sometimes lifts all hoofs simultaneously off the ground. **c** | Schematic illustrating the basic principle of apparent motion (AM) stimuli used in this Thesis. The motion of a bar from left to right can be reproduced by AM, displaying a static bar at two consecutive frame times ($t1$ and $t2$) at a slightly offset position in space. **d** | Schematic illustrating dichoptic AM stimuli used to probe the generation of direction selectivity in mouse V1. The motion of a bar from left to right can be mimicked by displaying the two consecutive frames ($t1$ and $t2$) each containing a single static bar, not to both eyes together as shown in (c), but each frame to one eye only, in a so-called dichoptic fashion. In this way, each eye will only view a single static bar, insufficient to detect any motion, thereby preventing any computation of direction selectivity in each retina. Neurons in the binocular region of mouse V1 (yellow region) can in principle extract motion direction by integrating visual input from the left and right eye. Therefore, binocular V1 neurons showing DS responses to dichoptic apparent motion would demonstrate that direction selectivity can be generated through thalamocortical and/or intracortical circuits, independently of any inheritance mechanism from the retina. The dichoptic viewing is achieved by using a haploscope, an apparatus consisting of two mirrors to redirect the field of view of each eye onto a separate monitor.

second, spatially offset position (Fig. 1.8c).

Crucially, the same bar motion can also be mimicked by displaying the two flashed static bars in a dichoptic fashion, i.e. separately to each eye: for example, the first bar is flashed only to the left eye and then the second bar only to the right eye, at a slightly different position (Fig. 1.8d). Technically, this can for example be achieved by means of two haploscope mirrors that redirect each eye's view onto a separate display monitor. In this way, while bar motion across both eyes can again be mimicked, each retina will only view a single static bar – insufficient to evoke any motion response –, thereby preventing any DS computation at the level of the retina. Conversely, binocular neurons in V1 can “view” (be stimulated by) both bars and, hence, are potentially able to extract motion direction. Critically, DS activation of V1 neurons in response to dichoptic AM can only be evoked if, in those same neurons, direction selectivity is generated via a retina-independent mechanism, i.e. through thalamocortical and/or intracortical circuits.

Dichoptic AM is thus a cyclopean stimulus. As defined by Béla Julesz in his influential work ‘Foundations of cyclopean perception’ (1971), a stimulus is cyclopean when the feature is not evident in the monocular image, but it is formed “centrally” – it can be said to bypass the retinae. As such, dichoptic AM is a cyclopean procedure, potentially allowing to infer that the origin of direction selectivity is, at least in part, beyond the retina (Howard and Rogers, 1995).

A similar approach was employed in the larval zebrafish, another vertebrate model system for vision research. In this species, the direction selectivity is present both at the level of the retina and the optic tectum, the largest retinorecipient structure and crucial for visual information processing. Dichoptic AM stimulation provided evidence that tectal neurons do not inherit DS signals from the retina, but rather generate direction selectivity *de novo*, through local circuits that provide asymmetric inhibition (Ramdya and Engert, 2008; Grama and Engert, 2012).

Here, I measured motion tuning of neurons in the binocular region of mouse V1 in response to a diverse repertoire of AM stimuli, displayed in a dichoptic fashion to prevent any retinal direction selectivity. Dichoptic AM stimuli evoked a surprisingly complex variety of neuronal responses in V1. A minority of neurons appeared to show DS responses to dichoptic AM stimuli, suggesting that the direction selectivity of these neurons was not inherited from the retina, but computed *de novo* via thalamocortical and/or intracortical circuits. However, the complexity of the response features disclosed by dichoptic AM stimulation probably reflected not only mechanisms of direction selectivity, but also other RF properties, like binocular disparity, which is a prominent feature of most binocular neurons in V1, as it will be demonstrated later in this Thesis.

Taken together, the results of this study did not allow making definitive statements on the actual contribution of visual motion computation in V1. Yet, despite complicated by confounding factors, the results are compatible with contributions of both retina-dependent and -independent mechanisms for cortical direction selectivity.

1.3 BINOCULAR DISPARITY PROCESSING

1.3.1 Visual depth cues and binocular disparity

The visibility of our three-dimensional surroundings is constrained by the optical apparatus of each eye, in which only a two-dimensional projection of the space can form on each retinal surface. Despite this dimensionality reduction, the visual system synthesizes a 3D representation of the visual world with a vivid sense of depth. To achieve this, the visual system exploits a number of visual depth cues, which can be categorized into three classes (Banks et al., 2016):

- (1) cues of light transmission and reflection, such as shading, occlusion, and atmospheric effects;
- (2) cues of perspective projection, such as linear perspective, relative size, texture gradients;
- (3) cues of triangulation, including blurring, motion parallax and binocular disparity.

Binocular disparity is the only visual depth cue to be binocular, i.e. it can provide depth information only when using both eyes together, producing a sense of depth called stereopsis. All other visual cues are monocular, as they allow to extract depth information already when viewing the scene with just one eye. The monocular cues can altogether provide a fairly good sense of depth. Indeed, 2-4% of people are “stereoblind” (Richards, 1970), specifically lacking stereoscopic depth perception, without major impairments in ordinary life and sometimes without even realizing it.² However, the monocular cues of the first two classes need to be interpreted using assumptions based on the statistics of the specific scene and on experience. As such, these cues tend to be more ambiguous and many animals have evolved to manipulate them to send deceptive signals as part of their defensive or predatory strategies (Read, 2015). The triangulation depth cues, instead, are less ambiguous because they stem from the geometrical configuration of the physical space and of the optical system of the observer (but see Yang and Purves, 2003). In motion parallax, for example, the animal’s head is laterally moved relative to the environment to sample different views over time. The retinal images of the viewed objects move with an angular velocity in function of object distance, enabling absolute distance judgments with an accuracy almost comparable to the one produced by stereopsis (Ferris, 1972). Motion parallax, on the other hand, requires head movements and is slower than other cues, making it easier to be detected by a prey or predator. While not essential for depth perception, it is by using binocular disparities that the visual system offers the most accurate 3D representation of the visual space

² «Stereoblind? Was I stereoblind? I looked around. The classroom didn’t seem entirely flat to me. I knew that the student sitting in front of me was located between me and the blackboard because the student blocked my view of the blackboard. When I looked outside the classroom window, I knew which trees were located further away because they looked smaller than the closer ones. The footpath outside the window appeared to narrow as it extended out into the distance. Through cues like these, I could judge depth and distance. I knew the world was in 3D. Yet, my professor implied that there was another, different way to see space and depth. He called this way of seeing stereopsis. I couldn’t imagine what he was talking about.» By Susan Barry, ‘Fixing my gaze’ (2009). Susan Barry first realizes her stereoblindness at a college neurobiology class, and only much later she was able to acquire stereopsis.

around us.³ Simply attempting to thread a needle using only one eye makes this evident (Fig. 1.9).

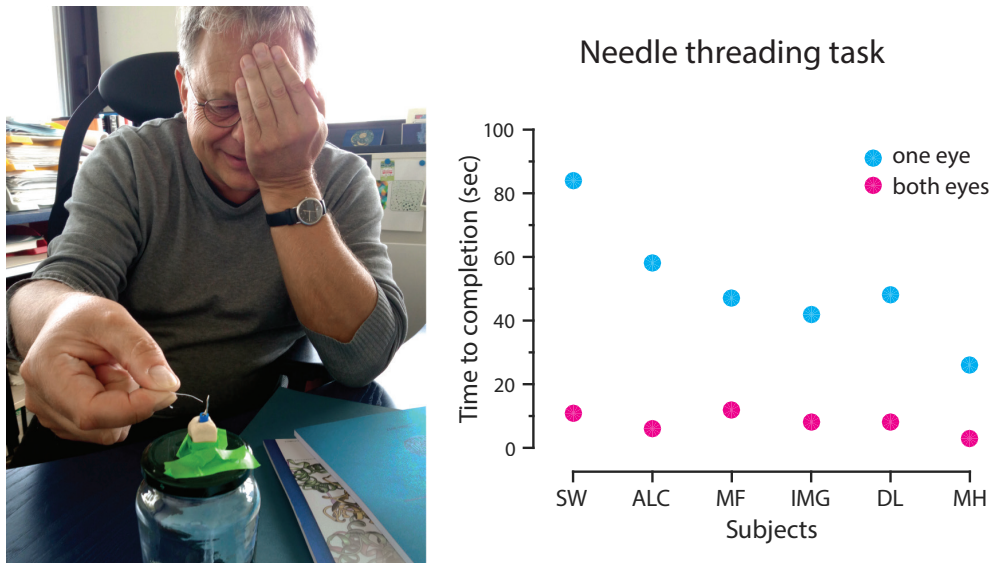


Figure 1.9 | Needle threading task to compare binocular and monocular depth perception.⁴
a | A subject (the Thesis supervisor) performing the needle threading task in the monocular condition. The experimental apparatus consisted of a small metal plate with a 1.5 mm hole, placed at a distance of about 50 cm. The task was to insert a thread (length 4 cm) through the hole using one hand, without contacting the table and the metal plate holder. Subjects were instructed to keep their head stable in order to minimize motion parallax. In the monocular condition, the subjects occluded one eye of their choice. **b** | Time to successful completion of the task, in the binocular (magenta) and monocular (cyan) condition. Note the marked increase in time needed by each subject for completing the task in the monocular condition compared to the binocular condition. Data points represents average of two trials for each subject and condition. Subjects participated on a purely volunteer basis (see also Acknowledgments).

Noteworthy, stereopsis is not only relevant for distance judgment *per se*. A major ability that arises from it is camouflage breaking. If viewed by a single eye, a certain object, say a predator or prey, might evade notice when its appearance makes it blend in with its surroundings. By contrast, a stereoscopic view could help making that object stand out from its background (Read, 2015; Nityananda and Read, 2017).⁵ Considering that camouflage is a crucial strategy exploited by both prey and predator species, it has been pro-

- 3 «I thought that I could see plants clearly. I thought I knew the forest. [But] binocular vision completely changed my experience of nature. I was strolling through a humble plantation of pines, I had an epiphany. I was amongst the trees, not looking out at them; they surrounded me in a way that was marvelously different than I'd previously experienced. The crenellations of bark and appliqué of moss were deeper, the edges clearer and the colors brighter. Most unusual, the space between the trees was apparent. It was as if I had stepped inside a painting that I had spent my whole life observing. The depth of space and emotion was overwhelming. I was awed and moved to tears. I had never experienced a forest in this way.» Rachel Hochman, formerly stereoblind, describes the moment she suddenly gained stereovision after vision therapy (Hochman, 2018).
- 4 «Just as I could not imagine a world in stereo depth, an individual with normal stereopsis cannot experience the worldview of a person who has always lacked stereopsis. This may be surprising because you can eliminate cues from stereopsis simply by closing one eye. What's more, many people do not notice a great difference when viewing the world with one eye or two. When a normal binocular viewer closes one eye, however, he or she still uses a lifetime of past experiences to re-create the missing stereo information.» By Susan Barry, 'Fixing my gaze' (2009)
- 5 «When we'd go out and people would look up and start discussing some bird in the tree, I would still be looking for the bird when they were finished. For everybody else, the bird

posed that stereopsis has actually evolved to support camouflage breaking (Julesz, 1971).

1.3.2 Demonstrating stereoscopic perception

Stereopsis fascinated scientists for centuries (Parker, 2016), but it was only in 1838 that Wheatstone first described this “remarkable, and hitherto unobserved” phenomenon of human binocular vision by inventing the stereoscope (Fig. 1.10a; Wheatstone, 1838). Obtaining a convincing proof of stereopsis is difficult because it requires to manipulate specifically binocular disparity without altering any other depth cue, by using some form of dichoptic viewing to display independent images to each eye, like in Wheatstone’s original stereoscope.

A major advance in stereopsis research has been enabled by the dichoptic presentation of random dot stereograms (RDS), already known in 1919 and successfully developed for binocular vision research by Béla Julesz (Julesz, 1960, 1971). These stimuli consist of a pair of images, one for each eye, made up of a set of black and white dots (Fig. 1.10b). The position and contrast of the dots are randomly assigned to generate the image for one eye; the image for the other eye is generated by copying the first image, with the dots located within a given region being displaced by a certain horizontal offset, i.e. introducing a binocular disparity. Importantly, RDS are a powerful form of cyclopean stimulation: each monocular image looks homogeneous and unstructured, without any distinctive feature. Only when fusing the left and right images via dichoptic viewing (i.e. by displaying the left and right image independently to each eye, for example by means of a stereoscope), the given region emerges from the noise, appearing to pop out or recede behind, depending on whether the binocular disparity is crossed or uncrossed, respectively.

By using RDS, not less than 130 years after Wheatstone’s discovery in humans, stereopsis could be first demonstrated in a non-human species. Macaque monkeys were able to discriminate between RDS of distinct binocular disparities, which produced distinct stereoscopic depth percepts (Bough, 1970). Not many species have been conclusively demonstrated to use stereopsis: monkeys (Bough, 1970), cats (Packwood and Gordon, 1975; Ptito et al., 1991), horses (Timney and Keil, 1999), owls (van der Willigen, 2011), falcons (Fox et al., 1977), toads (Collett, 1977) and praying mantises (Rossel, 1983; Nityananda et al., 2016, 2018). A demonstration of stereopsis in the mouse is still missing.

1.3.3 Neuronal mechanisms underlying stereopsis: binocular disparity processing

The first electrophysiological evidence of a neuronal substrate for stereopsis was provided by pioneering recordings in the anesthetized cat (Barlow et al., 1967; Pettigrew et al., 1968). When dichoptically presented with bars and edges, most individual neurons in V1 responded best within a specific range of retinal disparities, i.e. these neurons were disparity-tuned, with differ-

jumped out. But to me, it was just part of the background». Bruce Bridgeman, formerly stereoblind (<http://www.bbc.com/future/story/20120719-awoken-from-a-2d-world>)

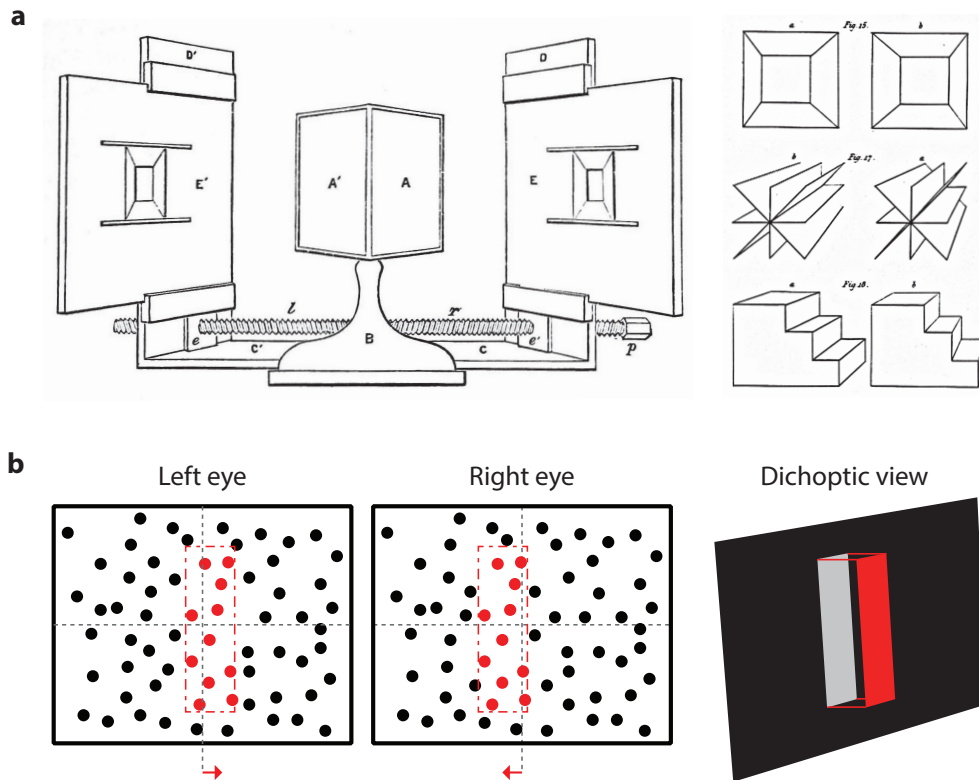
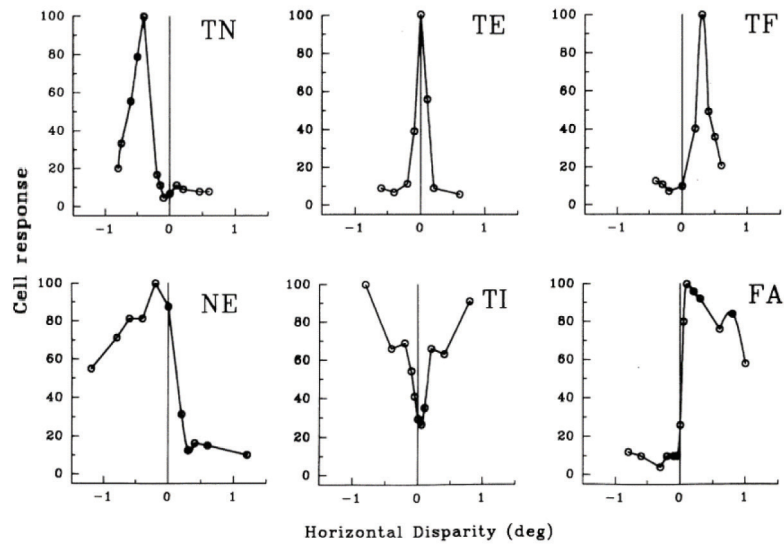


Figure 1.10 | Demonstrating stereopsis requires dichoptic presentation of stimuli. **a** | First stereoscope for dichoptic presentation of stimuli by Sir Charles Wheatstone (Wheatstone, 1838). Left, the apparatus consists of two mirrors at right angle (A, A') and two picture holders (D, D'). Right, three of the twenty pairs of pictures (stereograms) that Wheatstone used to demonstrate stereopsis. Reprinted with permission from Wheatstone (1838). **b** | Random dot stereograms (RDS). Left and middle panels, the basic construction of a RDS consists of generating a random pattern of dots to be viewed by one eye. The stimulus pattern for the other eye is generated by copying the first image, while introducing a binocular disparity by horizontally displacing a given region (red rectangles and arrows). The gap created by displacing the given region is filled with random dots. Right panel, when left and right images are viewed simultaneously but independently by the two eyes, by e.g. using a stereoscope, the dots within the displaced region appear to lie on a distinct depth plane from the other dots, depending on the binocular disparity. The schematic illustrates the simulated effect of binocular fusion of images with crossed binocular disparity as shown in the left and middle panels.

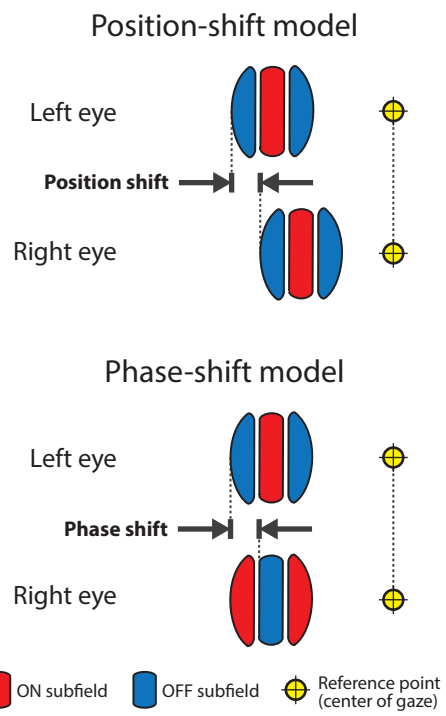
ent neurons tuned to different disparities. The high prevalence of disparity-tuned neurons was then confirmed in V1 as well as in extrastriate areas of the awake rhesus monkey (Poggio and Fischer, 1977; Poggio et al., 1988), paving the way to an intense investigation of the neurophysiology of disparity processing in this species (Gonzalez and Perez, 1998).

a

Disparity Tuning Functions of Cortical Visual Cells



b



c

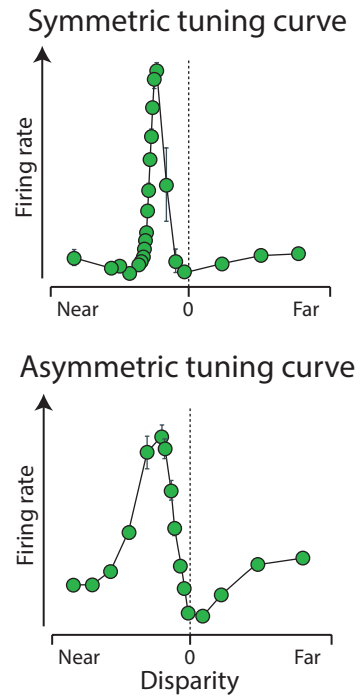


Figure 1.11 | **Tuning curves and possible mechanisms for binocular disparity.** **a** | Examples of tuning curves for binocular disparity, in which the firing rate of cortical neurons is plotted as a function of horizontal disparity. Tuned excitatory (TE) cells are activated over a narrow range of disparities centered around zero disparity, thereby encoding disparities at the horopter. Tuned near (TN) and tuned far (TF) cells have similarly shaped tuning curves as TE cells, but their response peaks at negative (crossed) and positive (uncrossed) disparities, respectively, thereby encoding disparities in front of or behind the horopter. Near (NE) and far (FA) cells, with tuning curves reciprocal to each other, are activated over a wide range of negative and positive disparities, respectively, and are suppressed by the opposite disparity. Tuned inhibitory (TI) cells are activated over most disparities but suppressed over a narrow range of disparities. Reprinted with permission, original data from Poggio et al. (1988) and redrawn from Gonzalez and Perez (1998). The tuning curves were measured in the awake macaque monkey using bar stimuli and plotted against normalized cell response. **b** | Two models for the generation of disparity selectivity in simple cells. For each model, the left eye and right eye RFs of a simple cell are depicted. ON subregions are in red, OFF subregions are in cyan. A reference point (yellow dot), e.g. the fovea in humans, is drawn to indicate the relative alignment of left and right RFs of the simple cell. Top, in the position-shift model, the left and right eye RFs have identical arrangements of ON and OFF subregions, but their relative position is spatially shifted. Bottom, in the phase-shift model, the left and right RFs are overall spatially aligned, but the arrangement of their ON and OFF subregions is swapped. **c** | Top, example of a symmetric (even-symmetric) tuning curve for binocular disparity, as predicted by the position shift model. Bottom, example of an asymmetric (odd-symmetric) tuning curve, as predicted by the phase-shift model.

1.3.3.1 Disparity tuning curves and underlying receptive field mechanisms

The tuning curves of disparity-tuned neurons exhibit a spectrum of shapes, describing different categories of disparity selectivity (Fig. 1.11a). For example, a cell whose tuning curve has a positive peak over a narrow range of negative disparities is called ‘tuned near’, as it encodes disparities produced by objects located closer than the fixation point (Fig. 1.11a, marked ‘TN’). As another example, a ‘tuned inhibitory’ cell displays a negative peak at near zero disparities, where its response is suppressed (Fig. 1.11a, marked ‘TI’).

How can a binocular neuron extract disparity information? What determines the shape of a neuron’s tuning curve? Two possible mechanisms have been put forward to explain the disparity selectivity of simple cells in the visual cortex (Qian, 1997; Cumming and DeAngelis, 2001; Westheimer, 2009). (1) In the position-shift model, the disparity tuning of a neuron arises from a spatial offset in the RF position between left and right eye, with the RF of each eye having the same spatial arrangement of ON and OFF subfields (Fig. 1.11b).

(2) Alternatively, the phase-shift model proposes that a disparity-tuned neuron has left and right eye RFs in the same retinal position, but with different subfield structures (Fig. 1.11b).

The position-shift mechanism produces a symmetric tuning curve for disparity, whereas the phase-shift mechanism produces an asymmetric (or odd-symmetric) tuning curve (Fig. 1.11c). Each of the two mechanisms appears to contribute to the disparity selectivity of individual simple cells, with a combination of the two mechanisms occurring for most cells (Tsao et al., 2003; Haefner and Cumming, 2008).

1.3.3.2 Role of disparity-tuned neurons in stereoscopic perception

Beyond V_1 , disparity-tuned neurons show a closer link to the perceptual qualities of stereopsis, including choice-related information about depth discrimination. For example, during a visual task in which a monkey is required

to decide whether an RDS stimulus is closer or farther than the fixation point, neurons can not only specifically respond to either disparity (near or far) of the stimulus according to their selectivity, but increase their firing in relation to the decision in the task. As such, the activity of these neurons allows predicting the behavioral output during the task, indicating a close correlation to perception (Parker, 2007; Parker et al., 2016). Most importantly, a causal relationship between disparity selective neurons in extrastriate areas and perception of stereoscopic depth has been established by using targeted intervention with electrical microstimulation (Krug et al., 2013; Krug et al., 2016; Parker et al., 2016). For example, in a classic study, a focal electrical stimulation was targeted to the monkey higher visual area MT, in which neurons are clustered according to their disparity preference (DeAngelis et al., 1998). During a near-far discrimination task, microstimulation shifted the perceptual judgments towards the disparity preference of the locally stimulated neurons.

Binocular disparity processing has proven to be a fruitful model for deciphering the neural basis of visual perception (Roe et al., 2007). It is a quite complex problem and yet well-defined and addressable in multiple species with a combination of electrophysiological, psychophysical and computational approaches. Furthermore, unlike the computation of stimulus motion that already occurs in the retina, the binocular (cyclopean) nature of stereopsis implies that its processing is largely, if not entirely, performed within the neocortex, thereby offering an ideal substrate for investigating cortical computation.

1.3.4 Stereopsis and binocular disparity processing in the mouse

Binocular disparity processing has been intensely investigated in cats and especially in primates (including humans), such that we have achieved a good understanding of both the psychophysics and the neuronal mechanisms of stereopsis in these species. However, much less is known about binocular disparity processing and stereopsis in other mammalian species (Nityananda and Read, 2017), including the mouse.

1.3.4.1 Behavioral evidence for binocular depth perception

Mice are amenable to a repertoire of powerful experimental tools, and they have become the most widely used model system for vision research in the last decade (Huberman and Niell, 2011; Luo et al., 2018). However, depth perception in this species has been largely neglected so far. Although the mouse has undoubtedly some form of depth discrimination, investigations on its behavioral significance and quantitative assessments of the contribution of specific depth cues, including binocular disparity, are lacking.

In an early report addressing their ability to evaluate distance, mice were placed on a disk platform at various elevations above a table (Fig. 1.12a) (Vaughn, 1910). The time to jump down decreased as a function of the platform's elevation, indicating that mice used visual cues to estimate the distance to the table to decide whether to jump down or not. Later, Fox (1965) introduced the so-called visual cliff test to assess depth perception in mice (Fig. 1.12b). The test apparatus consisted of a glass surface with a ridge separating a "shallow" (safe) side and a "cliff" (unsafe) side, with a checkerboard

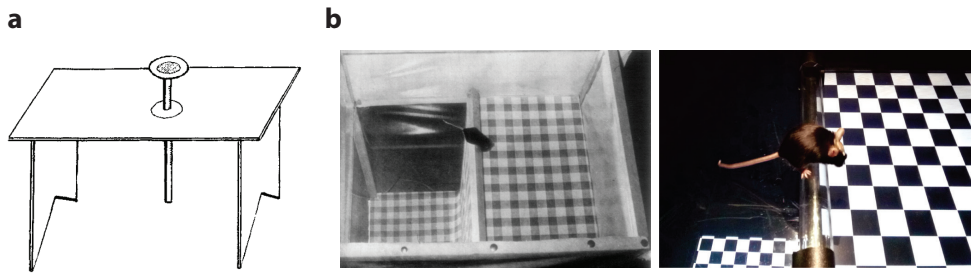


Figure 1.12 | Behavioral assessment of visual depth perception in mice. **a** | Original drawing from [Waugh \(1910\)](#) of the apparatus for studying mouse depth perception. A wooden disk 10 cm in diameter is raised at a certain height over a table, ranging between 4 and 18 cm. A mouse is placed on the disk and allowed to jump down. The time to jump down is taken as a measure of the mouse's ability to perceive depth. Animals took more time to jump down with the disk at higher elevations. Reprinted with permission from [Waugh \(1910\)](#). **b** | The visual cliff test as adapted by [Fox \(1965\)](#) for testing depth perception in mice. Left, original photo from [Fox \(1965\)](#) showing a mouse on the central ridge of the chamber. A positive choice is recorded if the animal steps on the "shallow" side on the right. On the left is the "cliff" side, where the chequered linoleum is placed 2 feet (61 cm) below the glass sheet. Reprinted with permission from [Fox \(1965\)](#). Right, a more recent implementation of the visual cliff test built in our lab. The checkerboard pattern is displayed on each of the two sides on a computer monitor, allowing to control, independently on each side, stimulus parameters like brightness, contrast, and size of the checkerboard.

floor immediately below or at a certain depth (e.g. 60 cm) beneath the glass. Mice, initially placed on the ridge, are free to step down to either side, and the number of safe choices along with decision time is recorded. Several studies used this test to show that mice are able to visually assess depth, as evidenced by a clear preference for the shallow side and avoidance of the cliff.

Nonetheless, the visual cliff test has been mostly used as a generic visual acuity test for mice rather than specifically addressing how depth perception in this species works. Indeed, this test is actually not very suitable for this purpose, because it does not allow the experimenter to precisely control the different visual cues and, particularly, to specifically manipulate binocular disparities. Two studies, though, used the visual cliff test to gain insight into the role of binocular vision for distance judgment, by testing mice with one eye occluded. Compared to binocular mice, the performance of monocular mice was significantly impaired, but still above chance level ([Mazziotti et al., 2017](#); see also [Leamey et al., 2007](#)). This finding indicates that mice exploit monocular visual cues, e.g. perspective and relative size, to assess depth in this task, and that the discrimination is facilitated when using both eyes. On the other hand, this evidence, albeit compatible, does not provide a direct demonstration that binocular disparity was used for perceiving depth. It is plausible, for example, that distance judgment relied exclusively on monocular cues and that that binocular vision simply improved detection sensitivity without stereopsis. In fact, [Leamey et al. \(2007\)](#) reported that the lower performance of monocular mice could be explained by accounting for the times the animals approached the cliff side using the open versus the occluded eye, indicating that any direct connection of mouse performance in this task to binocularity is at stake and highlighting the inadequacy of the visual cliff test to study stereopsis in mice.

Another insight into role of mouse binocular vision comes from recent experiments on prey-capture behavior and object exploration in mice ([Hoy et al., 2016](#); [Park et al., 2018](#)). [Hoy et al. \(2016\)](#) demonstrated that mice ex-

hibit robust prey capture behavior towards crickets, and that vision plays a crucial role for accurate long-range approach. Interestingly, after the detection of a cricket, it seems that mice first orient their head and body toward it, bringing the target from a more peripheral to a more central position within its visual field, and only after a short delay (~ 0.5 sec) initiate locomotion for approaching (Hoy et al., 2016). Park et al. (2018) investigated the circuitry underlying prey capture behavior to find that the optogenetic activation of specific projections from the medial preoptic area in the hypothalamus to the ventral periaqueductal gray in the midbrain induced strong chasing behavior toward prey and objects. Interestingly, by positioning an object at various locations within the visual field, it was found that the chasing behavior was reliably triggered only when the object was located within ± 15 deg from the vertical meridian. The findings of these two studies thus suggest that binocular vision may play an important role for robust chasing actions towards a target.

Therefore, further psychophysical experiments analyzing mouse depth perception are needed to determine the contributions of each of the monocular cues and, in particular, of binocular disparity.

1.3.4.2 *Neurophysiological evidence for binocular depth perception*

Neurophysiological experiments have revealed that the mouse visual system does contain the neuronal substrate required for stereopsis. Indeed, studies by Scholl et al. (2013; 2015) showed that the binocular region of mouse V1 contains a substantial fraction ($\sim 1/3$) of neurons sensitive to binocular disparities. In addition, it was found that disparity-tuned neurons in mouse V1 had overall similar tuning properties compared with those in cats (Scholl et al., 2013a). This suggests that the integration of eye signals underlying disparity selectivity and hence stereopsis relies on a computational logic common to all mammals (and probably, phyla; see also Nityananda and Read, 2017).

However, binocular disparity processing is still rarely studied in the mouse, as compared with cats and primates. For example, it is unknown whether neurons in higher areas of the mouse visual cortex integrate binocular inputs, and whether they encode binocular disparity. In primates, disparity is differentially distributed across higher visual cortical areas (Gonzalez and Perez, 1998; Parker, 2007). If binocular disparity is processed in multiple visual cortical areas in the mouse, it will be important to determine whether specialized representations exist in these areas. Comparison of binocular integration and disparity tuning across different mouse visual areas might help delineating their functional specializations, which are still largely unclear.

Therefore, I characterized binocular disparity in V1 and in two higher visual areas, LM and RL, which have a substantial retinotopic representation of the binocular field of view (Garrett et al., 2014; Zhuang et al., 2017). Visual areas were first identified with intrinsic signal imaging, using the established retinotopic organization of these areas. To record the activity of single neurons in the selected regions, I then performed two-photon imaging using the genetically encoded calcium indicator GCaMP6s.

Disparity tuning properties were measured by dichoptic presentation of oriented gratings at varying interocular phases as well as random dot stere-

ograms, which have not been used in the mouse before. With grating stimuli, I observed that across these areas most neurons were modulated by binocular disparity. Integration of binocular stimuli led to strong response facilitation at the cell's preferred disparity, and strong suppression at other disparities, even in neurons classified as monocular by conventional ocular dominance measurements.

Although disparity processing is highly distributed across neurons in areas V1, LM, and RL, the use of random dot stereograms revealed clear differences in preferred disparities: area RL contains a higher fraction of neurons tuned to near disparities compared to V1 and LM, indicating that RL is specialized for encoding nearby visual objects. Tuning for near disparities in RL was confirmed using oriented gratings for stimulation, and was also observed in the awake animal. Since recent data show that RL also contains many neurons responsive to whisker stimulation, I speculate that this area might contain a multimodal representation of the space immediately in front of the mouse.

1.4 *in vivo* TWO-PHOTON CALCIUM IMAGING

A major challenge in neuroscience is deciphering the principles of signal processing in the mammalian neocortex. A fundamental step toward this goal is mapping the activity of large numbers of neurons with high spatial and temporal resolution in the intact brain. Electrophysiological recordings have long been the “gold standard” for measuring neuronal activity of individual cells. However, they can typically sample a small number of neurons only. Multi-electrode extracellular recordings allow sampling hundreds of neurons simultaneously, but they lack spatial information and the possibility of distinguishing specific cell types (Jun et al., 2017). In addition, with electrophysiology it has been hardly possible to monitor the activity of the same cells over long periods (weeks). Over the past two decades, parallel progress in two-photon microscopy and fluorescence activity reporters have opened new powerful opportunities to study the functional organization of neuronal networks (Helmchen and Denk, 2005; Wilt et al., 2009; Grienberger and Konnerth, 2012; Lin and Schnitzer, 2016; Yang and Yuste, 2017).

PRINCIPLES OF TWO-PHOTON EXCITATION The essence of two-photon microscopy is the nonlinear process of two-photon excitation used to excite a fluorophore. In conventional fluorescence microscopy, the fluorophore is excited through the absorption of one photon, often in the ultraviolet/green spectrum, which has an energy equaling the energy gap between the electronic ground state and the excited state. However, the same excited state can be reached by near-simultaneous absorption of two photons (within ~0.5 fs) of about half the energy and, hence, of double the wavelengths (typically deep red to near infrared). Two-photon excitation is not a linear process, such that its probability is the product of the probability of each independent event of single photon absorption. Because each absorption event is proportional to the light intensity, two-photon excitation is a quadratic function of light intensity. Since in a focused light beam the intensity is maximum at the focus and declines with $1/z^2$, where z is the axial distance from the focus, fluorophores are excited exclusively in proximity of the focal point and

out-of-focus excitation is drastically minimized (Denk et al., 1990; Helmchen and Denk, 2005). Conversely, in confocal microscopy the one-photon absorption results in a cone of excitation whereby also out-of-focus fluorophores are excited.

These intrinsic characteristics of two-photon excitation confer to this microscopy technique crucial advantages that enable a nearly non-invasive analysis of neuronal activity in the intact brain *in vivo* with unprecedented detail. The light spectrum commonly used for two-photon excitation are in the near infrared range (800-1000 nm) which are less sensitive to scattering and less absorbed by endogenous chromophores. Given that the brain is a highly non-transparent, scattering medium, the use of longer wavelengths dramatically improves penetration depth in the tissue, while minimizing photo-induced toxicity. In addition, the excitation photons that are scattered by brain tissue can hardly contribute to out-of-focus signal, because they are too diluted for two-photon excitation. Crucially, it also follows that, because two-photon excitation is spatially highly confined, all emitted photons, both ballistic and scattered, constitute useful signal. Consequently, unlike in confocal microscopy, all the emitted light collected by the microscope objective is directly guided to the photo-detector without a pinhole, in a so-called non-descanned configuration, thereby incrementing signal-to-noise ratio of the emitted signal (Helmchen and Denk, 2005).

TWO-PHOTON MICROSCOPE Although the concept of two-photon excitation was first described in the 1931 (Göppert-Mayer, 1931), and the first experimental observations were done in the 1960s (Peticolas et al., 1963), two-photon imaging has been introduced in neuroscience laboratories only from the 1990s onwards, owing to the need of a nonstandard, optical apparatus (Denk et al., 1990; Denk and Svoboda, 1997). Indeed, for efficient two-photon absorption, a high density of photons at the focal point is required. This can be achieved by using a mode-locked, pulsed laser (commonly a Titanium:sapphire laser) that, instead of emitting a continuous flow of photons, concentrates photon emissions in very short pulses (pulse duration ~100 fs, repetition rate ~80 MHz) of high peak intensity while keeping a low average power (Helmchen and Denk, 2005).

The optical set-up of the two-photon microscope utilized for the experimental work of this Thesis is schematized in Figure 1.13. The pulsed laser beam output from the light source is first modulated in power. Then, the laser beam is directed onto a pair of fast scanning mirrors that deflect the beam along two dimensions for raster scanning of the laser focus in one focal plane within the tissue. After the scanning mirrors, the scan and tube lens form a telescope and expand the cross-section of the beam to match the back aperture of the objective. The emitted fluorescence signal from the tissue is collected by the microscope objective, which is a low-magnification, high numerical aperture one (16×, 0.8 NA) to maximize signal-to-noise ratio. The collected light is split into a separate green and red channel by a dichroic mirror and directed onto two photomultiplier tubes, which finally detect the fluorescence photons.

CALCIUM SIGNALING IN NEURONS In combination with technological advances in two-photon microscopy, development of fluorescence reporters have played a central role for allowing reliable monitoring of neuronal ac-

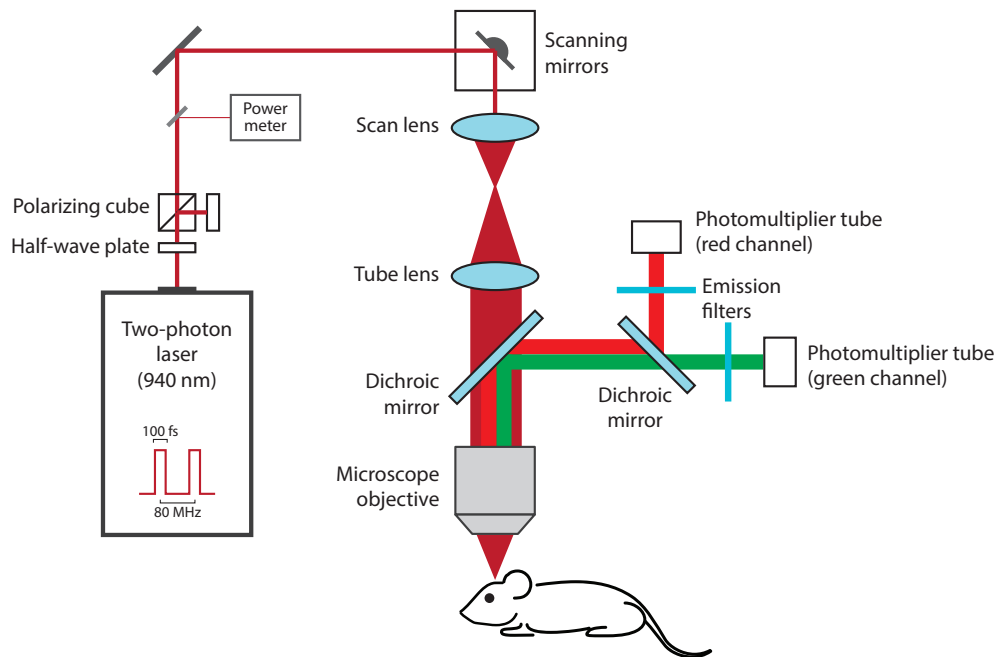


Figure 1.13 | Basic optical design of a two-photon laser scanning microscope. The schematic illustrates the optical set-up of the two-photon microscope used for *in vivo* calcium imaging. The light source is a Titanium:sapphire laser emitting photons at high-density, in ultrashort pulses (100 fs duration), with a repetition rate of 80 MHz. The wavelength can be tuned over a wide range in the red/near infrared spectrum (670–1040 nm). For exciting the calcium indicator GCaMP6, the wavelength is set to 940 nm. The intensity of the laser beam is first adjusted by means of a half-wave plate combined with a polarizing beam splitter cube. The laser beam is then directed onto pair of scanning mirrors, consisting of a resonant mirror oscillating at 8 kHz and a galvanometric mirror. The combination of scan and tube lens forms a telescope that expands the laser beam to fill the back aperture of the microscope objective. The objective focuses the excitation light into the brain tissue for two-photon excitation of the calcium indicator. Fluorescence light emitted by the fluorophores is collected by the objective and reflected by a dichroic mirror into the detection path. Another dichroic mirror splits the fluorescence light into a green and a red channel toward the photomultiplier tubes. The green channel contains the fluorescence signal emitted by GCaMP6, while the red channel contains the fluorescence signal emitted by a red fluorescent protein (e.g. mRuby2, used in Part 2 of the Thesis). The mouse is fixed under the microscope objective using a small head-post. For experiments under anesthesia, the mouse is placed on a heating pad to maintain body temperature. For experiments in awake animals, the mouse is free to run on a spherical treadmill while being head-fixed under the objective.

tivity. In neurons, synaptic input and action potential firing produce a brief rise in intracellular calcium, with increments of 10–100 times from a resting state of about 50–100 nM. These transient calcium increases, also referred to as “calcium transients”, typically show a sharp rise followed by a return to baseline by an exponential decay (with a time constant of ~0.5–1 sec). The calcium concentration increase during electrical activity mainly originates from calcium influx from the extracellular space mediated by voltage-gated calcium channels, ionotropic glutamate receptors, nicotinic acetylcholine receptors, and other mechanisms. The return to baseline level is mediated by calcium extrusion mechanisms, including calcium ATPases and sodium-calcium exchangers, and by intracellular molecules acting as calcium buffers (Grienberger and Konnerth, 2012).

CALCIUM INDICATORS Visualizing the dynamic changes of calcium activity requires reporter molecules, called calcium indicators, that modify their fluorescence or absorbance properties upon binding calcium. The fluorescence time course of calcium indicators depend on their calcium binding affinity, kinetic properties, dynamic range, and brightness. Until the last decade, the most widely used calcium indicators were synthetic small molecules derived from calcium chelators, such as Oregon Green BAPTA. Although synthetic indicators generally offer good fluorescence specifications, labeling of genetically defined neuronal populations is difficult and long-term, repeated measurements are hardly possible (Grienberger and Konnerth, 2012). These limitations have been largely overcome by the recent development of genetically encoded calcium indicators (GECIs), so called because these molecules are proteins encoded by a DNA sequence and directly expressed in neurons (Tian et al., 2012; Lin and Schnitzer, 2016). The most important class of GECIs is GCaMP. In these proteins, a modified version of the green fluorescent protein (a circularly permuted GFP) is fused with the calcium-binding protein Calmodulin (CaM) and with the CaM-interacting domain M13 (myosin light chain kinase). Upon calcium binding by CaM, the interaction CaM-M13 induces a conformational rearrangement of the GFP part, which in turn increases its fluorescence emission. Importantly, the most recently developed family of GCaMP6 (Chen et al., 2013b) offers, for the first time among GECIs, better sensitivity and kinetic specifications than synthetic indicators. Meanwhile, intense ongoing efforts will soon provide improved GECIs and expand this already powerful toolkit.

IN VIVO IMAGING WITH GECIS Another major advantage of GECIs is that their expression remains stable over several weeks or months, permitting to perform chronic recordings – of the same or different neurons – multiple times in the same animal. This enables a higher yield of neurons and the possibility of chronic monitoring of the same individual cells over long periods of time for studying stability and plasticity of their functional properties. The expression of the GECIs in the mouse brain can be obtained by direct gene transfer through *in utero* electroporation, by gene transfer through viral transduction, or by the generation of transgenic animals. Various levels of expression specificity can be achieved by using cell-type-specific or activity-dependent promoters, Cre-dependent systems and targeting sequences, allowing the labeling of genetically defined neuronal types or even of sub-cellular compartments (Grienberger and Konnerth, 2012; Luo et al., 2018).

Currently, a common approach (also used in this Thesis) is the expression of GCaMP6 under the control of a generic neuronal promoter (human synapsin promoter) induced via adeno-associated viruses (AAV), which are targeted to specific brain areas by means of stereotaxic injections (Chen et al., 2013b). The procedure for chronic imaging usually consists of the implantation of a small cranial window for optical access to the brain: a small piece of the skull (e.g. 4 mm) is surgically removed, viral vectors are injected to induce expression of the GECIs, and a permanent glass window is implanted. A small head-post is also implanted for fixing the mouse head under the microscope objective (Holtmaat et al., 2009; Goldey et al., 2014). After a few weeks of gene expression (e.g. 2-4 weeks), two-photon imaging allows large-scale activity measurements of hundreds of neurons simultaneously with high signal-to-noise ratio and sensitivity, within fields of view spanning a few hundred micrometers and at cortical depths up to several hundred micrometers.

In conclusion, two-photon microscopy in combination with genetically encoded fluorescent indicators of neuronal activity has transformed neuroscience research, allowing to monitor, with unprecedented spatial resolution, large brain networks of hundreds of neurons while they process information and perform computations.

2

MATERIALS AND METHODS

2.1 ETHICS

All experimental procedures were carried out in accordance with the institutional guidelines of the Max Planck Society and the local government (Regierung von Oberbayern).

2.2 VIRUS INJECTION AND CRANIAL WINDOW IMPLANTATION

For experiments on direction selectivity, cranial window implantations were performed on 8 female adult C57/BL6 mice (10–13 weeks of age at the start of the experiment). Mice were anesthetized by intraperitoneal injection of a mixture of Fentanyl (0.075 mg/kg), Midazolam (7.5 mg/kg), and Medetomidine (0.75 mg/kg). A general analgesic (Carprofen, 4 mg/kg, subcutaneous injection) was administered immediately before surgery and during post-surgical recovery. After an initial skin incision, a local analgesic (Lidocaine 10%) was topically applied. A circular craniotomy (4 mm diameter) was performed with a dentist drill, centered over the binocular region of the primary visual cortex in the right hemisphere (stereotaxic coordinates of the craniotomy center, relative to lambda: anterior, 1 mm; lateral, 3 mm).

The exogenous expression of the genetically encoded calcium indicator GCaMP6s was induced by viral gene transfer using adeno-associated viral vectors (AAV), carrying the sequence for GCaMP6s under the human synapsin promoter (Chen et al., 2013b). This resulted in a dense labeling of both excitatory and inhibitory neurons with GCaMP6s that, in combination with its high signal-to-noise ratio, enabled recordings of large numbers of neurons (~300 per imaging plane) with high sensitivity. In addition, the stable expression of the indicator over long periods of time (weeks to months) allowed performing recordings multiple times in the same animal and hence increasing the yield of cells.

Viral vectors were injected into V₁, approximately in the binocular region, and consisted of either AAV2/1.hSyn.GCaMP6s.WPRE.SV40 or AAV2/1.Syn.mRuby2.GSG.P2A.GCaMP6s.WPRE.SV40, diluted to reach a final titer of $1-1.5 \times 10^{13}$ genome copies/mL. The virus mixture was injected using glass pipettes and a pressure micro-injection system at 2-4 separate sites, each 200-450 μ m below the cortical surface (100-200 nL/injection, ~20 nL/min pressure injected at 0.25 Hz). After injections, the craniotomy was sealed flush with the brain surface using a glass cover slip (4 mm diameter) and cyanoacrylate glue (Histoacryl), without letting the glue contact the brain. A custom machined aluminum head-plate was attached to the skull using dental cement to allow head-fixation of the animal during imaging recordings. Expression of the transgene was allowed for 2.5–3 weeks before

imaging. For further details on single procedures, see also (Weiler et al., 2018).

For experiments on binocular disparity, cranial window implantations were performed on 13 female adult C57/BL6 mice (10–12 weeks of age), with procedures similar as described above, with minor changes. After skin incision and skull exposure, intrinsic optical imaging was performed through the skull to locate the binocular region of V₁. This facilitated the centering of the craniotomy (5 mm) and enhanced the accuracy and reproducibility of the targeted virus injections. Virus injections were performed at 3–5 separate sites into the binocular region of V₁ and ~0.5–1 μm more lateral (corresponding to the location of areas LM and RL), using AAV2/1.Syn.mRuby2.GSG.P2A.GCaMP6s.WPRE.SV4, diluted to reach a final titer of $\sim 1.5 \times 10^{13}$ genome copies/mL (100–150 nL/injection).

2.3 INTRINSIC SIGNAL IMAGING

Intrinsic signal imaging (Bonhoeffer and Grinvald, 1991; Bonhoeffer and Hübener, 2016) was used to localize the binocular region of the primary visual cortex for experiments on direction selectivity, and to localize areas V₁, LM, and RL for experiments on binocular disparity. Imaging was performed 2–4 weeks after cranial window implantation, under anesthesia by intraperitoneal injection of a mixture of Fentanyl (0.030 mg/kg), Midazolam (3.0 mg/kg), and Medetomidine (0.30 mg/kg). The surface of the brain was illuminated through the cranial window with red light from two sides using a 735-nm LED (bandpass filtered at 700/40 nm). Intrinsic signals were monitored as decreases in reflected light due to cortical activation in response to visual stimulation.

Images were collected through a 4× air objective (NA 0.28, Nikon) using a CCD camera (Teledyne Dalsa Xcelera-LVDS PX4; 12 bit; 512 × 512 pixels; 15 Hz; spatial binning, 3 × 3 pixels; temporal binning, 3 frames). The imaging plane was set 400–500 μm below the cortical surface. In addition, an image of the cortical surface was acquired by using green light from a 530-nm LED to visualize the blood vessel pattern, which was used as a reference to target two-photon imaging. Acquisition and analysis software were custom written in Matlab.

2.4 *in vivo* TWO-PHOTON IMAGING

Two-photon imaging was performed on mice (13–35 weeks of age) under anesthesia. Mice were initially anesthetized by intraperitoneal injection of a mixture of Fentanyl (0.030 mg/kg), Midazolam (3.0 mg/kg), and Medetomidine (0.30 mg/kg). Additional anesthetic mixture (25% of the induction level) was injected subcutaneously 60 min after the initial injection and then every 40 min to maintain anesthesia. Mice were placed on a heated blanket to ensure thermal homeostasis and fixed through the head-plate under the microscope.

Images were acquired using a custom-built two-photon microscope equipped with an 8 kHz resonant galvanometer scanner operated in bidirectional mode, resulting in frame rates of 17.6 Hz at an image resolution of 750 × 900 pix-

els ($330 \times 420 \mu\text{m}$). The illumination source was a Ti:Sapphire laser with a DeepSee pre-chirp unit (Spectra Physics MaiTai eHP, <100 fs pulse width, 80 MHz repetition rate). The excitation wavelength was set to 930 nm for GCaMP6s alone, or to 940 nm for co-expression of GCaMP6s with mRuby2. Laser power was modulated with a half-wave plate combined with a polarizing beam splitter cube, and was between 8–25 mW for all imaging experiments as measured after the objective ($16\times$, 0.8 NA, Nikon) with a photodiode. A mechanical blanker was positioned in the focal plane between the scan and tube lenses to block the laser beam at the scan turnaround points, where the beam moves slowly and hence would result in higher laser exposure of cortical tissue and distortions of images.

Photons collected from the objective passed through a beam splitter (FF560 dichroic) and were directed onto two separate photomultiplier tubes (PMT, Hamamatsu R6357) with a green (525/50–25 nm) and red (607/70–25 nm) band pass emission filter.

Data were acquired with a high-speed digitizer (NI-5761, National Instruments, 500 MHz) in combination with a field-programmable gate array (FPGA) to bin the PMT signal into pixels.

In some cases, for experiments on binocular disparity, mice were repeatedly imaged to increase yield. When a given visual area was targeted for a second time in the same animal, the new imaging plane was acquired at least $20 \mu\text{m}$ deeper than the previously recorded plane, which could be confidently re-identified using the structural marker mRuby2, thereby ensuring that there was no double sampling of cells.

Awake imaging was performed as described elsewhere (Dombeck et al., 2007). The animal was head-fixed on top of an air suspended Styrofoam ball (diameter 20 cm), allowing to run freely during stimulus presentation and data acquisition.

2.5 EYE TRACKING

During two-photon imaging, both eyes were continuously imaged with an infrared video camera (The Imaging Source, frame rate 30 Hz). Pupil position and diameter were monitored online using custom-written software (LabVIEW, National Instruments) based on (Sakatani and Isa, 2007). Analysis of pupil position was also performed *post hoc* to test whether either eye had changed position over the course of the experiment.

2.6 VISUAL STIMULATION

2.6.1 Retinotopic mapping with intrinsic signal imaging

To locate the binocular region of V_1 , retinotopic mapping was performed using small patches of drifting gratings (20–30 deg) presented at 8 to 15 different locations on a gray background (eight consecutive directions in a pseudorandom sequence; spatial frequency (SF), 0.04 cpd; temporal frequency (TF), 2 Hz; duration of each stimulus patch, 6 sec; inter-stimulus interval, 3 sec; number of stimulus trials, 3–4). The stimulus monitor (27 inches, Dell SE2717H, gamma corrected, refresh rate of 60 Hz, spatial resolution of 1920

$\times 1080$ pixels) was obliquely placed in the left (contralateral) visual hemifield, approximately 30 deg from the mouse's midline at a distance of 12 cm from the left eye, covering approximately from -20 to $+100$ deg in azimuth and -40 to $+40$ deg in elevation.

2.6.2 Mapping higher visual areas with intrinsic signal imaging

To locate higher areas of mouse visual cortex, retinotopic mapping employing a periodically drifting bar was used for both cardinal axis (Kalatsky and Stryker, 2003; Marshel et al., 2011). The bar consisted of a reversing checkerboard pattern (SF, 0.04 cpd; TF, 2 Hz) and was periodically swept over a gray background at 18–20 deg/sec for 30–45 times for each direction. The bar width was 20 deg, and spherical correction was applied to stimulate in spherical visual coordinates using a flat monitor. The stimulus monitor (27 inches, Dell SE2717H, gamma corrected, refresh rate 60 Hz, spatial resolution 1920×1080 pixels) was obliquely placed in the left (contralateral) visual hemifield, approximately 30 deg from the mouse's midline at a distance of 12 cm from the left eye, covering approximately between -20 to $+100$ deg in azimuth and -40 to $+40$ deg in elevation.

2.6.3 Dichoptic apparatus

The dichoptic apparatus consisted of a haploscope with two separate mirrors and two separate display monitors to enable independent stimulation of each eye (see Fig. 3.1a). Each mirror (silver coated, $25 \times 36 \times 1.05$ mm, custom-made, Thorlabs), mounted on a custom designed, 3D printed plastic holder, was independently positioned at an angle of approximately 30 deg to the longitudinal axis of the mouse, contacting the snout 2–4 mm anterior to the medial palpebral commissure of each eye. A shield made of black paper board and tape was used to prevent stimulus cross-talk between eyes and monitors (see also below). Each mirror redirected the field of view of each eye onto a separate display monitor located on each side of the animal at a distance of 21 cm, with an actual stimulation area subtending 65 deg in elevation and 70 deg in azimuth for each eye (the mirror and its holder occluded a vertical segment of the monitor view of ~ 25 deg). The two 21-inch LCD monitors (gamma corrected, refresh rate of 60 Hz, spatial resolution of 1600×900 pixels) were mounted on custom machined metal holders that allowed flexible and reproducible positioning of each monitor independently. To minimize light contamination of data images from visual stimulation, the LED backlight of the monitors were flickered at 16 kHz such that they were synchronized to the line clock of the resonant scanner (Leinweber et al., 2014). As a result, the LED backlight was only active during the turnaround intervals of the scan phase, which were not used for image generation (mean luminance with 16 kHz flickering: white, 5.2 cd/m^2 ; black 0.01 cd/m^2).

For dichoptic stimulation, it is crucial that visual stimuli directed to one eye do not reach the other eye. To verify the lack of cross-talk between the two stimulus monitors and eyes, a series of controls were performed. (1) With the dichoptic apparatus in place but without the animal, a photometer was located at the position of one eye. No luminance increase could be detected upon presentation of visual stimuli on the monitor dedicated to the other eye. (2) The videos used for pupil tracking were used for a

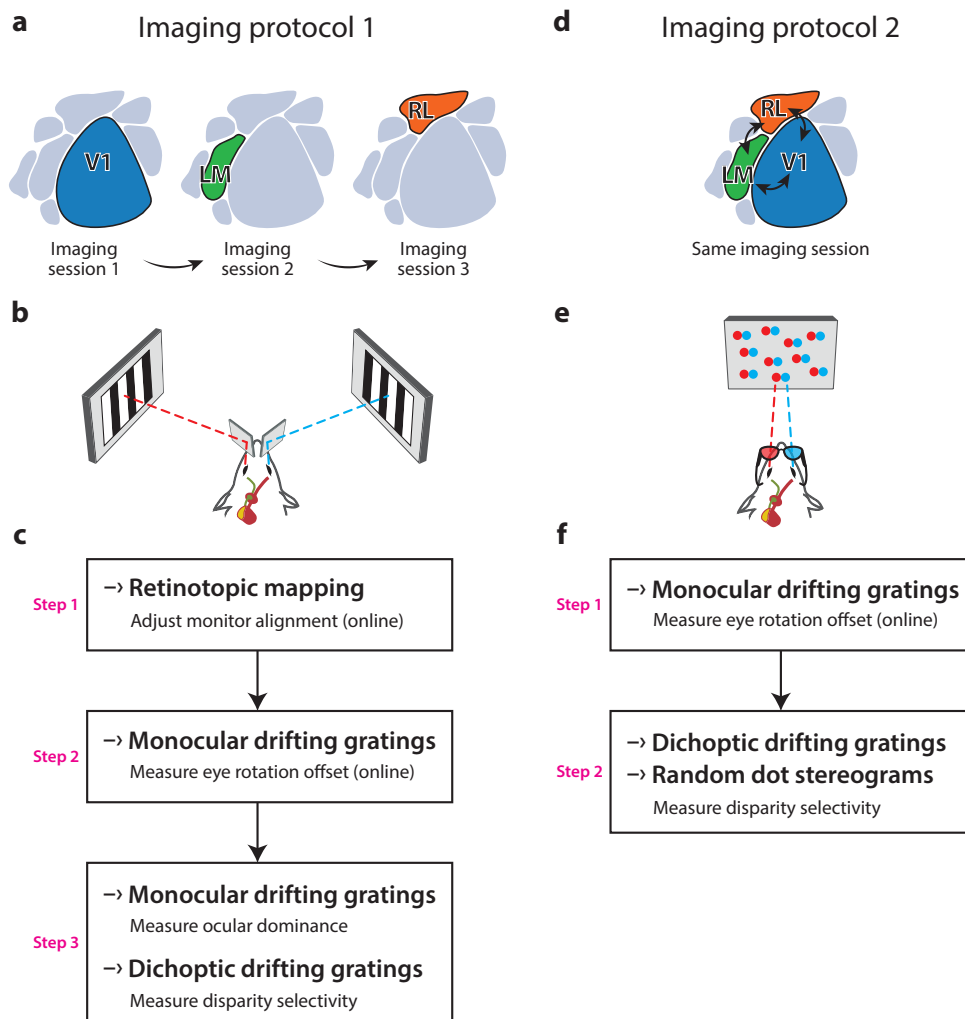


Figure 2.1 | The two imaging protocols adopted for two independent sets of experiments on binocular disparity. (a–c) Imaging protocol 1. **a** | Areas V1, LM, and RL are imaged in separate experiments, one area in each imaging session. **b** | Dichoptic presentation of stimuli is obtained using haploscope mirrors and two eye-specific computer monitors. **c** | Sequential steps of stimulus presentations and image recording. (d–f) Imaging protocol 2. **d** | Areas V1, LM, and RL are sequentially imaged during the same imaging session, recording at least one imaging plane in each of the three areas. The sequence of areas was randomly chosen for each imaging session. **e** | Dichoptic presentation of stimuli is achieved using shutter goggles and a single computer monitor. The monitor displays eye-specific frames in an alternate fashion and in temporal synchrony with the shutter goggles. **f** | Sequential steps of stimulus presentations and image recording.

pixel-based time-frequency analysis, which provided a sensitive way for assessing cross-talk. A Fourier transform was computed to extract the frequency components for each pixel. When a drifting grating at a given temporal frequency (e.g. 2 Hz) was presented on only one monitor, many pixels located on the eye directly stimulated by the drifting gratings contained a high power signal of that frequency component. By contrast, no signal at the stimulus frequency was detected for the other eye, suggesting that there was no optical cross-talk during dichoptic stimulation. (3) The ocular dominance distribution of neurons in the visual cortex should provide a sensitive, functional readout of potential light contaminations. If cross-talk was present, a monocular cell in principle driven by only one eye may appear responsive to stimulation to the other eye as well, resulting in ODI distributions overall

biased toward more binocular values. The ODI distributions obtained using the dichoptic apparatus of this study (Fig. 3.12a) were very similar to the ones obtained using conventional eye shutters, as reported in (Rose et al., 2016). Taken together, these indications suggest that the dichoptic stimulation used in this study had no significant cross-talk.

All visual stimuli presented during two-photon imaging were displayed through the dichoptic apparatus. Visual stimuli were generated using custom-written code for Matlab (MathWorks) with the Psychophysics Toolbox (Brainard, 1997; Pelli, 1997; Kleiner et al., 2007), running on a Dell PC (T7300) equipped with a Nvidia Quadro K600 graphics card. A Linux operating system was used to ensure better performance and timing in dual-display mode, as recommended (Kleiner, 2010).

For the experiments reported in Figures 3.17–3.20, eye shutter goggles (3D Vision 2, Nvidia) were used for dichoptic stimulus presentation (imaging protocol 2, Fig. 2.1; see also Fig. 3.17b). The goggles consisted of a pair of liquid crystal shutters, one for each eye, that rapidly (60 Hz) alternate their electro-optical state – i.e. either occluded or transparent to light. In one frame sequence, the left eye shutter is occluded while the right eye shutter is transparent, and vice versa for the next frame, with such alternations in temporal synchrony with the monitor refresh rate (120 Hz). Synchrony between the shutter goggles and the monitor is accomplished with an infra-red, wireless emitter.

The display monitor (Acer GN246HL, 24 inches, 120 Hz refresh rate, spatial resolution 1600×900 pixels) was placed in front of the mouse at a distance of 13 cm from the eyes (luminance measured through the transparent shutter: white, 21.6 cd/m^2 ; black 0.05 cd/m^2). To reduce light contamination of two-photon images from visual stimulation, the microscope objective was shielded using black tape. To generate visual stimuli and control the shutter goggles, custom-written code for Matlab (MathWorks) with the Psychophysics Toolbox (Brainard, 1997; Pelli, 1997; Kleiner et al., 2007) was used, running on a Dell PC (Precision T7500) under Windows 10 and equipped with a Nvidia Quadro K4000 graphics card.

2.6.4 Retinotopic mapping

For experiments on direction selectivity, a first, coarse retinotopic mapping was performed to ensure that the field of view of each eye was roughly redirected to the central region of the display monitors.

Visual stimuli consisted of small patches of drifting gratings presented to each eye, dividing each screen into a grid of 5×4 locations (size 18×15 deg; eight consecutive directions in pseudorandom sequence; SF, 0.04 cpd; TF, 2-3 Hz; duration of each stimulus patch, 3 sec; inter-stimulus interval, 2-3 sec; number of stimulus trials, 2-4; see Fig. 3.2a). Retinotopic maps for each eye were generated immediately after stimulation (see below for details on analysis). If the center of the ensemble receptive field (see below) of one eye was closer than 15 deg to any of the screen's edges, the position of the haploscope mirror of that eye was adjusted and the retinotopic mapping was repeated.

Next, a second, finer retinotopic mapping was performed to obtain a more precise localization of the center of each ensemble RF. Smaller patches of drifting gratings (9×8 deg) were presented to each eye at one of 16-20 loca-

tions centered on each ensemble RF (see Fig. 3.2b). This two-step procedure allowed for a fast yet precise determination of the center of each ensemble RF, which was subsequently used for positioning apparent motion stimuli. In a subset of experiments, RF mapping with sparse noise stimulation (Jones and Palmer, 1987) was performed to obtain the ON/OFF subfield arrangement of individual RFs (see Fig. 4.1c). Black or white squares (8×8 deg) were briefly flashed (duration 0.5 sec; inter-stimulus interval, 0.5 sec) on a gray background at 36 different positions in pseudorandomized sequence, over a grid of 6×6 covering a total of 48×48 deg. The stimulus sequence was repeated 15 times for each eye and square position.

For experiments on binocular disparity, when using the haploscope for dichoptic stimulation (imaging protocol 1, Fig. 2.1), retinotopic mapping was performed to ensure that the field of view of each eye was roughly redirected onto the more central area of the display monitor. Visual stimuli consisted of vertical and horizontal patches of drifting gratings, presented to each eye in 6 vertical (size 16×65 deg, $w \times h$) and 5 horizontal (size 70×13 deg, $w \times h$) locations (eight consecutive directions in pseudorandom sequence; SF, 0.05 cpd; TF, 2 Hz; duration of each stimulus patch, 4 sec; inter-stimulus interval, 2 sec; number of stimulus trials, 2–4). Retinotopic maps for each eye were generated immediately after completing stimulation (see below for details on analysis). If the center of the ensemble receptive field (RF) of one eye was closer than approximately 15 deg from any screen edge, the position of the haploscope mirror of that eye was adjusted and the retinotopic mapping was repeated.

2.6.5 Monocular drifting gratings

For experiments on direction selectivity, to measure the orientation and direction tuning of cortical neurons, as well as their ocular dominance, sinusoidal gratings were presented, to each eye separately, at 8 or 12 equally spaced drifting directions (0–315 or 0–330 deg). Gratings were displayed in full-field and at 100% contrast, at a SF of 0.04 cpd and a TF of 2 Hz. Each stimulus was displayed for 4 sec (8 grating cycles, randomized initial spatial phase) preceded by an inter-stimulus interval of 4 sec with a blank (gray) screen with the same mean luminance as during the stimulus period. During presentation of a grating stimulus on one monitor, the other monitor displayed a blank screen. Grating stimuli were presented in pseudorandomized sequence across drifting directions and eyes, repeating the stimulation block 4–6 times.

For experiments on binocular disparity, monocular drifting gratings were used to estimate a rotation offset between each eye's field of view (see below). Sinusoidal oriented gratings were presented, to each eye separately, similarly as described above, with the only differences being the stimulus parameters used: 12 or 16 equally spaced drifting directions (30–360 deg or 22.5–360 deg); SF of 0.05 cpd; TF of 2 Hz; stimulus interval of 3 sec; inter-stimulus interval of 2 sec; each stimulus was repeated for 2–3 trials. All subsequent stimuli were presented by correcting for the eye rotation offset, which was estimated by online ("on-the-fly") analysis of the responses (see below for details on the analysis).

In imaging protocol 1 (Fig. 2.1), to measure ocular dominance as well as facilitation/suppression, sinusoidal oriented gratings were presented with the

following stimulus parameters: two directions of drifting vertical gratings (90 deg, rightward; 270 deg, leftward); one of three possible SFs, spaced by 2 octaves, among 0.01 cpd, 0.05 and 0.10 cpd; TF of 2 Hz; stimulus interval of 2 sec; inter-stimulus interval of 4 sec; each stimulus was repeated for 6 trials, in pseudorandomized sequence across drifting directions and eyes, and interleaved with dichoptic drifting gratings as a part of the same stimulation block.

2.6.6 Apparent motion stimuli

All apparent motion (AM) stimuli were presented taking into account a potential rotation offset between each eye's field of view, which was functionally estimated by online analysis of the responses to drifting gratings (see below for details). The eye rotation offset was at least in part due to the dichoptic apparatus used here. For example, a grating originally displayed on the monitor with vertical orientation would appear at the level of the stimulated eye with a slightly offset orientation from vertical, because it is viewed through reflection of the haploscope mirror that has a small inclination angle from the vertical. Nonetheless, the eye rotation offset observed here (generally between 15 and 30 deg) was likely not entirely due to the dichoptic apparatus. Other studies that used anesthetized mice without any apparatus reported a rotation offset of 15-20 deg between the eyes (Wang et al., 2010; Longordo et al., 2013; Sarnaik et al., 2014; Gu and Cang, 2016; Mazziotti et al., 2017).

In the following, the three different types of apparent motion (AM) stimulation will be described in detail.

APPARENT MOTION WITH BARS

AM bar stimuli consisted of two consecutively flashed bright bars (width 8 deg, height 80 deg), displayed on a gray background at one of four different orientations (two cardinals and two obliques). For each orientation and eye, bars could appear in one of four adjacent positions (distance of adjacent positions, 8 deg) within a region spanning a total of 32 deg, centered on each eye's ensemble RF, as measured beforehand (see Fig. 3.2c). For each stimulus, the two consecutive bars (of matching orientation) appeared for 0.5 sec (30 screen frames), one after the other with a single frame (0.0167 sec) of blank screen between the two bars. After the second bar, during the inter-stimulus interval, a blank screen was presented for 2 sec.

AM bar stimuli were presented both monocularly to each eye and dichoptically. For monocular stimulation, the two consecutive bars were presented with matching orientation to the same eye, in any of the four possible positions (16 monocular combinations per eye, per orientation). For dichoptic stimulation, the first bar was flashed to one eye and the second bar to the other eye, encompassing all possible combinations of positions across eyes and eye sequences (16 combinations for each eye sequence (first left then right, and vice versa), for a total of 32 dichoptic combinations per orientation). Monocular and dichoptic stimulus combinations were presented interleaved in a pseudorandomized manner, repeating the whole stimulus sequence at least 8 times, totaling ~90 min of stimulation distributed over 3 separate blocks, allowing for additional administration of anesthesia between blocks.

TWO-GRATING AM

In a different set of experiments, AM stimuli consisted of two consecutively flashed, static sinusoidal gratings (full-field; 100% contrast; SF, 0.04 cpd), displayed at one of four different orientations (two cardinals and two obliques). For each stimulus, the two consecutively flashed gratings (of matching orientation) appeared for 0.133 sec (8 screen frames), one after the other with a single frame (0.0167 sec) of blank screen between the two gratings. Using this stimulus interval, the AM is equivalent to a grating drifting at a TF of 1.88 Hz in the +90 deg phase direction, or a grating drifting three-fold faster at a TF of 5.63 Hz in the -270 deg phase direction. After the second grating, an inter-stimulus interval with blank screen was presented for 2 sec.

For each orientation and eye, gratings could appear in one of four different spatial phases (0, 90, 180, 270 deg phase). For monocular stimulation, the two consecutive flashes of gratings were presented to the same eye with a spatial phase difference between each other of ± 90 deg phase (8 combinations: 0–90, 90–180, 180–270, 270–0, and in reverse order as well; 8×2 eyes = 16 monocular combinations per orientation). For dichoptic stimulation, the first grating was flashed to one eye and the second grating to the other eye (see Fig. 3.7b), encompassing all possible combinations of spatial phases and eye sequences ($16 \times 2 = 32$ dichoptic combinations per orientation). Monocular and dichoptic stimulus combinations were presented interleaved in a pseudorandomized manner, repeating the whole stimulus sequence at least 8 times.

CONTRAST-MODULATED AM

In a third set of experiments, AM stimuli consisted of stationary sinusoidal gratings (full-field; 100% contrast; SF, 0.05 cpd), presented in dichoptic fashion (Fig. 3.7c). For each stimulus, the grating presented to the left eye had a spatial phase of s_0 at the onset of the stimulus. The contrast of the grating was modulated with a sinewave function with a TF of 2 Hz. As such, the grating contrast was 100% at stimulus onset, 0.125 sec later the contrast was 0% (gray screen with mean luminance), and at 0.25 sec the contrast was -100% (contrast reversed compared to onset; the spatial phase of the grating at this time point is $s_0 + \frac{\pi}{2}$), with this cycle repeating every 0.5 sec. The grating presented to the right eye had a spatial phase of $s_0 + \delta_S$ at the onset of the stimulus and its contrast modulation was temporally out of phase by a quarter cycle ($\delta_T = \frac{\pi}{4}$) relative to the grating presented to the left eye (Fig. 3.7c). Each stimulus period lasted 3 sec, with an inter-stimulus interval of 3 sec, during which a blank (gray) screen was displayed.

To align the gratings to each eye's ensemble RF, the spatial phase of the grating presented to each eye was offset, taking the respective ensemble RF as a reference, i.e. the spatial phase of 0 deg phase corresponded to the white band of the grating being aligned to the center of the ensemble RF.

The stimulus set encompassed only gratings in the vertical orientation, in all combinations of four different values of s_0 (0, 45, 90, 135 deg phase) and eight values of δ_S (0–315 deg phase), for a total of 32 combinations. The stimulus sequence was repeated 6–10 times.

Interleaved with contrast-modulated AM stimuli, dichoptic drifting gratings for assessing binocular disparity were also presented at 8 different interocular phase disparities (0–315 deg phase) and two motion directions of vertical

orientation (see Fig. 3.10d and paragraph below for details), amounting to 16 additional combinations, each presented 4–6 times.

2.6.7 Dichoptic drifting gratings

In imaging protocol 1 (Fig. 2.1), to assess sensitivity for binocular disparity, drifting vertical gratings were dichoptically presented to both eyes at the same time, at varying interocular disparities. Different interocular grating disparities were generated by varying the initial phase (position) of the grating presented to one eye relative to the phase of the grating presented to the other eye, systematically across the entire grating cycle (see Fig. 3.10d). Eight equally spaced phase disparities (45–360 deg phase) were used. For each stimulus, drift direction, TF, and SF were kept constant across eyes. The other grating stimulus parameters were the same as for the monocular drifting gratings.

In imaging protocol 2 (Fig. 2.1), dichoptic drifting gratings were presented at 12 equally spaced phase disparities (30–360 deg phase), at a single SF of 0.01 cpd, with a stimulus interval of 2 sec and an inter-stimulus interval of 2 sec. Dichoptic gratings were presented in pseudorandomized sequence across disparities and drifting directions, with 4 trials for each stimulus condition, interleaved with random dot stereograms (see below) as a part of the same stimulation sequence.

2.6.8 Random dot stereograms

In imaging protocol 2 (Fig. 2.1), random dot stereograms (RDS) were additionally employed to assess disparity tuning. The stimulus consisted of a pattern of random dots, simultaneously presented to both eyes in a dichoptic fashion; between the left and the right eye images, a spatial offset along the horizontal axis was introduced to produce interocular disparities (see Fig. 3.17a). Unlike grating stimuli for which interocular disparity is expressed as the relative phase differences because of the circular nature of the stimulus, the interocular disparity of RDS is given in degrees of visual angle. A total of 23 different RDS conditions were presented, covering a range of disparities between -31.3 deg and $+31.3$ deg. The different RDS conditions were obtained by subdividing the entire range of disparities into 23 non-overlapping bins (bin width 2.6 deg) and assigning each bin to one RDS condition (e.g. $[-1.3 + 1.3]$, $[+1.3 + 3.9]$, etc.). Each RDS stimulus was presented for 5 sec, during which a new random pattern of dots was displayed every 0.15 sec. In each pattern, all dots had the same interocular disparity, randomly chosen within the 2.6 deg bin of that particular RDS condition. The dots (diameter 12 deg) were bright against a gray background with an overall density of 25%. Each RDS condition was presented for 8–10 stimulus trials, with individual trials separated by an inter-stimulus interval of 2 sec. RDS stimuli were presented in pseudorandomized sequence, interleaved with dichoptic gratings as part of the same stimulation sequence.

2.7 IMAGE ANALYSIS

All analyses of two-photon imaging data were performed using custom-written Matlab code (MathWorks). Imaging data were processed in three steps: (1) image registration, (2) selection of regions of interest (ROIs), (3) extraction of calcium fluorescence time courses.

(1) Motion artifacts, mainly consisting of small, slow drifts in brain position that occurred during imaging, were corrected by rigid translational registration based on 2D cross-correlation and applied to down-sampled fast Fourier transforms of all frames, using the average of the initial 200 frames of the recording as a reference.

(2) ROIs were selected by manually drawing circular shapes around cell somas, which were morphologically identified by inspecting the average of all registered frames of the recording, combined with examination of activity and direction tuning maps. Regions with overlapping somas were excluded from the analysis.

(3) Since the signal from any somatic ROI might be contaminated by out-of-focus fluorescence from surrounding neuropil and other cells, neuropil contamination was corrected by generating a peri-somatic neuropil ROI for each soma ROI, consisting of an annular region extending from 3 μm (6.7 pixels) to 13 μm from the border of the somatic ROI. Pixels belonging to other somatic ROIs were excluded from neuropil ROIs.

The raw fluorescence time course of each cell was extracted by averaging all pixels within the somatic ROI ($F_{\text{cell_raw}}$). Similarly, the fluorescence time course from the annular neuropil ROI (F_{neuropil}) was extracted. The true fluorescence time course of a cell was estimated as:

$$F_{\text{cell_corrected}} = F_{\text{cell_raw}} - r \times F_{\text{neuropil}}$$

with a contamination factor r set to 0.7 (Kerlin et al., 2010; Chen et al., 2013b). After neuropil correction, the fluorescence signals were filtered with the Savitsky-Golay method (second order polynomial, 10 data points, 0.5 sec). Relative changes in fluorescence signals ($\Delta F/F_0$) were calculated, for each stimulus trial independently, as $(F - F_0)/F_0$, where F_0 was the average over a baseline period of 1 sec immediately before onset of the visual stimulus.

2.8 DATA ANALYSIS

All data analyses were performed using custom-written Matlab code (MathWorks).

2.8.1 Retinotopic mapping of V1

Images were high-pass-filtered to calculate blank-corrected image averages for each stimulus condition, and thresholded (image background mean + $3 \times$ standard deviation). The signal in response to visual stimulation (23 frames during presentation of a given visual stimulus) was referenced against the mean of 15 baseline frames (prior to stimulus presentation), resulting in a percentage signal decrease for each pixel. A map of retinotopy was generated

by assigning a color to each pixel based on the stimulus location that evoked the strongest response and encoding the response strength by pixel intensity.

2.8.2 Retinotopic mapping of higher visual areas

Retinotopic maps for azimuth and elevation were generated using the temporal phase method introduced by (Kalatsky and Stryker, 2003) on images obtained with intrinsic signal imaging. Briefly, camera pixels showing a similar temporal phase in response to the vertical or horizontal periodic bar encode, respectively, iso-azimuth or iso-elevation coordinates in the visual field. To compute maps, first, the time course of each pixel was high-pass filtered using a moving average (with a time window equaling the duration of the moving bar cycle, ~10 sec) to remove slow artifactual changes in reflected light intensity not evoked by visual stimulation (Mayhew et al., 1996). Next, a Fourier transform was computed to extract the phase and the power of the frequency component at the bar drifting frequency. The phase indicates the location of the bar driving the response of a pixel, and the power indicates the strength of its response. The phase, however, does not directly provide the absolute retinal location, because the response is lagged by the hemodynamic delay. To compute maps of absolute retinotopy, the response time to the bar drifting in one direction was subtracted from the response time to the opposite drift direction. Since the hemodynamic delay should be the same in both cases, the subtraction eliminated the delay and produced maps showing the absolute retinal location on the stimulus monitor (Kalatsky and Stryker, 2003). From these maps of absolute retinotopy, contour lines of equally spaced iso-azimuth and iso-elevation lines were extracted, color-coded for visual field location, and overlaid on top of the image of the blood vessel pattern.

The boundary between V₁ on one side and areas LM, AL, and RL on the other side was identified by a reversal at the vertical meridian, as the longer axis of the elliptically shaped contour at the vertical meridian. The boundaries between LM and AL, and between AL and RL were identified as a reversal near the horizontal meridian (Kalatsky and Stryker, 2003; Marshel et al., 2011; Garrett et al., 2014). The binocular regions of areas V₁, LM, and RL were then specifically targeted for two-photon imaging, by using the blood vessels as landmarks, which could be reliably recognized in the two-photon images.

2.8.3 Retinotopic mapping online analysis

Data images of the recording were analyzed online ("on-the-fly") pixel by pixel, by calculating a $\Delta F/F$ for each pixel and grating patch location, averaged across trials, for each eye independently. An eye-specific retinotopic map (as shown in Fig. 3.2a,b) was generated by counting, for each stimulus location presented to one eye, the number of pixels that best responded to it (only pixels with an averaged $\Delta F/F_0$ above zero for any given location were considered).

The center of the each eye's ensemble RF was determined by a two-dimensional Gaussian fit. Given the high number of total pixels in the images (675k), analyzed regardless of individual cell's ownership, this online analysis provided a good estimate of the center of the overall RF across cells

from that imaging plane, as confirmed by comparison to individual cells' RFs analyzed *post hoc* (data not shown).

For retinotopic mapping with vertical and horizontal patches of gratings (experiments on binocular disparity), azimuth and elevation maps were generated for each eye by counting, for each vertical and horizontal stimulus location presented to one eye, the number of pixels that best responded to it (only pixels with an averaged $\Delta F/F$ above zero for any given location were considered).

2.8.4 Eye rotation offset online analysis

Data images containing responses to drifting gratings were analyzed online ("on-the-fly") pixel by pixel, by calculating a $\Delta F/F$ for each pixel and grating direction, averaged across trials, for each eye independently.

For each eye independently, responsive and orientation-tuned pixels were selected on the basis of an orientation selectivity index (OSI), scaled by the maximum relative fluorescence change, with OSI calculated for each pixel as a normalized length of the mean response vector (Ringach et al., 2002; Mazurek et al., 2014):

$$\text{OSI} = \left| \frac{\sum_k R(\Theta_k) \exp(i\Theta_k)}{\sum_k R(\Theta_k)} \right|$$

where $R(\Theta_k)$ is the mean $\Delta F/F$ response to the orientation angle Θ_k . The angle of the same mean response vector was taken as the preferred orientation of that pixel. For pixels that were selected for both eye-specific stimuli, the difference in preferred orientation between left and right eye was calculated and the average across all selected pixels was taken as the rotational offset between the eyes' fields of view (dO). Subsequent stimulations (either AM stimuli or dichoptic gratings) were presented by correcting stimulus orientation by $-dO/2$ and $+dO/2$ for stimuli presented to the left and right eye, respectively.

2.8.5 Responsive cells

Cells were defined visually responsive when $\Delta F_{\text{peak}}/F_0 > 4 \times \sigma_{\text{baseline}}$ in at least 50% of the trials of the same stimulus condition (e.g. grating drifting at 90 deg direction, presented to the contralateral eye), where ΔF_{peak} is the peak $\Delta F/F_0$ during the stimulus period of each trial, and σ_{baseline} is the standard deviation calculated across the F_0 of all stimulus trials and conditions of the recording.

For drifting gratings, contrast-modulated AM, and RDS stimuli, the mean $\Delta F/F_0$ over the entire stimulus interval of each trial was calculated.

For AM bars, the mean $\Delta F/F_0$ for each trial was calculated including data points from 0.5 sec to 2 sec after the onset of the first bar.

For two-grating AM, the mean $\Delta F/F_0$ for each trial was calculated including data points from 0 sec to 1 sec after the onset of the first grating.

For RDS stimuli, the responsiveness of cells was additionally determined using a one-way ANOVA ($p < 0.01$) on the mean $\Delta F/F_0$ of single stimulus trials across disparities. When plotting the disparity preference averaged

across neurons of each imaging plane (Fig. 3.18a,c), only imaging planes with at least 5 neurons were used for averaging.

2.8.6 Ocular dominance index

Ocular dominance was determined for responsive cells by calculating the ocular dominance index (ODI) using eye-specific responses to drifting gratings:

$$\text{ODI} = \frac{R_{\text{contra}} - R_{\text{ipsi}}}{R_{\text{contra}} + R_{\text{ipsi}}}$$

where R_{contra} and R_{ipsi} are the mean $\Delta F/F_0$ responses (across trials) to the preferred grating direction presented to either the contra- or ipsilateral eye, respectively. Contralateral and ipsilateral dominance are indicated by an ODI of 1 or -1 , respectively. A cell equally activated by either eye stimulation has an ODI = 0. Cells were defined binocular if $-0.7 < \text{ODI} < 0.7$.

2.8.7 Direction selectivity index

For each responsive cell, the direction selectivity index (DSI) was calculated using eye-specific responses to drifting gratings as follows:

$$\text{DSI} = \frac{R(\Theta_{\text{pref}}) - R(\Theta_{\text{opp}})}{R(\Theta_{\text{pref}}) + R(\Theta_{\text{opp}})}$$

where $R(\Theta_{\text{pref}})$ is the mean $\Delta F/F_0$ across trials to the grating direction evoking the strongest response, and $R(\Theta_{\text{opp}})$ is the mean $\Delta F/F_0$ across trials to the grating of the opposite direction ($\Theta_{\text{opp}} = \Theta_{\text{pref}} + 180$).

DSI values closer to 1 indicate a preferential response to a single motion direction, whereas values closer to 0 indicate no preference between opposite motion directions. Cells were defined direction-selective (DS) if $\text{DSI} > 0.3$.

For cells responsive to AM stimuli, a separate DSI was also calculated as described above, but using $\Delta F/F_0$ responses to AM stimuli.

The definition of binocular or DS cells was based on arbitrary thresholds, since ODI and DSI showed a continuum of scores across their respective ranges (for an example ODI distribution see Fig. 3.12a). Using different thresholds for ODI ($-0.5 < \text{ODI} < 0.5$, or $-0.3 < \text{ODI} < 0.3$) and DSI ($\text{DSI} > 0.2$, or $\text{DSI} > 0.5$) did not qualitatively change the results of the experiments on direction selectivity (data not shown).

2.8.8 Direction tuning curve fit

To compare the direction preferences of individual cells across drifting gratings and AM stimuli (as in Fig. 3.4 and Fig. 3.8), direction preferences were calculated by fitting the tuning curves with a double Gaussian function using single trial responses:

$$\begin{aligned} R(\Theta) = & R_{\text{baseline}} + R_{\text{pref}} \times \exp\left(-\frac{\text{wrap}(\Theta - \Theta_{\text{pref}})^2}{2\sigma^2}\right) \\ & + R_{\text{opp}} \times \exp\left(-\frac{\text{wrap}(\Theta + 180 - \Theta_{\text{pref}})^2}{2\sigma^2}\right) \end{aligned}$$

where R_{baseline} is the baseline response, R_{pref} is the response to the preferred direction, R_{opp} is the response to the direction opposite to the preferred one ($\Theta_{\text{pref}} + 180$), σ is the tuning width, and the function $\text{wrap}(\Theta)$ wraps angles onto the interval between 0 and 180 deg:

$$\text{wrap}(\Theta) = \min(|\Theta|, |\Theta + 360|, |\Theta - 360|).$$

Direction preference was defined as the angle corresponding to the peak of the fitted tuning curve.

2.8.9 Disparity selectivity index

For each cell responsive to dichoptic gratings, a disparity selectivity index (DI) was calculated, given by the normalized length of the mean response vector across the eight phase disparities of the drifting direction that elicited the stronger activation (Scholl et al., 2013a, 2015, 2017a; based on similar measurements of orientation and direction selectivity, Ringach et al., 2002; Mazurek et al., 2014):

$$\text{DI} = \left| \frac{\sum_k R(\Theta_k) \exp(i\Theta_k)}{\sum_k R(\Theta_k)} \right|$$

where $R(\Theta_k)$ is the mean $\Delta F/F$ response to the interocular phase disparity Θ_k . Cells were defined disparity-tuned (DT) if $\text{DI} > 0.3$.

Using more stringent criteria for defining responsive cells ($\Delta F_{\text{peak}}/F_0 > 8 \times \sigma_{\text{baseline}}$) did not result in a significant change in the DI distribution for each area and SF (data not shown), indicating that signal-to-noise issues did not affect the measurement of disparity selectivity.

Note that the calculation of DI is based on a circular metric. As such, DI could be computed only for responses to dichoptic gratings, but not for responses to RDS, which are not circular. Cells were defined DT to RDS when at least 50% of the tuning curve variance (R^2) could be accounted for by the model fit (see below).

2.8.10 Disparity tuning curve fit

Disparity tuning curves obtained with dichoptic gratings were fitted with an asymmetric Gaussian function using single trial responses, as follows:

$$R(\Theta) = \begin{cases} R_{\text{baseline}} + R_{\text{pref}} \times \exp\left(-\frac{\text{wrap}(\Theta - \Theta_{\text{pref}})^2}{2\sigma_1^2}\right) & \text{if } \Theta < \Theta_{\text{pref}} \\ R_{\text{baseline}} + R_{\text{pref}} \times \exp\left(-\frac{\text{wrap}(\Theta - \Theta_{\text{pref}})^2}{2\sigma_2^2}\right) & \text{if } \Theta \geq \Theta_{\text{pref}} \end{cases}$$

where R_{baseline} is the baseline response, R_{pref} is the response to the preferred disparity, σ_1 and σ_2 are the tuning width parameters for the left and right sides, respectively, and the function $\text{wrap}(\Theta)$ wraps angles onto the interval between 0 and 180 deg:

$$\text{wrap}(\Theta) = \min(|\Theta|, |\Theta + 360|, |\Theta - 360|).$$

Disparity tuning curves obtained with RDS were fit with a similar asymmetric Gaussian function, where a simple angular difference was used ($\Theta - \Theta_{\text{pref}}$), instead of the wrap function.

2.8.11 Noise correlations

Noise correlations were calculated between all possible pairs of DT neurons from the same recording. The single-trial $\Delta F/F_0$ responses of a given cell to dichoptic gratings were Z-scored with respect to the mean across trials. Pair-wise noise correlations were then computed using the Pearson's linear correlation coefficient. Since neighboring cells might "contaminate" each other's fluorescence signal, only pairs separated by at least 20 μm were considered.

2.8.12 Population decoding with SVM

To estimate whether the joint activity of populations of neurons encode AM stimuli, I exploited a population decoding approach based on data classification with machine learning. Support vector machines (SVM; Cortes and Vapnik, 1995) were used to find the hyperplane that best separated neuronal activity data points of one class (stimulus condition) from those of another class ("binary classification"). The accuracy in classifying data points of the two stimulus conditions with increasing number of neurons was evaluated. The binary classifiers consisted of SVM with a linear kernel. The decoding procedures were performed using custom-written routines based on the function *fitcsvm* (kernel scale, 1; box constraint, 1) as part of the Statistics and Machine Learning Toolbox in Matlab (Mathworks).

For population decoding of responses to drifting gratings, binary classifiers were used with datasets consisting of the mean $\Delta F/F_0$ responses to drifting gratings calculated over the stimulus period for each trial.

For each decoding session, the single trial responses of a population of N neurons to two adjacent grating directions were considered (binary classification with the two directions corresponding to the two "classes"). The N neurons were randomly selected among all the ones deemed responsive to drifting gratings from the same recording. A matrix of responses was obtained, with N columns (neurons, corresponding to the "features") and $t \times d$ rows (trials \times directions, corresponding to the "observations"). Thus, each element of the matrix is a single response value (the mean $\Delta F/F_0$) of a given neuron for a given trial of one of the two grating directions.

$t \times d$ decoders were trained on a training set consisting of the response matrix in which one row was systematically held out to be used as a test set after training ("leave-one-out cross-validation"). The identity of each trial of the training set was also provided to the decoder ("supervised classification"). The binary classifier obtained was then probed on the previously held-out responses to predict the identity of the test set. For each population of N neurons, binary decoders for all possible pairs of adjacent grating directions were trained and their accuracy evaluated by cross-validation. This procedure was then repeated 20 times, using a different random subsampling of N neurons, and the outcomes of these iterations averaged to generate a measure of decoding performance for a given experiment, as shown in Fig. 3.6. Significance levels for classification accuracy were determined by using a similar decoding procedure, but training decoders on training sets in which

the identities of the stimulus trials were randomly shuffled, repeating the shuffling 500 times (Jurilli and Datta, 2017) and taking the 95th percentile.

For population decoding of responses to AM bars that were presented monocularly, a decoding procedure similar to the one for drifting gratings was adopted. The four stimulus orientations were analyzed independently from each other. For binary classifications, each of the two classes included the single trial responses to all three possible AM combinations of, respectively, one or the other direction (e.g. rightward direction in one class: L1–L2, L2–L3, L3–L4; leftward direction in the other class: L2–L1, L3–L2, L4–L3, as denoted in Fig. 3.2c). Populations of N neurons randomly selected among the ones deemed responsive to monocular AM of any of these 3 + 3 combinations were considered. For each population of N neurons, 20 different random resamplings were performed, and the outcomes were averaged to generate a measure of decoding performance for a given experiment.

For population decoding of responses to AM bars that were presented dichoptically, a decoding procedure similar to the one used for monocular AM bars was adopted, with the main difference being the stimulus combinations used and the configurations of the two classes. Among all possible dichoptic combinations of a given orientation, only the pairs of bar positions that appeared “adjacent across eyes” were considered (e.g. L1–R2/R2–L1, but not L1–R3/R3–L1, as denoted in Fig. 3.2c). Each of the two classes included responses to all six dichoptic combinations producing AM in one of the two opposite directions (three different pairs of bar positions and two eye sequences per direction; e.g. rightward direction: L1–R2, R1–L2, L2–R3, R2–L3, L3–R4, R3–L4, leftward direction: L2–R1, R2–L1, L3–R2, R3–L2, L4–R3, R4–L3). For each population of N neurons, randomly sampled among the ones deemed responsive to any of the stimulus combinations considered, 20 different random resamplings were performed, and the outcomes were averaged to generate a measure of decoding performance for a given experiment.

For population decoding with sequential inclusion of neurons in the order of decoding contribution (forward feature selection), an initial subpopulation of $N = 2$ neurons was randomly sampled from the population of neurons deemed responsive to any of the stimulus combinations considered in the two classes. All possible subpopulations of $N = 3$ neurons including the previous two neurons were used to train distinct decoders and the subpopulation resulting in highest classification accuracy was selected. The selection iterations were then repeated until $N = 15$. The whole procedure was performed on 20 different randomly sampled, initial subpopulations of $N = 2$, and outcomes were averaged to generate a measure of decoding performance for a given experiment.

For population decoding with sequential exclusion of neurons on the basis of their decoding contribution (backward feature selection), an initial subpopulation of $N = 15$ neurons was randomly sampled from the population of neurons deemed responsive to any of the stimulus combinations considered in the two classes. All possible subpopulations of $N = 14$ sampled by systematically leaving one neuron out were used to train distinct decoders and the subpopulation resulting in highest classification accuracy was selected. The selection iterations were then repeated until $N = 2$. The whole procedure was performed 20 times, starting from different initial subpopulations of $N = 15$, and outcomes were averaged to generate a measure of decoding performance for a given experiment.

The feature selection procedures were performed using custom-written routines based on the function *fitcsvm* (kernel scale, 1; box constraint, 1) and *sequentialfs* as a part of the Statistics and Machine Learning Toolbox in Matlab (Mathworks).

To estimate how much information about binocular disparity is carried by the joint activity of populations of neurons in each area, a population decoding approach based on support vector machines (SVM; Cortes and Vapnik, 1995) was employed, similarly as described above, but with several differences in the implementation.

The dataset consisted of pseudo-populations generated by pooling neurons, from a given area and responsive to dichoptic gratings of a given SF, from all individual recordings across animals. To take into account that distributions of disparity preferences had a population peak disparity that was characteristic for each individual recording (see Fig. 3.13a), the tuning curves of neurons from a given recording were shifted by dP deg phase, where dP is the difference between the population peak disparity characteristic of that recording and 180 deg phase.

For each neuron in the dataset, the $\Delta F/F_0$ response of each trial was split in $b = 6$ bins of 0.5 sec, including 4 bins during the stimulus period (2 sec) and 2 bins immediately after it, and the mean $\Delta F/F_0$ of each bin was taken as one activity data point. As such, for each neuron and disparity, there were ap activity points, with $ap = t \times b$, where $t = 6$ trials for each disparity and $b = 6$ bins.

The decoding approach was designed to estimate which disparity, among all eight possible disparities, was actually presented. This discrimination among eight distinct classes was redefined as a series of binary classifications (“multi-class classification”). For each decoding session, a subpopulation of N neurons was randomly sampled from the pseudo-population. A matrix of data points was constructed, with N columns (neurons, corresponding to the “features”) and $ap \times d$ rows (activity points \times disparities, corresponding to the “observations”).

The data matrix was divided into two separate sets, a training set and a test set. The training set included $0.9 \times ap$ randomly chosen activity points for each disparity; the test set included the remaining $0.1 \times ap$ activity points (“10-fold cross-validation”). A multi-class decoder was constructed by training 28 distinct binary classifiers, each considering only two different disparities as the two classes, and exhausting all combinations of disparity pairs (“one-vs-one”). The identity of each observation of the training set was also provided to every classifier (“supervised classification”).

Then, the multi-class decoder was probed on the test set. Each observation of the test set was evaluated by each of the 28 binary classifiers to predict its class (disparity). The class identity that was more frequently predicted across the 28 classifications was taken as the predicted class identity of that observation. This evaluation was performed for every observation of the test set. The procedure was then repeated on a different training set and test set, across all 10 folds, to produce an average accuracy estimate of the decoder for a given subpopulation of N neurons. 20 different random resampling of N neurons from the pseudo-population were performed and the outcomes were averaged to generate a measure of decoding performance of a given N , as reported in Fig. 3.16.

Significance levels for classification accuracy were determined by using a

similar decoding procedure but training decoders on training sets in which the identities of the observations were randomly shuffled, repeating the shuffling 100 times. The binary classifiers consisted of SVM with a linear kernel. The decoding procedures were performed using custom-written routines based on the function `fitecoc` (kernel scale, 1; box constraint, 1) as part of the Statistics and Machine Learning Toolbox in Matlab (Mathworks).

2.9 STATISTICS

Statistical analyses were performed using Matlab (MathWorks). Sample sizes were not estimated in advance. No randomization or blinding was performed during experiments or data analysis. Data are reported as mean with standard error of the mean (mean \pm SEM), or as median with interquartile range (median \pm IQR), as reported in Figures and Figure legends. Data groups were tested for normality using the Shapiro-Wilk test in combination with a skewness test and visual assessment (Ghasemi and Zahediasl, 2012). Then, comparisons were made using the appropriate tests (t-test, one-way ANOVA, two-way ANOVA with unbalanced design, Kruskal-Wallis test). For multiple comparisons, Bonferroni correction was used. All tests were two sided. Correlation coefficients were calculated as Pearson's correlation coefficient. When comparing the direction preferences showed by individual cells across drifting gratings and AM stimuli (Fig. 3.4, Fig. 3.8), two-sided binomial tests were used with the null hypothesis that 50% of the cells would show a difference in direction preference in the interval 0–90 deg. The statistical significances are reported in the Figures, with asterisks denoting significance values as follows: * $p < 0.05$, ** $p < 0.01$, *** $p < 0.001$.

3 | RESULTS

In this thesis, I investigated two fundamental receptive field properties of neurons in the mouse visual cortex – direction selectivity and binocular disparity. First, I studied the origin of cortical direction selectivity, examining to which degree it is inherited from the retina and to which extent it is generated *de novo* in V1. Second, I studied the integration of inputs from both eyes in cortical neurons, characterizing binocular disparity in V1, and in two higher-order visual areas, LM and RL.

3.1 ORIGIN OF DIRECTION SELECTIVITY IN MOUSE VISUAL CORTEX

3.1.1 Identification of direction-selective and binocular neurons in V1

To measure response properties of neurons in V1, I employed two-photon population calcium imaging in anesthetized mice. In each experiment, about ~200 L2/3 neurons expressing the genetically encoded calcium indicator GCaMP6s were recorded at single-cell resolution, sampling 1588 neurons in total across 8 imaging planes and 6 animals. The neurons recorded were located in upper L2/3, 120–240 μm below the cortical surface (Fig. 3.1b). Two-photon imaging was targeted to the binocular region of V1, which was previously located in each mouse using intrinsic signal imaging (Fig. 1.3 Introduction). For dichoptic visual stimulation, the two haploscope mirrors were placed directly in front of the eyes to redirect each eye's view onto a separate display monitor (Fig. 3.1a). The approach based on dichoptic apparent motion (AM) to probe retina-dependent and -independent mechanisms for cortical direction selectivity requires neurons that are both DS and binocular. Thus, DS and binocular neurons were first identified by displaying drifting gratings at eight or twelve different directions to each eye separately (Fig. 3.1c). By measuring visually evoked calcium responses to monocular stimulation, two direction tuning curves, one for each eye, were generated for each responsive cell (Fig. 3.3a,b). The direction selectivity index (DSI, see Materials and Methods, paragraph 2.8.7) was calculated from each tuning curve, where values closer to 1 indicate a preferential response to a single motion direction, whereas values closer to 0 indicate no preference between opposite motion directions. To quantify the degree of binocularity of each cell, the ocular dominance index (ODI) was calculated, with values ranging from -1 , for a cell responding exclusively to ipsilateral eye stimulation, to 1 , for a cell responding exclusively to contralateral eye stimulation; a binocular cell equally activated by either eye stimulation has an $\text{ODI} = 0$. A visually responsive neuron was defined DS and binocular if it had $\text{DSI} > 0.3$ to either eye's tuning curve and $-0.7 < \text{ODI} < 0.7$ (see Materials and Methods for details), making up about 10% of the responsive neurons ($11\% \pm 2\%$ mean \pm SEM across experiments).

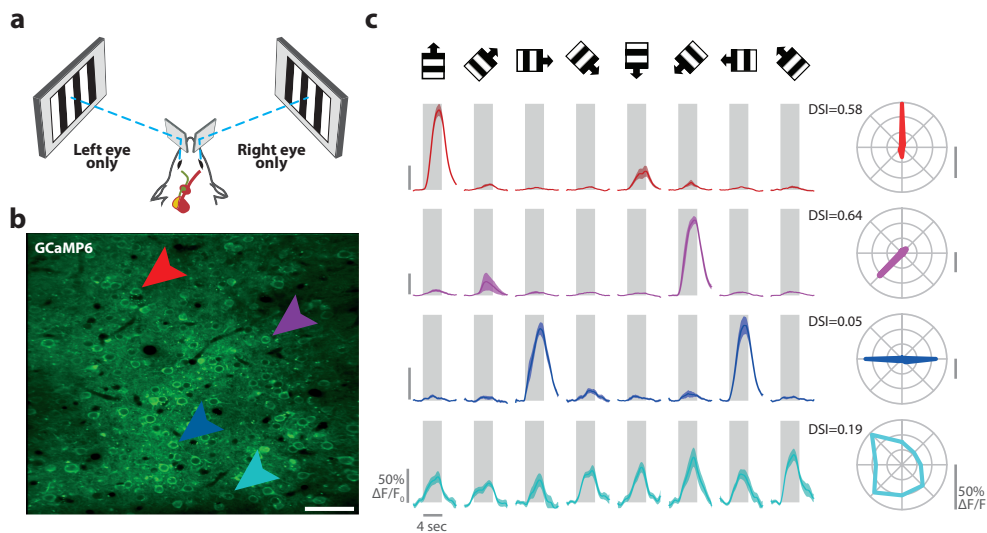


Figure 3.1 | Identification of direction-selective and binocular neurons in mouse V1 with two-photon calcium imaging. **a** | Haploscope apparatus for dichoptic presentation of stimuli. Two mirrors are used to redirect the field of view of each eye onto display monitors for independent stimulation of each eye. The direction selectivity of neurons in V1 is characterized for each eye separately. **b** | The activity of V1 neurons in response to drifting gratings is measured using two-photon imaging of GCaMP6s. Example of a frame-averaged imaging plane acquired at a cortical depth of 220 μm , showing V1 neurons expressing GCaMP6s. Scale bar, 50 μm . **c** | Left, fluorescence time courses ($\Delta F/F_0$) of the four example neurons in (b) in response to eight grating directions presented to the contralateral eye. The fluorescence time courses are plotted as mean \pm SEM (lines with shaded regions) calculated across stimulus trials. The gray boxes illustrate the period of stimulus presentation (4 sec), with its bottom edge indicating the baseline level (0% $\Delta F/F_0$). Right, polar plots with mean fluorescence responses across the eight directions, showing the direction tuning of each cell with the corresponding DSI value. The top two neurons (red and purple) show clear DS responses. The third neuron (blue) shows selective responses for vertical orientation, with no preference for either motion direction. The bottom neuron (cyan) is broadly tuned.

3.1.2 Neuronal responses to monocular apparent motion

In order to apply the dichoptic AM paradigm used here, it was essential to verify that V1 neurons would, in general, be able to respond to AM stimuli in a DS manner. Specifically, do cells exhibit DS responses to AM stimuli presented to either eye? And, do responses to AM stimuli resemble the direction tuning probed with drifting gratings? To test this, AM stimuli were initially displayed monocularly to either eye. I could thus assess whether AM stimuli can elicit DS responses, and compare these responses to the ones evoked by conventional drifting gratings.

To ensure that AM stimuli were in principle positioned such as to activate neurons, a two-step retinotopic mapping was performed presenting small patches of drifting gratings to either eye (Fig. 3.2a,b). A first, coarse retinotopic mapping was used to verify the alignment of the stimulus monitors (Fig. 3.2a), followed by a finer retinotopic mapping step (Fig. 3.2b) used to determine the position of AM stimuli to be presented in the following step. The retinotopic maps were extracted by pixel-based, online analysis, including responsive pixels from all neurons and neuropil recorded in that particular imaging field to generate two ensemble RFs, one per eye. The center of each eye's ensemble RF was then used as a reference to position AM stimuli (Fig. 3.2c). For each eye, four possible adjacent bar positions were chosen to be centered on the ensemble RF. Each monocular AM stimulus consisted

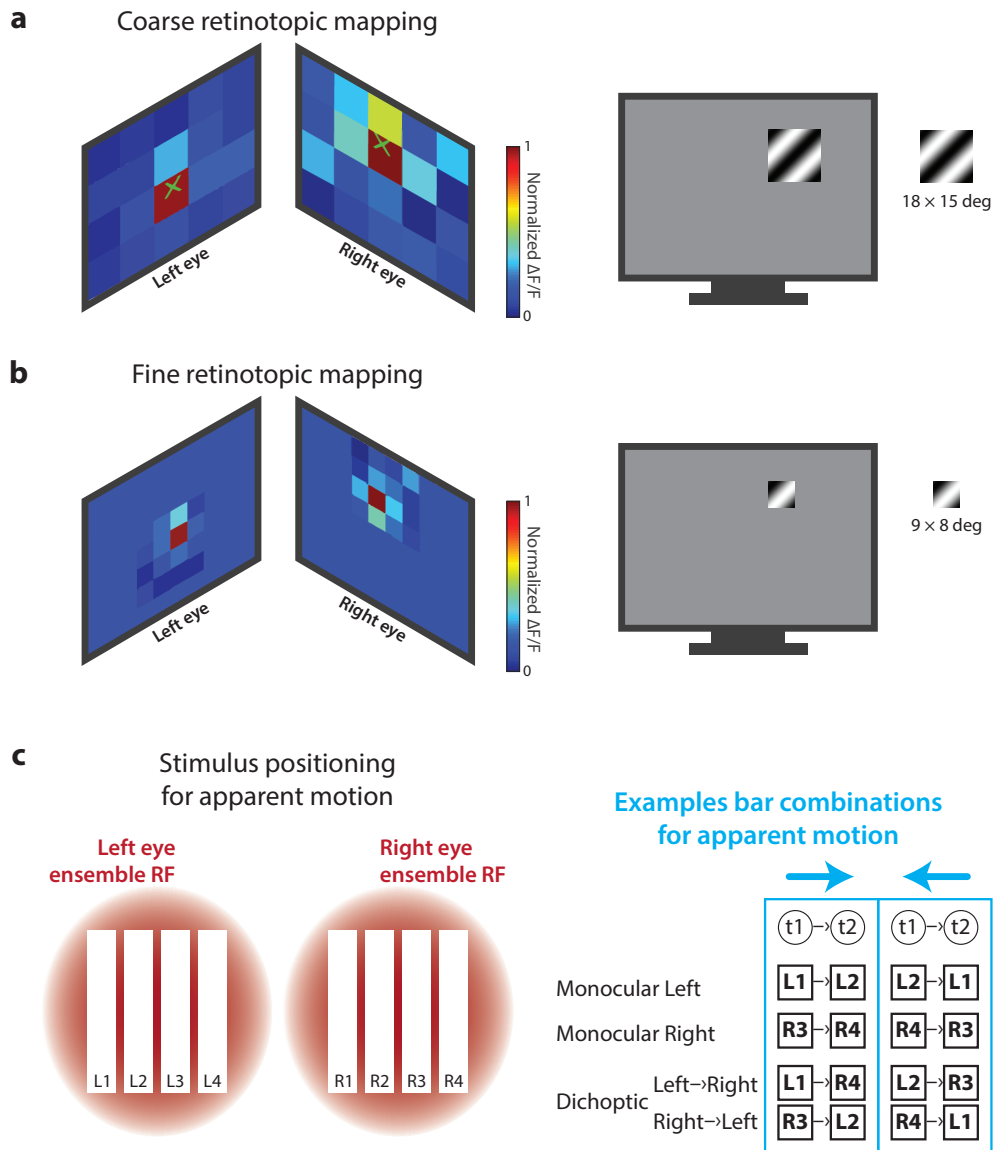


Figure 3.2 | Retinotopic mapping and positioning of bars for apparent motion. **a** | Since the field of view of each eye is deviated by means of the haploscope mirrors, coarse retinotopic mapping was used to verify the alignment of the monitors and ensure that the field of view of each eye was roughly redirected to the central region of the display monitors. Left, example of ensemble RFs for each eye obtained by pixel-based, online analysis of fluorescence responses to small patches of moving gratings. The color code of each map shows the response strength averaged across all responsive pixels to stimuli presented at 20 different locations to each eye. Right, schematic illustrating the patches of drifting gratings presented to each eye for coarse mapping of retinotopy. **b** | A more accurate retinotopic mapping was then carried out to obtain a more precise localization of the center of each ensemble RF. Smaller patches were used, presented only in the portion of field of view containing the ensemble RF measured with the coarse mapping. This two-step mapping procedure allowed for a fast yet accurate measurement of the center of each eye's ensemble RF, which was subsequently used for positioning AM bar stimuli. **c** | Schematics illustrating how the positions of bar stimuli for AM were selected. Left, for a given orientation, four adjacent bar positions for each eye were chosen to be centered on the ensemble RF (red shaded circle). The example shows four vertical positions for the left eye (L1 to L4) and four positions for the right eye (R1 to R4). Right, example combinations of two bar positions flashed at two consecutive time points (t1 and t2), which produce either leftward or rightward AM. AM was presented monocularly to each eye, and across eyes in dichoptic fashion. Note that for dichoptic AM two possible eye sequences were possible: first left then right eye, and vice versa. For more details on all AM combinations, see paragraph 2.6.6 in Materials and Methods.

of two static bars flashed in sequence (one after the other) in two adjacent positions of the same eye (Fig. 3.2c). As a result, for each of the two opposite AM directions of one orientation (out of four orientations), three different combinations of bars were possible. Of the three possible AM combinations per direction, only the one eliciting the strongest response for any given neuron was considered as the response to that particular AM direction and was used to construct the cell's tuning curve for AM over the total of eight AM directions (Fig. 3.3c,d).

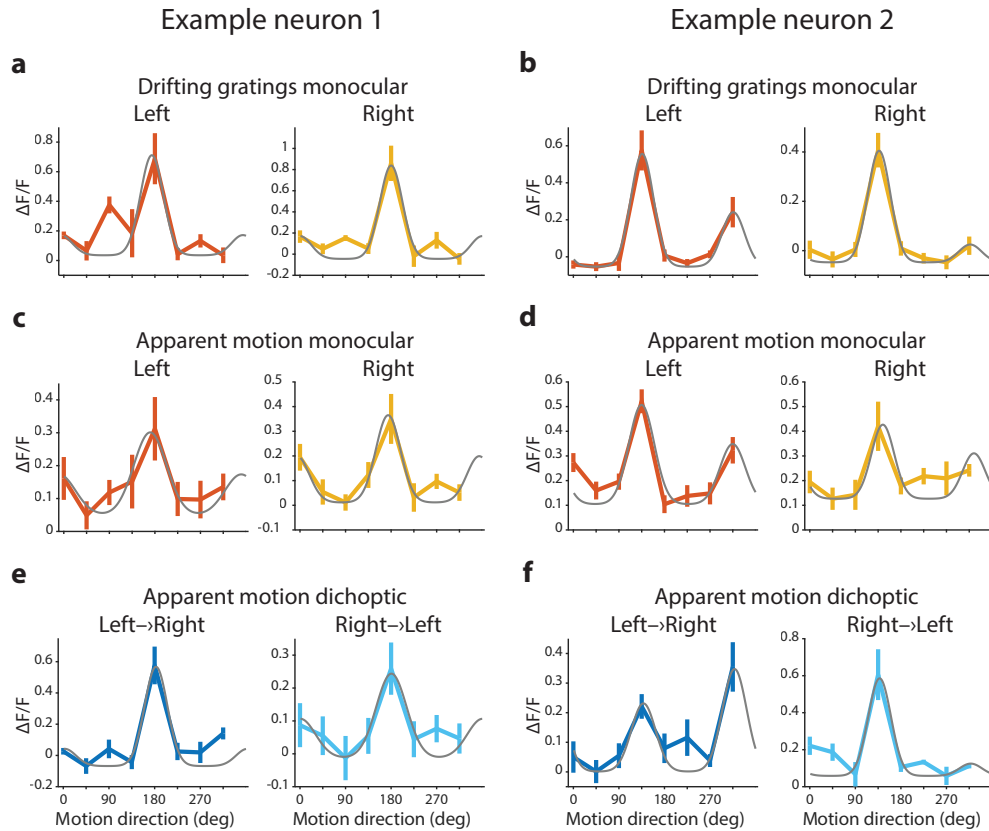


Figure 3.3 | Direction tuning for drifting gratings and apparent motion. Representative tuning curves for two individual neurons. For each panel, the mean fluorescence responses calculated across stimulus trials are plotted in function of the eight motion directions, with error bars indicating \pm SEM. The gray curve shows the double Gaussian curve fit. **a,b** | Tuning curves obtained with drifting gratings presented monocularly to either left (orange) or right eye (yellow). **c,d** | Tuning curves obtained in response to AM bars presented monocularly to either left (orange) or right eye (yellow). **e,f** | Tuning curves obtained in response to AM bars presented dichoptically with a left-right eye sequence (dark blue) or right-left eye sequence (cyan). Note that the neuron in (f) shows opposite direction selectivity between the two possible eye sequences of dichoptic stimulus presentation.

On average, neurons were only weakly activated by AM stimuli, as response strengths were generally much lower compared to drifting gratings, and a smaller fraction of neurons was responsive to any of the monocular AM stimuli (fraction responsive neurons: 28% monocular AM bars vs. 58% monocular gratings; mean response amplitude $\Delta F/F$ 0.31 vs. 0.67). Only a minority of cells were responsive to both monocular drifting gratings and monocular AM bars (14% for the contralateral eye, 9% for the ipsilateral eye). For these cells, the direction tuning curves obtained with the two stimulation paradigms were compared by determining preferred direction from both tuning curves independently (Fig. 3.3a-d), and calculating the differ-

ence. Between monocular drifting gratings and AM bars, a larger proportion of neurons showed a similar direction preference between monocular drifting gratings and monocular AM bars (Fig. 3.4a; difference in direction preference ≤ 45 deg, 57% neurons across contralateral and ipsilateral eye stimulation), while a smaller proportion of neurons showed opposite preferred direction (Fig. 3.4a; difference in direction preference ≥ 135 deg, 37%). These data show that, with stimuli presented to only one eye, AM bars elicited DS responses that in about half of the neurons matched the motion tuning obtained with drifting gratings.

The inversion of direction preference between AM and drifting gratings found in a fraction of neurons might depend on the specific parameters of the AM presentation, in particular the spatial offset and time interval between the two consecutive bars. This phenomenon is known from human psychophysics, whereby apparent motion can lead to the perception of opposite directions, depending on stimulus parameters (Bours et al., 2009). At the level of individual cells in the context of these experiments, the inversion of direction preference might in principle arise from the specific way AM stimuli stimulate the cell's RF, which would depend on both the specific spatiotemporal properties of the RF and the AM stimulus parameters, such as time interval, bar size, luminance polarity and location relative to ON/OFF subfields of the cell's RF (Duijnhouwer and Krekelberg, 2016). Note that in the experiments reported here, only the position of the stimuli was varied, while the other parameters remained constant (time interval, bar size, brightness).

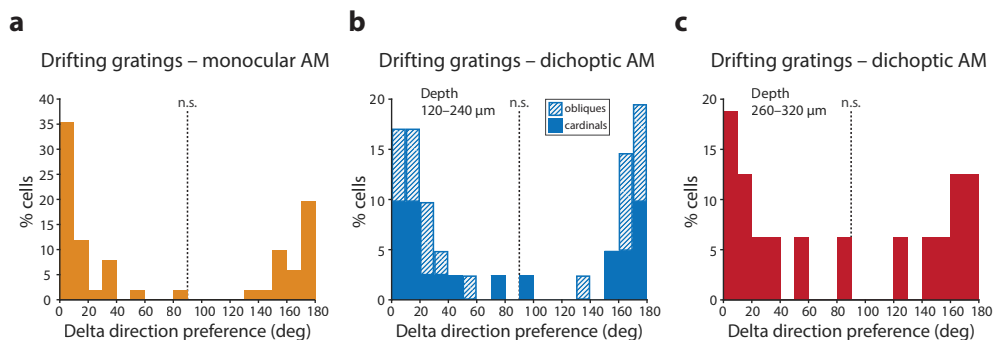


Figure 3.4 | Comparison of direction preferences between drifting gratings and apparent motion bars. **a** | Distribution of differences in direction preference between drifting gratings and monocular AM calculated for each neuron individually. Binomial test, $p = 0.16$. **b** | Distribution of differences in direction preference between drifting gratings and dichoptic AM. Only neurons located in upper L2/3 (cortical depths 120–240 μm) are included ($n = 41$ neurons, across 8 imaging planes in 6 animals). Neurons with preferences for cardinal ($n = 21$) and oblique ($n = 20$) directions are plotted with different fill patterns. Binomial test, calculated pooling together cardinal and oblique directions, $p = 0.53$; binomial test for cardinal directions, $p = 0.66$; binomial test for oblique directions, $p = 0.82$. **c** | Distribution of differences in direction preference between drifting gratings and dichoptic AM. Only neurons located in lower L2/3 (cortical depths of 260–320 μm) are included ($n = 16$ neurons, across 3 imaging planes and 3 animals). Binomial test, $p = 0.80$. For each distribution in (a–c), a two-sided binomial test was used with the null hypothesis that 50% of the cells would show a difference in direction preference in the interval 0–90 deg.

3.1.3 Neuronal responses to dichoptic apparent motion

Can AM stimuli, in particular when presented in a dichoptic fashion, reproduce the direction tuning obtained with drifting gratings? When AM stimuli

are presented dichoptically, such that the first bar is presented to one eye and the second one to the other eye, the computation of direction selectivity cannot occur in the retina because each eye views only a static stimulus (Fig. 1.8d Introduction). Hence, any DS responses of V1 neurons to dichoptic AM stimuli indicate that, in these neurons, direction selectivity is generated through thalamocortical and/or intracortical circuits, independently of any retinal mechanism for direction selectivity. To examine this, I measured responses to AM bars presented in a dichoptic fashion at eight different AM directions. For one orientation, 16 different dichoptic AM combinations were possible for each of the two eye sequences (first left eye then right eye, and vice versa), amounting to 32 possible dichoptic AM combinations per orientation. For any given cell, the specific combinations corresponding to the two opposite dichoptic AM directions were determined based on the monocular AM combinations previously determined for each eye (see Materials and Methods for more details). As a result, for each neuron, two separate direction tunings for dichoptic AM were constructed, one per eye sequence (Fig. 3.3e,f). To be included in this analysis, neurons had to be (a) binocular and DS as previously defined with drifting gratings, (b) responsive to monocular AM to each eye, (c) responsive to dichoptic AM in either of the two eye sequences ($n = 118$ neurons; see Materials and Methods for more details; modest changes in one or more selection parameters did not qualitatively affect the results of this study).

The large set of diverse stimuli used here generated a complexity of multiple response types. Often, cells showed responses and direction preferences that were inconsistent across monocular drifting gratings and AM to either eye, and dichoptic AM in either eye sequence (Fig. 3.3f). To deal with this variety of responses, the analysis was further restricted to neurons showing similar direction preferences between stimuli monocularly presented to the contralateral and ipsilateral eye (drifting gratings and AM, separately; see Materials and Methods for more details). These subsampling criteria reduced the sample size to 78 cells.

In general, three different types of responses were observed in these neurons, as illustrated in Figure 3.5. First, in the response type depicted in Figure 3.5a, the example neuron shows clear DS responses to both drifting gratings and dichoptic AM bars, with similar direction tuning in both stimulation paradigms. This potentially indicates that such a neuron does not inherit DS signals from the retina, but that its directional tuning is generated via retina-independent mechanisms, i.e. through thalamocortical and/or intracortical circuits.

The second response type (Fig. 3.5b) is characterized by similar orientation tuning between stimulation paradigms, but, interestingly, opposite direction preferences. Since any contribution of retinal DS signals is excluded by dichoptic AM stimulation, the direction tuning of such a cell, though inverted, would still point toward a retina-independent generation of direction selectivity.

In the third response type (Fig. 3.5c), the orientation tuning is similar for both stimuli, but no preference for dichoptic AM direction is evident ($DSI < 0.3$), while there are clear DS responses to drifting gratings. Since such a neuron does not appear to compute stimulus direction from dichoptic AM, this response type is compatible with an inheritance mechanism of direction selectivity from the retina.

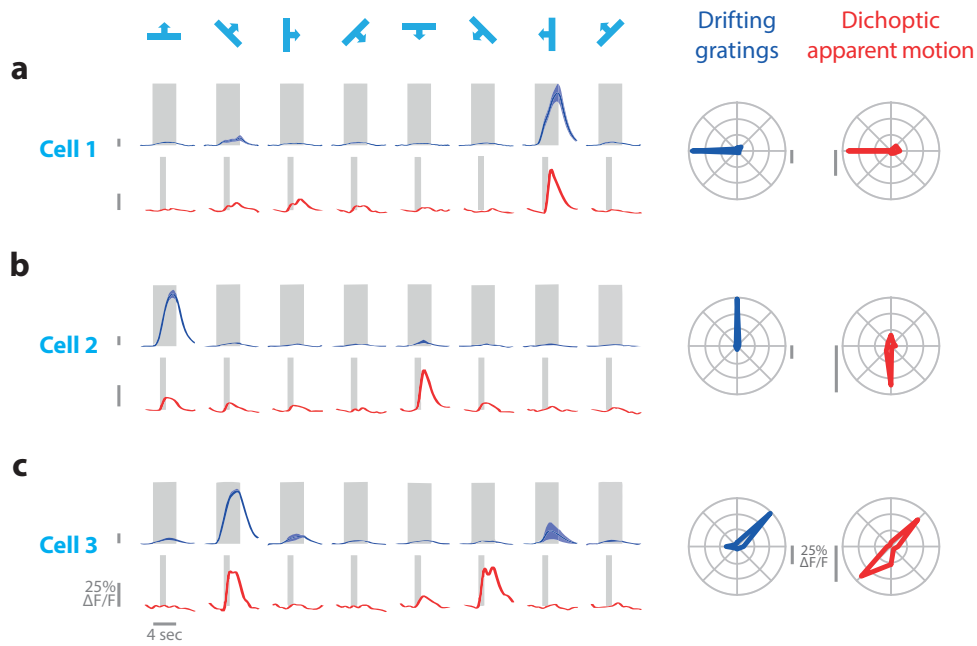


Figure 3.5 | Different types of responses to dichoptic apparent motion. Representative examples of fluorescence responses to drifting gratings (blue) and dichoptic AM bars (red) of three individual neurons (a–c). **a** | Example cell showing clear DS responses to both drifting gratings and dichoptic AM bars, with similar direction selectivity between the two stimulation paradigms. **b** | Example cell showing clear DS responses to both drifting gratings and dichoptic AM bars, but with opposite direction selectivity between the two stimulation paradigms. **c** | Example cell showing a clear DS response to drifting gratings, but with no direction selectivity for dichoptic AM. All three example cells have direction tuning to monocular drifting gratings similar between eyes, but only the responses to the strongest eye are shown (blue). Likewise, the direction tuning to dichoptic AM is similar between the two possible eye sequences (left–right or right–left), but only the responses to strongest eye sequence are shown (red). Left panels, fluorescence time courses ($\Delta F/F_0$) in response to eight directions of drifting gratings (blue, top row of each cell) and dichoptic AM (red, bottom row of each cell). The fluorescence time courses are plotted as mean $\Delta F/F_0$ (lines) calculated across stimulus trials, with \pm SEM (shaded regions) for drifting gratings. The gray boxes illustrate the period of stimulus presentation (4 sec for drifting gratings, 1 sec for AM), with its bottom side indicating the baseline level ($0\% \Delta F/F_0$). Right panels, polar plots with mean fluorescence responses for each direction, showing the direction tuning of each cell to drifting gratings (blue) and dichoptic AM (red).

For cells showing DS responses to dichoptic AM ($DSI > 0.3$) and consistent direction preferences between the two eye sequences of dichoptic AM (first and second response type, 41/1588 neurons), the direction tuning curves obtained with drifting gratings and dichoptic AM were compared by determining preferred direction from both tuning curves independently (Fig. 3.3a,b,e,f), and calculating the difference. Between drifting gratings and dichoptic AM bars, 20 out of 41 selected cells showed a similar direction preference between drifting gratings and dichoptic AM bars (Fig. 3.4b; difference in direction preference ≤ 45 deg, 49%; binomial test, $p = 0.53$). 16 out of 41 showed opposite preferred direction (Fig. 3.4b; difference in direction preference ≥ 135 deg, 39%; binomial test, $p = 0.53$).

Four types of DS retinal ganglion cells were reported in the literature, each tuned to one of the four cardinal directions (Huberman et al., 2009; Kay et al., 2011; Rivlin-Etzion et al., 2011). Hillier et al. (2017) provided evidence that the retina-dependent form of cortical direction selectivity is biased for the horizontal cardinal axis in the posterior direction. Moreover, early in development DS responses in mouse V1 are mainly tuned to the four car-

dinal directions, and only later in development oblique directions become significantly represented (Rocheffort et al., 2011; Hoy and Niell, 2015). These findings suggest that retina-dependent and -independent mechanisms for cortical direction selectivity may be differentially recruited for computing, respectively, cardinal and oblique directions in V1. To test this, I calculated the difference in direction preference between drifting gratings and dichoptic AM stimuli separately for cardinal and oblique directions. No significant difference between cardinal and oblique axes, or across the individual directions, was found (Fig. 3.4b; cardinal directions: $n = 21$ neurons, binomial test, $p = 0.66$; oblique directions: $n = 20$ neurons, binomial test, $p = 0.82$).

Evidence from viral trans-synaptic tracing (Cruz-Martín et al., 2014) indicates that the retina-dependent circuit for cortical direction selectivity may be anatomically segregated within the retino-geniculo-cortical pathway and may specifically carry DS signals only to the superficial layers of V1 (L1 and upper L2/3). In addition, the response properties of neurons in mouse V1 can vary substantially with cortical depth, even within L2/3 itself (Kreile et al., 2011; Hoy and Niell, 2015; O'Herron et al., 2018). For example, neurons in upper L2/3 were found to be more biased for the horizontal axis than those in lower L2/3 (Kreile et al., 2011). To test whether responses to dichoptic AM stimuli might be dependent on cortical depth, I performed a subset of recordings deeper in L2/3 (260–320 μm below the cortical surface, 520 neurons in total across 3 imaging planes and 3 animals). The fraction of neurons showing DS responses to AM stimuli was comparable to that in upper L2/3 (34% lower L2/3 vs. 28% upper L2/3). The difference in direction preference between drifting gratings and dichoptic AM stimuli also showed a similar distribution to the one obtained from upper L2/3 (Fig. 3.4c; no difference in fraction of neurons with similar or opposite direction preference between drifting gratings and dichoptic AM bars, binomial test, $p = 0.80$). Note, however, the small number of neurons sampled in lower L2/3 ($n = 16$), which would call for further experiments.

The observation that V1 neurons, albeit few, show DS responses to drifting gratings as well as to dichoptic AM stimuli suggests that cortical direction selectivity is at least in part generated *de novo* through thalamocortical and/or intracortical mechanisms. At the same time, the V1 neurons found to be unselective to dichoptic AM stimuli suggest an inheritance mechanism from the retina. Therefore, these findings in principle support the hypothesis that cortical direction selectivity arises via diverse mechanisms comprising both retina-dependent and -independent circuits, in line with recent evidence (Hillier et al., 2017). However, the small sample size and the overall variety of response types generated using a large set of bar combinations, which often resulted in inconsistent direction tuning curves across eyes and specific stimulus combinations, requires caution: the interpretation of the data is in fact complicated by several factors that might explain the responses to dichoptic stimuli of individual cells, regardless of the specific mechanisms of direction selectivity potentially involved. These confounding factors will be examined in detail in the Discussion (section 4.1.1 [Complexity of responses to apparent motion](#)). Consequently, it was not possible to make definitive statements on the actual contributions of retina-dependent and -independent mechanisms for cortical direction selectivity.

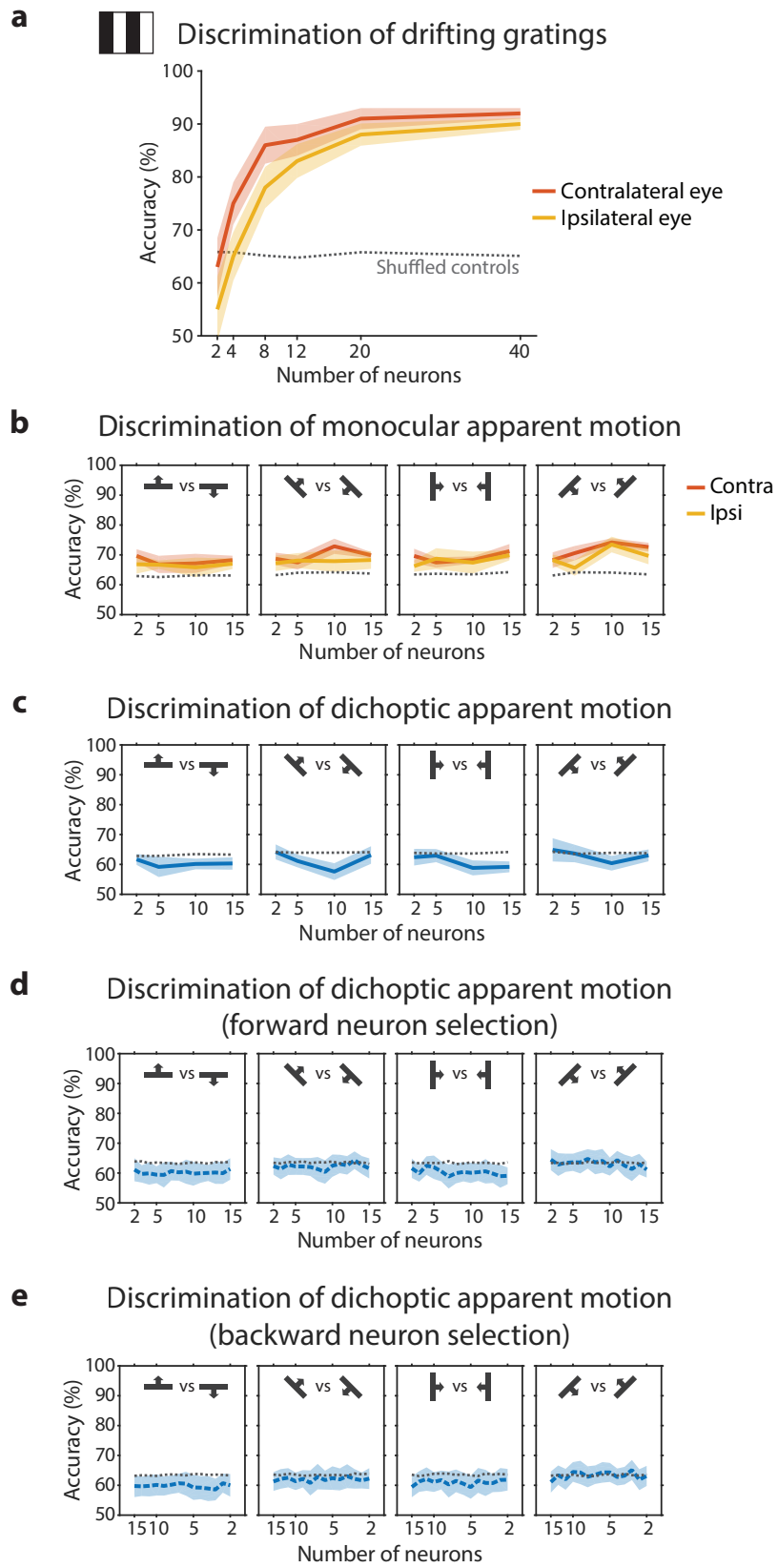


Figure 3.6 | Population decoding of drifting gratings and apparent motion stimuli. In each panel, the classification accuracy of linear SVM decoders is plotted as a function of the number of neurons used for training the decoders. **a** | Accuracy of decoders trained to discriminate between two neighboring directions of drifting gratings presented to either the contralateral (orange) or ipsilateral eye (yellow). **b** | Accuracy of decoders trained to discriminate between two opposite directions of AM bars presented monocularly to either the contralateral (orange) or ipsilateral eye (yellow). Each of the four panels shows the decoding performed the two opposite directions of a given orientation. **c** | As in (b), but showing decoder accuracy in discriminating between two opposite directions of dichoptically presented AM bars. **d** | Decoder accuracy in discriminating between two opposite directions of dichoptic AM bars, in which neurons for decoder training were progressively added to an initial population of $n = 2$, based on their contribution to classification accuracy. Note that performance does not improve significantly compared to decoders in which the neurons used for training are randomly sampled from the pool of responsive neurons, as shown in (c). **e** | Decoder accuracy in discriminating between two opposite directions of dichoptic AM bars, in which an initial population of $n = 15$ neurons was progressively depleted of neurons based on their contribution to classification accuracy. Note that also this approach, similarly to the approach used in (d), does not improve classification accuracy compared to decoders trained as in (c). In all plots, lines indicate the mean accuracy across decoding iterations, with \pm SEM indicated by the shaded regions. Dashed lines indicate 95% confidence level, calculated as the 95th percentile of the decoding accuracy after shuffling stimulus identity labels. See paragraph 2.8.12 in Materials and Methods for details.

3.1.4 Population decoding of apparent motion

The analysis performed so far assumes that AM stimuli are encoded by single neurons individually. It is conceivable, though, that V1 forms a representation of AM stimuli based on the joint activity of multiple neurons. If this is the case, a single-cell analysis might not be particularly revealing, whereas an approach based on population decoding might be more appropriate for assessing whether V1 encodes motion direction of dichoptic AM stimuli. To test this, I employed a population decoding approach based on support vector machines (SVM; Cortes and Vapnik, 1995) to classify neuronal responses to AM stimuli (see paragraph 2.8.12 in Materials and Methods for details). I trained a decoder using AM stimulus-evoked calcium activity from a population of neurons and tested the decoder's ability to discriminate between the two opposite AM directions for a given orientation. This approach assumes that decoding performance reflects the capacity of this neuronal population to encode AM direction. The dataset for each decoding session consists of single-trial responses of a group of neurons recorded within the same experiment to multiple presentations of the two opposite directions of AM stimuli. A subset of single-trial responses is used to train the decoder, to which the class identity of each trial is also provided as input (supervised classification). A distinct subset of single-trial responses, previously unused for decoder's training, is then used to test the performance of the decoder, which aims to predict the class identity of these responses.

To benchmark this approach, I verified whether decoders were able to discriminate between any two neighboring directions of drifting gratings presented to either eye (e.g. 0 versus 45 deg of motion direction). The decoders were trained with an increasing number of neurons to probe how decoding performance varied as a function of the population size. The decoders proved to effectively determine the direction of the presented grating, showing a significant accuracy already at small population sizes and progressively improving by including more neurons (Fig. 3.6a; significance level by shuffle controls).

I next examined population decoding of AM stimuli. To test whether decoders were able to extract AM direction from the joint activity of a neuronal population, decoders were initially trained using AM bars presented monocularly to each eye, and evaluated for their ability to discriminate between two opposite AM directions at a given orientation. The decoders showed a moderate but significant accuracy, with a slight overall improvement with increasing population size (Fig. 3.6b). It is also notable that the decoding accuracy was generally higher for stimuli presented to the contralateral eye, likely reflecting that binocular V1 is overall driven more strongly by the contralateral eye.

Can information about the direction of dichoptically presented AM stimuli be extracted from the joint activity of neuronal populations? The decoder's ability to predict the direction of dichoptic AM would point toward a *de novo* generation of cortical direction selectivity, via retina-independent mechanisms. To address this question, decoders were trained on dichoptic AM bars, and their ability to discriminate between two opposite AM directions was evaluated, similarly as described above for monocular AM bars. It turned out that the decoders were ineffective at determining the direction of the presented AM bars, with no difference across cardinal and oblique axes (Fig. 3.6c). Moreover, as shown in Figure 3.6c, decoding accuracy decreased with more neurons used for training. This degradation of decoder performance with larger population size hints at neurons tending to have noisy calcium signals or unreliable responses (Graf et al., 2011). These observations might be interpreted in favor of a retina-dependent mechanism as a major source of cortical direction selectivity. However, while SVM are considered to be generally accurate and robust, even when applied to sparse and noisy data, they still have important limitations when used with small datasets consisting of relatively few stimulus trials (Meyers and Kreiman, 2012; Combrisson and Jerbi, 2015; Kassraian-Fard et al., 2016). The datasets used here were rather small (~10 repetitions for each stimulus) compared to typical SVM applications (Combrisson and Jerbi, 2015) and with overall relatively low signal-to-noise. For these reasons, no convincing conclusion could be drawn from the results of the population decoding regarding the contribution of retina-dependent and -independent mechanisms for direction selectivity.

It is conceivable that only a small fraction of neurons in each dataset actually carries relevant information about the direction of dichoptic AM stimuli, but that their contribution, within a potentially noisy population of neurons, is cluttered and cannot be captured by the decoder. To test this possibility, instead of randomly sampling subpopulations of neurons, two alternative approaches were tested: (1) incrementally including neurons that, in each iteration, led to higher decoding accuracies (forward neuron selection, Fig. 3.6d); (2) initially providing the decoder with a large population of neurons and progressively removing the ones which led to lower decoding accuracies in each iteration (backward neuron selection, Fig. 3.6e; see paragraph 2.8.12 in Materials and Methods for details). Neither approach, however, significantly improved decoding, nor revealed the existence of a subpopulation of highly informative neurons encoding dichoptic AM direction. Therefore, the population decoding approach applied to these data did not prove insightful with respect to the mechanisms underlying cortical direction selectivity.

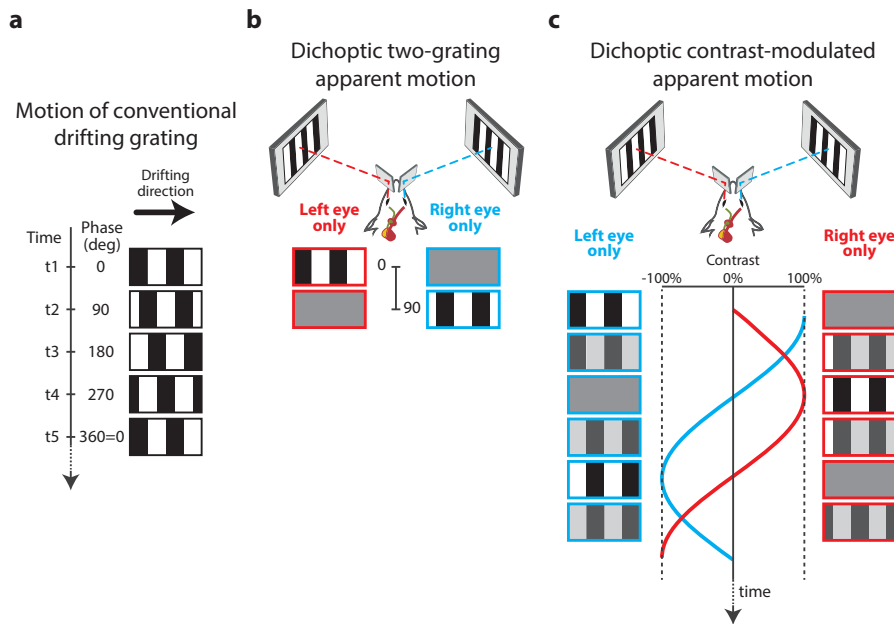


Figure 3.7 | Apparent motion stimuli based on gratings. **a** | Motion of a conventional grating drifting in the rightward direction. Five frames of the grating animation are depicted at five equally spaced time points, with the respective grating position expressed in deg phase. **b** | Dichoptic two-grating AM. A static grating is first flashed to one eye at a given phase position (e.g. 0 deg phase) and, immediately thereafter, it is flashed to the other eye with a phase offset of 90 deg phase. Owing to the circularity of gratings, the two flashed frames produce AM with rightward direction (+90 deg phase direction) or with leftward direction at three-fold speed (−270 deg phase direction), **c** | Dichoptic contrast-modulated AM. Each eye is presented with a stationary grating that gradually and continuously reverses contrast following a sinewave modulation. The gratings across the two eyes have a phase offset of 90 deg phase and their respective sinewave contrast modulations are temporally offset by 90 deg phase. Binocular fusion of the gratings produces a single sinusoidal grating with AM in one specific direction (rightward in the schematic).

3.1.5 Apparent motion stimuli based on gratings

A potential problem of the calcium imaging data obtained with dichoptically presented AM bars could be that they were generally of low amplitude and reliability, thereby limiting both single-cell and population analysis. To address this issue, I devised two different types of AM stimuli based on gratings, each trying to overcome specific weaknesses of the single, dichoptically presented bars. In the following, I will briefly report on the specific rationales and results obtained with these two types of AM stimuli, hereafter referred to as two-grating AM and contrast-modulated AM.

3.1.5.1 Two-grating apparent motion

In one type of AM stimulation, I took advantage of the fact that gratings generally evoke stronger neuronal activity than single bars. Instead of mimicking motion by subsequently presenting a static bar at two slightly offset positions (Fig. 1.8c,d Intro), a full-field grating was flashed at two different phase positions, with a spatial offset of 90 deg phase (i.e. one fourth of the grating cycle) and a temporal offset corresponding to 2 Hz (Fig. 3.7b). Owing to the circularity of gratings, motion of +90 deg phase in one direction is equivalent to motion of −270 deg phase, i.e. in the opposite direction and at three-fold speed (6 Hz). Despite this ambiguity, most neurons in V1 are more likely activated by the +90 deg phase motion, because of their average range

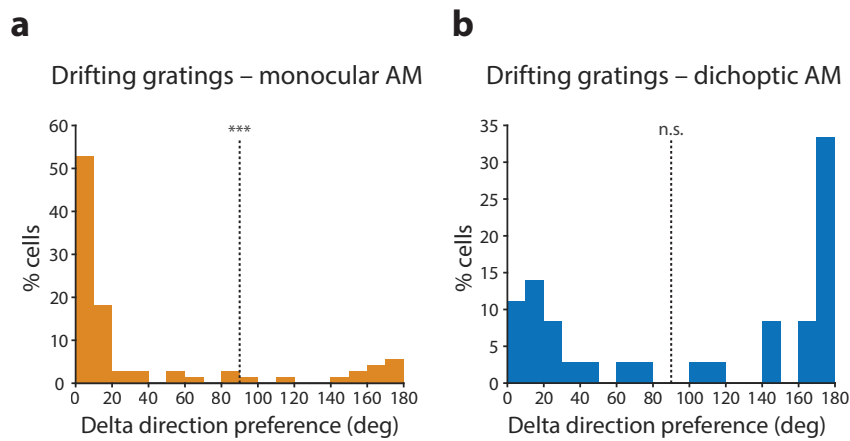


Figure 3.8 | Comparison of direction preferences between drifting gratings and two-grating apparent motion. **a** | Distribution of differences in direction preference between drifting gratings and monocular two-grating AM, calculated for each neuron individually ($n = 72$ neurons, across 3 imaging planes and 3 animals). Binomial test, $p < 0.0001$. **b** | Distribution of differences in direction preference between drifting gratings and dichoptic two-grating AM ($n = 36$ neurons). Binomial test, $p = 0.62$. For each distribution in (a–b), a two-sided binomial test was used with the null hypothesis that 50% of the cells would show a difference in direction preference in the interval 0–90 deg.

of preferences for temporal frequencies (0.5 – 2 Hz; [Marshel et al., 2011](#); [Mura-kami et al., 2015](#); for details on stimulus parameters see paragraph 2.6.6 in Materials and Methods).

As expected, the two-grating AM evoked responses from a higher fraction of neurons than AM bars (35% with two-grating AM vs. 28% with AM bars; 615 neurons in total across 3 imaging planes and 3 animals). Under monocular stimulation conditions, a larger proportion of cells showed a similar direction tuning for drifting gratings and two-grating AM (difference in direction preference ≤ 45 deg, 76%, 55/72 neurons), as compared to neurons showing opposite preferred directions for these two stimulus paradigms ([Fig. 3.8a](#); difference in direction preference ≥ 135 deg 14%, 10/72 neurons; binomial test, $p < 0.0001$). This indicates that the ambiguity of grating phase positions did not appear to be problematic, as the +90 deg phase motion was in fact the direction most neurons were tuned to, rather than the –270 deg phase direction.

When presenting dichoptic two-grating AM, motion direction tuning was on average not preserved, as the proportion of neurons with a similar direction preference between monocular and dichoptic AM was not significantly different from the proportion of neurons showing opposite preferred direction ([Fig. 3.8b](#); similar direction preference: 36%, 13/36 neurons; opposite direction preference: 50%, 18/36 neurons; binomial test, $p = 0.62$). While not significant, there appeared to be a trend for an inversion of direction tuning in response to dichoptic two-grating AM. It is worthwhile noting that, analogously to what I have argued for the responses to AM bars depicted in [Fig. 3.5b](#), this inversion in direction tuning with dichoptic two-grating AM compared to monocular AM is, in principle, not speaking against a cortical mechanism for the generation of direction selectivity, but rather might support this circuit model. However, as observed for AM bars, the inconsistencies in direction preferences between drifting gratings and AM stimuli, shown by single neurons between eyes and/or dichoptic eye sequences (sim-

ilarly to the example response to AM bars shown in Fig. 3.3f), were rather frequent (32/68 neurons). This observation, combined with the small number of cells left after the multiple selection criteria (responsiveness, $DSI > 0.3$ to both drifting gratings and AM; see Materials and Methods for more details), does not allow to make any confident interpretation of these data. Thus, although two-grating AM evoked stronger neuronal activation than AM bars, it did not permit to provide deeper insight into mechanisms of cortical direction selectivity as compared to AM bars.

3.1.5.2 Contrast-modulated apparent motion

A second type of AM stimulation was designed with the intent to activate neurons more strongly and to circumvent the potentially major confounding effects of binocular disparity selectivity. Binocular disparity is the relative difference in image location on the two retinae of an object as viewed by the left and right eye (see section 1.1.9.7 and Fig. 1.5 in the Introduction). As it will be demonstrated below, a large proportion of neurons in the binocular region of mouse V1 are sensitive to binocular disparity, which is manifested through substantial facilitatory and suppressive effects depending on the specific interocular location of the stimuli within the left and right eye RF of each cell. Disparity selectivity of individual neurons can be assessed by using dichoptically presented drifting gratings at varying interocular phase disparities (Fig. 3.10d). Disparity-tuned neurons, like the ones shown in Figure 1.5f and Figure 3.11a, exhibit a clear response modulation upon grating phase disparities, with a peak response at a certain preferred disparity, which is characteristic for each cell.

Contrast-modulated AM is generated by presenting each eye with a stationary sinusoidal grating that gradually and continuously reverses contrast following a sinewave modulation (Fig. 3.7c). The luminance of the stimulus presented to one eye can be expressed at each point by:

$$L(x, t) = L_0 + L_0 C_0 \sin(2\pi f x + s_0) \sin(2\pi \omega t) \quad (1)$$

$L(x, t)$ is the luminance at position x and time t , with the first sinewave term describing the spatial modulation and the second one the temporal modulation; f is the spatial frequency in cycles per degree, s_0 is the initial spatial phase offset, ω is the temporal frequency in Hz, L_0 is the mean luminance, and C_0 is the luminance contrast.

The second eye is presented with a similar stationary sinusoidal grating, but with spatial (δ_S) and temporal (δ_T) modulations offset by 90 deg phase relative to the first eye ($\delta_S = \frac{\pi}{4}$, $\delta_T = \frac{\pi}{4}$):

$$\begin{aligned} L'(x, t) &= L_0 + L_0 C_0 \sin(2\pi f x + s_0 + \delta_S) \sin(2\pi \omega t + \delta_T) \\ &= L_0 + L_0 C_0 \sin\left(2\pi f x + s_0 + \frac{\pi}{4}\right) \sin\left(2\pi \omega t + \frac{\pi}{4}\right) \\ &= L_0 + L_0 C_0 \cos(2\pi f x + s_0) \cos(2\pi \omega t) \end{aligned} \quad (2)$$

Note that the grating presented to each eye shows only a periodic inversion of contrast, without any motion. A simple summation of the two eye chan-

nels, representing the integration of signals from the two eyes, produces a single sinusoidal grating with AM in one specific direction:

$$L + L' = 2L_0 + L_0 C_0 \cos[2\pi(fx + s_0 - \omega t)] \quad (3)$$

The opposite direction of the fused sinusoidal grating is generated by setting the temporal modulation offset δ_T to -90 deg phase (instead of $+90$ deg phase in the second term of Equation 2).

By dichoptically presenting the two stationary sinusoidal gratings to each eye, human observers perceive a grating smoothly drifting in the predicted direction (according to Equation 3) over a broad range of spatial and temporal frequencies (Shadlen and Carney, 1986; personal observation).

This concept can in principle be applied to individual binocular neurons: a cell preferentially activated by only one of the two possible dichoptic AM directions, and with direction preference matching that observed with conventional drifting gratings, likely derives its direction selectivity from a retina-independent computation.

To generate the fused AM grating of the correct direction, it is important to take into account the disparity preference of each individual neuron. In Equations 1–3, the disparity is assumed to be zero. With a cell's disparity preference of D , to produce the expected direction of dichoptic AM, the grating presented to the second eye (Equation 2) requires a spatial modulation offset of $\delta_S = \frac{\pi}{4} - D$ (and not just $\frac{\pi}{4}$ as in the first term of Equation 2) to cancel out the binocular disparity tuning of the cell. Importantly, the possibility of accounting for the disparity tuning of individual neurons could provide a way of circumventing this major confounder. Note, on the other hand, that failing to accurately account for the cell's disparity preference can lead to spurious binocular fusion for that cell, up to producing the exact opposite AM direction when $\delta_S = \frac{3\pi}{4} - D$. This highlights the strong impact of binocular disparity on interpreting responses of each cell to dichoptic stimuli.

Another advantage of this type of AM stimulation is that, in contrast to AM bars and two-grating AM, stimuli are not just briefly flashed to each eye, but are continuously displayed for any amount of time set by the experimenter (4–5 seconds in these experiments). Stimulating neurons continuously and for longer periods should evoke stronger and more reliable responses, as compared with other types of AM stimulation.

To take the disparity preference of individual neurons into account, contrast-modulated AM was dichoptically presented at eight different values of δ_S , ranging from 0 to 315 deg phase. With such a range of δ_S , it was thus possible to account for eight different disparity preferences. To measure the disparity preference D of each neuron, drifting gratings at eight different interocular phases were also dichoptically presented (Fig. 3.10d; for more explanations on identification and characterization of disparity-tuned cells, see section 3.2). This allowed, for each disparity-tuned cell, to constrain the analysis of contrast-modulated AM based on the respective disparity preference measured. In addition, to better cover the range of possible spatial phase combinations, contrast-modulated AM of any given δ_S was presented in one of four initial spatial phase offsets s_0 (from 0 to 135 deg phase, such that the entire grating cycle is covered, considering the contrast reversal). With gratings being displayed only in the vertical orientation at a single SF of 0.05 cpd, the AM stimulus set comprised 32 different combinations (8 values of $\delta_S \times 4$ values of s_0), plus 16 stimuli for assessing disparity selectivity

(8 interocular phase disparities \times 2 directions; for details see Materials and Methods, paragraph 2.6.6).

Contrast-modulated AM generally evoked stronger responses compared to AM bars and two-grating AM, activating a large proportion of cells (23%; 201 out of 886 neurons in total, across 4 imaging planes and 4 animals; note that only one stimulus orientation was used here, compared to four orientations for AM bars and two-grating AM). For each of the four s_0 , responses to the eight possible δ_S were plotted as a tuning curve for each responsive cell (Fig. 3.9a,b). By restricting the analysis to disparity-tuned cells only, the disparity preference D of each cell could be used to determine the two values of δ_S that, for a given cell, in principle generated the two opposite AM directions, as predicted by Equation 3 (one direction given by $\delta_S = \frac{\pi}{4} - D$, and the opposite direction given by $\delta_S = \frac{3\pi}{4} - D$). Note that the values of δ_S other than those two should in principle produce spurious binocular fusion with unclear AM direction (indicated by red question marks in Fig. 3.9a,b). Across neurons, tuning curves for δ_S were in general broad or noisy, with cells responding rather indistinctly to the different δ_S values (Fig. 3.9a,b). By manual inspection of tuning curves across all selected neurons, it was not possible to identify cells that convincingly showed a preferential activation to only one of the two possible dichoptic AM directions, with consistent responses across the different spatial phase combinations (i.e. across the four s_0), and with direction preference matching that observed with conventional drifting gratings. The example neuron in Figure 3.9c shows an example of the inconsistencies in the responses to contrast-modulated AM observed across the four values of s_0 . Thus, this visual stimulation paradigm generated a great variety of neuronal response patterns, which could not easily be interpreted as supporting one or the other mechanism for the generation of direction selectivity in mouse V1.

In an attempt to manage this complexity of responses, only the value of s_0 eliciting the strongest activation was considered for each cell and its AM direction preference was determined. The frequency of cells showing the same or opposite direction preference between contrast-modulated AM and conventional drifting gratings was then calculated. Approximately half of these neurons (35/65 neurons) showed a similar direction preference between contrast-modulated AM and conventional drifting gratings, while the other half showed opposite direction preferences for the two stimulations, with no significant bias (30/65; binomial test, $p = 0.62$). A separate analysis including neurons preferring either leftward or rightward direction produced comparable results (data not shown). Altogether, the results obtained with contrast-modulated AM might be in principle interpreted against a *de novo* generation and in support of an inheritance from the retina for cortical direction selectivity. However, the complexity and potential pitfalls of this AM stimulation type, along with the overall inconsistency of the evoked responses, demand particular caution such that no clear statement could be made.

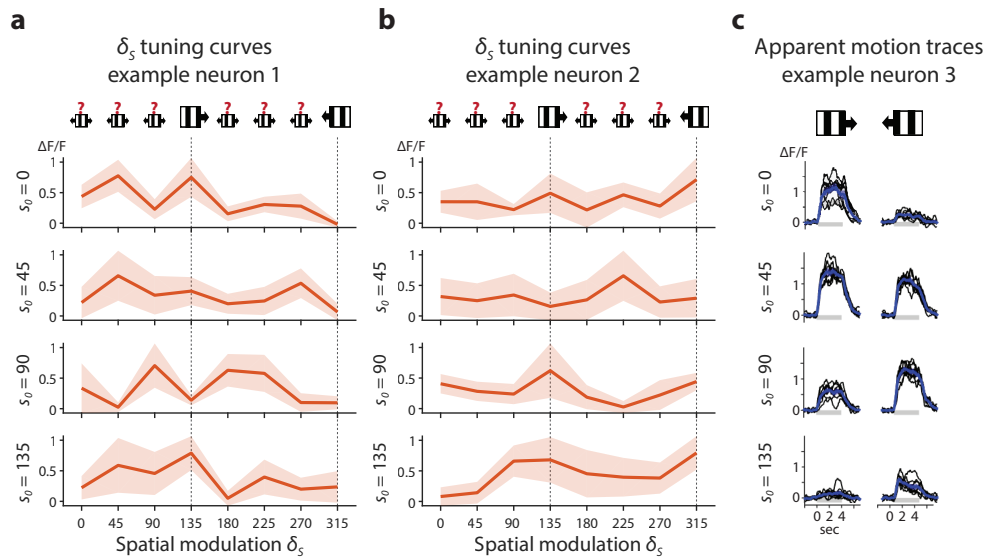


Figure 3.9 | Complexity of neuronal responses to contrast-modulated apparent motion. **a,b** | Tuning curves for dichoptic contrast-modulated AM of two example neurons with preference for rightward motion as measured with conventional drifting gratings. The mean fluorescence response across stimulus trials is plotted in function of the eight values of spatial modulation offset δ_S of the contrast-modulated AM stimulus. Shaded regions indicate \pm SEM. From top to bottom, each panel shows the tuning curve for each of the four values of initial spatial phase offset s_0 of the contrast-modulated AM stimulus. Each tuning curve is shifted to have the two δ_S values producing coherent AM in the two opposite AM directions aligned at $\delta_S = 135$ deg phase and $\delta_S = 315$ deg phase (vertical dashed lines). The other δ_S values producing incoherent AM are marked with red question marks. Note that the four s_0 tuning curves of each neuron are rather noisy and do not show consistent responses across the four s_0 values. **c** | Fluorescence time courses of another example neuron in response to the two opposite dichoptic AM directions. The neuron prefers rightward motion as measured with conventional drifting gratings. Panels from top to bottom, the responses to stimuli at each of the four values of initial spatial phase offset s_0 are shown. The fluorescence time courses of single-trial responses are plotted (black lines) along with mean $\Delta F/F_0$ (blue lines). Note how the neuron's preference for AM direction varies by changing the initial spatial phase offset s_0 of the contrast-modulated stimuli, showing the complexity of responses elicited by this stimulation.

3.2 BINOCULAR DISPARITY PROCESSING IN MOUSE VISUAL CORTEX

To investigate binocular integration and disparity selectivity in the mouse visual cortex, I performed *in vivo* two-photon population imaging in three areas of mouse visual cortex, the primary visual cortex (V₁), and areas LM and RL. These three areas were selected because they overall contain the largest, continuous cortical representation of the central, binocular part of the visual field.

3.2.1 Identification and targeting of areas V₁, LM, and RL for two-photon imaging

To localize areas V₁, LM, and RL for subsequent targeting by two-photon imaging, I first employed intrinsic signal imaging combined with periodic visual stimulation to obtain retinotopic maps of the visual cortex (Kalatsky and Stryker, 2003; Marshel et al., 2011; see Materials and Methods for details). A stimulus monitor was positioned in the contralateral field of view of the mouse (Fig. 3.10a). Neural activity in V₁ and higher visual areas was evoked by an elongated bar drifting either horizontally or vertically, generating two orthogonal retinotopic maps with precise vertical and horizontal meridians. By using the established visual field representations in mouse visual cortex (Marshel et al., 2011; Garrett et al., 2014), the boundaries among areas V₁, LM, and RL could be reliably identified (Fig. 3.10b).

Next, I specifically targeted areas V₁, LM, and RL for two-photon imaging (Fig. 3.10e,f). The visually-evoked activity of individual neurons in each of these areas was measured using the genetically encoded calcium indicator GCaMP6s (Chen et al., 2013b), which was co-expressed with the structural marker mRuby2 (Rose et al., 2016). Since the baseline fluorescence signal of GCaMP6s is quite low, the structural marker provided three main benefits: (1) it facilitated the navigation through the labeled cortex and imaging planes, by enabling rapid recognition of neurons; (2) it aided image registration for correcting motion artifacts; (3) it improved the identification of neurons for drawing regions of interest from which calcium activity traces could be extracted.

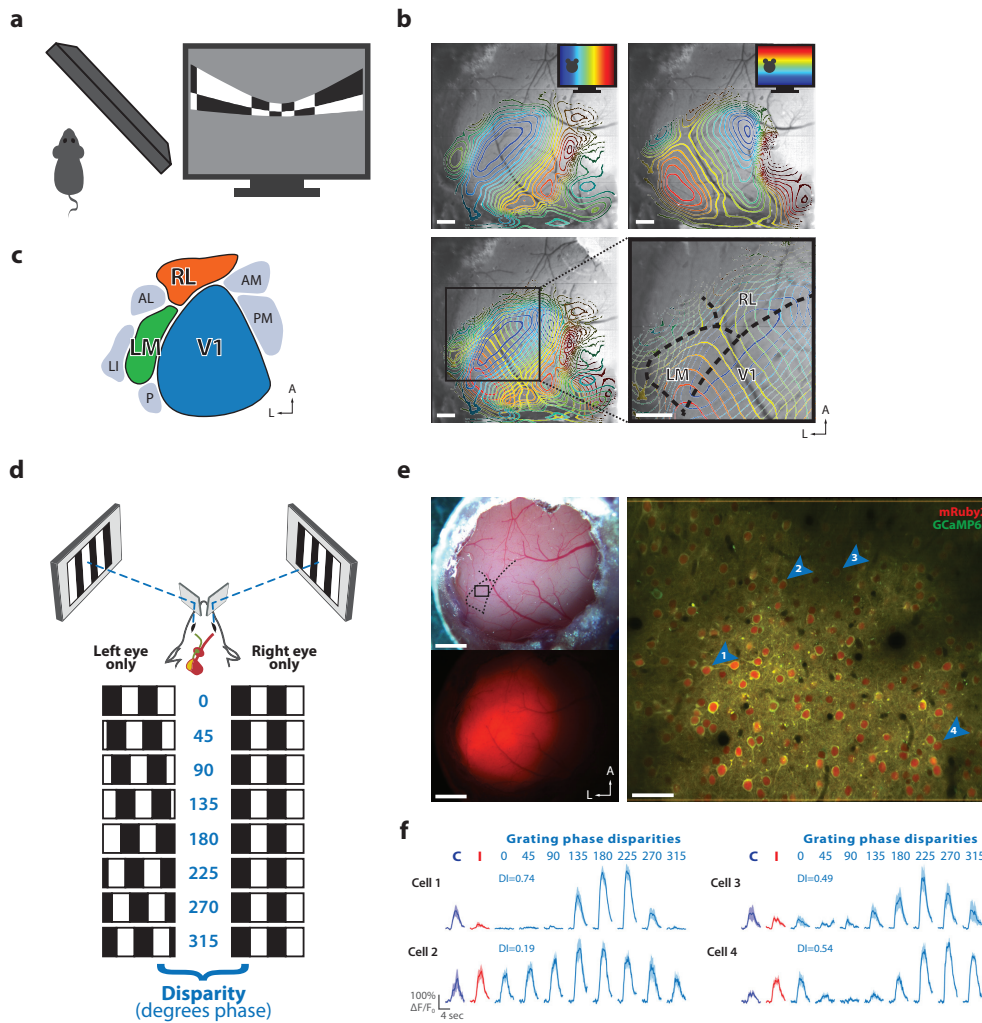


Figure 3.10 | Identification and targeting of areas V1, LM, and RL for two-photon calcium imaging. (a–c) Intrinsic signal imaging was used to localize V1 and higher visual areas LM and RL. **a** | Stimulus presentation for mapping the retinotopic organization of the visual cortex. Left, top view of the stimulation layout. Right, screenshot of the periodic bar stimulus displayed with spherical correction to stimulate in spherical visual coordinates using a flat monitor. **b** | Retinotopic maps from an example mouse. Contour plots of retinotopy are overlaid with an image of the brain surface. Contour lines depict equally spaced, iso-elevation and iso-azimuth lines as indicated by the color code (from blue to red). Top left, contour plots for azimuth. Top right, contour plots for elevation. Bottom left, overlay of azimuth and elevation contours. Bottom right, enlarged view of the cortical region where areas V1, LM, and RL are located. The boundaries between these areas are reliably delineated (dashed black line). Scale bars, 500 μm . **c** | Schematic overview of the location of V1 and several higher-order areas of the mouse visual cortex in the left hemisphere. The color code for areas V1 (blue), LM (green), and RL (orange) is used throughout the Figures. (d–f) Characterization of binocular disparity tuning with single-cell two-photon calcium imaging. **d** | Schematic illustrating the dichoptic gratings. Top, haploscope apparatus for dichoptic presentation of visual stimuli. Bottom, drifting gratings are dichoptically presented at varying interocular phase disparities. Eight equally spaced interocular grating disparities (0–315 deg phase) are produced by systematically varying the initial phase (position) of the grating presented to one eye relative to the phase of the grating presented to the other eye. **e** | Two-photon imaging of the calcium indicator GCaMP6s co-expressed with the structural marker mRuby2. Top left, image of the cranial window 5 weeks after implantation. Bottom left, epifluorescence image showing the virus bolus of expression, with fluorescence signal from mRuby2. Right, example two-photon imaging plane acquired 180 μm below the cortical surface in area LM. The image is a mean-intensity projection with fluorescence signal from GCaMP6s (green) and mRuby2 (red). The cortical location of the imaging plane is indicated by the black rectangle in the top left panel. Scale bars: left panels, 1 mm; right panel, 50 μm . **f** | Visually-evoked calcium transients ($\Delta F/F_0$) of four example neurons indicated by the blue arrowheads in (e). For each cell, the responses to monocular drifting gratings presented to either the contralateral (blue) or ipsilateral eye (red) are shown on the left. Responses to the eight interocular phase disparities of dichoptic gratings are shown on the right (cyan), along with the corresponding disparity selectivity index (DI). The fluorescence time courses are plotted as mean $\Delta F/F_0$ and SEM (lines and shaded areas) calculated across stimulus trials.

3.2.2 Binocular disparity is encoded by large fractions of neurons in areas V1, LM, and RL

Disparity tuning properties were characterized by using drifting vertical gratings displayed in a dichoptic fashion at varying interocular disparities (Fig. 3.10d,f). Eight different grating disparities were generated by systematically varying the initial phase (position) of the grating presented to one eye relative to the phase of the grating presented to the other eye, while drift direction, speed, and spatial frequency (SF) were kept constant across eyes. Note that, given the circular nature of grating stimuli, interocular disparities of gratings are also circular and are expressed in degrees of grating phase (deg phase), ranging across eight values from 0 to 315 deg phase in steps of 45 deg phase (one eighth of the full grating cycle). In addition to dichoptic gratings for assessing disparity selectivity (hereafter referred to as “dichoptic gratings”), gratings were also displayed to each eye separately (“monocular gratings”) to measure ocular dominance (OD) and compare monocular with binocular responses in individual cells. Moreover, since individual neurons in mouse visual cortex are typically sensitive to only a SF band of ~2 octaves on average (Niell and Stryker, 2008), every combination of binocular and monocular gratings was presented at each of three SFs, spaced by 2 octaves, 0.01 cycles per degree (cpd), 0.05 cpd, and 0.10 cpd. This allowed collecting a broader range of visually evoked responses from each area and examining binocular interactions in relation to the stimulus SF.

A total of 2166, 1836, and 1605 neurons were recorded in areas V1, LM, and RL, respectively (V1: 8 experiments in 6 animals; LM: 7 experiments in 7 animals; RL: 6 experiments in 5 animals). Across these neuronal populations, 15% of neurons were responsive to dichoptic gratings at 0.01 cpd and 0.05 cpd, and ~5% at 0.10 cpd (Table 1; see Materials and Methods for responsiveness criteria). Altogether, the mean response magnitude was similar across areas (Table 1). For each responsive cell, a disparity tuning curve was computed by plotting its average calcium response in function of the interocular disparity of the dichoptic gratings (Fig. 3.11a). Typically, across areas, disparity tuning curves of neurons showed a strong modulation. To quantify the magnitude of modulation caused by binocular disparity, the disparity selectivity index (DI), based on the vectorial sum of responses across disparities (Scholl et al., 2013a; see Materials and Methods for details), was calculated for each cell, with values closer to one for highly selective cells and values closer to zero for less selective cells. Cells were defined as disparity-tuned (DT) when their DI values were above 0.3.

To determine whether any of the three areas was more specialized for encoding binocular disparity, I first plotted the frequency distribution of DI over the entire populations of neurons from each area, separately for each SF (Fig. 3.11b). Notably, the majority of neurons from each area showed at least some degree of modulation to binocular disparity at the two lower SFs (> 75% of DT neurons, Table 1). Conversely, the DI distribution at the highest SF (0.10 cpd) was dramatically shifted toward zero, such that only ~20% of cells were DT at this SF across areas (Table 1). Using more stringent criteria for defining responsive cells did not result in a significant change in the DI distribution for each area and SF (data not shown), indicating that signal-to-noise issues did not affect the measurement of disparity selectivity and could not explain the low average DI observed at 0.10 cpd. By

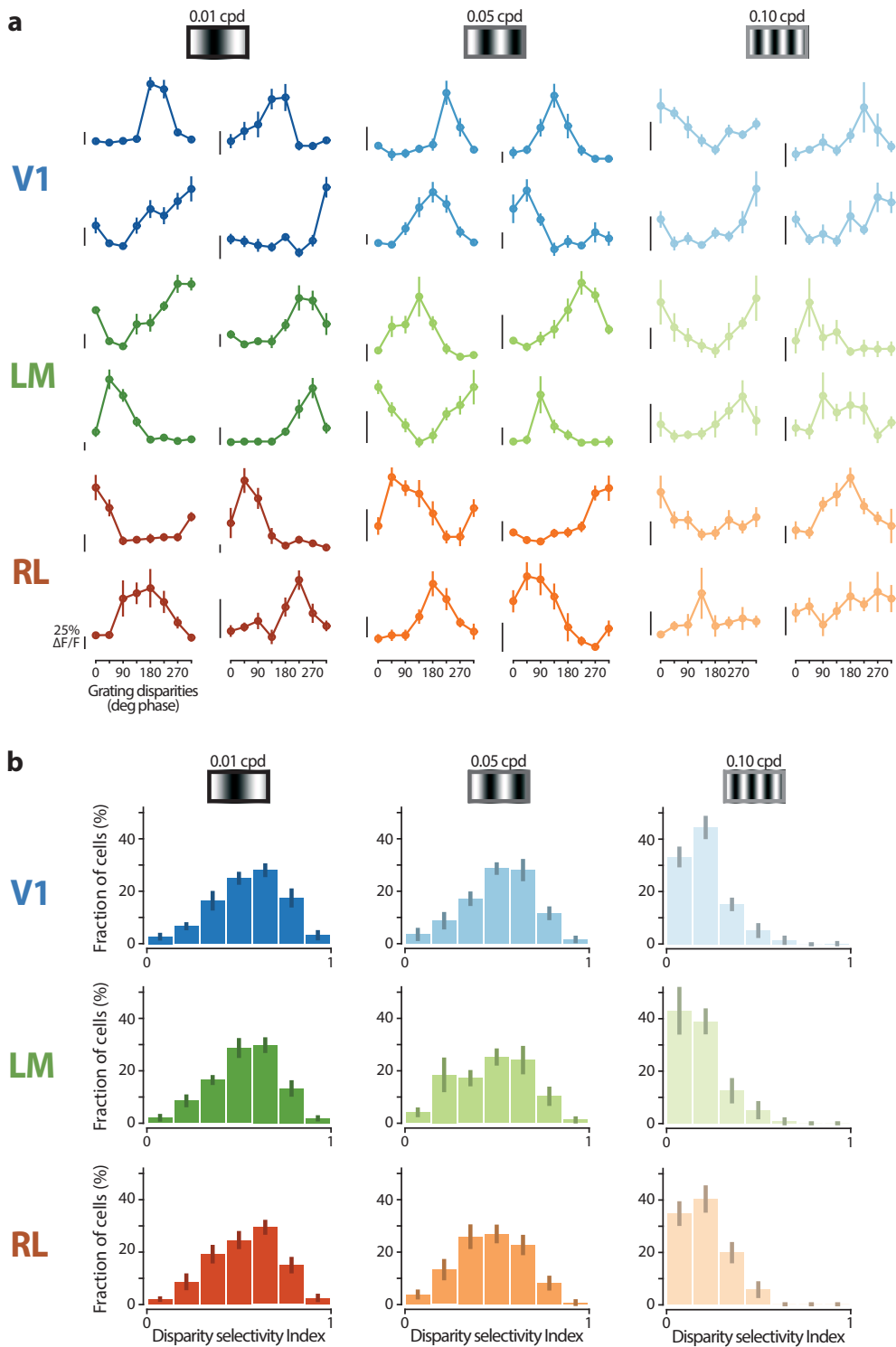


Figure 3.11 | Functional characterization of disparity-tuned neurons in areas V1, LM, and RL. **a** | Example tuning curves for binocular disparity, each from a different cell located in one of areas V1, LM, and RL as indicated by the color code. The mean fluorescence response is plotted as a function of the eight grating disparities. Error bars indicate SEM across trials. Scale bars for neuronal response indicate 25% $\Delta F/F$, with the bottom end of each scale bar indicating the baseline level (0% $\Delta F/F$). **b** | Distributions of disparity selectivity index (DI) for each area and spatial frequency. In all areas, large fractions of neurons are disparity-tuned.

Table 1 | Fractions of disparity-tuned neurons in each area.

Area	Cells (n)	Exps (n)	Mice (n)	% Responsive			Mean $\Delta F/F$			% Disparity-tuned		
				0.01 cpd	0.05 cpd	0.10 cpd	0.01 cpd	0.05 cpd	0.10 cpd	0.01 cpd	0.05 cpd	0.10 cpd
V1	2166	8	6	14.5 ± 3.8	17.2 ± 4.6	7.3 ± 2.5	0.57 ± 0.03	0.63 ± 0.03	0.42 ± 0.03	89.0 ± 1.3	86.6 ± 4.4	21.4 ± 3.2
LM	1836	7	7	15.0 ± 4.1	12.9 ± 3.8	4.8 ± 1.6	0.65 ± 0.06	0.66 ± 0.05	0.42 ± 0.05	88.4 ± 2.7	80.7 ± 4.0	23.3 ± 3.8
RL	1605	6	5	18.1 ± 3.2	12.2 ± 3.9	3.5 ± 1.1	0.55 ± 0.03	0.60 ± 0.04	0.44 ± 0.02	88.3 ± 2.1	75.8 ± 6.8	16.0 ± 4.9

Total number (n) of neurons ("Cells"), imaging planes ("Exps"), and animals ("Mice") for each cortical area. Percentage of total cells responsive to dichoptic gratings (see Materials and Methods for responsiveness criteria) at each SF (0.01 cpd, 0.05 cpd, 0.10 cpd), averaged across cells of each imaging plane, mean ± SEM across planes. Mean $\Delta F/F$ averaged across cells of each imaging plane, mean ± SEM across planes. Percentage of responsive cells defined disparity-tuned (DI > 0.3), averaged across cells of each imaging plane, mean ± SEM across planes.

comparing the population distributions of DI across areas, overall similar degrees of disparity selectivity were observed (two-way ANOVA, SF as a factor: $F_{2,54} = 185.85$, $p < 0.0001$; area as a factor: $F_{2,54} = 1.43$, $p = 0.248$; interaction SF and area: $F_{4,54} = 0.41$, $p = 0.799$). In addition, all three areas showed continuous DI distributions, indicating a continuum of disparity tunings without pointing to the existence of any distinct subset of highly tuned cells.

These data demonstrate that binocular disparity processing is prominent not only in V1 (Scholl et al., 2013a, 2015), but also in higher areas LM and RL. Large fractions of neurons across the three areas encode the interocular disparity of gratings at lower SFs, with a comparable amount of selectivity across populations in the three areas. Conversely, only a minor fraction of neurons in each area encodes interocular disparities of high SF gratings.

3.2.3 Ocular dominance is similar across visual areas and is not correlated to disparity selectivity

To encode binocular disparity, a neuron is required to integrate input from both eyes, i.e. DT neurons are binocular. However, the binocularity of a neuron is conventionally assessed by measuring its ocular dominance based on responses to monocular stimuli only. How are disparity selectivity and ocular dominance, which represent two different ways of describing a neuron's binocularity, related to each other? To answer this question, I first computed the ocular dominance index (ODI) using the neuronal responses to monocular gratings presented to each eye separately. An ODI value of +1 or -1 indicates that a cell is responding exclusively to monocular gratings presented to either the contralateral or ipsilateral eye, respectively, whereas an ODI value of 0 indicates an equal response to each eye. As previously reported (Dräger, 1975; Gordon and Stryker, 1996; Mrsic-Flogel et al., 2007), the distribution of ODI values for mouse V1 is considerably biased toward the contralateral eye (Fig. 3.12a). Neurons in areas LM and RL, for which OD measurements have not been reported yet, were also more strongly driven by the contralateral eye and showed ODI distributions comparable to V1 (ODI median, V1: 0.40, LM: 0.40, RL: 0.44; ODI mean ± SEM across experiments, V1: 0.17 ± 0.07, LM: 0.25 ± 0.06, RL: 0.21 ± 0.09; Kruskal-Wallis test for medians $\chi^2(2) = 0.84$, $p = 0.658$).

I then analyzed the relationship between ocular dominance and disparity selectivity by plotting DI values against ODI values for individual cells in each area. DT neurons homogeneously covered the entire range of ODI val-

ues, even though neurons preferentially driven by the ipsilateral eye ($ODI < -0.7$) tended to have slightly higher disparity selectivity (Fig. 3.12b; Pearson's correlation, V1: $r = -0.09, p = 0.066$; LM: $r = -0.15, p < 0.0001$; RL: $r = -0.02, p = 0.697$; one-way ANOVA with *post hoc* multiple comparisons, see Fig. 3.12b for *p* values). Notably, neurons classified as monocular by OD measurements ($ODI \approx 1$ or $ODI \approx -1$) could be DT, hence clearly reflecting integration of inputs from both eyes. This finding indicates that there is no obvious relationship between ocular dominance and disparity selectivity, in line with other studies in mice, cats, and monkeys (Ohzawa and Freeman, 1986; LeVay and Voigt, 1988; Prince et al., 2002a; Read and Cumming, 2003; Scholl et al., 2013a). This is perhaps not surprising, considering that cortical neurons non-linearly transform synaptic input into spiking (e.g. Priebe and Ferster, 2008, 2012). For instance, a neuron might receive synaptic inputs from both eyes, but only through stimulation of one of the two eyes the cell passes its spike threshold and fires action potentials. On the other hand, the contribution of subthreshold inputs from the other eye could be uncovered upon stimulation of both eyes: dichoptic gratings would lead to integration of the synaptic input from both eyes and, potentially, result in disparity-modulated responses. Such a cell would thus appear monocular according to OD measurements ($ODI \approx 1$ or -1) but binocular according to disparity measurements ($DI > 0.3$).

3.2.4 Most neurons exhibit strong disparity-dependent facilitation and suppression

To examine the integration of visual inputs from both eyes, I next compared the response amplitudes evoked by dichoptic and monocular gratings. Neurons often showed strong binocular interactions, as evidenced by the specific modulation by interocular grating disparity (Fig. 3.11a). The response at the optimal binocular disparity was generally much larger than the sum of the two monocular responses for most neurons, indicating a facilitatory effect of the binocular disparity interaction (Fig. 3.12c). At the same time, the disparity modulation also included strong suppressive binocular interactions: at the weakest grating disparity, the response was generally absent or smaller than the larger of the two monocular responses (Fig. 3.12c). To quantify the response facilitation or suppression at the most preferred or least-preferred binocular disparity, respectively, a facilitation index (FI) and a suppression index (SI) was computed for every neuron responsive to both dichoptic and monocular gratings, at the neuron's preferred SF, defined as:

$$FI = \frac{R_{binoc_peak}}{R_{monoc_contra} + R_{monoc_ipsi}}$$

$$SI = \frac{R_{binoc_null}}{\max(R_{monoc_contra}, R_{monoc_ipsi})}$$

R_{binoc_peak} and R_{binoc_null} are, respectively, the highest and weakest response evoked among the eight disparities of dichoptic gratings at a given SF; R_{monoc_contra} and R_{monoc_ipsi} are the responses to monocular gratings presented, respectively, at either the contralateral or ipsilateral eye. A value of $FI > 1$ indicates a facilitatory interaction of the eye-specific inputs in a given cell, because the peak binocular response is higher than the sum

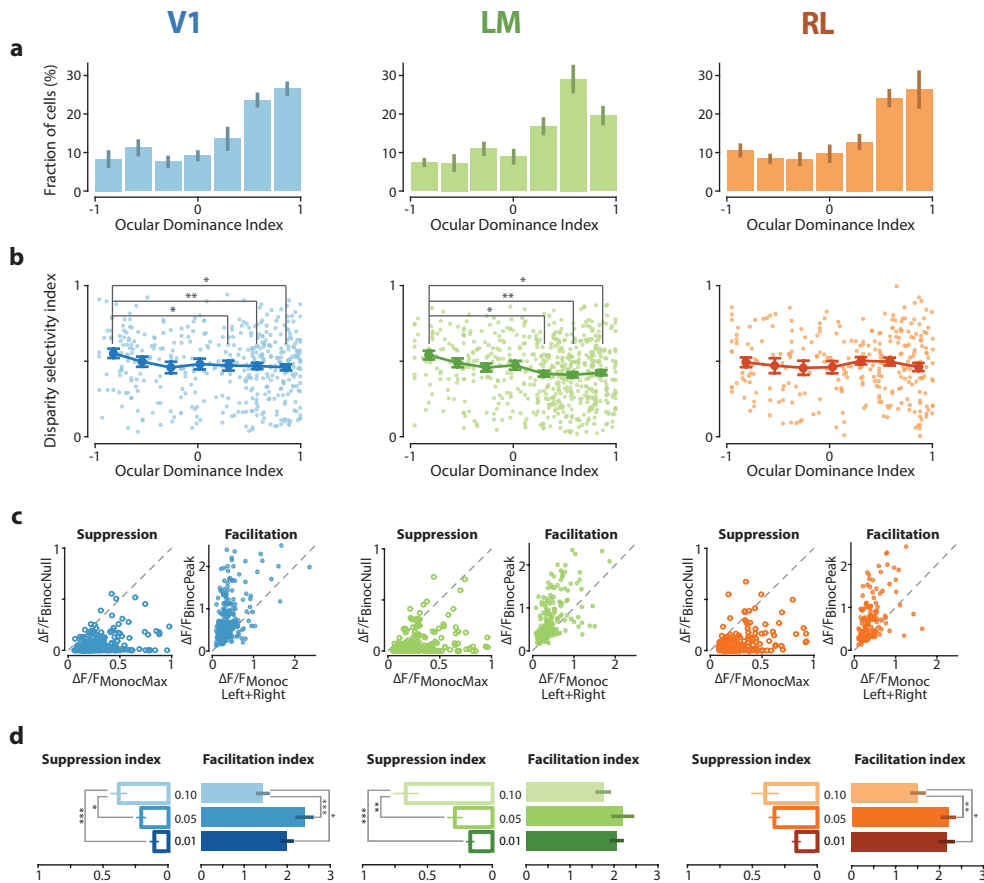


Figure 3.12 | Ocular dominance and binocular interaction of individual neurons across visual areas. **a** | Ocular dominance index (ODI) distributions in areas V1, LM, and RL, plotted as mean across experiments with error bars indicating \pm SEM. The ODI distributions are similar across areas (ODI median, V1: 0.40, LM: 0.40, RL: 0.44; ODI mean \pm SEM across experiments, V1: 0.17 ± 0.07 , LM: 0.25 ± 0.06 , RL: 0.21 ± 0.09 ; Kruskal-Wallis test for medians $\chi^2(2) = 0.84$, $p = 0.658$). **b** | Scatter graphs plotting the relationship between ODI and disparity selectivity index. Lines with error bars plot the mean \pm SEM across neurons, with individual cells indicated with circles in lighter shading. Ipsilateral-dominated neurons (ODI values closer to -1) tend to have higher disparity selectivity (one-way ANOVA followed by multiple comparisons with Bonferroni correction, * $p < 0.05$, ** $p < 0.01$). (c–d) Facilitatory and suppressive interactions upon binocular stimulation. **c** | For each area, the graph on the left plots the weakest response to dichoptic (binocular) gratings ($\Delta F/F_{\text{BinocNull}}$) against the strongest monocular response ($\Delta F/F_{\text{MonocMax}}$) for individual neurons, showing a strong overall response suppression with binocular stimulation at the least preferred (null) disparity. For each area, the graph on the right plots the strongest response to dichoptic (binocular) gratings ($\Delta F/F_{\text{BinocPeak}}$) against the sum of the strongest contralateral and ipsilateral responses ($\Delta F/F_{\text{MonocLeft+Right}}$) for individual neurons, showing a strong overall response facilitation with binocular stimulation at the preferred disparity. Only responses to gratings at the middle spatial frequency (0.05 cpd) are shown here for clarity. **d** | Bar plots of suppression and facilitation indexes for each area and spatial frequency, with mean \pm SEM across experiments (one-way ANOVA followed by multiple comparisons with Bonferroni correction, * $p < 0.05$, ** $p < 0.01$, *** $p < 0.001$).

of the two monocular responses. A value of $SI = 1$ indicates that a given cell does not exhibit any suppression of responses to dichoptic compared to monocular gratings, whereas a SI closer to 0 indicate a suppressive binocular interaction, because all binocular responses of that cell are smaller than its monocular responses. Each of the three areas exhibited on average strong facilitation and suppression at the two lower SFs (Fig. 3.12d). Interestingly, at the highest SF, neurons showed significantly weaker disparity-dependent facilitation and suppression, consistent with the poor overall disparity selec-

tivity evident at this SF. Moreover, a FI higher than 1 should in principle indicate a non-linear integration mechanism through which a given cell facilitates its response. However, it should be borne in mind that the responses measured in this study consist of the visually-evoked calcium fluorescence activity of GCaMP6s, which provides an indirect measure of the spiking activity of neurons (Hendel et al., 2008; Grienberger and Konnerth, 2012; Lütcke et al., 2013; Rose et al., 2014). Owing to the non-linear relationship between action potential firing and the GCaMP6 fluorescence signal, only the presence of facilitation or suppression can be reported, without inferring the precise linear/non-linear nature of the binocular interaction shown by a cell.

These data show that, in most neurons across the three areas, the inputs from both eyes are integrated with strong response facilitation as well as suppression as a function of binocular disparity. At high SFs, however, neurons are considerably less susceptible to binocular interactions.

3.2.5 No large-scale spatial organization for disparity tuning in the visual cortex

In the visual cortex of primates and cats, spatially organized maps for binocular disparity have been observed (DeAngelis and Newsome, 1999; Chen et al., 2008; Kara and Boyd, 2009; Goncalves et al., 2015; Nasr and Tootell, 2016). While the absence of any apparent large-scale spatial arrangement for orientation preference and OD as compared with cats and primates (see also paragraph 1.1.7.3 in the Introduction) makes it unlikely, I nonetheless tested whether the mouse visual cortex features a spatial organization for disparity preference. To examine this, a color-coded, disparity map was generated for each imaging plane, in which the hue of each cell body indicates its disparity preference (Fig. 3.13a). Inspection of these maps did not give any clear indication for a large-scale layout of DT neurons. To investigate whether any spatial organization exists on a finer scale, as it has been shown for orientation tuning (Kondo et al., 2016; Maruoka et al., 2017; Scholl et al., 2017b), I next plotted the difference in disparity preference between every pair of cells in each disparity map as a function of their respective cortical distance (Fig. 3.13b; data shown only for low and middle SF). None of the three areas showed a clear dependence of tuning similarity on cortical distance, indicating a lack of a large-scale spatial arrangement of DT cells. However, specifically at the low SF, adjacent neurons, located within 10 μm from each other, had a significantly more similar disparity preference. This suggests that DT neurons with the same disparity preference show some degree of spatial clustering on the scale of 10 μm . Note, however, that an effect of fluorescence signal contamination across adjacent cells cannot be completely ruled out, despite the neuropil correction applied to the data (see Materials and Methods, paragraph 2.7).

The spatial scale of clustering observed here for disparity is consistent with the spatial clustering reported for orientation and SF tuning (at the scale of $\sim 35 \mu\text{m}$; (Ringach et al., 2016; Scholl et al., 2017b)), and consistent with the fine-scale organization reported for orientation tuning and ocular dominance (in the range of 5–20 μm) in which neurons with similar functional properties have been shown to be arranged into microcolumns (Kondo et al., 2016; Maruoka et al., 2017).

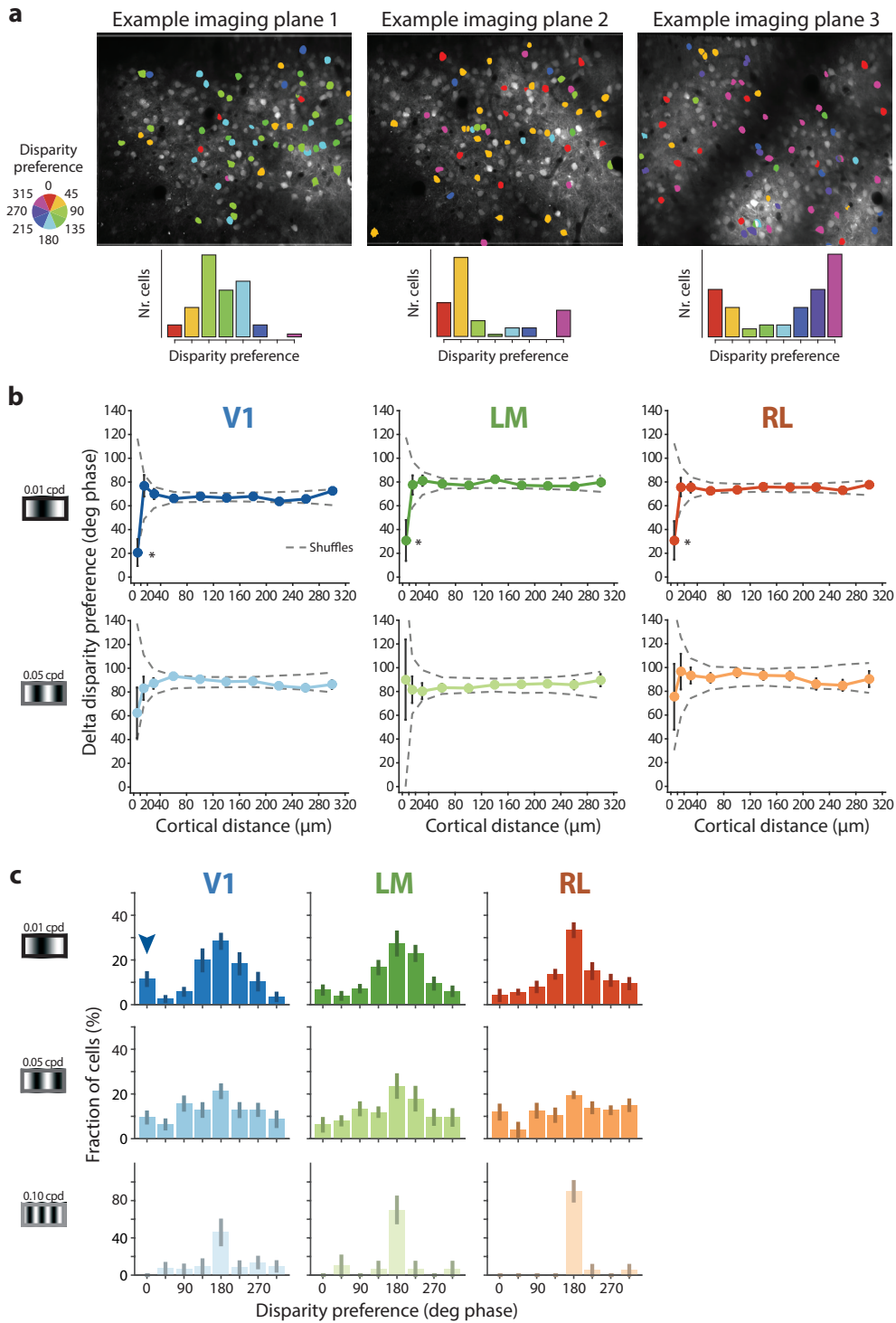


Figure 3.13 | Spatial and functional organization of disparity-tuned neurons. **a** | Top, example disparity maps from three different imaging planes, with neurons color-coded for disparity preference. Bottom, disparity preferences show non-uniform distributions, with a population peak disparity characteristic for each individual experiment. **b** | Spatial organization for disparity tuning. Difference in disparity preference between every pair of DT cells in each imaging plane plotted as a function of the cortical distance between cells. Top panels, low SF (0.01 cpd). Bottom panels, middle SF (0.05 cpd). Plot lines and error bars indicate mean \pm SEM across neurons. The dashed lines indicate the 95% confidence interval, as determined by random shuffles of disparity preferences and cell xy positions in each imaging plane (* $p < 0.05$ at the 10 μm bin of cortical distance). **c** | Peak aligned distributions of disparity preferences, averaged across experiments. The population peak was arbitrarily set to 180 deg phase. The arrowhead on the top left panel for area V1 and low SF indicates a secondary peak of cells with disparity preference at 0 deg phase.

3.2.6 Non-uniform distribution of disparity preferences in individual experiments

While there was no obvious spatial organization for disparity preference, in each individual experiment I found that some disparities were more frequently represented than others (Fig. 3.13a). I therefore analyzed the range of binocular disparities encoded by neurons in each mouse and area. Indeed, disparity preferences showed non-uniform distributions, with a population peak disparity that was characteristic for each individual experiment. This population peak disparity, though, varied over the whole range from experiment to experiment, showing no systematic relationship across experiments, animals or areas.

I consider it unlikely that the variation of apparent population peak disparity across mice reflects a true biological phenomenon. Rather, two technical factors probably contribute to it, namely (1) the positioning of the haploscope mirrors for dichoptic stimulation and (2) the position of the mouse eyes. Both factors could not be experimentally controlled with the necessary precision, in particular because the mouse's eye optical axis is very hard to determine. As such, they were likely not consistent across imaging sessions, resulting in varying alignment of the eyes from one experiment to the other and hence causing variability of the population peak disparity. It follows that the disparity preference distribution in each experiment might be related to the actual optical axes of the mouse eyes in that imaging session. For example, the population peak disparity might reflect the visual field location of retinal correspondence between eyes, i.e. a vertical meridian of zero retinal disparity. This is plausible, since studies in cats and monkeys, in which the optical axes of the eyes were determined, generally found that a higher proportion of DT neurons, measured with elongated bars or random dot stereograms, showed a preference around zero retinal disparity, whereas more convergent or divergent disparities were less represented (Barlow et al., 1967; Nikara et al., 1968; LeVay and Voigt, 1988; Prince et al., 2002b; DeAngelis and Uka, 2003).

In order to analyze the overall range of binocular disparity preferences in each area, the disparity preference distributions of individual experiments were aligned by setting the population peak arbitrarily to 180 deg phase and averaging the distributions across experiments (Fig. 3.13c). It is evident that the range of disparity preferences strongly depends on grating SF. For all areas, the distributions of disparity preferences at the lowest SF was substantially more peaked than at the middle SF, which showed a more homogeneous representation of disparities. Interestingly, the few DT neurons identified in each experiment at the highest SF had very similar disparity preferences, resulting in sharply peaked distributions. I further observed that, at any given SF, the disparity preference distributions were comparable across areas. However, specifically to area V1 and at lower SF, a higher fraction of cells with a disparity preference of 0 deg phase was present, which is the most distant disparity value from the main population peak (see arrowhead in Fig. 3.13c). Moreover, no correlation of disparity preferences with DI and FI/SI was found (data not shown).

It is worth stressing that, in these experiments, only one area at a time was recorded during each imaging session. Thus, owing to the two technical limitations pointed out above, differences in the average disparity preference

across areas, e.g. a systematic shift in the disparity distribution of one area compared to another one, could not be revealed in this set of experiments. Such differences, however, were investigated in a separate set of experiments described below.

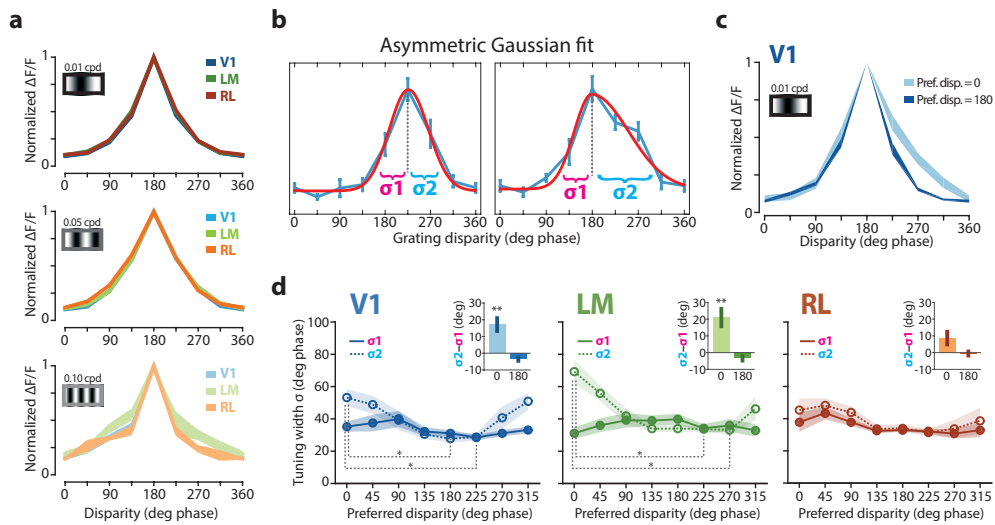


Figure 3.14 | Analysis of disparity tuning curves. **a** | Disparity tuning curves averaged across DT neurons for each area and SF. For averaging, each individual tuning curve was peak aligned to 180 deg phase and the response amplitudes normalized to the peak response. Shaded regions are \pm SEM calculated across DT neurons (DI > 0.3). **b** | Tuning curve fit with an asymmetric Gaussian function. Two examples curve fits are shown, illustrating the tuning width parameters for the left and right sides (σ_1 and σ_2). The asymmetry of a tuning curve is quantified as the difference between the two width parameters ($\sigma_2 - \sigma_1$). Left, example of a symmetric tuning curve. Right, example of asymmetric tuning curve. **c** | Disparity tuning curves averaged across DT neurons in V1 at low SF (0.01 cpd), with separate averaging for neurons with disparity preference of 180 deg phase (dark blue) and 0 deg phase (light blue). Shaded regions are \pm SEM. DT neurons with a disparity preference of 0 deg phase show tuning curves skewed to the right side of the peak. **d** | Tuning width parameters plotted as a function of the disparity preference of each DT cell. Only data at the low SF (0.01 cpd) are shown. Lines with shaded regions indicate mean \pm SEM calculated across experiment for the left (solid line) and right (dotted line) tuning width parameter. One-way ANOVA followed by multiple comparisons with Bonferroni correction, * $p < 0.05$. Insets, difference between right and left width parameters ($\sigma_2 - \sigma_1$) for neurons with disparity preference of 0 deg phase or 180 deg phase. Bar plots indicate mean \pm SEM calculated across neurons. One sample t-test against zero, ** $p < 0.01$.

3.2.7 Subsets of neurons in areas V1 and LM have asymmetric disparity tuning curves

Observing a secondary peak in the distribution of disparity preferences in V1 prompted me to analyze the tuning properties of DT neurons in more detail. Indeed, this observation might point toward the existence of a specific subset of neurons with distinct properties. Initially, I plotted the average raw tuning curves across the entire populations of DT neurons from each area (Fig. 3.14a). Overall, the three areas showed a similar sharpness in disparity tuning. Next, I fitted the disparity tuning curves of individual neurons with an asymmetric Gaussian function with separate width parameters for the left (σ_1) and right side (σ_2 ; Fig. 3.14b; see Materials and Methods for details). This function can also capture potential asymmetries in the tuning curve, which result in dissimilar values of left and right width parameters. Interestingly, the tuning asymmetry, calculated as the difference

between the two width parameters ($\sigma_2 - \sigma_1$), was dependent on the cell's disparity preference, but only at the lowest SF (Fig. 3.14d). Neurons in the primary population peak of the disparity preference distributions (disparity preference of 180 deg phase) showed symmetric tuning curves (Fig. 3.14c,d). By contrast, neurons in areas V1 and LM with a disparity preference of 0 deg phase exhibited a significant average asymmetry, such that their tuning curves were consistently skewed to the right (Fig. 3.14c,d). To further examine this observation, the asymmetry in disparity tuning was correlated with other response properties, including DI, direction selectivity, response amplitude, ODI, and FI/SI, but no correlation was found (data not shown) and no further insights were gained. While somewhat puzzling, a possible interpretation of this finding is provided in the Discussion (paragraph 4.2.3.1).

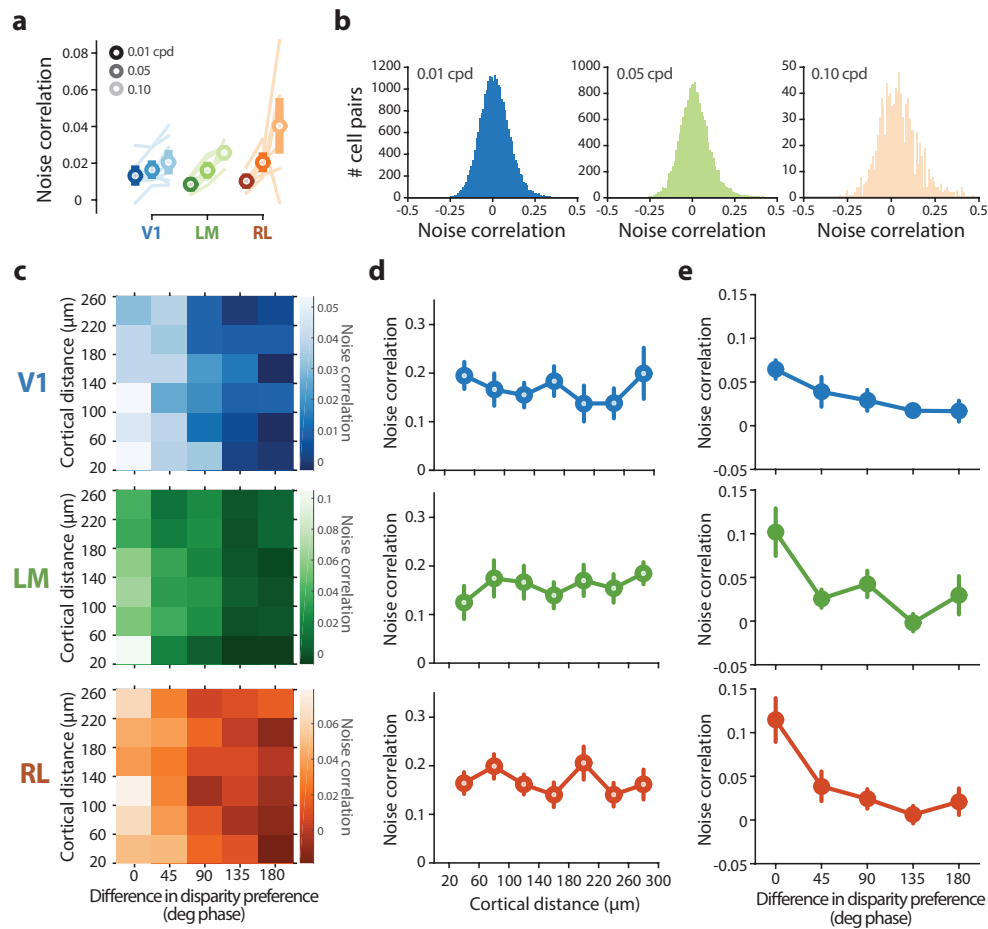


Figure 3.15 | Noise correlations are higher between neurons with similar disparity preference.

a | Pairwise noise correlations averaged across experiments. Mean across neurons of individual experiments are indicated with plot lines. **b** | Distributions of pairwise noise correlations. Only one distribution for each area at the indicated SF is shown as an example. Note the small positive tail in the distributions. **c** | Dependence of noise correlations on both cortical distance and difference in disparity preference between each cell pair. **d** | Pairwise noise correlation as a function of cortical distance between each cell pair. **e** | Pairwise noise correlation as a function of difference in disparity preference between each cell pair. For computing pairwise noise correlations, only cell pairs separated by at least 20 μm were considered.

3.2.8 Noise correlations are higher between neurons with similar disparity preference

I next exploited the so-called noise correlation analysis to infer the functional connectivity among neurons. Neurons stimulated multiple times with the same visual stimulus do not always respond with the same amplitude, but rather show a certain variability (the “noise”) in their responses. The fluctuations in response strength between pairs of neurons can be more or less correlated on a trial-to-trial basis: neurons that jointly respond above and below their respective average activation show a higher noise correlation, whereas neurons responding independently from each other across trials have near zero noise correlations. The amount of variability shared between neurons has considerable implications for neural coding, and it is assumed to reflect their anatomical connectivity (Averbeck et al., 2006; Cohen and Kohn, 2011; Ko et al., 2011; Schulz et al., 2015; Kohn et al., 2016). Generally, neurons with higher noise correlations are more highly interconnected or share more common inputs than neurons with lower noise correlations. For example, the connection probability between neurons in mouse V1 was found to increase significantly with increase in noise correlation and similarity in orientation preference, as measured by using paired recordings (Ko et al., 2011).

Over the entire populations in each area, the pairwise noise correlations were weak on average, but significantly higher than zero (Fig. 3.15a,b), in line with previous reports in the mouse visual cortex (Ko et al., 2011; Montijn et al., 2014; Rose et al., 2016; Khan et al., 2018). All distributions of noise correlations showed a small positive tail, consisting of a small number of highly correlated pairs (Fig. 3.15b). Moreover, noise correlations were progressively higher with increasing SF (Fig. 3.15a).

Are nearby neurons or similarly tuned neurons more correlated in their response fluctuations? To answer this question, for each pair of DT neurons, the value of their noise correlation was related to both their cortical distance and their disparity preference (Fig. 3.15c–e). Nearby and distal neurons showed comparable noise correlations, indicating no dependence of noise correlations on cortical distance (Fig. 3.15d). Notably, cell pairs with a similar disparity preference (< 45 deg phase) showed substantially higher similarity in their response fluctuations compared to pairs with dissimilar preference (Fig. 3.15c,e). These data suggest that neurons with similar disparity preference are more strongly interconnected or share common input.

3.2.9 Neuronal populations across visual areas effectively discriminate between grating disparities

Forming an accurate representation of binocular disparity requires the joint contribution of a population of neurons, since individual neurons alone are likely insufficient for this task, considering the narrow range of their response properties (Scholl et al., 2013a; Burge and Geisler, 2014; Kato et al., 2016). Having shown that large numbers of individual neurons in all three areas encode binocular disparity, I next investigated how much information is carried, in each area, by the joint activity of multiple neurons together, rather than by single neurons.

To address this question, I employed a population decoding approach based on support vector machines (SVM; Cortes and Vapnik, 1995), trained using the calcium transients of populations of neurons. For each area separately,

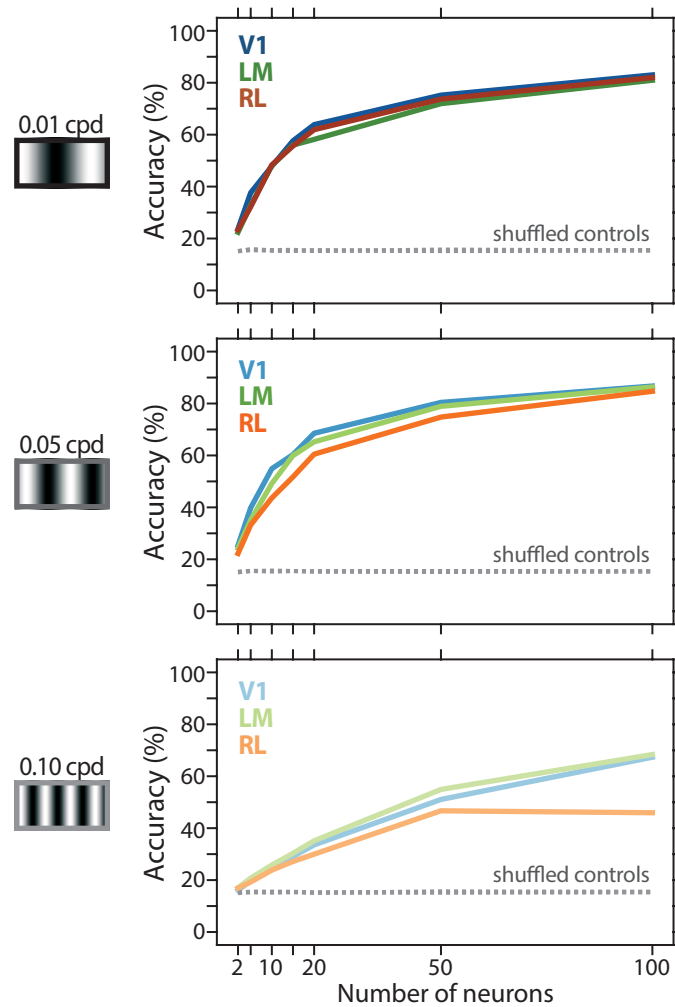


Figure 3.16 | Population decoding of binocular disparity. Accuracy of linear SVM decoders trained to estimate which grating disparity, among all eight possible disparities, was actually presented. The classification accuracy of linear SVM decoders are plotted as a function of the number of neurons used for training the decoders, with neurons of each area (color code) and at each SF independently (panels from top to bottom). Plot lines indicate the mean accuracy across decoding iterations. Dashed lines indicate the 95% confidence level, calculated as 95th percentile of the decoding accuracy after shuffling stimulus identity labels. See Methods for more details.

the SVM decoders were used to estimate, on a trial-to-trial basis, which of the eight grating disparities was actually presented to the mouse (see Materials and Methods, paragraph 2.8.12). Decoding performance is taken as a measure of how accurate the encoding of binocular disparity by neuronal populations in each area is. Across areas, decoders were able to effectively estimate binocular disparity at lower SFs, since populations with as few as two neurons allowed significantly correct prediction of stimulus disparity, with steep improvements with increasing population sizes (Fig. 3.16). In contrast, discrimination accuracy at high SF was substantially worse, though still significant. The three areas showed a similar capacity of discriminating disparity over the entire range of population sizes tested (Fig. 3.16). Moreover, a decoder built on a pseudo-population consisting of neurons pooled together from all three areas indistinctly, showed a curve of discrimination accuracy comparable to decoders trained on populations from each area separately (data not shown), thereby indicating that neurons from the different areas were interchangeable from the perspective of the decoder and hence

contributed similarly to decoding.

Together, these data indicate that populations of neurons in areas V₁, LM, and RL efficiently encode binocular disparity and can effectively discriminate between grating disparities, with a comparable accuracy across areas.

3.2.10 Characterization of disparity tuning of mouse visual areas using random dot stereograms

I found that the processing of binocular disparity is prominent and distributed across areas V₁, LM, and RL, with similar degrees of selectivities. In cats and primates, disparity processing is widely distributed across their visual system, but DT neurons in different areas show distinct response properties (Gonzalez and Perez, 1998; Parker, 2007), which were revealed by using random dot stereograms (RDS; see also Fig. 1.10b). For example, primate higher visual area MT appears to be specialized in encoding nearby visual objects, as it contains a higher proportion of neurons tuned to near disparities compared to V₁ (DeAngelis and Uka, 2003).

I set out to determine whether such specializations also exist across areas of the mouse visual cortex through a series of specifically designed experiments, in which the disparity selectivity of neurons from all three areas was characterized during the same imaging session using both dichoptic gratings and RDS (see Fig. 2.1 in Materials and Methods). Each of the three areas was sequentially imaged, characterizing neurons from one imaging plane in one of the areas and then moving to another area, acquiring at least one imaging plane per area during the same imaging session. The area sequence was randomly chosen for each imaging session and the animal's eyes were monitored to rule out any position change over the course of the recordings. Thus, a direct comparison of disparity tuning across the three areas was possible in these experiments, excluding any effect caused by varying positions of an animal's eyes from one recording session to the next.

The other key feature of the experiments presented below is that disparity tuning was probed using dichoptic gratings as well as RDS (Fig. 3.17a). RDS are cyclopean stimuli that enable, upon binocular fusion, to precisely locate the dots in depth either in front or behind the display, depending on the exact magnitude of crossed or uncrossed interocular disparity. Crucially, unlike gratings, RDS allow measuring absolute disparities, in which tuning curves are expressed as a function of visual (retinal) angles, thus avoiding the ambiguity deriving from the circular nature of gratings. Furthermore, RDS are more spatially homogeneous than gratings, without any motion and orientation component, thereby allowing to better isolate the disparity component of a cell's response. While routinely used in primates, RDS have never been employed in mice; conversely, grating stimuli have been extensively used in mice and are known to strongly activate visual cortical neurons, whose tuning properties in response to these stimuli are well characterized (Niell and Stryker, 2008; Andermann et al., 2011; Marshel et al., 2011; Roth et al., 2012; Allen Brain Observatory, 2016). In addition, differently from the experiments described above, dichoptic stimulation was achieved employing eye shutter goggles (Fig. 3.17b). The use of a single display monitor for both eyes, as compared to using two haploscope mirrors and two monitors, simplified stimulus presentation and resulted in more consistent stimulus positions relative to the mouse eyes across experiments, overcoming the technical limitation of the previously used dichoptic apparatus.

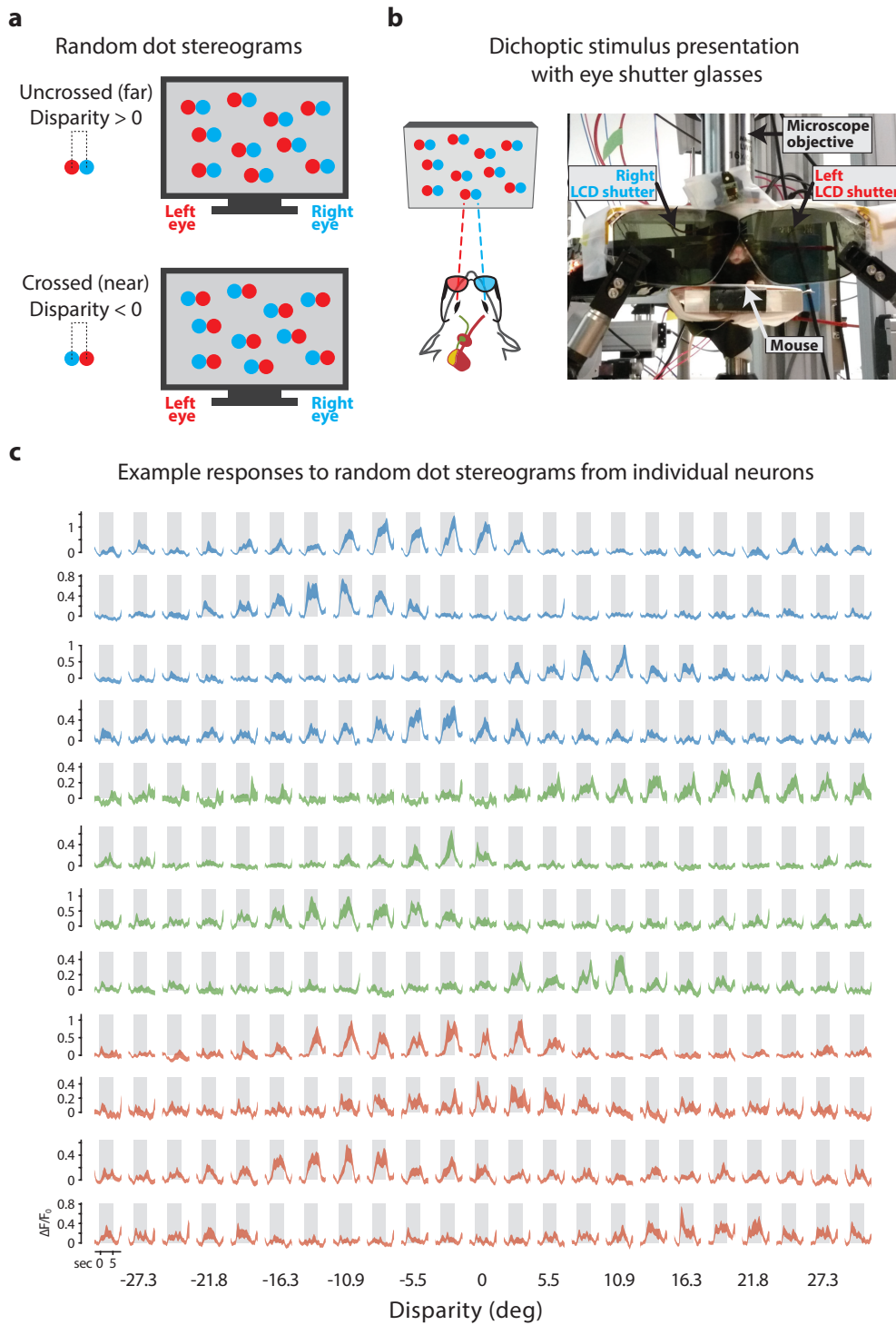


Figure 3.17 | Characterization of disparity tuning of mouse visual areas using random dot stereograms. **a** | Random dot stereograms (RDS) for assessing binocular disparity selectivity. RDS stimuli are pairs of images, one for each eye, consisting of a pattern of dots with randomly assigned positions. The same pattern of dots is displayed to each eye, introducing a certain horizontal displacement between left and right eye dots to produce binocular disparities. Each RDS stimulus is presented for 5 sec, during which a new random pattern of dots is displayed every 0.15 sec. Top, positive horizontal displacements cause binocular disparities equivalent to far object distances. Bottom, negative horizontal displacements cause binocular disparities equivalent to near object distances. **b** | Dichoptic presentation of stimuli through eye shutter goggles. Left, schematic of the dichoptic presentation of RDS stimuli through eye shutter goggles. The red-cyan color code illustrates only the eye specificity of the dots; in reality, dots are displayed all in white on a gray background. Right, front view of a mouse with eye shutter goggles, head-fixed under the microscope objective for two-photon imaging. **c** | Example calcium traces ($\Delta F/F_0$) in response to RDS stimuli of twelve different neurons, four from each area (V1, blue; LM, green; RL, orange). Shaded regions are \pm SEM calculated across stimulus trials (8–10 repetitions).

3.2.11 Area RL contains more near-tuned cells compared to V1 and LM

A total of 3304, 3696, and 4084 neurons were recorded in areas V1, LM, and RL, respectively, across 13 separate imaging sessions, in which at least one imaging plane in each of the three areas was acquired (number of imaging planes in V1: $n = 11$, LM: $n = 13$, RL: $n = 15$; 5 animals; see also Fig. 2.1 in Materials and Methods). RDS activated $\sim 20\%$ of neurons in each area, generally evoking weaker and less reliable responses than drifting gratings ($\Delta F/F$ in response to RDS, mean \pm SEM across neurons, V1: 0.34 ± 0.05 , LM: 0.31 ± 0.05 , RL: 0.28 ± 0.06). Notably, a fraction of neurons exhibited clear tuning curves in response to RDS, with reliable activation to a limited range of disparities (Fig. 3.17c). The tuning curves obtained with RDS were fit with an asymmetric Gaussian function, similarly as described above for grating stimuli. Since the calculation of the disparity index DI is based on a circular metric, but RDS stimuli are not, the DI could not be computed for disparity curves obtained with RDS (unlike those based on gratings). Cells were defined disparity selective to RDS when at least 50% of the tuning curve variance (R^2) could be accounted for by the model fit. Approximately 20% of the neurons that responded to RDS were defined as DT, showing clear disparity selectivity, with comparable proportions across areas (mean \pm SEM across experiments, V1: $22.5\% \pm 4.5\%$, LM: $19.4\% \pm 4.2\%$, RL: $16.9\% \pm 3.5\%$; Fig. 3.17b).

Are DT neurons in the three areas investigated tuned to different disparities? For each DT neuron, its disparity preference was calculated by taking the disparity value corresponding to the peak of the fitted tuning curve. Remarkably, clear differences in the ranges of disparities covered by each area became evident by plotting the disparity preferences of all individual DT neurons from each area (Fig. 3.18b). Although the distributions of disparity preferences in all three areas were biased toward near (negative/crossed) disparities, area RL contained a significantly higher fraction of neurons tuned to near disparities compared to areas V1 and LM (Fig. 3.18b; mean \pm SEM across neurons, V1: -3.15 ± 0.63 deg, LM: -3.88 ± 0.53 deg, RL: -7.24 ± 1.00 deg; median across neurons, V1: -3.7 deg, LM: -4.5 deg, RL: -5.6 deg; one-way ANOVA, $F_{2,458} = 7.29$, $p = 0.00077$; V1 versus LM: $p = 1$; V1 versus RL: $p = 0.00056$; LM versus RL: $p = 0.0066$, Bonferroni correction for multiple comparisons). The over-representation of near disparities in area RL compared to V1 and LM was also evident by plotting the disparity preference averaged across neurons of each imaging plane, showing a consistent trend across animals and imaging sessions (Fig. 3.18a; mean \pm SEM across experiments, V1: -3.37 ± 1.24 deg, LM: -3.75 ± 0.76 deg, RL: -7.62 ± 0.95 deg; one-way ANOVA, $F_{2,20} = 4.36$, $p = 0.0268$; V1 versus LM: $p = 1$; V1 versus RL: $p = 0.0358$; LM versus RL: $p = 0.0694$, Bonferroni correction for multiple comparisons).

Therefore, these data show that area RL is specialized for encoding binocular disparities corresponding to nearby visual objects.

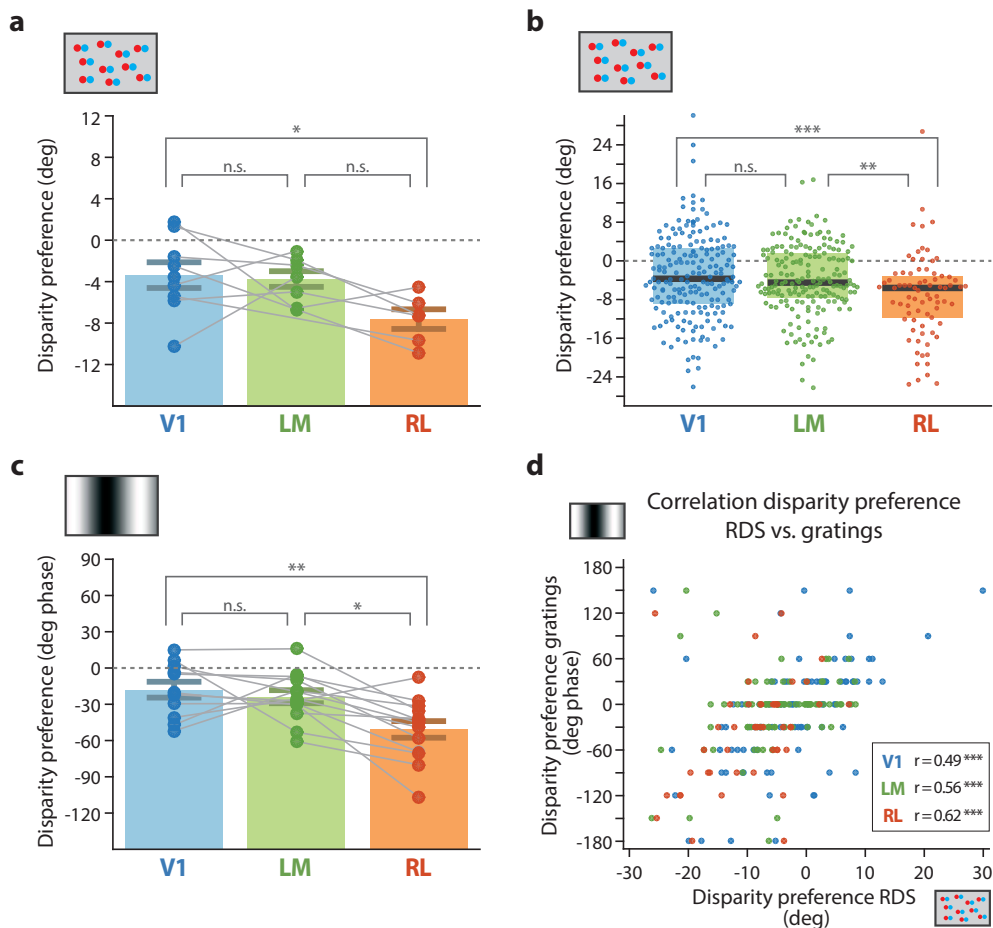


Figure 3.18 | Area RL contains more near-tuned cells compared to V1 and LM. **a** | Disparity preference measured with RDS, averaged across neurons of each imaging plane. Bar plots with error bars indicate the mean \pm SEM calculated across imaging planes. Individual data points indicate the mean disparity preference calculated across neurons of each imaging plane. The gray lines connect imaging plane data points acquired across visual areas during the same imaging session. Only imaging planes with at least $n = 5$ DT neurons are shown and were used for averaging (number of imaging planes used for averaging, V1: $n = 9/11$, LM: $n = 8/13$, RL: $n = 6/15$; 5 animals). Mean \pm SEM across experiments, V1: -3.37 ± 1.24 deg, LM: -3.75 ± 0.76 deg, RL: -7.62 ± 0.95 deg; one-way ANOVA, $F_{2,20} = 4.36$, $p = 0.0268$; V1 versus LM: $p = 1$; V1 versus RL: $*p = 0.0358$; LM versus RL: $p = 0.0694$, Bonferroni correction for multiple comparisons. **b** | Disparity preference measured with RDS, averaged across neurons from all imaging planes in each area (number of DT neurons, V1: $n = 196$, LM: $n = 191$, RL: $n = 87$). Box plots indicate median \pm interquartile range. Individual data points indicate the disparity preference of each DT cell. Mean \pm SEM across neurons, V1: -3.15 ± 0.63 deg, LM: -3.88 ± 0.53 deg, RL: -7.24 ± 1.00 deg; median across neurons, V1: -3.7 deg, LM: -4.5 deg, RL: -5.6 deg. One-way ANOVA, $F_{2,458} = 7.29$, $p = 0.00077$; V1 versus LM: $p = 1$; V1 versus RL: $***p = 0.00056$; LM versus RL: $**p = 0.0066$, Bonferroni correction for multiple comparisons. **c** | Disparity preference measured with dichoptic gratings, averaged across neurons of each imaging plane. Bar plots with error bars indicate the circular mean \pm SEM calculated across imaging planes. Individual data points indicate the mean disparity preference calculated across neurons of each imaging plane. The gray lines connect imaging plane data points acquired across visual areas during the same imaging session. Only imaging planes with at least $n = 5$ DT neurons are shown and were used for averaging (number of imaging planes used for averaging, V1: $n = 11/11$, LM: $n = 13/13$, RL: $n = 13/15$; 5 animals). **d** | Correlation between disparity preference measured with RDS and dichoptic gratings, for individual neurons tuned to both stimuli. Correlation coefficient between a circular and a linear variable (Berens, 2009) (V1: $r = 0.49$, $p < 0.0001$; LM: $r = 0.56$, $p < 0.00001$; RL: $r = 0.62$, $p < 0.001$).

3.2.12 Near disparity tuning of RL cells also revealed by grating stimuli

Having observed clear differences in overall disparity preference across areas using RDS, I next asked whether similar differences were also seen with dichoptic drifting gratings. To examine this, I computed disparity tuning curves for individual neurons in response to drifting gratings, which were presented at twelve interocular phase disparities (0–330 deg phase, step size 30 deg phase), randomly interleaved along with RDS stimuli. Dichoptic gratings generally evoked stronger responses than RDS ($\Delta F/F$ in response to gratings, mean \pm SEM across neurons, V1: 0.67 ± 0.02 , LM: 0.65 ± 0.03 , RL: 0.61 ± 0.03), activating one third of cells across areas (mean \pm SEM across experiments, V1: $32.7\% \pm 2.4\%$, LM: $33.7\% \pm 2.2\%$, RL: $33.5\% \pm 2.0\%$), of which $\sim 85\%$ were DT ($DI > 0.3$). From each cell's tuning curve obtained with gratings, the disparity preference was extracted and averages across the populations of each area were calculated (Fig. 3.18c). Notably, the range of phase disparities covered by neurons in area RL is significantly biased toward negative (crossed) values compared to V1 and LM (mean \pm SEM across experiments, V1: -17.9 ± 6.6 deg phase, LM: -23.7 ± 5.4 deg phase, RL: -50.8 ± 6.9 deg phase; one-way ANOVA, $F_{2,34} = 7.39$, $p = 0.0022$; V1 versus LM: $p = 1$; V1 versus RL: $p = 0.0037$; LM versus RL: $p = 0.0136$, Bonferroni correction for multiple comparisons).

It should be borne in mind, however, that a crossed disparity of -30 deg phase is equivalent to an uncrossed disparity of 330 deg phase, owing to the circularity of gratings. Despite this ambiguity, at a SF of 0.01 cpd, neurons are more likely activated by the smaller of the two possible phase disparities (-30 deg phase rather than 330 deg phase), because the crossed phase disparity of -30 deg phase corresponds to 8.3 absolute degrees at this SF (a full grating cycle at 0.01 cpd corresponds to 100 absolute degrees), whereas the uncrossed phase disparity of 330 deg phase correspond to 91.7 absolute degrees, which is unrealistically large to be the disparity a neuron responds best to. Thus, by showing that area RL has on average a distinct disparity preference compared to V1 and LM, likely corresponding to more crossed/near values, the data obtained with dichoptic gratings corroborate the specialization of RL for near disparities observed with RDS.

Is disparity preference measured with both RDS and drifting gratings correlated? To address this, for all neurons tuned to both stimuli (V1: 2.8% , $n = 96$; LM: 2.4% , $n = 89$; RL: 1.1% , $n = 47$), the disparity preference measured with RDS was plotted against the disparity preference measured with dichoptic gratings (Fig. 3.18d). Noteworthy, the two independently measured disparity tunings were highly correlated in all three areas (correlation coefficient between a circular and a linear variable (Berens, 2009), V1: $r = 0.49$, $p < 0.0001$; LM: $r = 0.56$, $p < 0.00001$; RL: $r = 0.62$, $p < 0.001$). The fact that the results obtained with drifting gratings closely matched those observed with RDS, considering the fundamental differences between these two stimuli, strongly supports the existence of distinct representations of binocular disparity across these visual areas.

3.2.13 Is disparity tuning related to elevation in visual field?

Although the binocular regions of areas V1, LM, and RL contain similar representations of the visual field in azimuth (central/peripheral visual field), they cover substantially different amounts of the visual field in elevation (lower/upper visual field; see Fig. 1.4c in the Introduction; Garrett et al., 2014; Zhuang et al., 2017). Binocular V1 covers both the lower and the upper visual field, more or less homogeneously along the rostrocaudal axis of the cortex. The retinotopic representation of area LM covers mainly the upper visual field, approximately spanning from the horizon upward (Garrett et al., 2014; Zhuang et al., 2017). Conversely, the retinotopic representation of RL covers mainly the lower visual field, approximately spanning from the horizon downward (Garrett et al., 2014; Zhuang et al., 2017). Thus, the distinct disparity tuning of RL, as compared to V1 and LM, might be related to the different visual field representations that these areas show in elevation.

I addressed this in a preliminary experiment ($n = 1$ mouse), in which three imaging planes were recorded in the binocular region of V1, separated along the rostrocaudal axis and hence at distinct retinotopic elevations (Fig. 3.19b). During the same imaging session, two imaging planes in RL were also recorded (cortical depth of 150 μm and 180 μm , same xy location). The three imaging planes in V1, labeled $V1_{up}$ to $V1_{low}$, progressed from the upper to the lower visual field, with $V1_{low}$ corresponding roughly to the same elevation as the imaging planes in RL. The disparity tuning of individual neurons in all imaging planes were probed using dichoptic gratings. The average disparity preference of neurons in each of the three locations in V1 shifted toward more negative (crossed) disparities when moving from upper to lower visual field (Fig. 3.19c). Noticeably, the location $V1_{low}$ showed a similar disparity preference as the imaging region in area RL. While a larger sample size is needed for any definitive statement, these preliminary data suggest that disparity tuning might correlate with retinotopic elevation: neurons with RFs in the upper visual field are biased for far disparities, while neurons with RFs in the lower visual field are biased for near disparities. This interpretation is also indirectly supported by the fact that 8 out of 11 planes imaged in V1 in the experiments depicted in Figure 3.18 were at about the same location as region $V1_{up}$ in Figure 3.19b.

If confirmed by further experiments, this finding implies that the specialization of RL for near disparities might in fact result from its retinotopic overrepresentation of the lower visual field, rather than arising from dedicated, area-specific circuits. Notwithstanding, these data show a clear area-specific segregation of disparity preferences across different areas of mouse visual cortex.

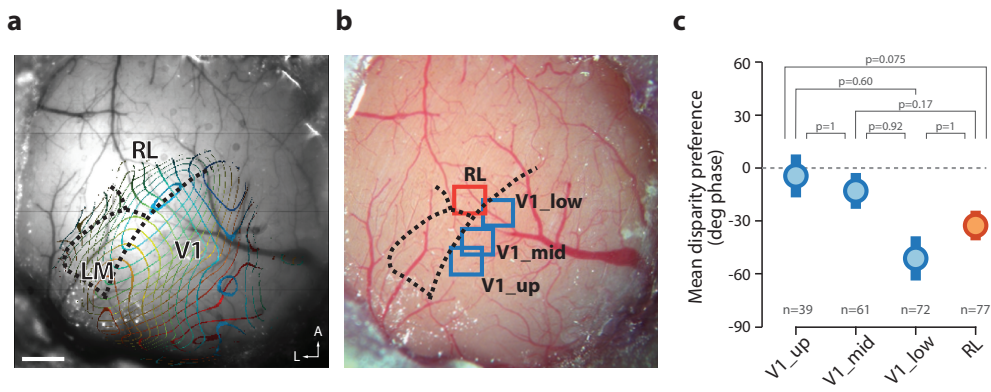


Figure 3.19 | Relation between retinotopic representation in elevation and disparity tuning. **a** | Retinotopic contour plots of azimuth and elevation overlaid with an image of the brain surface acquired with green light. The boundaries between areas V1, LM, and RL are indicated with dashed black lines. **b** | Corresponding image of the cranial window, showing the exact cortical locations of the three imaging planes recorded in V1 (blue rectangles) and the two planes in RL (same xy location, different depths below the cortical surface; orange rectangle). The three locations in V1 have different retinotopic representations in elevation, from upper (V1_up) to lower visual field (V1_low). The plane V1_low corresponds roughly to the same elevation as the planes in RL (see also Fig. 1.4 in the Introduction for more retinotopic maps of visual cortical areas). Scale bars, 500 μm . **c** | Disparity preference measured with dichoptic gratings, averaged across neurons from each imaging plane. Shaded circles with error bars indicate circular mean \pm SEM calculated across neurons. Neurons from the two imaging planes in RL were analyzed together. One-way ANOVA, $F_{3,245} = 2.87$, $p = 0.0369$, followed by multiple comparisons with Bonferroni correction (p values and number of cells indicated in the panel).

3.2.14 Two-photon imaging and dichoptic stimulation in the awake mouse

Retinal disparities are not only determined by the distance of visual objects, but they are also directly related to the position of the eyes. For this reason, eye position needs to be carefully controlled and monitored when investigating binocular disparity, by performing experiments on anesthetized and paralyzed animals, or with subjects (monkeys or humans) that can keep their eyes immobile by actively fixating on a certain point. Even though mouse eyes do not seem to be involved in coordinated vergence movements (Wallace et al., 2013; Meyer et al., 2018) and, especially in head-fixed animals, show rather limited movements (Keller et al., 2012; Wallace et al., 2013), controlling eye position is still of particular concern. For this study, mice were kept under anesthesia, and their pupils were monitored to rule out any effect due to eye movements on measurements of disparity. Nevertheless, it is of interest to test whether disparity selectivity could also be characterized in awake mice, and how disparity response properties of individual neurons compare between the awake and the anesthetized condition.

To start exploring these questions, I performed two-photon imaging in a preliminary experiment in the awake mouse ($n = 1$). The animal was head-fixed on top of an air suspended Styrofoam ball, allowing the mouse to run during stimulus presentation and data acquisition (Dombeck et al., 2007). Crucially, despite the animal being awake, the eye shutter goggles could be accurately positioned and appeared to be tolerated by the mouse, making dichoptic visual stimulation possible during awake recording. Two-photon imaging was specifically targeted to neurons in areas V1 and RL that were previously recorded under anesthesia 21 days earlier. The structural marker mRuby2 enabled confident re-identification of the same neurons between

the awake and anesthetized imaging sessions (Fig. 3.20a).

Disparity tuning of individual neurons was characterized using RDS, with the same stimulation protocol used in the anesthetized and awake condition. Responses in the awake state were substantially stronger compared to the anesthetized state, activating a higher fraction of neurons and with larger calcium transients on average (data not shown). The number of DT neurons identified in the awake state was remarkably higher (percentage DT neurons out of responsive neurons in awake, V1: 77%, RL: 67%, compared to ~20% in anesthetized).

Fig. 11b illustrates the comparison of responses to RDS between the anesthetized and the awake state for three different neurons. Noticeably, the disparity tuning curves were consistent between states, even though responses in the awake state were larger and more reliable for many cells. The consistency of the average tuning curves for individual cells, along with the consistency of responses across individual stimulus trials, indicate that eye movements of the awake animal did not particularly affect measurements of disparity tuning. Furthermore, the disparity tuning curve of the third example neuron in Figure 3.20b clearly identifies, in the awake recording, a so-called “tuned inhibitory” cell (see also Fig. 1.11a in the Introduction; Poggio et al., 1988; Cumming and DeAngelis, 2001). Strikingly, this class of DT cells, which is typically found in cats and monkeys, was very rarely encountered in the anesthetized recordings of this study (< 3% of all DT neurons), but accounted for up to ~20% of all DT neurons characterized in this experiment.

Is the over-representation of area RL for near disparities also evident in the awake mouse? The disparity preference of DT neurons identified in area RL of the awake animal was, on average, substantially biased toward negative values compared to V1, in line with the anesthetized recordings (Fig. 3.20c; two-sample t-test, $p = 6.86 \times 10^{-4}$). Even though additional experiments in awake animals are needed, this finding further supports the specialization of area RL for near disparities.

Finally, these data show for the first time that dichoptic stimulation and measurements of disparity selectivity can be reliably achieved also in awake mice.

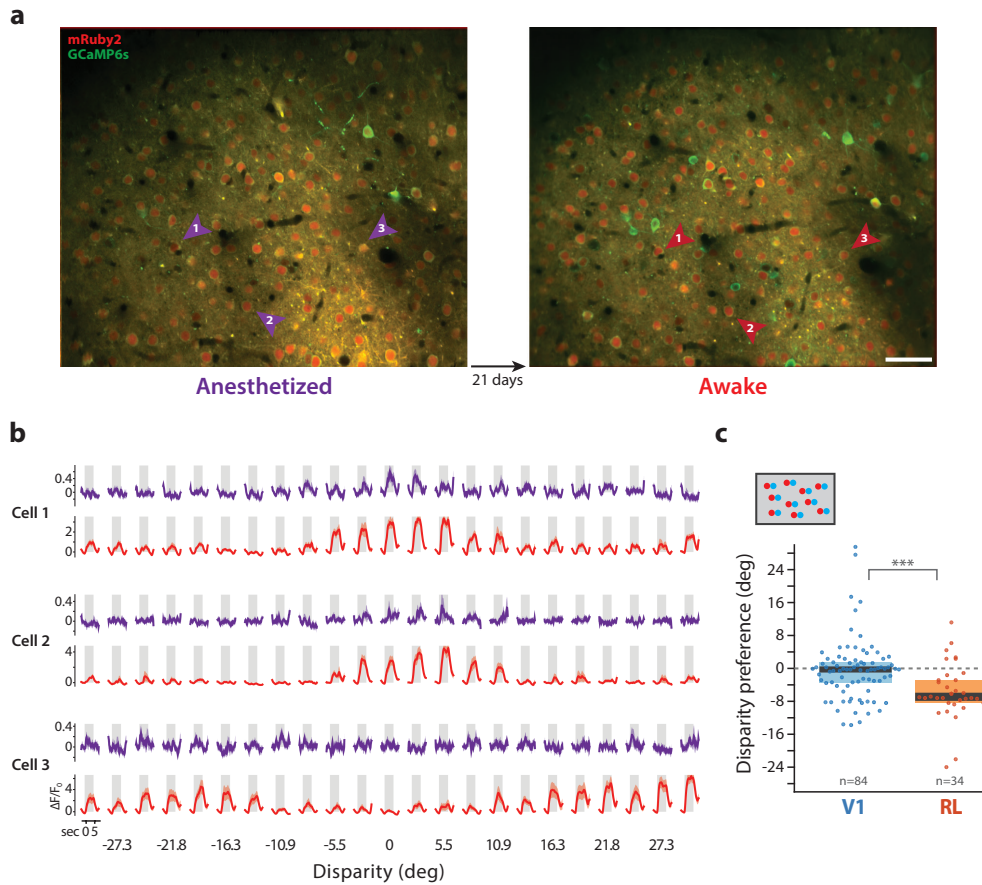


Figure 3.20 | Imaging in the awake mouse reveals strong disparity-tuned responses to RDS and near disparity tuning in RL. **a** | Re-identification of the same neurons between two separate imaging sessions. Left, frame-averaged two-photon images of an imaging plane recorded in area V1 in the anesthetized animal. Right, same imaging plane as shown on the left, acquired 21 days later in the awake animal. Scale bar, 50 μm . **b** | Comparison of visually-evoked responses between the anesthetized and the awake state. Calcium traces ($\Delta F/F_0$) in response to RDS stimuli of three example neurons, each measured in both the anesthetized (purple) and awake (red) animal. The soma location of the three cells are indicated by the arrowheads in (a). Shaded regions represents \pm SEM calculated across stimulus trials (10 repetitions). **c** | Disparity preference measured with RDS, averaged across neurons from each imaging plane recorded in area V1 and RL (number of DT neurons, V1: $n = 84$, RL: $n = 34$). Box plots indicate median \pm interquartile range. Individual data points indicate the disparity preference of each DT cell. Two-sample t-test, *** $p = 0.00069$.

4 | DISCUSSION

4.1 ORIGIN OF DIRECTION SELECTIVITY IN MOUSE VISUAL CORTEX

4.1.1 The complexity of responses to apparent motion stimuli: possible interpretations

In this study, I designed a series of dichoptic visual stimuli that distribute information about motion direction over both eyes, leaving no motion information to either eye's retina alone. Under this stimulation condition, if a binocular V₁ neuron shows DS responses, then thalamocortical and/or intracortical circuits are sufficient, in the absence of any retinal motion computation, to generate direction selectivity *de novo*.

All dichoptic visual stimuli used evoked a complex variety of neuronal responses. Consistent DS responses could be elicited only in a minority of neurons, while the rest of the cells did not show clear dichoptic DS responses. These results can lead to two possible interpretations. According to one, the dichoptic DS responses shown by those neurons, albeit few, provide evidence that at least part of the direction selectivity present in V₁ is not due to inheritance from the retina, but is generated *de novo* through thalamocortical and/or intracortical mechanisms. Concurrently, those V₁ neurons that showed unselective responses to AM stimuli support an inheritance mechanism from the retina. Thus, the results suggest that both retina-dependent and retina-independent circuits contribute to cortical direction selectivity, in line with recent evidence (Hillier et al., 2017).

Alternatively, the complexity of the multiple response types generated using a large set of diverse stimuli, along with the small sample of neurons showing dichoptic DS responses, call for a more cautious (and in my view more likely) interpretation of the data, and warrant a careful examination of potential confounders. In the following, these confounders will be discussed.

(a) Positioning of AM stimuli relative to the RFs of the recorded neurons

The bar positions used for all combinations of AM stimulation were chosen, for each experiment, based on the retinotopic mapping performed immediately before the direction selectivity measurements. However, within the ensemble RF generated online across all neurons and neuropil from that particular imaging plane, the scatter and variability of each cell's RF could lead to a variable efficacy in evoking neuronal responses, depending on the exact position of a given bar relative to the ON/OFF subfields of each neuron's RF (Fig. 4.1a).

In an attempt to circumvent this problem, in a subset of experiments I mapped in more detail the RF structure of the recorded neurons by using sparse noise stimulation with black or white patches (Fig. 4.1c). This mapping allowed computing separately ON and OFF subfields of individual neurons, for each eye's RF. However, in only ~15% of the neurons it was possible

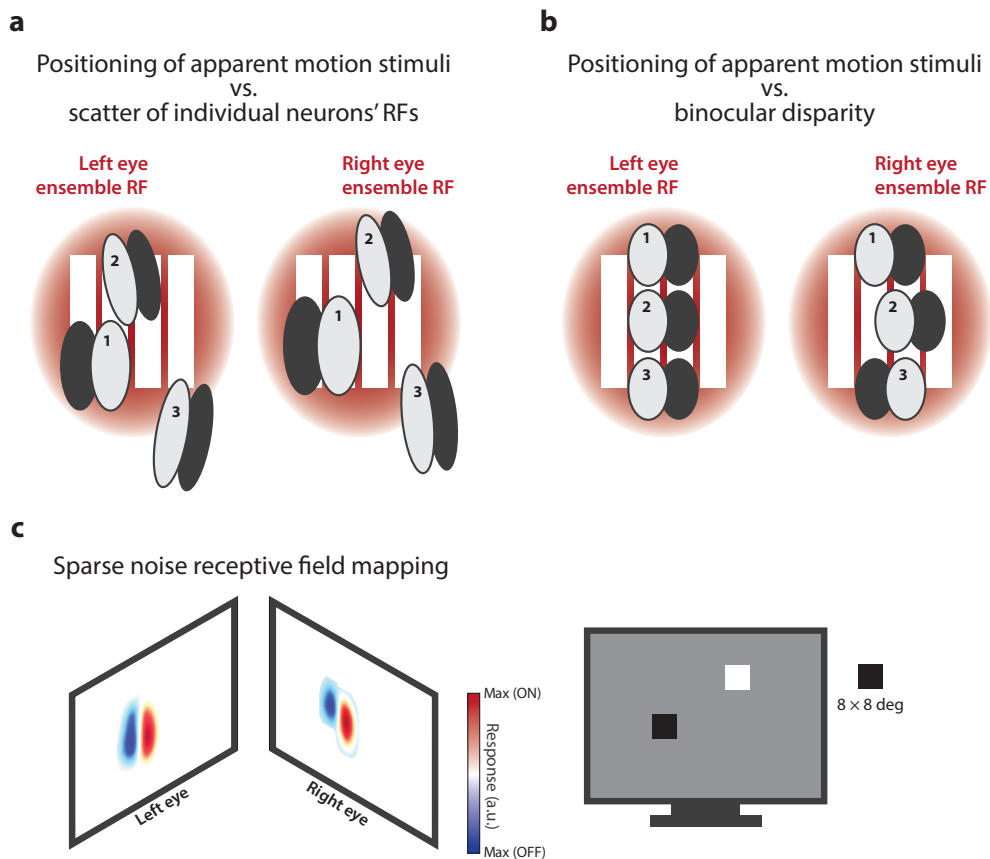


Figure 4.1 | The variability of left and right eye receptive fields of individual binocular neurons. **a** | Schematic illustrating that the variability of individual neurons' RFs contributes to the complexity of responses to AM stimuli. The RFs of three example binocular neurons are shown (denoted by the numbers 1–3), with ON/OFF subfields indicated in gray/black shading. The ensemble RF measured for each eye across all recorded neurons is depicted with a red shaded circle. Due to the scattering and diversity of subfield arrangement of RFs, individual neurons can have RFs with different spatial positions relative to each ensemble RF. Consequently, the vertical bars (white) used for AM stimulation can hit the individual RFs at different locations, thereby leading to variable efficacy in evoking neuronal responses. **b** | Schematic illustrating how binocular disparity of individual binocular neurons can affect their responses depending on the interocular position of AM stimuli. Example arrangements of left and right RFs of three different disparity-tuned neurons (denoted by the numbers 1–3). The first neuron shows the same spatial position relative to the ensemble RF and the same arrangement of ON/OFF subfields between each eye's RF. The second neuron shows a shift in spatial position between left and right eye RFs (position-shift mechanism for disparity selectivity). The third neurons shows the same RF position between eyes, but different arrangements of ON/OFF subfields (phase-shift mechanism). **c** | Mapping of ON and OFF subregions of individual neurons with sparse noise stimulation. Left, spatial maps of left and right eye RFs of an example neuron. Red regions indicate ON subfields; blue regions indicate OFF subfields. Peak intensity within each color represents the maximum response compared to baseline. Right, schematic illustrating the black or white patches presented to each eye for mapping ON and OFF subregions within RFs of individual neurons. Each stimulus consists of a black or white square flashed for 0.5 sec at a random location over a 6×6 grid.

to characterize both contralateral and ipsilateral eye RFs of a same cell, because sparse noise stimuli generally do not strongly activate cells and their RFs had to be mapped for each eye independently. This subsampling, in addition to the other selection criteria for including cells in the dichoptic AM analysis, caused the sample size to drop below statistically acceptable values. Moreover, accurate RF mapping with sparse noise required more time compared to mapping with patches of drifting gratings (> 35 min versus ~ 15

min), forcing to reduce the number of presentation trials for the following battery of AM stimuli.

(b) Binocular interactions and ocular dominance

The problem of stimulus positioning is further complicated by the fact that stimuli needed to be displayed to both eyes, thus stimulating the left and right eye RF of each cell. Each cell's activity in response to dichoptic AM bars results from the specific binocular interaction of signals deriving from its left and right eye RF, characterized by spatial, temporal and relative eye strength properties that, for the very same cell, can be different between the two eyes (Dräger, 1975; Tsao et al., 2003; Liu et al., 2010; Sarnaik et al., 2014). The ocular dominance of a cell, for instance, describes the relative activation strengths of left and right eye RF. One could expect the responses of a cell to dichoptic stimuli to be linked in some way to its ocular dominance. For example, cells with balanced relative eye strength ($ODI \approx 0$) might more consistently exhibit the same direction preference between the two possible eye sequences of dichoptic AM (first left eye then right eye, or vice versa); by contrast, an unbalanced binocular cell ($ODI \approx \pm 0.7$) might show opposite DS responses between the two dichoptic AM sequences, possibly owing to some peculiarity in binocular interaction. Attempting to take neurons' ocular dominance into account, e.g. by varying the selection criteria of cells across different ODI ranges (e.g. $-0.3 < ODI < 0.3$ or $|ODI| > 0.6$; see also Materials and Methods), did not make the interpretation of the data more straightforward. This is perhaps not too surprising, because the ODI is determined by stimulating each eye individually using full-field drifting gratings. This measure, however, does not capture key aspects of a cell's binocularity that are likely to emerge when presenting dichoptic AM bars, such as subthreshold activation, local specificities of binocular RFs (e.g. ON/OFF subfield organization) and interactions of the two eyes' inputs, which could lead to facilitatory or suppressive effects. Subsampling neurons for larger amplitudes of responses to drifting gratings and/or AM stimuli (e.g. $\Delta F/F > 1$) further reduced the sample size without making the data more interpretable.

(c) Binocular disparity

The most prominent of these binocular interactions is binocular disparity. Disparity-tuned cells have left and right eye RF that frequently do not match in terms of retinotopic position and/or arrangement of the ON and OFF subfields (for more details see Introduction, paragraph 1.3.3.1; Cumming and DeAngelis, 2001; Tsao et al., 2003; Westheimer, 2009). As a result, the specific interocular position of AM stimuli will have a strong impact on the firing of these cells (Fig. 4.1b).

Toward overcoming this problem, I specifically designed a different set of AM stimuli, i.e. contrast-modulated AM, that in principle allows to account for each cell's disparity preference. Using dichoptic contrast-modulated AM, no convincing cases of cells with clear DS responses were found, which might support the hypothesis of an inheritance mechanism from the retina as the only source of cortical direction selectivity. However, the interpretation of the responses to these AM stimuli requires caution because it strongly relies on the accurate alignment of the stimuli with respect to the measured disparity preference of each cell, and even small inaccuracies that may es-

cape the experimenter's control could result in spurious interpretations of the data. The variety of neuronal responses that was observed, with frequent inconsistencies across specific stimulus conditions, likely reflects the complexity of this AM stimulation type and does not allow ruling out that a *de novo* generation of cortical direction selectivity is actually at play.

(d) Sensitivity and non-linearity of calcium indicator

Despite the in general high sensitivity of the calcium indicator GCaMP6s (Chen et al., 2013b), it is possible that, under the imaging conditions of these experiments, weak neuronal responses (one or few action potentials) might not be reliably detected. AM stimuli were overall less effective in activating neurons than drifting gratings, often evoking only small calcium transients, some of which might go undetected. Furthermore, the relationship between action potential firing and the GCaMP6 fluorescence signal is not linear (Rose et al., 2014; Theis et al., 2016), and this non-linearity is more marked at lower firing rates. Together, the combination of a low signal-to-noise ratio and the non-linearity of GCaMP6, which tends to occur with AM bar stimulation, could affect the quantification of neuronal responses. A possible way of ameliorating this problem is restricting the analysis to responses consisting of large calcium transients (e.g. $\Delta F/F > 1$), but this approach, too, did not improve data interpretation. Jointly, these confounders might have the effect that responses to dichoptic AM stimuli do actually not result from a cell's direction selectivity only, but might also reflect different phenomena influencing the measured neuronal activity in a hardly predictable way. Thus, despite the observation of dichoptic DS responses, these arguments do not allow to confidently claim that part of cortical direction selectivity is generated *de novo* through thalamocortical and/or intracortical mechanisms. On the other hand, the overall failure of a variety of different dichoptic stimuli to elicit clear DS responses in a substantial fraction of cells is, in principle, in line with the hypothesis that most, or even all, direction selectivity in L2/3 of V1 is inherited from the retina. It is possible, though, that part of cortical direction selectivity does originate independently of any retinal mechanism, but the approach based on dichoptic presentation of AM, as specifically implemented in this study, is not able to reveal it.

Therefore, the data in this study do not allow conclusive statements but are compatible with both a retina-dependent and -independent mechanism for the computation of motion direction in V1 (Hillier et al., 2017), tentatively supporting the hypothesis that the retina-dependent computation may be the predominant mechanism.

4.1.2 Are retina-dependent and -independent mechanisms for direction selectivity functionally specific?

In the mouse retina, four types of DS retinal ganglion cells (DSGCs) were reported in the literature, each mainly tuned to one of the four cardinal directions (Huberman et al., 2009; Kay et al., 2011; Rivlin-Etzion et al., 2011) with an over-representation for the nasal-to-temporal (posterior) motion direction (Sabbah et al., 2017). As a result, if inheritance from the retina is the predominant mechanism for cortical direction selectivity and if no mixing of DS signals occurs in V1, it can be hypothesized that the direction preferences of

V1 neurons should also be biased for cardinal directions. This in fact appears to be the case: early in development, DS responses in mouse V1 are mainly tuned to the four cardinal directions and only later in development oblique directions occur more often, although they remain under-represented compared to the cardinals (Rocheport et al., 2011; Hoy and Niell, 2015). The second hypothesis that follows is that retina-dependent and -independent mechanisms for cortical direction selectivity may be differentially recruited for computing, respectively, cardinal and oblique directions in V1.

Hillier et al. (2017) found a strong over-representation of posterior motion sensitivity across L2/3 neurons. In addition, it was previously reported that DSGCs of the ON-OFF subtype monotonically increase their firing with stimulus speeds up to about 40 deg/sec. Interestingly, Hillier et al. observed that the fraction of neurons preferring the posterior direction steadily increased with stimulus speed up to the highest value tested of 40 deg/sec. Crucially, disrupting retinal direction selectivity did not alter the overall degree of direction selectivity in V1, but resulted in the abolishment of the over-representation for posterior motion, with a similar effect induced by either disrupting retinal direction selectivity along the horizontal axis only or along all axes. The reduction of the over-representation for posterior motion was much more pronounced at high speed stimuli (26.6 deg/sec and 40 deg/sec) and was not significant when probed at lower speed (10 deg/sec and 16.6 deg/sec). Thus, these findings provide evidence that both retina-dependent and -independent mechanisms contribute to cortical direction selectivity, each with distinct functional properties: a retina-dependent mechanism is responsible for cortical direction selectivity tuned for higher speed, posterior motion; part of cortical direction selectivity, more evenly distributed across direction and speed tunings, is generated *de novo* through retina-independent circuits. The specialization of retina-dependent circuits for high speed and posterior motion might reflect an adaptation of the visual system to the image statistics produced by optic flow during forward locomotion. Notably, the disruption of retinal direction selectivity did not reduce the overall number of DS neurons in V1. This is consistent with compensatory plasticity mechanisms, induced by the permanent manipulation, that increase the component of cortical direction selectivity computed through retina-independent circuits. This increase would lead to the recruitment of new DS cells that were previously untuned or to a shift in the direction preference of V1 cells that were previously tuned for the posterior direction.

In the present study, which was conducted before the publication by Hillier et al. (2017), the acute, non-invasive blocking of retinal direction selectivity using dichoptic AM, did not provide evidence for a link between DS mechanisms and specific cardinal/oblique directions. While the responses to AM stimuli were comparable across motion directions, distinguishing between the various directions reduced the statistical power of the analyses. Moreover, contrast-modulated AM stimuli were presented only along the horizontal axis, with an apparent speed of drifting equivalent to 40 deg/sec, matching the highest speed tested in Hillier et al. (2017). It is thus conceivable that the stimulus parameters used here were optimally suited to drive V1 neurons with a retina-dependent computation of direction selectivity, which however was blocked by the nature of dichoptic AM; by contrast, the stimulus parameters were less well-suited to unmask cells showing signatures of retina-independent direction selectivity. Note also that, unlike

Hillier et al. who displayed stimuli in the mouse monocular visual field on an oblique plane with respect to the animal, in the present study the stimuli were presented in the central visual field on a frontoparallel plane, such that a leftward/rightward direction could be defined along the horizontal axis, but not a posterior/anterior direction. A similar argument about stimulus speed parameters applies to the other two AM stimulation types that were used: although those stimuli were presented also at directions other than the horizontal ones, the stimulus speed used was on the high end, equivalent to ~ 32 deg/sec for AM bars, and ~ 38 deg/sec for two-grating AM. Therefore, further experiments to increase the sample size and a more careful examination of the responses to cardinal/oblique directions of motion in relation to stimulus speed would be important.

4.1.3 Are retina-dependent and -independent mechanisms for direction selectivity differentially distributed across cortical layers?

Recent evidence suggests that retina-dependent and -independent circuits for cortical direction selectivity might be part of two functionally and anatomically distinct channels in the retino-geniculo-cortical pathway, transmitting DS and unselective signals from the retina to different layers in V₁ (Cruz-Martín et al., 2014). In the study by Cruz-Martín et al. a recently developed method for retrograde trans-synaptic tracing was used, which takes advantage of the ability of the rabies virus to spread between connected neurons (Callaway and Luo, 2015). The rabies virus is specifically engineered to limit its infection across only one synapse and to induce the expression of a fluorescent marker in the cells that are presynaptic to the initially infected cell, thereby allowing the retrograde labeling of monosynaptic connections. Using this approach, Cruz-Martín et al. demonstrated the existence of a di-synaptic circuit transmitting DS signals from DSGCs in the retina to V₁, specifically to the superficial layers (L₁ and upper L_{2/3}). By contrast, unselective signals from the retina are conveyed to deeper layers of V₁ (L₄). Contrary to this finding, another study used two-photon calcium imaging of dLGN axons in V₁ observing that dLGN cells provide DS signals, likely inherited from the retina, across all cortical depths of V₁, including L₄ (Sun et al., 2016). In the work by Hillier et al. (2017) providing evidence for retina-dependent and -independent mechanism for cortical direction selectivity as described above, only neurons in L_{2/3} were measured and a distinction between the upper and lower portion within this layer was not made. In addition, the response properties of neurons in mouse V₁ can vary substantially with cortical depth, even within L_{2/3} itself (Kreile et al., 2011; Hoy and Niell, 2015; O'Herron et al., 2018). For example, neurons in upper L_{2/3} were found to be more biased for the horizontal axis than in lower L_{2/3} (Kreile et al., 2011). One would thus expect to see a change in the proportion of neurons that show signatures of retina-dependent direction selectivity with cortical depth.

To test this possibility in the present study, a subset of experiments ($n = 3$) was performed in lower L_{2/3}, while most data were recorded from neurons in upper L_{2/3} (Fig. 3.4b). The proportion of neurons showing DS responses to AM stimuli did not change between upper and lower L_{2/3}, and no evidence of a dependence of responses to AM stimuli on L_{2/3} depth was found. A larger sample size at lower L_{2/3}, however, would be needed for a more

thorough examination of the effects of cortical depth.

It would also be worth probing responses to dichoptic AM from layers deeper than L2/3. Owing to increased light scattering in brain tissue and a general lack of GCaMP6 expression in L4 (Liebscher et al., 2016), the recording of V1 neurons in L4 or deeper using calcium imaging is generally challenging (e.g. Sun et al., 2016; Jaepel et al., 2017). A more targeted expression of GCaMP6 in deeper layers (e.g. specific labeling of L4 neurons by Cre-dependent expression of GCaMP6 in Scnn1a-Tg3-Cre transgenic mice) could be employed. Alternatively, recently developed red-shifted calcium indicators (Dana et al., 2016), not yet available during the course of this study, should more easily allow imaging neurons in deeper cortical layers with sufficient signal-to-noise.

4.1.4 Is anesthesia a major confounder for dichoptic apparent motion?

In addition to the confounding factors discussed above, another important consideration is that the recordings of this study were performed in anesthetized animals. It is well documented that anesthesia can have strong effects on cortical dynamics and sensory processing (Niell and Stryker, 2010; Haider et al., 2013; Vaiceliunaite et al., 2013; Sugawara and Nikaido, 2014; Goltstein et al., 2015; Durand et al., 2016; Adesnik, 2017). Haider et al. (2013) showed that in the awake state, V1 activity is dominated by stronger inhibition, resulting in shorter and more spatially selective responses to flashed bars, compared to the anesthetized state, during which responses were prolonged and could be evoked from a larger region of the visual field. Importantly, a recent study showed that anesthesia increased responses of V1 neurons to non-preferred directions and resulted in overall reduced direction selectivity (Goltstein et al., 2015; see also Zhang et al., 2014), potentially caused by an impairment of cortical inhibitory function (Lee et al., 2012; Haider et al., 2013; Vaiceliunaite et al., 2013; Sugawara and Nikaido, 2014). Thus, in contrast to orientation selectivity that does not seem to be substantially affected (Niell and Stryker, 2010; Goltstein et al., 2015; Durand et al., 2016), anesthesia might have a stronger impact on the computation of motion direction and other complex RF properties (Guo et al., 2004; Durand et al., 2016). Consistent with this view, I observed that responses to random dot stereograms, which are dichoptic stimuli for assessing the complex RF property of binocular disparity, were overall substantially stronger in the awake state as compared to anesthetized (Fig. 3.20).

It is also plausible that this effect might be more profound for cortical circuits of direction selectivity than retinal circuits, in particular for such cortical direction selectivity circuit models that feature mechanisms of asymmetric inhibition, whereby direction selectivity relies on inhibition to suppress responses to non-preferred directions (see Introduction, section 1.2.4 for more explanations on possible mechanisms for cortical direction selectivity).

Moreover, the potential impact of anesthesia on the computation of direction selectivity might be more severe under the specific stimulation conditions of this study, which resemble the flashed bar stimuli used in Haider et al. (2013). In the present study, motion direction needed to be extracted by the precise spatiotemporal and binocular integration of only two, briefly flashed stimuli (at least for AM bars and two-grating AM). By contrast, with real, continu-

ous motion stimuli such as a grating drifting for several seconds, the effect of anesthesia might be less evident (Durand et al., 2016).

4.1.5 Dichoptic apparent motion in the zebrafish

A similar approach based on the dichoptic presentation of AM stimuli as employed here, has previously been used by only one other study, performed in the larval zebrafish (Ramdya and Engert, 2008). In this work, Ramdya and Engert aimed to investigate the mechanisms underlying the emergence of binocular RF properties in the visual system, by artificially inducing a second retinal input to the optic tectum, which is the largest retino-recipient structure that normally receives only monocular input. In these binocularly rewired tecta, dichoptic AM was employed to test the sufficiency of tectal circuitry for computing direction selectivity: tectal neurons exhibited DS responses when presented with dichoptic AM stimuli, indicating that those neurons did not inherit DS signals from the retina, but direction selectivity was generated *de novo* through tectal circuits.

In addition to potential differences in the mechanisms of direction selectivity between mice and these rewired larval zebrafish, considerations on basic RF properties might explain why the interpretation of responses to dichoptic AM stimuli was seemingly more difficult in the present study compared to zebrafish. Tectal cells typically have complex-like RFs (lacking clear ON/OFF subfields), covering a large portion of visual space (ranging 10–90 deg, with a mean of 40 deg; Sajovic and Levinthal, 1982; Niell and Smith, 2005; Bergmann et al., 2018; Förster & Baier, unpublished). Given these RF properties, the exact positioning of AM stimuli with respect to the RFs might have been less problematic than in the mouse, where most V1 neurons in L2/3 have smaller (~25 deg), simple-like RFs, particularly sensitive to the specific location and other parameters of stimulation (e.g. size, luminance; see also confounders (a–c) in section 4.1.1; Niell and Stryker, 2008). Furthermore, the AM stimuli used in Ramdya and Engert (2008) did not cover the whole set of possible combinations. AM stimuli were presented monocularly only to the contralateral eye, without probing responses to AM presented to the ipsilateral eye. In addition, of the total of four dichoptic AM combinations (consisting of 2 directions \times 2 eye sequences) only two were actually presented. The sample size selected for this analysis amounted to only 18 cells, across 278 neurons and 4 fish, with only 3 trials for each stimulus. Overall, this implies that the interpretations of the data were potentially based on a partial characterization of the cells' response properties and, hence, might need further analysis.

4.1.6 Outlook and future experiments

Further investigations based on the dichoptic AM approach developed here would potentially be very informative. In light of the results of recent publications (Cruz-Martín et al., 2014; Hillier et al., 2017), future experiments should analyze neuronal responses to dichoptic AM with particular attention to cortical depth, direction of motion, and stimulus speed, as discussed above. Ideally, to preserve the functionality of the inhibitory system, responses to dichoptic AM should be measured in the awake animal, by adopting the awake dichoptic paradigm (Fig. 3.20). This paradigm features the use

of eye shutter goggles and a single stimulus monitor for both eyes, thereby making stimulus presentation much simpler and consistent across experiments (Fig. 3.17b), as compared to using two haploscope mirrors and two monitors as done here.

As an alternative to two-photon imaging, patch clamp recordings from individual neurons might be better suited for the questions addressed in this study, since they are less susceptible to the confounders discussed above. Tailoring the precise stimulus parameters to just one cell at a time, together with a high fidelity in recording the cell's firing, this technique would potentially enable a better characterization of the properties of a cell's RF and, hence, a better assessment of its responses to dichoptic AM. One key feature of two-photon population calcium imaging is the possibility of recording the activity of hundreds of neurons at the same time. It was indeed expected that a denser sampling would be advantageous when aiming to record a specific subpopulation of neurons (i.e. cells that are both binocular and DS). In fact, this potential advantage did not hold the multiple selection criteria for response reliability and consistency, direction selectivity, and binocularity, eventually resulting in a small sample size. Moreover, patch clamp recordings could potentially be used to measure also the subthreshold activity of the cells, thereby permitting the examination of synaptic mechanisms underlying direction selectivity and spatiotemporal input integration (Longordo et al., 2013; Adesnik, 2017; Lien and Scanziani, 2018).

4.1.6.1 Investigating intracortical circuits underlying direction selectivity

The approach based on dichoptic AM for blocking retinal direction selectivity and, likewise the manipulations adopted by Hillier et al. (2017), allow, at least in principle, to determine the relative contribution of retina-dependent and -independent circuits to cortical direction selectivity. However, with these approaches, it is hardly possible to investigate the exact wiring of the thalamocortical and/or intracortical circuits for *de novo* generation of cortical direction selectivity, which are still far less understood compared to retinal direction selectivity.

For the *de novo* generation of cortical direction selectivity, two fundamental circuit models have been put forward (see Fig. 1.7). The asymmetric excitation model relies on the integration of excitatory inputs with appropriate RF position and time delays to generate DS responses of V1 neurons. Potential sources of this spatiotemporal offset are at the convergence of thalamocortical connections; or alternatively, through intracortical connections, hence occurring entirely within the cortex. Conversely, the asymmetric inhibition model relies on the cortical inhibitory system that asymmetrically suppresses responses to non-preferred directions. A very recent study by Lien and Scanziani (2018) provided clear evidence in favor of the asymmetric excitation model, showing that the primary bias for the direction selectivity of neurons in mouse L4 (the major thalamo-recipient layer) arises at the convergence of spatially and temporally offset thalamocortical inputs. Nevertheless, it is well possible that inhibition still plays a critical role for cortical direction selectivity, by providing a complementary mechanism for selectivity sharpening (Isaacson and Scanziani, 2011; Li et al., 2015; Li et al., 2017) or also as a main mechanism in cortical layers outside L4 or for specific subsets of DS cells. For example, it was shown that the optogenetic activation of cortical inhibitory neurons of the parvalbumin subtype enhanced direction selectivity.

ity of nearby DS neurons in mouse V1 (Lee et al., 2012), thereby supporting the inhibition-based models. However, the precise mechanisms behind the contribution of inhibition are not clear.

Future experimental work should test the asymmetric inhibition model. Genetic strategies as used by Hillier et al. (2017) or dichoptic AM stimuli might first be employed to identify cells with retina-independent direction selectivity. Next, such cells could be targeted for trans-synaptic rabies virus tracing (Wertz et al., 2015) to identify the presynaptic inhibitory inputs. One prediction of the asymmetric inhibition model is that, given the retinotopic organization of V1, the spatial distribution of the somata of such inhibitory presynaptic cells is asymmetric with respect to the location of the postsynaptic DS cell and should be correlated with its preferred direction – a circuit arrangement very much resembling the asymmetric connectivity between DSGCs and starburst amacrine cells in the retina (see Introduction, paragraph 1.2.3). According to the model, inhibitory cells should preferentially be located on the “non-preferred side” of the DS cell. It is conceivable, however, that the asymmetric inhibition might not be evident at such a coarse anatomical level, but it may emerge functionally via asymmetries in connection strengths and/or temporal properties.

One approach to tackle this question is using two-photon optogenetics in combination with calcium imaging to perturb the activity of specific inhibitory cells with high spatial and temporal resolution. Calcium imaging with GCaMP6 is used to characterize the RF locations and selectivities of V1 neurons in the imaging plane. A specific subtype of cortical inhibitory cells, e.g. the parvalbumin-positive subtype, is specifically targeted to express an optogenetic tool such as ChR2, the newly developed ChroME optimized for two-photon activation (Mardinly et al., 2018), or the red-shifted ChrimsonR (Klapoetke et al., 2014) for reducing cross-talk with GCaMP6. Photostimulation with two-photon light, enabling improved penetration depth and spatial specificity compared to one-photon light (Emiliani et al., 2015; Mardinly et al., 2018), is used to activate selected inhibitory neurons at specific timings with respect to the visual sensory input, while analyzing the effects on the DS output of nearby neurons simultaneously. If asymmetric inhibition is at play, one can predict the perturbation effects on the DS output to be correlated with the physical location and/or RF locations of the perturbed inhibitory cells and with the specific preferred direction.

By using an analogous approach, testing the asymmetric excitation circuit via intracortical connections (rather than via thalamocortical connections) could also be possible. The activity of cortical excitatory neurons could be manipulated by targeting them to express an inhibitory optogenetic tool such as the red-shifted halorhodopsin eNpHR3.0 (Gradinaru et al., 2010) or the newly released GtACR1 optimized for two-photon activation (Mardinly et al., 2018). In this way, one could try to interfere with the time delay between specific excitatory inputs with distinct spatial locations.

In conclusion, the extraction of motion direction from the visual scene offers an ideal substrate for investigating how circuits of the visual system perform a neural computation. Therefore, future work aimed at a better understanding of the generation of cortical direction selectivity will also contribute to solve essential questions in neuroscience about principles of neural computation in the mammalian visual cortex.

4.2 BINOCULAR DISPARITY PROCESSING IN MOUSE VISUAL CORTEX

4.2.1 How do rodents use binocular vision?

In carnivorans and primates, a key function of the visual cortex is integrating signals from the two eyes, as the vast majority of neurons in visual cortical areas are binocular, while the input from LGN is eye-specific. One important function of binocular integration is extracting retinal disparities – the building blocks from which the visual system can construct stereoscopic depth perception. The processing of stereoscopic depth in the visual system of these species is remarkably widespread, suggesting the importance and high demand of this task. Individual neurons sensitive to binocular disparities are found in almost all regions of the visual cortex of cats and monkeys (Poggio, 1995; Gonzalez and Perez, 1998; Parker, 2007; Parker et al., 2016). Human fMRI studies also showed that disparity-selective responses involve a broad expanse of the cortex, even beyond visual areas (Minini et al., 2010; Welchman, 2016).

The mouse features the essential components for binocular vision, even though binocularity is less prominent compared to species with forward-facing eyes. Despite sideways-facing, both eyes in the mouse can sample the same central ~40 degrees segment of visual field in front of the head. This region of binocular overlap is, relative to more peripheral space, over-represented in the cortical territory of the primary visual cortex (V₁) and, in particular, in some higher-order visual areas like LM and RL. Yet, while ocular dominance plasticity has become one of the most prominent models for experience-dependent plasticity, surprisingly little is known about the function and cortical mechanisms of the binocular visual system of mice.

In this study, I have shown that large fractions of neurons in the binocular regions of areas V₁, LM, and RL integrate input from both eyes to encode retinal disparities. The information about binocular disparity that these neurons carry is potentially critical for depth perception, because it is the essential data that the visual system needs to construct stereopsis. Thus, the abundance of disparity-selective signals found in all three areas strongly suggests that mice do use binocular disparity as a depth cue to estimate object distances. One should acknowledge, however, that stereopsis in this species has not been formally proven. A conclusive demonstration of stereoscopic depth perception in mice will require behavioral experiments in which disparity in a binocular depth task is specifically manipulated (see also paragraph 1.3.2 [Demonstrating stereoscopic perception](#)). This can be ideally achieved with dichoptic viewing in awake mice under head-fixed conditions, allowing for optimum control over visual stimulation and other physical parameters (e.g. eye positions). The awake recordings of this study are the proof-of-principle that this experimental approach can be effectively adopted to test stereopsis in the mouse.

In a recent publication, Wallace et al. (2013) suggested that rats do not likely have stereopsis. They characterized eye movements in freely moving rats using head-mounted cameras and found that rats' eyes often move in a disconjugate and asymmetrical fashion, which is inconsistent with the animal showing any binocular fixation while moving around. In addition, Wallace et al. emphasize that the rat's eye movements keep the visual fields of

the two eyes continuously overlapping above the animal's head, thus concluding that both eyes are jointly used for a more efficient detection of predators appearing overhead, rather than for stereopsis. However, as correctly pointed out by [Meister and Cox \(2013\)](#), the data presented by Wallace et al. contradict their own main claim and rather clearly indicate that the rats' eyes are moved such that the binocular field is in fact centered on the horizon straight ahead of the animal – and not overhead. Furthermore, in the work by Wallace et al. rat's eye movements were characterized in animals during locomotion and while performing body and head movements, whereas eye movements were not studied under stationary conditions. Indeed, as shown in Wallace et al. and as it seems to hold true for mice too ([Meyer et al., 2018](#)), a large fraction of eye movements can be explained by the vestibulo-ocular reflex, which induces eye movements in the direction opposite to head movement to stabilize the images on the retinas.

It is conceivable that rodents show two different viewing modes, depending on the behavioral context. (1) In one mode, during locomotion, rodents show eye movements mostly driven by the vestibulo-ocular reflex and often disconjugate. This mode would result in a more efficient visual field coverage and a spatial mapping of the surrounding environment in relation to the animal's own head/body position, and ultimately in more effective predator detection. Indeed, during locomotion in open areas, it is likely more important for rodents to enhance predator detection, also at the expense of stereopsis. In fact, predators would more often appear at distant (infinity) locations, where binocular disparities cannot contribute anymore to depth discrimination. This mode might be primarily mediated by the superior colliculus, which has been shown to play a key role in predator avoidance ([Shang et al., 2015](#); [Almada et al., 2018](#); [Evans et al., 2018](#); [Li et al., 2018](#)), and to contain motor maps for eye ([Wang et al., 2015](#)) and head movements ([Wilson et al., 2018b](#)).

(2) In another viewing mode, rodents in a safer and more stationary condition might show absent or more coordinated eye movements, thereby enabling binocular vision to support behaviors such as terrain traversability assessment, distance estimation for gap jumping, object interaction, food selection, and prey-capture. Consistent with this view, it has been observed that eye movements in mice are more restricted during quiescence, grooming and eating than during active exploration ([Meyer et al., 2018](#)). In addition, it seems that during prey-capture behavior in mice, the mouse first orients its head and body toward the prey, then maintains a stationary position for a small amount of time (~0.5 sec), and finally initiates locomotion for approaching ([Hoy et al., 2016](#)). It is thus tempting to speculate that such a behavior is consistent with bringing the target to a more central location of the mouse visual field to enable stereoscopic judgment of prey position and hence more accurate long-range approach behavior (see also paragraph [1.3.4.1 Behavioral evidence for stereopsis](#) and [Park et al., 2018](#)).

4.2.2 Wide distribution of disparity selectivity in mouse visual areas V1, LM, and RL

In this study, I found that > 75% of visually responsive cells were disparity-tuned (DT) in response to dichoptic gratings at lower SFs (0.01 cpd and 0.05

cpd), with a comparable amount of selectivity across neurons in areas V₁, LM, and RL.

4.2.2.1 *Comparison with the reported disparity selectivity in mouse V₁*

In previous reports in the mouse, Scholl et al. (2015; 2017) found that only about one third of V₁ neurons were DT, using a similar visual stimulus (dichoptic gratings with SF 0.02–0.04 cpd and TF 1–4 Hz) and similar criteria for quantifying disparity selectivity compared to the present study. One reason for this discrepancy could be that different calcium indicators were employed. Scholl et al. (2015; 2017) used the synthetic indicator Oregon Green BAPTA-1 (OGB-1), which is substantially less sensitive (~2-fold) compared to GCaMP6s (Chen et al., 2013b). In addition, GCaMP6s shows a higher non-linearity in the relationship between action potential firing and the fluorescence signal, compared to OGB-1, which might also contribute to explaining this difference (Hendel et al., 2008; Rose et al., 2014).

Another reason for the lower fraction of DT cells is that Scholl et al. (2013; 2015; 2017) did not measure and account for possible optical rotations of the visual field between left and right eye, which might be artificially introduced by the haploscope mirrors used for dichoptic stimulation (see Materials and Methods, paragraph 2.8.4 for details). In the present study, the rotational offset was measured and found to range between 15 and 30 degrees across different experiments, and the stimuli were then displayed such as to correct for this offset. Failing to correct for the rotational offset, might result in an overall decreased disparity selectivity, because a mismatched orientation between RFs of individual neurons, albeit small, might lead to suboptimal binocular integration and hence reduced disparity selectivity (Ohzawa and Freeman, 1986; Smith et al., 1997; Vickery and Morley, 1999; Longordo et al., 2013).

4.2.2.2 *Comparison with disparity selectivity in cat and monkey*

In cats and monkeys, large fractions of DT neurons are found as early as in V₁, and across extrastriate areas. Many of the studies in these species were conducted under variable experimental conditions (i.e. stimuli, anesthesia/awake, disparity selectivity criteria) and with limited sample sizes. Thus, some differences are present across studies in terms of the fractions of DT cells and their tuning characteristics, such that comparisons with the results of the present study are somewhat difficult. Nonetheless, at least half of the visually responsive neurons across monkey visual areas, including V₁, V₂, V₃, V₄ and MT were reported to be DT, both using dichoptic gratings (Smith et al., 1997) and, more often, RDS stimuli (Poggio et al., 1985; Adams and Zeki, 2001; Prince et al., 2002b; DeAngelis and Uka, 2003; Hinkle and Connor, 2005; Gonzalez et al., 2010). Comparably large proportions were also reported in visual areas of the cat (Ohzawa and Freeman, 1986; Vickery and Morley, 1999; for a review see Gonzalez and Perez, 1998).

4.2.2.3 *Disparity processing is distributed across multiple areas*

The overall high disparity selectivity found across mouse visual areas V₁, LM, and RL, which harbor the largest, continuous representation of the

binocular visual field in the visual cortex, resembles the widespread distribution of disparity processing throughout most of the visual system of cats and primates. Studies in these species have long sought to identify a cortical region specifically dedicated to stereoscopic depth processing, but failed in achieving this goal. For other visual features, it has been possible to identify specific cortical regions playing a more preeminent role, among multiple areas involved. For example, primate areas V₄ and MT have been considered crucial centers for color and motion perception, respectively (Kandel et al., 2013).

Why is binocular disparity processing so widespread across multiple areas? One possibility is that disparity processing is highly distributed, relying on the concomitant recruitment of several areas. Similar disparity signals generated in these areas might then be differentially combined with information about other aspects of visual stimuli, such as motion, contrast, and shape, or with information deriving from other sensory modalities, in order to construct the percept of a 3D object. Another possibility is that different areas do form specialized representations of binocular disparity, thereby playing distinct disparity-related roles in constructing a 3D percept (Roe et al., 2007), such as encoding near or far space, supporting reaching movements (for more discussions see paragraph 4.2.7 [Does RL contain a visuo-tactile representation of nearby space?](#)), or computing visual object motion across depth (Czuba et al., 2014; Sanada and DeAngelis, 2014).

4.2.3 Tuning characteristics of disparity-tuned neurons

Evidence indicates that different visual areas in the primate form specialized representations of disparity, also in relation to the distinct specialization of the dorsal and ventral streams (Poggio, 1995; Gonzalez and Perez, 1998; Parker, 2007; Goncalves et al., 2015; Verhoef et al., 2016; Welchman, 2016). Such specializations for binocular disparity tend to emerge when investigated with complex visual stimuli in alert animals engaged in perceptual tasks dependent on disparity (e.g. Anzai and DeAngelis, 2010; Krug and Parker, 2011). Nevertheless, some differences in basic disparity tuning properties have been found, too, across visual areas. In monkey V₁, neurons are more frequently found to have a symmetric tuning curve, whereas a larger fraction of neurons in extrastriate areas show asymmetric tuning curves (Gonzalez and Perez, 1998; Cumming and DeAngelis, 2001). In addition, neurons in extrastriate areas show a coarser disparity tuning (i.e. wider peaks of the tuning curve) than V₁ neurons and overall cover wider range of disparities than V₁ (Cumming and DeAngelis, 2001; Parker, 2007; Parker et al., 2016).

4.2.3.1 *Asymmetric disparity tuning curves*

In the present study, the disparity tuning width of individual neurons was on average similar across areas V₁, LM, and RL. The majority of neurons in these areas showed symmetric tuning. A small, specific subset of cells (~15%) in areas V₁ and LM when tested with a SF of 0.01 cpd, exhibited an asymmetric tuning curve (Fig. 3.14c). Most of these cells had a disparity preference maximally different (180 deg phase) from the overall peak in the distribution of disparity preferences in each recording. While somewhat puz-

zling, one possible interpretation of the disparity tuning asymmetry of some cells might be related to the two proposed mechanisms underlying disparity selectivity: the position-shift and the phase-shift mechanism, which generate symmetric and asymmetric disparity tuning curves, respectively (see Fig. 1.11b). A disparity phase difference of 180 deg corresponds to 50 absolute deg (a full grating cycle at 0.01 cpd corresponds to 100 absolute deg). Assuming that the population peak disparity reflects the visual field location of retinal correspondence between the eyes (vertical meridian of zero retinal disparity), a position-shift mechanism alone would require a spatial offset between left and right eye RF of 50 absolute degrees. This value is unrealistically large, considering the typical RF size of cells in V1 and LM (average diameter of ~25 and ~40 deg, respectively; Van den Bergh et al., 2010; Smith and Häusser, 2010; Bonin et al., 2011; Vaiceliunaite et al., 2013; Smith et al., 2017), and that left and right eye RFs are at least partially overlapping in most V1 neurons (Sarnaik et al., 2014). It follows that cells in V1 and LM with a disparity preference of 0 deg phase might predominantly rely on a phase-shift mechanism, hence showing asymmetric tuning curves. By contrast, neurons in RL, possibly due to larger RFs compared to V1 and LM (D'Souza et al., 2017), might rely less on a phase-shift mechanism.

4.2.3.2 Overall near bias in the disparity ranges encoded in each area

In the first set of experiments, the disparity preference distributions for any given grating SF were comparable across the three areas, indicating that the ranges of disparities covered in each area were similarly wide. However, the disparity distributions of each area were all aligned to have the population peak at 180 deg phase, to account for technical limitations (as pointed out in paragraph 3.2.6). This means that in principle the ranges of disparities covered in one area could be actually shifted compared to another area, without being able to reveal such a difference in that set of experiments.

In a separate set of experiments, each of the areas V1, LM, and RL was imaged during the same imaging session, allowing for a direct comparison of the disparities represented in the different areas (see also Fig. 2.1 in Materials and Methods). Another key aspect of these experiments was the use of RDS stimuli in addition to grating stimuli. The use of RDS, albeit at the expense of characterizing fewer cells compared to gratings, enabled the measurement of tuning curves as a function of absolute disparities (i.e. disparities in terms of visual angles, and not in terms of grating phase), without the ambiguity caused by the circular nature of grating stimuli.

I found that all three areas exhibited an over-representation of near disparities. Importantly, however, area RL covered a range of disparities significantly more shifted toward near values compared to V1 and LM, thereby indicating a specialization of RL for encoding nearby visual objects. The near bias observed across these three mouse areas is overall in line with a bias for near disparity preferences generally found across areas of the monkey visual system, including V1 (Prince et al., 2002a; Gonzalez et al., 2010; Samonds et al., 2012), V2 (Chen et al., 2008; Gonzalez et al., 2010; Hubel et al., 2013), V3 (Adams and Zeki, 2001; Hubel et al., 2013), V4 (Watanabe et al., 2002; Hinkle and Connor, 2005; Tanabe et al., 2005), and MT (Maunsell and Van Essen, 1983; DeAngelis and Uka, 2003), even though these disparity biases might partly reflect a biased sampling with respect to visual field location (see below paragraph 4.2.8; Sprague et al., 2015). The overall bias

for near disparities present across areas of both mouse and monkey visual system might reflect a higher behavioral relevance of the space near the animal compared to objects located farther away (Hoffman and Richards, 1984), or might be related to figure-background segregation of the visual scene (Hinkle and Connor, 2005).

4.2.4 Potential area correspondences between mouse and primate visual cortex

Similarly to mouse area RL, the primate higher-order visual area MT shows a stronger over-representation of near disparities compared to V1 and other visual areas (DeAngelis and Uka, 2003; Parker et al., 2016). A parallel between mouse RL and primate MT has been suggested on the basis of some similarities (Juavinett and Callaway, 2015). Both RL and MT prefer high velocity stimuli (Born and Bradley, 2005; Marshel et al., 2011; Tohmi et al., 2014; Murakami et al., 2017), and both areas contain a retinotopic representation biased to the lower visual field (Maunsell and Newsome, 1987; Garrett et al., 2014; Zhuang et al., 2017). Moreover, anatomical and functional studies put forward RL as a node of the supposed dorsal stream of the mouse visual system (Wang et al., 2012), as MT is considered to be in the primate visual system (Maunsell and Newsome, 1987; Born and Bradley, 2005).

Despite some similarities, the hypothesis of a correspondence between mouse RL and primate MT is still largely speculative, but it could be experimentally explored in more detail. For example, neurons in primate MT, unlike V1, show perceptually relevant signals in binocular depth tasks and have been causally implicated in stereoscopic judgments (for more details see also paragraph 1.3.3.2 [Role of disparity-tuned neurons in stereopsis](#); DeAngelis et al., 1998; Krug, 2004; Krug et al., 2013; Parker et al., 2016). Neurons in the mouse RL might be monitored during a binocular depth task, e.g. in which the animal is required to discriminate between near and far RDS disparities, and the presence of neuronal activity related to the perceptual choice could be assessed. In addition, a causal evidence for a role of DT neurons in binocular depth discrimination might be provided through manipulations such as lesions and pharmacology, or intervening more selectively with optogenetic tools.

Ultimately, establishing interspecies homology requires anatomical and cytoarchitectural similarity. This, however, is often difficult because of evolutionary distance, brain and body size differences, anatomical and functional reorganizations during evolution, even when comparing monkey to human visual areas (Serenó and Tootell, 2005; Laramée and Boire, 2014). This implies that interspecies correspondence needs to be strongly based on functional similarity as well (Mantini et al., 2012; Wager and Yarkoni, 2012), which likely becomes even more important when attempting to relate mouse and primate brains.

Sensitivity to binocular disparity, as a hallmark of many neurons in primate visual cortex with distinct characteristics across different areas, may act as a valuable functional marker to help delineating the roles of mouse cortical areas for visual processing, which are still largely unclear. The present study provides clear evidence for distinct representations of binocular disparities across areas of mouse visual cortex. While any real comparison with primate visual areas would be premature, the functional specialization of

RL shown here reveals something arguably more relevant than previous attempts to chart mouse visual areas, which mainly focused on basic stimulus selectivities, such as SF, TF, orientation and direction tuning, and often led to controversial distinctions among areas (see also paragraph 4.2.7 [Does RL contain a visuo-tactile representation of nearby space?](#); for more details on published works of functional characterization of higher visual areas, see paragraph 1.1.8 in the Introduction).

4.2.4.1 *Absolute and relative disparity*

Two important aspects of binocular disparity – absolute/relative disparity and binocular correlation/anticorrelation – are differentially processed across visual areas and streams in primates, but were not explored in the present study and might help to understand the role of mouse areas in visual processing and possibly facilitate a comparison with primate areas. In the following paragraphs, these two aspects of binocular disparity will be considered.

Binocular disparity comes in two flavors, absolute and relative disparity (Parker, 2007; Roe et al., 2007; Anzai and DeAngelis, 2010; Patten and Murphy, 2012; Verhoef et al., 2016; Welchman, 2016). The absolute disparity of an object is determined by a retina-anchored coordinate system, i.e. with reference to each eye’s fovea. The relative disparity of an object is measured with reference to another object in space, eliminating the retina as the frame of reference (Neri et al., 2004; Parker, 2007). The advantage of relative over absolute disparities relies on their independence from eye movements and the actual fixation depth. Conversely, absolute disparities are altered when the eyes move, because the retinal image of a given object moves along with the eyes. Human perception of stereoscopic depth is quite insensitive to absolute disparity and relies primarily on the computation of relative disparities, as evidenced by psychophysical studies (Parker, 2007). In the primate visual system, V1 neurons carry information about absolute disparity only (Cumming and Parker, 1999), while neurons in higher visual areas, starting from V2, have been found to additionally encode relative disparity (Thomas et al., 2002; Neri et al., 2004; Parker, 2007; Welchman, 2016). This also indicates that primate V1 cannot account for key properties of binocular depth perception, which seems to require extrastriate areas beyond V1.

In the mouse visual system, the present study assessed neuronal sensitivity to absolute disparities, leaving open the question whether a distinction between absolute and relative disparity processing is present in the mouse visual cortex, too. To probe sensitivity to relative disparity in primate studies, visual stimulation typically consists of RDS stimuli in which different portions of the stimuli display different absolute disparities, e.g. in a center-surround arrangement (Cumming and Parker, 1999; Thomas et al., 2002; Krug and Parker, 2011; Norcia et al., 2017). Having shown in the present study that neurons in mouse visual cortex across three distinct areas can be reliably driven and characterized using RDS, future experiments could focus on whether these areas display specialized encoding for absolute versus relative disparity, by employing variations of the RDS stimuli established here. If such a distinction is made at the level of single neurons, behavioral experiments might explore the contribution of absolute and relative disparity for binocular depth perception in mice. For example, mouse performance might be tested on two different near-far discrimination tasks,

each with same amount of disparity difference between near and far stimuli, but defined in either relative or absolute terms. It might be hypothesized that mouse stereoscopic perception may rely primarily on relative disparity, considering that mice are likely not capable of controlling the actual fixation depth (no evident fixation movements (Wallace et al., 2013; Meyer et al., 2018), that mouse eyes lack a well-defined fovea and accommodation (de la Cera et al., 2006; Chalupa and Williams, 2008), and that eye movements are largely driven by the vestibulo-ocular reflex (Wallace et al., 2013; Meyer et al., 2018).

4.2.4.2 *Binocular correlation and anticorrelation*

Another important aspect of binocular disparity, showing different properties across primate visual areas, is related to the role of binocular neurons to operate as correlation detectors between left and right eye signals, which is assessed by comparing their disparity tuning for correlated and anticorrelated stimuli. For instance, when every visual stimulus feature on one retina matches in brightness the feature on the other retina (i.e. bright with bright, dark with dark), the input signal is perfectly correlated; conversely, when left and right eye images have opposite contrasts (i.e. bright with dark, dark with bright), the input signal is anticorrelated.

When probed with RDS stimuli with opposite contrast between the two eyes, neurons along the primate visual pathway can react differently to correlated and anticorrelated stimuli. For example, neurons in V1 and V2 invert their tuning curve in response to anticorrelated stimuli (i.e. disparities eliciting the highest response to correlated stimuli evoke the lowest response with anticorrelated stimuli and vice versa), whereas responses to anticorrelated stimuli in visual areas of the ventral stream are diminished or abolished (Cumming and Parker, 1997; Parker, 2007). Anticorrelated stimuli have a strong impact on stereoscopic depth, often inducing disruption of depth perception (Julesz, 1971; Cumming and Parker, 1997; Neri et al., 1999). As for absolute/relative disparity, also the response properties to correlated/anticorrelated stimuli in the primate visual system indicate that visual areas higher than V1 are more relevant for binocular depth perception.

Future work using anticorrelated RDS stimuli in the mouse could address questions as for which forms of interocular signal correlations may be performed by individual neurons, and what area specializations may underlie these computations. This might also facilitate a comparison of visual areas between mouse and primate.

4.2.5 **Most binocular disparity information is contained in low and middle spatial frequencies**

By assessing disparity selectivity with a range of different grating SFs, I found that the majority of neurons were strongly and similarly sensitive to binocular disparity at the low and middle SFs tested (0.01 and 0.05 cpd). Conversely, at the highest SF tested (0.10 cpd), neurons were dramatically less sensitive to binocular disparity, suggesting that high SFs do not carry useful information for extracting binocular disparities. This dependence of disparity selectivity on SF was paralleled by the degree of binocular facilitation and suppression manifested in the response to dichoptic gratings compared

to monocular stimulation. At low and middle SF, neurons exhibited strong response facilitation and suppression at preferred and null disparity, respectively. By contrast, at high SF, neurons were much less susceptible to facilitation and suppression. The high SFs used here are, however, well within the range of visual acuity of the mouse (Wong and Brown, 2006) and well within the range of SFs encoded by neurons in areas V1 and LM, though less so in area RL which is more biased toward lower SFs (Niell and Stryker, 2008; Marshel et al., 2011; Murakami et al., 2017). Yet, a comparable low amount of disparity selectivity at high SF was observed across all three areas, while area RL was in comparison slightly less capable of discriminating middle and high SF grating disparity at the population level (Fig. 3.16), consistent with the SF tuning ranges of these areas.

Previous reports in the mouse did not probe disparity selectivity in function of SF, neither measured binocular facilitation and suppression (Scholl et al., 2013a, 2015, 2017a). In cats and monkeys, the majority of DT neurons typically show both a substantial facilitation and suppression at preferred and null disparity, respectively, similarly to the present study (Ohzawa and Freeman, 1986; Smith et al., 1997). Data in these species, in which the relation between disparity tuning and SF was systematically examined, are scarce. In one study, in which disparity tuning of neurons in primate V1 was measured using dichoptic gratings at various SFs, almost all cells tested (15 out of 16) responded with higher disparity selectivity at lower SFs within the range of SFs that each cell was tuned to and decreased progressively at increasing SF (Smith et al., 1997).

The negative correlation of disparity selectivity with SFs observed here might seem somewhat counterintuitive. In general, for accurately estimating binocular disparity under natural viewing conditions, one would rather expect high SFs to carry a substantial amount of information. In fact, a given spatial phase displacement corresponds to smaller absolute displacements at high SFs compared to low SFs, thus making high SFs potentially more sensitive to small changes in binocular disparity. Interestingly, it is known from human psychophysical studies that spatial stereo-resolution, which is the finest sinusoidal modulation in disparity-defined depth, is relatively poor. Humans lose the ability to detect disparity modulations at SFs beyond a certain threshold, which is lower than that expected by taking into account factors like high acuity and high stereo-resolution for luminance, which is the smallest luminance variation that can be dichoptically detected (Tyler, 1974; Banks et al., 2004). One study tried to develop an intuition for this phenomenon by modeling binocularly viewed natural images and found that most information for estimating disparity is concentrated in low to middle SFs (Burge and Geisler, 2014). The same analysis as performed in the aforementioned study, but adapted to mouse stereo-geometry (Fig. 4.2a), predicted that the most useful range of SFs for the mouse to estimate disparity is between 0.01 cpd and 0.10 cpd, with progressively more information carried by lower SFs (Scholl et al., 2013a). The data of the present study thus corroborate these predictions, although they do not show a smooth progressivity over SFs; rather, sensitivity for binocular disparity is present to a similar degree at 0.01 cpd and 0.05 cpd, and abruptly dropped at 0.10 cpd. Moreover, while several mechanisms have been proposed for explaining the poor spatial stereo-resolution for binocular disparity in humans, data addressing this issue are scant (Banks et al., 2004; Nienborg et al., 2004). Intriguingly,

the mouse data of this study, by showing a remarkably poor disparity tuning of individual neurons at high SFs, provide a possible neural substrate underlying the psychophysical phenomenon present in humans.

4.2.6 Area RL encodes visual objects located in close proximity to the mouse

The data of this study clearly show that mouse area RL contains a larger proportion of neurons tuned for near disparities compared to V1 and LM, thereby indicating a specialization of RL for encoding visual objects located at a shorter distance to the mouse. Based on the disparity preferences measured in this study using RDS, it is possible to extrapolate the absolute distances of visual objects encoded by the three areas. Considering the stereo-geometry of the mouse visual system (Fig. 4.2a), the relationship between binocular disparity and object depth distance, under the small angle approximation, is described by the following equation (Fig. 4.2b; Scholl et al., 2013a):

$$\delta = \frac{-\Delta \cdot I}{(d_{pref} + \Delta) \cdot d_{pref}} = \frac{-I \cdot (d_{object} - d_{pref})}{d_{object} \cdot d_{pref}} \quad (4)$$

from which follows:

$$d_{object} = \frac{I \cdot d_{pref}}{I - \delta \cdot d_{pref}} \quad (5)$$

where δ is the binocular disparity (in radians), I is the interocular distance, d_{pref} is the preferred binocular viewing distance, and Δ is the depth of an object defined as the difference between the distance of the object d_{object} and the preferred viewing distance $\Delta = d_{object} - d_{pref}$.

Using the interquartile ranges of disparity values as plotted in Fig. 3.18b and applying Equation 2, area V1 is estimated to best encode visual objects at distances from the mouse eyes' between 3.9 and 18.3 cm, area LM between 4.3 and 13.9 cm, and area RL between 3.2 and 6.5 cm. Thus, area RL is estimated to cover a narrower range of distances substantially closer to the mouse (Fig. 4.2c).

Interestingly, the range of distances that the mouse visual system can in principle encode, as estimated in Scholl et al. (2013a) by solely using assumptions based on stereo-geometry, is from 5.3 to 96.3 cm, which is very similar to the actual range of disparities that neurons across the three areas are most sensitive to, as could be measured in this study using RDS. It is also worth pointing out that the extrapolations made here were enabled by the use of RDS stimuli, which permit the measurement of absolute disparity preferences in visual angles, as already pointed out above. Conversely, Scholl et al. (2013a) were not in a position to extrapolate absolute distances, because only phase disparity preferences could be measured with grating stimuli.

Note that the distance ranges estimated here indicate a range in which depth judgments of visual objects could, in principle, be made through stereopsis. Such distance ranges might seem surprisingly short for us as humans, but they are likely not so for mice, when rescaled to their proportions. In fact, much of the visually salient information, deriving during behaviors like ground assessment, object/food interaction, or prey capture, occurs within these estimated distances for a mouse. Beyond this range, mice would still be capable of seeing distant objects, like overhead predators or navigation

cues (as experimentally used in the Morris water maze), but depth judgments would be in principle possible only through monocular depth cues, like perspective or relative size. Nonetheless, for aversive visual stimuli like predators, it is likely more important for the mouse to detect the threat and actuate a defense strategy (freeze or escape) as quickly as possible, rather than accurately determining the distance of the potential threat. Similarly, more distant navigation cues are likely exploited for orientating in an environment, such that an enhanced depth judgment by stereopsis would not be particularly advantageous.

Finally, a number of neurons tuned for disparities were found to be well outside the estimated range of useful disparities. A disparity outside this range can be considered “impossible”, because it cannot be generated by the same object viewed by both eyes. A recent computational study attributed to neurons tuned to such impossible disparities an important role in extracting depth from natural images. By signaling unlikely interocular matches, such neurons could help identifying the “correct matches” of visual objects between the two retinal images (Goncalves and Welchman, 2017; see also Read and Cumming, 2007; Read and Cumming, 2017).

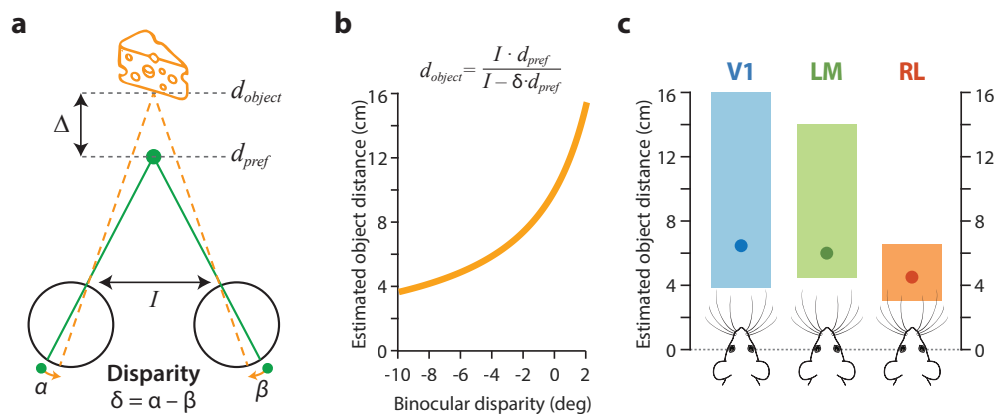


Figure 4.2 | Estimation of object distances encoded by disparity-tuned neurons. **a** | Stereogeometry of the mouse visual system (adapted with permission from Scholl et al., 2013a). The parameters of preferred binocular viewing distance (10 cm) and interocular distance (1.0 cm) are used to estimate the absolute distance of an object from the binocular disparity that the object causes. The preferred binocular viewing distance is estimated to be 10 cm from the eyes, considering the fact that the refractive error of mouse eyes of +10.0 diopters should enable optimal focus of objects located at 10 cm (de la Cera et al., 2006). **b** | Functional relationship between binocular disparity and absolute distance of an object from the observer, given by Equation 2. **c** | Estimated range of distances that are best encoded by disparity-tuned neurons in areas V1, LM, and RL. The range of distances is estimated by applying Equation 2 to transform the interquartile ranges of disparity preferences as plotted in Fig. 3.18b (V1: 3.9–18.3 cm, LM: 4.3–13.9 cm, RL: 3.2–6.5 cm). The dots represent the estimated distances corresponding to the mean disparity preference across neurons from each area as plotted in Fig. 3.18b (V1: 6.3 cm, LM: 6.0 cm, RL: 4.3 cm). In the mouse schematics, the eyes are aligned at zero (dotted line), with the interocular distance of 1 cm and whiskers in scale with the y-axis.

4.2.7 Does RL contain a visuo-tactile representation of nearby space?

By using the whiskers on their snouts, mice can extract accurate information about object location, shape, and texture, forming a tactile representation of the space around their head. The tactile signals from the whiskers are processed in the barrel cortex of the primary somatosensory area, where individual whiskers are represented in discrete units referred to as barrels.

The rostro-lateral area (RL) of the mouse visual cortex is anatomically located between V₁ and the barrel cortex, and from each of these two areas receives strong projections (Gămănuț et al., 2018). The retinotopic map of RL covers a more nasal, central portion of the visual field, with a bias toward the lower quadrant (Fig. 1.4c in the Introduction). The results of this study showed that RL is specialized for encoding nearby visual object as reflected in the cells' disparity preferences. This finding is consistent with the overall range of SFs and TFs that RL is tuned to: compared to the other areas, tunings of RL neurons are markedly shifted toward lower SFs and higher TFs (Murakami et al., 2017), corresponding to (moving) objects at closer distance to the eyes.

Intriguingly, based on cells' disparity tunings measured with RDS, RL is estimated to best encode object distances in a range, centered around 4 cm from the eyes, that is well within reach of the whiskers (Fig. 4.2c). Indeed, mouse whiskers can be as long as 3–4 cm (Ibrahim and Wright, 1975) originating from the whisker pad that is located ~1 cm rostral to the eyes. Moreover, mice have a specialized musculature that enables the fine scale control of individual whiskers during tactile sensing, resembling the way in which primates make use of their hands and fingers to map out their surroundings. During exploration of novel environments, rodents perform the so-called “foveal whisking”, in which their whiskers are thrust forward and stretched toward an object of interest, making small amplitude oscillations maintaining the protracted position. Conversely, in a familiar context such protraction occurs less frequently (Berg and Kleinfeld, 2003; O'Connor et al., 2010; Deschênes et al., 2012; Pammer et al., 2013; Sofroniew et al., 2014; Sofroniew and Svoboda, 2015).

A recent study demonstrated that mouse RL is in fact not a unimodal visual area, but rather a multisensory area that houses layer- and cell-specific circuits mediating visuo-tactile integration (Olcese et al., 2013). The largest fraction of neurons in RL is responsive to both, visual and whisker stimulation, while smaller fractions consist of unisensory neurons responsive to either sensory input.

Therefore, these features of RL, in combination with the properties of the whisker system, raise the hypothesis that this area might contain a visuo-tactile representation of the space in front of the mouse, potentially important for object interaction jointly mediated by binocular vision and whisker touch.

While the barrel cortex is typically viewed as containing a discrete somatotopic representation of individual whiskers, a very recent study revealed that neurons in the upper layers, when tested with all whiskers intact, actually form a highly ordered map of near touch-space, which in its smoothness very much resembles the retinotopic maps in visual cortex (Pluta et al., 2017; see also Lee and Barth, 2017). This finding thus supports the view that RL might contain a matched visual and touch sensory map to form a multi-modal representation of the space directly in front of the mouse.

Following this view, it is also tempting to compare the possible interplay between vision and whisking in mice with object interaction in primates, whereby vision and arm/hand movements are used together in a coordinated fashion. In these species, a so-called “parietal reach region” within the posterior parietal cortex, which RL might belong to in the mouse cortex (Marshel et al., 2011), has been specifically implicated in visually-guided

arm-reaching behaviors and found to contain “reaching-grasping neurons” (Rizzolatti et al., 1990; Andersen and Buneo, 2002). Moreover, it is known that the primate brain contains a modular representation of space, with some cortical regions processing the so-called peri-personal space, corresponding to the surroundings with which direct interaction is possible, and other cortical regions processing extra-personal space (Cléry et al., 2015). A study in macaques, using fMRI in a naturalistic 3D environment, has recently shown that the extra-personal space cannot be considered as a unique entity. Rather, there is an additional distinction between near and far space processing in the brain, with two dedicated functional networks involving different cortical regions (Cléry et al., 2018). This finding might offer a new framework for analyzing the specific contributions of individual visual areas to disparity processing and stereopsis, which is still relatively unclear even in primates, not to speak of rodents.

To effectively exploit both vision and whiskers together when interacting with nearby objects, the retinotopic map should be in register with the spatial map derived from the whiskers. Since the mouse barrel cortex develops before eye opening (O’Leary et al., 1994; Erzurumlu and Gaspar, 2012), the alignment of these two sensory maps would likely require experience-dependent plasticity. This hypothesis is supported by a study in which the relationship between visual and whisker inputs was altered by using a monocular prism to deviate the visual field of one eye by 30 deg (Yoshitake et al., 2013). Wearing the monocular prism for 5–7 days during the critical period of the visual cortex induced a shift of the retinotopic map in V1. Interestingly, for the prism-induced visual map shift to occur, tactile input from whiskers was crucial. This suggests that abnormal visuo-tactile input integration, rather than only abnormal visual input, was responsible for this reorganization, thereby implying that eye- and whisker-derived spatial signals are tightly linked and are aligned over experience-dependent development. Although Yoshitake et al. observed the prism-induced visual map shifts in V1 (no other areas were examined), the primary neural substrate behind the visuo-tactile map alignment unlikely resides in V1, since functional evidence to date indicates scant, if at all, tactile information in this area, unlike RL.

A series of classic studies in the barn owl pioneered by Knudsen and colleagues, using manipulations like lid suture, ear plugging, and prisms, demonstrated that an auditory space map is formed in the external nucleus of the inferior colliculus is transmitted to the optic tectum, where it merges with a visual space map derived from retinotopic inputs. As a result, the optic tectum of owls harbors a multimodal representation of space, which is used for more effective orienting behavior compared to either modality alone (Knudsen, 1982; Knudsen, 1983; Knudsen and Knudsen, 1985; Knudsen and Brainard, 1991; Knudsen, 2002; for reviews see Peña and DeBello, 2010; Grothe, 2018). The higher order area RL in the mouse visual cortex, by integrating visual and tactile inputs from near space, seems to be in an ideal anatomical and functional position to play a crucial role for such space map alignment.

Finally, the multisensory function hypothesized for area RL suggests a perspective according to which, for better delineating their functional role, visual areas should be viewed more as functional units that, engaged in specific behavioral contexts, process rich sensory information deriving from

complex visual stimuli and other sensory modalities as well (Ghazanfar and Schroeder, 2006).

4.2.8 Is disparity tuning related to visual field elevation?

In preliminary experiments, I observed that neurons with RFs in the upper visual field are on average biased toward farther disparities, while neurons with RFs in the lower visual field are biased for near disparities (Fig. 3.19), indicating a dependence of disparity tuning on retinotopic elevation, which will require further experiments to be verified. Such finding would then suggest the possibility that the specialization of RL for near disparities may not arise from area-specific circuit mechanisms, but may be explained by its retinotopic representation, which mostly covers the lower visual field (Fig. 1.4c). In either case, the hypothesis of area RL containing as a visuo-tactile representation of nearby space would still fully hold.

Surprisingly, none of the many studies using electrophysiological recordings in cats or monkeys directly examined the potential relationship between disparity tuning and retinotopic elevation. However, a very recent study re-analyzed data on DT neurons in monkey V1 collated across several original publications, in which the disparity preferences as well as RF positions of neurons were given. It was found that, in line with my preliminary finding in the mouse, neurons representing the lower visual field preferred on average crossed (near) disparities, whereas neurons representing the upper visual field tended to prefer uncrossed (far) disparities (Sprague et al., 2015). These data are in line with a very recent fMRI study in humans, showing that near and far stimuli preferentially activated disparity-selective cortical columns located in the lower and upper visual field, respectively (Nasr and Tootell, 2016).

The natural distribution of binocular disparities has been recently examined in humans performing everyday tasks, such as walking indoors or outdoors, making a sandwich and ordering coffee (Sprague et al., 2015). Using a head-mounted device, the disparities during these tasks were measured and related to their position in the images. It was found that disparities are distributed along a clear gradient in elevation, with crossed (near) disparities in the lower portion of the images and uncrossed (far) disparities in the upper, thereby matching the lower/crossed, upper/uncrossed pattern of DT neurons as measured in the preliminary results of this study. It is likely that a similar distribution of disparities characterizes natural viewing in mice too, if not with even a more marked vertical gradient, considering the environment they live in and the way they interact with it.

Furthermore, the inhomogeneous distribution of visual features in natural images, observed also for features other than disparity, such as orientation, luminance, and color (Geisler, 2008), suggest that information on RF position in visual space should be taken into account when examining RF properties in general (Sprague et al., 2015). As also suggested by the preliminary data discussed here, caution should be exercised in ascribing specific visual feature selectivities to certain areas, considering that the retinotopic representation can be considerably different across areas and even within the same area. It is plausible, for example, that certain inconsistencies in stimulus selectivities of mouse visual areas reported across studies might be in part explained by different samplings in relation to the retinotopic location of the

recordings, which was often not taken into account (e.g. [Andermann et al., 2011](#); [Marshel et al., 2011](#); [Roth et al., 2012](#)).

The fact that the elevation-dependent distribution of disparity preferences reflects the statistics of naturally occurring disparities may provide another prime example of how visual experience sculpts RF properties during development, potentially also pointing to the true physiological role of ocular dominance (OD) plasticity. OD plasticity has long been a classic example of how neuronal circuits are shaped by experience. Typically, OD plasticity is experimentally induced by monocular visual deprivation during the critical period, leading to dramatic shifts in the binocular responses of neurons in the visual cortex toward the open eye. However, under normal visual experience during development, OD plasticity serves to align eye-specific inputs at the level of individual binocular neurons, resulting in matched orientation preference between left and right eye RF ([Wang et al., 2010](#)). The matching of orientation tuning across eyes might then be necessary for generating normal disparity tuning and, ultimately, optimal binocular vision.

It is also interesting to note a certain synchrony between the critical period for OD plasticity, which is generally considered to peak between postnatal day 28 and 32 ([Gordon and Stryker, 1996](#); [Levelt and Hübener, 2012](#)), and the developmental growth of the mouse skull, which largely declines at postnatal day 28 after a rapid growth earlier ([Vora et al., 2016](#)). The inter-eye distance (i.e. inter-zygomatic arch width) passes from ~8 mm at postnatal day 14 (corresponding to eye opening) to ~10 mm at postnatal day 28, after which no substantial increase follows ([Vora et al., 2016](#)). Taking into account the stereo-geometry of the mouse visual system, as described above, objects located in a range of distances of [3, 20] cm are estimated to correspond to binocular disparities of [-10.7, 2.3] deg with an inter-eye distance of 8 mm, and to binocular disparities of [-13.4, 2.9] deg with an inter-eye distance of 10 mm. Furthermore, the timing of OD plasticity and skull growth is also paralleled by the development of the refractive state of the mouse eye, with mice showing a strong myopic refractive error at young age that improves rapidly and disappears at postnatal day 32 ([Tkatchenko et al., 2010](#)). Thus, it seems plausible that a period of increased plasticity, matching the critical period for OD, might be useful for DT neurons to adapt to changes in visual input due to skull and eye development. Analogously, a correlation between skull development and neural plasticity of the auditory system of barn owls has been found ([Carr and Boudreau, 1996](#); [Knudsen, 2002](#)). The developmental increase in the inter-ear distance leads to changes in the interaural timing differences, which are key sound localization cues resulting from the interaction of head and ears with incoming sound stimuli. Such a phenomenon could contribute to explaining the critical period timing in the barn owl auditory system ([Carr and Boudreau, 1996](#); [Knudsen, 2002](#)).

Therefore, there seems to be a tight relationship between the statistical contents of natural images and binocular neuronal properties, whereby visual experience might play a key role for achieving the best adaptation to a 3D visual environment. Questions about the exact mechanisms mediating this refined adaptation, how much they rely on experience or to what extent they are hard-wired, still need to be understood. For example, the interocular matching of RF orientations as a prerequisite for developing normal sensitivity to binocular disparity, and the role of visual experience therein, could be investigated by adapting a protocol using prism goggles to optically rotate

the visual field between the two eyes (Shinkman and Bruce, 1977; Kreile et al., 2011). In addition, it will be valuable to measure the actual image statistics of mouse viewing using a similar approach as in Sprague et al. (2015). This would allow analyzing specific RF properties as a function of image statistics, and might help understanding how the visual system comes to encode image features with optimal efficiency.

Finally, this crossed/uncrossed disparity biases in lower/upper visual fields would also provide a neural mechanism explaining certain known distance misjudgments in humans, in which objects below the line of sight appear closer than they actually are, whereas object distance is overestimated in the upper visual field (Breitmeyer et al., 1977; Wallach and O’Leary, 1982; Ooi et al., 2001; Yang and Purves, 2003). This might also contribute to explaining the moon illusion, in which the moon looks larger near the horizon than near the zenith (Kaufman and Kaufman, 2000; Antonides and Kubota, 2016).

4.2.9 Outlook and future experiments: Dendritic mechanisms of binocular integration

Numerous studies in cats and monkeys have investigated the processing of binocular disparity, providing a basic understanding of the underlying neuronal and circuit mechanisms. However, our knowledge is mostly based on single unit extracellular recordings, which can only measure the action potential output of individual neurons. As such, the actual synaptic mechanisms underlying disparity selectivity remain largely unexplored, with most insights coming from theoretical studies (Koch and Poggio, 1987; Qian, 1997; Mel et al., 1998a,b; Archie and Mel, 2000). To address such questions experimentally, the mouse model might prove to be particularly valuable.

According to an influential model proposed by Archie and Mel (2000), disparity selectivity could be generated at the single-dendrite level, by synergistic interactions of neighboring, eye-specific synaptic inputs. Left- and right-eye inputs located on the same stretch of dendrite cover a specific region of each eye’s visual field, with a systematic spatial offset between the visual field of the two eyes. The nonlinear interaction of these neighboring inputs, dependent on the spatiotemporal distribution of synapses and on active dendritic properties (e.g. voltage-dependent sodium, calcium, and NMDA spikes; London and Häusser, 2005; Stuart and Spruston, 2015; Tran-Van-Minh et al., 2015), can lead to binocular, disparity-specific facilitation. This model could be experimentally tested by exploiting *in vivo* two-photon calcium imaging of dendritic spines in the mouse (Grienberger et al., 2014). This method allows measuring local calcium signals in dendrites and single dendritic spines (the postsynaptic sites of most excitatory synapses) evoked by synaptic input activation. On a given dendrite of a binocular cell, the RFs of individual synaptic inputs could be mapped for each eye by using sparse noise visual stimuli (as illustrated in Fig. 4.1c), similarly to previous reports (Iacaruso et al., 2017). Using this approach, the organization of eye-specific inputs on individual dendrites could be examined, potentially helping to understand the synaptic mechanisms underlying binocular disparity. Moreover, since binocular cells integrate signals from two well-defined sensory sources (i.e. the two eyes), each under precise experimental control, they potentially

offer an excellent model system for studying dendritic integration *in vivo*, which has not been exploited yet.

In conclusion, it is worth pointing out that the intricacies of dendritic binocular integration, as outlined above, can give a hint as to why, in the study about the origin of direction selectivity in the first part of this thesis, dichoptic apparent motion produced a complex variety of neuronal responses whose interpretation proved to be so difficult.

4.2.10 Concluding remarks

This part of the Thesis demonstrates that binocular integration is strongly represented among individual neurons in mouse cortical areas V1, LM, and RL. In many cells, binocular integration endows these cells with sensitivity for retinal disparities. Although all three areas are engaged in disparity processing, the respective representations of binocular disparities show clear differences, with area RL being more specialized for near visual objects, compared to V1 and LM.

These findings were enabled by using, for the first time in the mouse, 3D stimuli based on random dot stereograms, which have been crucial for stereopsis research in primates. The development of this experimental paradigm opens up the possibility for further investigations into disparity processing and stereopsis in both anesthetized and awake mice.

While most thoroughly investigated in primates, and largely neglected in mice so far, studying mouse binocular vision promises to be particularly valuable, as indicated by this study. Mice offer unmatched opportunities to monitor and manipulate specific neurons and circuits through an arsenal of well-established methods, including transgene expression, trans-synaptic tracing of neuronal connections, and optogenetics (Kim et al., 2017; Daigle et al., 2018; Luo et al., 2018). The small, lissencephalic cortex of the mouse allows an easier accessibility to most cortical regions for large-scale recordings, such that even multiple areas could be monitored and manipulated at the same time (Goard et al., 2016; Sofroniew et al., 2016; Stirman et al., 2016). In addition, the attention that the mouse model has received in the last decade has led to a number of behavioral paradigms that have already produced a great amount of evidence for clear and quantifiable visually-mediated behaviors (Busse et al., 2011; Carandini and Churchland, 2013; Glickfeld et al., 2013a; Burgess et al., 2017; Marques et al., 2018). Therefore, the experimental tractability of the mouse will likely be of great importance for dissecting the cellular and network principles underlying binocular vision in mammals.

BIBLIOGRAPHY

- Adams, D. L. and S. Zeki
2001 "Functional organization of macaque V3 for stereoscopic depth." *Journal of Neurophysiology*, 86, 5, pp. 2195-203, DOI: [10.1152/jn.2001.86.5.2195](https://doi.org/10.1152/jn.2001.86.5.2195).
- Adesnik, H.
2017 "Synaptic mechanisms of feature coding in the visual cortex of awake mice." *Neuron*, 95, 5, 1147-1159.e4, DOI: [10.1016/j.neuron.2017.08.014](https://doi.org/10.1016/j.neuron.2017.08.014).
- Ahmadlou, M. and J. A. Heimel
2015 "Preference for concentric orientations in the mouse superior colliculus", *Nature Communications*, 6, p. 6773, DOI: [10.1038/ncomms7773](https://doi.org/10.1038/ncomms7773).
- Almada, R. C., A. J. Genewsky, D. E. Heinz, P. M. Kaplick, N. C. Coimbra, and C. T. Wotjak
2018 "Stimulation of the nigroretectal pathway at the level of the superior colliculus reduces threat recognition and causes a shift from avoidance to approach behavior", *Frontiers in Neural Circuits*, 12, May, pp. 1-9, DOI: [10.3389/fncir.2018.00036](https://doi.org/10.3389/fncir.2018.00036).
- Alonso, J. M., W. M. Usrey, and R. C. Reid
2001 "Rules of connectivity between geniculate cells and simple cells in cat primary visual cortex." *Journal of Neuroscience*, 21, 11, pp. 4002-15, DOI: [10.1523/JNEUROSCI.2111-00.2001](https://doi.org/10.1523/JNEUROSCI.2111-00.2001).
- Andermann, M. L., A. M. Kerlin, D. K. Roumis, L. L. Glickfeld, and R. C. Reid
2011 "Functional specialization of mouse higher visual cortical areas." *Neuron*, 72, 6, pp. 1025-39, DOI: [10.1016/j.neuron.2011.11.013](https://doi.org/10.1016/j.neuron.2011.11.013).
- Andersen, R. A. and C. A. Buneo
2002 "Intentional maps in posterior parietal cortex." *Annual Review of Neuroscience*, 25, 1, pp. 189-220, DOI: [10.1146/annurev.neuro.25.1.142922](https://doi.org/10.1146/annurev.neuro.25.1.142922).
- Antonides, J. and T. Kubota
2016 "Binocular disparity as an explanation for the moon illusion", *arXiv*, i, pp. 1-8, arXiv: [1301.2715](https://arxiv.org/abs/1301.2715).
- Anzai, A. and G. C. DeAngelis
2010 "Neural computations underlying depth perception", *Current Opinion in Neurobiology*, 20, 3, pp. 367-375, DOI: [10.1016/j.conb.2010.04.006](https://doi.org/10.1016/j.conb.2010.04.006).
- Archie, K. A. and B. W. Mel
2000 "A model for intradendritic computation of binocular disparity." *Nature Neuroscience*, 3, 1, pp. 54-63, DOI: [10.1038/71125](https://doi.org/10.1038/71125).
- Averbeck, B. B., P. E. Latham, and A. Pouget
2006 "Neural correlations, population coding and computation." *Nature Reviews Neuroscience*, 7, 5, pp. 358-366, DOI: [10.1038/nrn1888](https://doi.org/10.1038/nrn1888).
- Ayaz, A., A. B. Saleem, M. L. Schölvinc, and M. Carandini
2013 "Locomotion controls spatial integration in mouse visual cortex." *Current Biology*, 23, 10, pp. 890-4, DOI: [10.1016/j.cub.2013.04.012](https://doi.org/10.1016/j.cub.2013.04.012).

- Baden, T., P. Berens, K. Franke, M. Roman-Roson, M. Bethge, and Euler
 2016 "The functional diversity of mouse retinal ganglion cells", *Nature*, pp. 1-21, DOI: [10.1038/nature16468](https://doi.org/10.1038/nature16468).
- Banks, M. S., S. Gepshtein, and M. S. Landy
 2004 "Why is spatial stereoresolution so low?", *Journal of Neuroscience*, 24, 9, pp. 2077-89, DOI: [10.1523/JNEUROSCI.3852-02.2004](https://doi.org/10.1523/JNEUROSCI.3852-02.2004).
- Banks, M. S., D. M. Hoffman, J. Kim, and G. Wetzstein
 2016 "3D Displays", *Annual Review of Vision Science*, 2, 1, pp. 397-435, DOI: [10.1146/annurev-vision-082114-035800](https://doi.org/10.1146/annurev-vision-082114-035800).
- Barlow, H. B., R. M. Hill, and W. R. Levick
 1964 "Retinal ganglion cells responding selectively to direction and speed of image motion in the rabbit", *Journal of Physiology*, 173, pp. 377-407, DOI: doi.org/10.1113/jphysiol.1964.sp007463.
- Barlow, H. B. and W. R. Levick
 1965 "The mechanism of directionally selective units in rabbit's retina." *Journal of Physiology*, 178, 3, pp. 477-504, DOI: doi.org/10.1113/jphysiol.1965.sp007638.
- Barlow, H. B., C. Blakemore, and J. D. Pettigrew
 1967 "The neural mechanism of binocular depth discrimination", *Journal of Physiology*, 193, 2, pp. 327-342, DOI: [10.1113/jphysiol.1967.sp008360](https://doi.org/10.1113/jphysiol.1967.sp008360).
- Barlow, H. B. and R. M. Hill
 1963 "Selective sensitivity to direction of movement in ganglion cells of the rabbit retina", *Science*, 139, 3553, pp. 412-412, DOI: [10.1126/science.139.3553.412](https://doi.org/10.1126/science.139.3553.412).
- Barry, S. R.
 2009 *Fixing my gaze*, Basic Books, New York, p. 272.
- Beer, Z., C. Chwiesko, T. Kitsukawa, and M. M. Sauvage
 2013 "Spatial and stimulus-type tuning in the LEC, MEC, POR, PrC, CA1, and CA3 during spontaneous item recognition memory", *Hippocampus*, 23, 12, pp. 1425-1438, DOI: [10.1002/hipo.22195](https://doi.org/10.1002/hipo.22195).
- Berens, P.
 2009 "CircStat: A MATLAB toolbox for circular statistics", *Journal of Statistical Software*, 31, 10, pp. 1-21, DOI: [10.1002/wics.10](https://doi.org/10.1002/wics.10).
- Berg, R. W. and D. Kleinfeld
 2003 "Rhythmic whisking by rat: retraction as well as protraction of the vibrissae is under active muscular control." *Journal of Neurophysiology*, 89, 1, pp. 104-117, DOI: [10.1152/jn.00600.2002](https://doi.org/10.1152/jn.00600.2002).
- Bergmann, K., P. Meza Santoscoy, K. Lygdas, Y. Nikolaeva, R. MacDonald, V. Cunliffe, and A. Nikolaev
 2018 "Imaging neuronal activity in the optic tectum of late stage larval zebrafish", *Journal of Developmental Biology*, 6, 1, p. 6, DOI: [10.3390/jdb6010006](https://doi.org/10.3390/jdb6010006).
- Bleckert, A., G. W. Schwartz, M. H. Turner, F. Rieke, and R. O. L. Wong
 2014 "Visual space is represented by nonmatching topographies of distinct mouse retinal ganglion cell types", *Current Biology*, 24, 3, pp. 310-315, DOI: [10.1016/j.cub.2013.12.020](https://doi.org/10.1016/j.cub.2013.12.020).

- Bocci, T., M. Pietrasanta, C. Cerri, L. Restani, M. Caleo, and F. Sartucci
 2014 "Visual callosal connections: Role in visual processing in health and disease", *Reviews in the Neurosciences*, 25, 1, pp. 113-127, DOI: [10.1515/revneuro-2013-0025](https://doi.org/10.1515/revneuro-2013-0025).
- Bonhoeffer, T. and A. Grinvald
 1991 "Iso-orientation domains in cat visual cortex are arranged in pinwheel-like patterns", *Nature*, 353, 6343, pp. 429-431, DOI: [10.1038/353429a0](https://doi.org/10.1038/353429a0).
- Bonhoeffer, T. and M. Hübener
 2016 "Intrinsic optical imaging of functional map development in mammalian visual cortex", *Cold Spring Harbor Protocols*, 2016, 6, pdb.top089383, DOI: [10.1101/pdb.top089383](https://doi.org/10.1101/pdb.top089383).
- Bonin, V., M. H. Histed, S. Yurgenson, and R. C. Reid
 2011 "Local diversity and fine-scale organization of receptive fields in mouse visual cortex." *Journal of Neuroscience*, 31, 50, pp. 18506-21, DOI: [10.1523/JNEUROSCI.2974-11.2011](https://doi.org/10.1523/JNEUROSCI.2974-11.2011).
- Born, R. T. and D. C. Bradley
 2005 "Structure and function of visual area MT", *Annual Review of Neuroscience*, 28, 1, pp. 157-189, DOI: [10.1146/annurev.neuro.26.041002.131052](https://doi.org/10.1146/annurev.neuro.26.041002.131052).
- Borst, A. and M. Helmstaedter
 2015 "Common circuit design in fly and mammalian motion vision", *Nature Neuroscience*, 18, 8, DOI: [10.1038/nn.4050](https://doi.org/10.1038/nn.4050).
- Bough, E. W.
 1970 "Stereoscopic vision in the macaque monkey: A behavioural demonstration", *Nature*, 225, 5227, pp. 42-44, DOI: [10.1038/225042a0](https://doi.org/10.1038/225042a0).
- Bours, R. J., M. C. Kroes, and M. J. Lankheet
 2009 "Sensitivity for reverse-phi motion", *Vision Research*, 49, 1, pp. 1-9, DOI: [10.1016/j.visres.2008.09.014](https://doi.org/10.1016/j.visres.2008.09.014).
- Brainard, D. H.
 1997 "The Psychophysics Toolbox", *Spatial Vision*, 10, 4, pp. 433-436, DOI: [10.1163/156856897X00357](https://doi.org/10.1163/156856897X00357).
- Breitmeyer, B., F. Battaglia, and J. Bridge
 1977 "Existence and implications of a tilted binocular disparity space", *Perception*, 6, 2, pp. 161-164, DOI: [10.1068/p060161](https://doi.org/10.1068/p060161).
- Briggman, K. L., M. Helmstaedter, and W. Denk
 2011 "Wiring specificity in the direction-selectivity circuit of the retina." *Nature*, 471, 7337, pp. 183-8, DOI: [10.1038/nature09818](https://doi.org/10.1038/nature09818).
- Burge, J. and W. S. Geisler
 2014 "Optimal disparity estimation in natural stereo images", *Journal of Vision*, 14, 2, pp. 1-, DOI: [10.1167/14.2.1.doi](https://doi.org/10.1167/14.2.1.doi).
- Burgess, C. P., A. Lak, N. A. Steinmetz, P. Zátka-Haas, C. Bai Reddy, E. A. K. Jacobs, J. F. Linden, J. J. Paton, A. Ranson, S. Schröder, S. Soares, M. J. Wells, L. E. Wool, K. D. Harris, and M. Carandini
 2017 "High-yield methods for accurate two-alternative visual psychophysics in head-fixed mice", *Cell Reports*, 20, 10, pp. 2513-2524, DOI: [10.1016/j.celrep.2017.08.047](https://doi.org/10.1016/j.celrep.2017.08.047).
- Busse, L., A. Ayaz, N. T. Dhruv, S. Katzner, A. B. Saleem, M. L. Scholvinck, A. D. Zaharia, and M. Carandini
 2011 "The detection of visual contrast in the behaving mouse", *Journal of Neuroscience*, 31, 31, pp. 11351-11361, DOI: [10.1523/JNEUROSCI.6689-10.2011](https://doi.org/10.1523/JNEUROSCI.6689-10.2011).

- Callaway, E. M. and L. Luo
 2015 "Monosynaptic circuit tracing with glycoprotein-deleted rabies viruses", *Journal of Neuroscience*, 35, 24, pp. 8979-8985, DOI: [10.1523/JNEUROSCI.0409-15.2015](https://doi.org/10.1523/JNEUROSCI.0409-15.2015), arXiv: [NIHMS150003](https://arxiv.org/abs/1508.0003).
- Carandini, M. and A. K. Churchland
 2013 "Probing perceptual decisions in rodents", *Nature Neuroscience*, 16, 7, pp. 824-831, DOI: [10.1038/nn.3410](https://doi.org/10.1038/nn.3410).
- Carr, C. E. and R. E. Boudreau
 1996 "Development of the time coding pathways in the auditory brainstem of the barn owl", *Journal of Comparative Neurology*, 373, 4, pp. 467-83, DOI: [10.1002/\(SICI\)1096-9861\(19960930\)373:4<467::AID-CNE1>3.0.CO;2-#](https://doi.org/10.1002/(SICI)1096-9861(19960930)373:4<467::AID-CNE1>3.0.CO;2-#).
- Cerri, C., L. Restani, and M. Caleo
 2010 "Callosal contribution to ocular dominance in rat primary visual cortex", *European Journal of Neuroscience*, 32, 7, pp. 1163-1169, DOI: [10.1111/j.1460-9568.2010.07363.x](https://doi.org/10.1111/j.1460-9568.2010.07363.x).
- Chalupa, L. M. and R. W. Williams
 2008 *Eye, Retina, and Visual System of the Mouse*, Cambridge, MA: MIT Press.
- Chapman, B., K. R. Zahs, and M. P. Stryker
 1991 "Relation of cortical cell orientation selectivity to alignment of receptive fields of the geniculocortical afferents that arborize within a single orientation column in ferret visual cortex." *Journal of Neuroscience*, 11, 5, pp. 1347-58, DOI: doi.org/10.1523/JNEUROSCI.11-05-01347.1991.
- Chen, G., J. A. King, N. Burgess, and J. O'Keefe
 2013a "How vision and movement combine in the hippocampal place code", *Proceedings of the National Academy of Sciences*, 110, 1, pp. 378-383, DOI: [10.1073/pnas.1215834110](https://doi.org/10.1073/pnas.1215834110).
- Chen, G., H. D. Lu, and A. W. Roe
 2008 "A map for horizontal disparity in monkey V2", *Neuron*, 58, 3, pp. 442-450, DOI: [10.1016/j.neuron.2008.02.032](https://doi.org/10.1016/j.neuron.2008.02.032).
- Chen, T.-W., T. J. Wardill, Y. Sun, S. R. Pulver, S. L. Renninger, A. Baohan, E. R. Schreier, R. a. Kerr, M. B. Orger, V. Jayaraman, L. L. Looger, K. Svoboda, and D. S. Kim
 2013b "Ultrasensitive fluorescent proteins for imaging neuronal activity", *Nature*, 499, 7458, pp. 295-300, DOI: [10.1038/nature12354](https://doi.org/10.1038/nature12354).
- Cheong, S. K., C. Tailby, S. G. Solomon, and P. R. Martin
 2013 "Cortical-like receptive fields in the lateral geniculate nucleus of marmoset monkeys", *Journal of Neuroscience*, 33, 16, pp. 6864-6876, DOI: [10.1523/JNEUROSCI.5208-12.2013](https://doi.org/10.1523/JNEUROSCI.5208-12.2013).
- Chung, S. and D. Ferster
 1998 "Strength and orientation tuning of the thalamic input to simple cells revealed by electrically evoked cortical suppression", *Neuron*, 20, 6, pp. 1177-89, DOI: [10.1016/S0896-6273\(00\)80498-5](https://doi.org/10.1016/S0896-6273(00)80498-5).
- Cleland, B. G. and W. R. Levick
 1974 "Properties of rarely encountered types of ganglion cells in the cat's retina and on overall classification", *Journal of Physiology*, 240, 2, pp. 457-492, DOI: [10.1113/jphysiol.1974.sp010618](https://doi.org/10.1113/jphysiol.1974.sp010618).

- Cléry, J., O. Guipponi, S. Odouard, C. Wardak, and S. Ben Hamed
 2018 "Cortical networks for encoding near and far space in the non-human primate", *NeuroImage*, 176, April, pp. 164-178, DOI: [10.1016/j.neuroimage.2018.04.036](https://doi.org/10.1016/j.neuroimage.2018.04.036).
- Cléry, J., O. Guipponi, C. Wardak, and S. Ben Hamed
 2015 "Neuronal bases of peripersonal and extrapersonal spaces, their plasticity and their dynamics: Knowns and unknowns", *Neuropsychologia*, 70, pp. 313-326, DOI: [10.1016/j.neuropsychologia.2014.10.022](https://doi.org/10.1016/j.neuropsychologia.2014.10.022).
- Cohen, M. R. and A. Kohn
 2011 "Measuring and interpreting neuronal correlations." *Nature Neuroscience*, 14, 7, pp. 811-819, DOI: [10.1038/nn.2842](https://doi.org/10.1038/nn.2842).
- Coleman, J. E., K. Law, and M. F. Bear
 2009 "Anatomical origins of ocular dominance in mouse primary visual cortex", *Neuroscience*, 161, 2, pp. 561-571, DOI: [10.1016/j.neuroscience.2009.03.045](https://doi.org/10.1016/j.neuroscience.2009.03.045).
- Collett, T.
 1977 "Stereopsis in toads", *Nature*, 267, 5609, pp. 349-51, DOI: [10.1038/267349a0](https://doi.org/10.1038/267349a0).
- Combrisson, E. and K. Jerbi
 2015 "Exceeding chance level by chance: The caveat of theoretical chance levels in brain signal classification and statistical assessment of decoding accuracy", *Journal of Neuroscience Methods*, 250, pp. 126-136, DOI: [10.1016/j.jneumeth.2015.01.010](https://doi.org/10.1016/j.jneumeth.2015.01.010).
- Cooke, S. F., R. W. Komorowski, E. S. Kaplan, J. P. Gavornik, and M. F. Bear
 2015 "Visual recognition memory, manifested as long-term habituation, requires synaptic plasticity in V1", *Nature Neuroscience*, 18, 2, pp. 262-271, DOI: [10.1038/nn.3920](https://doi.org/10.1038/nn.3920), arXiv: [15334406](https://arxiv.org/abs/15334406).
- Cortes, C. and V. Vapnik
 1995 "Support-Vector Networks", *Machine Learning*, 20, 3, pp. 273-297, DOI: [10.1023/A:1022627411411](https://doi.org/10.1023/A:1022627411411).
- Crapse, T. B., H. Lau, and M. A. Basso
 2017 "A role for the superior colliculus in decision criteria", *Neuron*, 97, 1, 181-194.e6, DOI: [10.1016/j.neuron.2017.12.006](https://doi.org/10.1016/j.neuron.2017.12.006).
- Cruz-Martín, A., R. N. El-Danaf, F. Osakada, B. Sriram, O. S. Dhande, P. L. Nguyen, E. M. Callaway, A. Ghosh, and A. D. Huberman
 2014 "A dedicated circuit links direction-selective retinal ganglion cells to the primary visual cortex", *Nature*, 507, 7492, pp. 358-361, DOI: [10.1038/nature12989](https://doi.org/10.1038/nature12989).
- Cumming, B. G. and G. C. DeAngelis
 2001 "The physiology of stereopsis", *Annual Review of Neuroscience*, 24, pp. 203-38, DOI: [10.1146/annurev.neuro.24.1.203](https://doi.org/10.1146/annurev.neuro.24.1.203).
- Cumming, B. G. and A. J. Parker
 1999 "Binocular neurons in V1 of awake monkeys are selective for absolute, not relative, disparity." *Journal of Neuroscience*, 19, 13, pp. 5602-5618, DOI: [10.1523/JNEUROSCI.19-13-05602.1999](https://doi.org/10.1523/JNEUROSCI.19-13-05602.1999).
- Cumming, B. G. and A. J. Parker
 1997 "Responses of primary visual cortical neurons to binocular disparity without depth perception." *Nature*, 389, 6648, pp. 280-3, DOI: [10.1038/38487](https://doi.org/10.1038/38487).

- Czuba, T. B., A. C. Huk, L. K. Cormack, and A. Kohn
 2014 "Area MT encodes three-dimensional motion", *Journal of Neuroscience*, 34, 47, pp. 15522-33, DOI: [10.1523/JNEUROSCI.1081-14.2014](https://doi.org/10.1523/JNEUROSCI.1081-14.2014).
- D'Souza, R. D. and A. Burkhalter
 2017 "A laminar organization for selective cortico-cortical communication", *Frontiers in Neuroanatomy*, 11, August, pp. 1-13, DOI: [10.3389/fnana.2017.00071](https://doi.org/10.3389/fnana.2017.00071).
- D'Souza, R. D., Q. Wang, W. Ji, A. Meier, H. Kennedy, K. Knoblauch, and A. Burkhalter
 2017 "A hierarchical organization of mouse visual cortical areas", *Program No. 312.13. 2017 Neuroscience Meeting Planner. Washington, DC: Society for Neuroscience, 2017. Online.*
- Daigle, T. L., L. Madisen, T. A. Hage, M. T. Valley, U. Knoblich, R. S. Larsen, M. M. Takeno, L. Huang, H. Gu, R. Larsen, M. Mills, A. Bosma-Moody, L. A. Siverts, M. Walker, L. T. Graybuck, Z. Yao, O. Fong, T. N. Nguyen, E. Garren, G. H. Lenz, M. Chavarha, J. Pendergraft, J. Harrington, K. E. Hirokawa, J. A. Harris, P. R. Nicovich, M. J. McGraw, D. R. Ollerenshaw, K. A. Smith, C. A. Baker, J. T. Ting, S. M. Sunkin, J. Lecoq, M. Z. Lin, E. S. Boyden, G. J. Murphy, N. M. da Costa, J. Waters, L. Li, B. Tasic, and H. Zeng
 2018 "A suite of transgenic driver and reporter mouse lines with enhanced brain-cell-type targeting and functionality", *Cell*, 174, 2, pp. 465-480, DOI: [10.1016/j.cell.2018.06.035](https://doi.org/10.1016/j.cell.2018.06.035).
- Dana, H., B. Mohar, Y. Sun, S. Narayan, A. Gordus, J. P. Hasseman, G. Tsegaye, G. T. Holt, A. Hu, D. Walpita, R. Patel, J. J. Macklin, C. I. Bargmann, M. B. Ahrens, E. R. Schreiter, V. Jayaraman, L. L. Looger, K. Svoboda, and D. S. Kim
 2016 "Sensitive red protein calcium indicators for imaging neural activity", *eLife*, 5, MARCH2016, pp. 1-24, DOI: [10.7554/eLife.12727](https://doi.org/10.7554/eLife.12727).
- De Franceschi, G., T. Vivattanasarn, A. B. Saleem, and S. G. Solomon
 2016 "Vision guides selection of freeze or flight defense strategies in mice", *Current Biology*, 26, 16, pp. 2150-2154, DOI: [10.1016/j.cub.2016.06.006](https://doi.org/10.1016/j.cub.2016.06.006).
- De la Cera, E. G., G. Rodríguez, L. Llorente, F. Schaeffel, and S. Marcos
 2006 "Optical aberrations in the mouse eye", *Vision Research*, 46, 16, pp. 2546-2553, DOI: [10.1016/j.visres.2006.01.011](https://doi.org/10.1016/j.visres.2006.01.011).
- DeAngelis, G. C., B. G. Cumming, and W. T. Newsome
 1998 "Cortical area MT and the perception of stereoscopic depth." *Nature*, 394, August, pp. 677-680, DOI: [10.1038/29299](https://doi.org/10.1038/29299).
- DeAngelis, G. C. and W. T. Newsome
 1999 "Organization of disparity-selective neurons in macaque area MT." *Journal of Neuroscience*, 19, 4, pp. 1398-1415, DOI: doi.org/10.1523/JNEUROSCI.19-04-01398.1999.
- DeAngelis, G. C. and T. Uka
 2003 "Coding of horizontal disparity and velocity by MT neurons in the alert macaque." *Journal of Neurophysiology*, 89, 2, pp. 1094-1111, DOI: [10.1152/jn.00717.2002](https://doi.org/10.1152/jn.00717.2002).
- Denk, W., J. Strickler, and W. Webb
 1990 "Two-photon laser scanning fluorescence microscopy", *Science*, 248, 4951, pp. 73-76, DOI: [10.1126/science.2321027](https://doi.org/10.1126/science.2321027).

- Denk, W. and K. Svoboda
 1997 "Photon upmanship: Why multiphoton imaging is more than a gimmick", *Neuron*, 18, 3, pp. 351-357, DOI: [10.1016/S0896-6273\(00\)81237-4](https://doi.org/10.1016/S0896-6273(00)81237-4).
- Denman, D. J., J. H. Siegle, C. Koch, R. C. Reid, and T. J. Blanche
 2016 "Spatial organization of chromatic pathways in the mouse dorsal lateral geniculate nucleus", *Journal of Neuroscience*, 37, 5, pp. 1102-1116, DOI: [10.1523/JNEUROSCI.1742-16.2016](https://doi.org/10.1523/JNEUROSCI.1742-16.2016).
- Deschênes, M., J. Moore, and D. Kleinfeld
 2012 "Sniffing and whisking in rodents", *Current Opinion in Neurobiology*, 22, 2, pp. 243-250, DOI: [10.1016/j.conb.2011.11.013](https://doi.org/10.1016/j.conb.2011.11.013).
- Dhande, O. S. and A. D. Huberman
 2014 "Visual circuits: Mouse retina no longer a level playing field", *Current Biology*, 24, 4, R155-R156, DOI: [10.1016/j.cub.2013.12.045](https://doi.org/10.1016/j.cub.2013.12.045).
- Dhande, O. S., B. K. Stafford, J.-H. A. Lim, and A. D. Huberman
 2015 "Contributions of retinal ganglion cells to subcortical visual processing and behaviors", *Annual Review of Vision Science*, 1, 1, pp. 291-328, DOI: [10.1146/annurev-vision-082114-035502](https://doi.org/10.1146/annurev-vision-082114-035502).
- Dombeck, D. A., A. N. Khabbaz, F. Collman, T. L. Adelman, and D. W. Tank
 2007 "Imaging large-scale neural activity with cellular resolution in awake, mobile mice", *Neuron*, 56, 1, pp. 43-57, DOI: [10.1016/j.neuron.2007.08.003](https://doi.org/10.1016/j.neuron.2007.08.003).
- Dougherty, K., M. A. Cox, J. A. Westerberg, and A. Maier
 2018 "Binocular modulation of monocular V1 neurons", *bioRxiv*, DOI: <http://dx.doi.org/10.1101/320218>.
- Dräger, U. C.
 1975 "Receptive fields of single cells and topography in mouse visual cortex", *Journal of Comparative Neurology*, 160, 3, pp. 269-289, DOI: [10.1002/cne.901600302](https://doi.org/10.1002/cne.901600302).
 1978 "Observations on monocular deprivation in mice", *Journal of Neurophysiology*, 41, 1, pp. 28-42, DOI: [10.1152/jn.1978.41.1.28](https://doi.org/10.1152/jn.1978.41.1.28).
- Dräger, U. C. and J. F. Olsen
 1980 "Origins of crossed and uncrossed retinal projections in pigmented and albino mice", *Journal of Comparative Neurology*, 191, 3, pp. 383-412, DOI: [10.1002/cne.901910306](https://doi.org/10.1002/cne.901910306).
- Duijnhouwer, J. and B. Krekelberg
 2016 "Evidence and counterevidence in motion perception", *Cerebral Cortex*, 26, 12, pp. 4602-4612, DOI: [10.1093/cercor/bhw221](https://doi.org/10.1093/cercor/bhw221).
- Durand, S., R. Iyer, K. Mizuseki, S. de Vries, S. Mihalas, and R. C. Reid
 2016 "A comparison of visual response properties in the lateral geniculate nucleus and primary visual cortex of awake and anesthetized mice", *Journal of Neuroscience*, 36, 48, pp. 12144-12156, DOI: [10.1523/JNEUROSCI.1741-16.2016](https://doi.org/10.1523/JNEUROSCI.1741-16.2016).
- Eagleman, D. M.
 2001 "Visual illusions and neurobiology", *Nature Reviews Neuroscience*, 2, 12, pp. 920-6, DOI: [10.1038/35104092](https://doi.org/10.1038/35104092).
- Ellis, E. M., G. Gauvain, B. Sivyer, and G. J. Murphy
 2016 "Shared and distinct retinal input to the mouse superior colliculus and dorsal lateral geniculate nucleus", *Journal of Neurophysiology*, 116, 2, pp. 602-610, DOI: [10.1152/jn.00227.2016](https://doi.org/10.1152/jn.00227.2016).

- Emerson, R. C. and G. L. Gerstein
 1977 "Simple striate neurons in the cat. II. Mechanisms underlying directional asymmetry and direction selectivity", *Journal of Neurophysiology*, 40, 1, pp. 136-155, DOI: [10.1152/jn.1977.40.1.136](https://doi.org/10.1152/jn.1977.40.1.136).
- Emiliani, V., A. E. Cohen, K. Deisseroth, and M. Häusser
 2015 "All-optical interrogation of neural circuits", *Journal of Neuroscience*, 35, 41, pp. 13917-13926, DOI: [10.1523/JNEUROSCI.2916-15.2015](https://doi.org/10.1523/JNEUROSCI.2916-15.2015).
- Erisken, S., A. Vaiceliunaite, O. Jurjut, M. Fiorini, S. Katzner, and L. Busse
 2014 "Effects of locomotion extend throughout the mouse early visual system", *Current Biology*, 24, 24, pp. 2899-2907, DOI: [10.1016/j.cub.2014.10.045](https://doi.org/10.1016/j.cub.2014.10.045).
- Erulkar, S. D. and M. Fillenz
 1960 "Single-unit activity in the lateral geniculate body of the cat." *Journal of Physiology*, 154, 1, pp. 206-18, DOI: doi.org/10.1113/jphysiol.1960.sp006574.
- Erzurumlu, R. S. and P. Gaspar
 2012 "Development and critical period plasticity of the barrel cortex", *European Journal of Neuroscience*, 35, 10, pp. 1540-1553, DOI: [10.1111/j.1460-9568.2012.08075.x](https://doi.org/10.1111/j.1460-9568.2012.08075.x), arXiv: [NIHMS150003](https://arxiv.org/abs/NIHMS150003).
- Euler, T., P. B. Detwiler, and W. Denk
 2002 "Directionally selective calcium signals in dendrites of starburst amacrine cells", *Nature*, 418, 6900, pp. 845-852, DOI: [10.1038/nature00931](https://doi.org/10.1038/nature00931).
- Evans, D. A., A. V. Stempel, R. Vale, S. Ruehle, Y. Lefler, and T. Branco
 2018 "A synaptic threshold mechanism for computing escape decisions", *Nature*, 558, 7711, pp. 590-594, DOI: [10.1038/s41586-018-0244-6](https://doi.org/10.1038/s41586-018-0244-6).
- Feinberg, E. H. and M. Meister
 2015 "Orientation columns in the mouse superior colliculus", *Nature*, 519, 7542, pp. 229-232, DOI: [10.1038/nature14103](https://doi.org/10.1038/nature14103).
- Ferris, S. H.
 1972 "Motion parallax and absolute distance." *Journal of Experimental Psychology*, 95, 2, pp. 258-263, DOI: [10.1037/h0033605](https://doi.org/10.1037/h0033605).
- Ferster, D., S. Chung, and H. Wheat
 1996 "Orientation selectivity of thalamic input to simple cells of cat visual cortex", *Nature*, 380, 6571, pp. 249-252, DOI: [10.1038/380249a0](https://doi.org/10.1038/380249a0).
- Fox, M.
 1965 "The visual cliff test for the study of visual depth perception in the mouse", *Animal Behaviour*, 13, 2-3, 232-IN3, DOI: [10.1016/0003-3472\(65\)90040-0](https://doi.org/10.1016/0003-3472(65)90040-0).
- Fox, R., S. Lehmkuhle, and R. Bush
 1977 "Stereopsis in the falcon", *Science*, 197, 4298, pp. 79-81, DOI: [10.1126/science.867054](https://doi.org/10.1126/science.867054).
- Fried, S. I., T. a. Münch, and F. S. Werblin
 2002 "Mechanisms and circuitry underlying directional selectivity in the retina." *Nature*, 420, 6914, pp. 411-4, DOI: [10.1038/nature01179](https://doi.org/10.1038/nature01179).
- Gale, S. D. and G. J. Murphy
 2014 "Distinct representation and distribution of visual information by specific cell types in mouse superficial superior colliculus", *Journal of Neuroscience*, 34, 40, pp. 13458-13471, DOI: [10.1523/JNEUROSCI.2768-14.2014](https://doi.org/10.1523/JNEUROSCI.2768-14.2014).

- Gămănuț, R., H. Kennedy, Z. Toroczkai, D. V. Essen, K. Knoblauch, and A. Burkhalter
2018 "The mouse cortical connectome characterized by an ultra dense cortical graph maintains specificity by distinct connectivity profiles", *Neuron*, pp. 698-715, DOI: [10.1101/156976](https://doi.org/10.1101/156976).
- Garrett, M. E., I. Nauhaus, J. H. Marshel, and E. M. Callaway
2014 "Topography and areal organization of mouse visual cortex", *Journal of Neuroscience*, 34, 37, pp. 12587-12600, DOI: [10.1523/JNEUROSCI.1124-14.2014](https://doi.org/10.1523/JNEUROSCI.1124-14.2014).
- Gavornik, J. P. and M. F. Bear
2014 "Higher brain functions served by the lowly rodent primary visual cortex", *Learning & Memory*, 21, 10, pp. 527-533, DOI: [10.1101/lm.034355.114](https://doi.org/10.1101/lm.034355.114).
- Geisler, W. S.
2008 "Visual perception and the statistical properties of natural scenes", *Annual Review of Psychology*, 59, 1, pp. 167-192, DOI: [10.1146/annurev.psych.58.110405.085632](https://doi.org/10.1146/annurev.psych.58.110405.085632).
- Ghasemi, A. and S. Zahediasl
2012 "Normality tests for statistical analysis: A guide for non-statisticians", *International Journal of Endocrinology and Metabolism*, 10, 2, pp. 486-489, DOI: [10.5812/ijem.3505](https://doi.org/10.5812/ijem.3505).
- Ghazanfar, A. A. and C. E. Schroeder
2006 "Is neocortex essentially multisensory?", *Trends in Cognitive Sciences*, 10, 6, pp. 278-285, DOI: [10.1016/j.tics.2006.04.008](https://doi.org/10.1016/j.tics.2006.04.008), arXiv: [NIHMS150003](https://arxiv.org/abs/NIHMS150003).
- Ghodrati, M., S.-M. Khaligh-Razavi, and S. R. Lehky
2017 "Towards building a more complex view of the lateral geniculate nucleus: Recent advances in understanding its role", *Progress in Neurobiology*, 156, pp. 214-255, DOI: [10.1016/j.pneurobio.2017.06.002](https://doi.org/10.1016/j.pneurobio.2017.06.002).
- Glickfeld, L. L., M. H. Histed, and J. H. R. Maunsell
2013a "Mouse primary visual cortex is used to detect both orientation and contrast changes", *Journal of Neuroscience*, 33, 50, pp. 19416-19422, DOI: [10.1523/JNEUROSCI.3560-13.2013](https://doi.org/10.1523/JNEUROSCI.3560-13.2013).
- Glickfeld, L. L. and S. R. Olsen
2017 "Higher-order areas of the mouse visual cortex", *Annual Review of Vision Science*, 3, 1, annurev-vision-102016-061331, DOI: [10.1146/annurev-vision-102016-061331](https://doi.org/10.1146/annurev-vision-102016-061331).
- Glickfeld, L. L., R. C. Reid, and M. L. Andermann
2014 "A mouse model of higher visual cortical function", *Current Opinion in Neurobiology*, 24, 1, pp. 28-33, DOI: [10.1016/j.conb.2013.08.009](https://doi.org/10.1016/j.conb.2013.08.009).
- Glickfeld, L. L., M. L. Andermann, V. Bonin, and R. C. Reid
2013b "Cortico-cortical projections in mouse visual cortex are functionally target specific." *Nature Neuroscience*, 16, 2, pp. 219-26, DOI: [10.1038/nn.3300](https://doi.org/10.1038/nn.3300).
- Goard, M. J., G. N. Pho, J. Woodson, and M. Sur
2016 "Distinct roles of visual, parietal, and frontal motor cortices in memory-guided sensorimotor decisions." *eLife*, 5, pp. 1-30, DOI: [10.7554/eLife.13764](https://doi.org/10.7554/eLife.13764).
- Goldey, G. J., D. K. Roumis, L. L. Glickfeld, A. M. Kerlin, R. C. Reid, V. Bonin, D. P. Schafer, and M. L. Andermann
2014 "Removable cranial windows for long-term imaging in awake mice." *Nature Protocols*, 9, 11, pp. 2515-2538, DOI: [10.1038/nprot.2014.165](https://doi.org/10.1038/nprot.2014.165).

- Goltstein, P. M., J. S. Montijn, and C. M. a. Pennartz
 2015 "Effects of isoflurane anesthesia on ensemble patterns of Ca²⁺ activity in mouse V1: Reduced direction selectivity independent of increased correlations in cellular activity", *PLoS ONE*, 10, 2, e0118277, DOI: [10.1371/journal.pone.0118277](https://doi.org/10.1371/journal.pone.0118277).
- Goncalves, N. R., H. Ban, R. M. Sanchez-Panchuelo, S. T. Francis, D. Schluppeck, and A. E. Welchman
 2015 "7 tesla fMRI reveals systematic functional organization for binocular disparity in dorsal visual cortex", *Journal of Neuroscience*, 35, 7, pp. 3056-3072, DOI: [10.1523/JNEUROSCI.3047-14.2015](https://doi.org/10.1523/JNEUROSCI.3047-14.2015).
- Goncalves, N. R. and A. E. Welchman
 2017 ""What not" detectors help the brain see in depth", *Current Biology*, 27, 10, 1403-1412.e8, DOI: [10.1016/j.cub.2017.03.074](https://doi.org/10.1016/j.cub.2017.03.074).
- Gonzalez, F. and R. Perez
 1998 "Neural mechanisms underlying stereoscopic vision." *Progress in Neurobiology*, 55, 3, pp. 191-224, DOI: [10.1016/S0301-0082\(98\)00012-4](https://doi.org/10.1016/S0301-0082(98)00012-4).
- Gonzalez, F., M. A. Bermudez, A. F. Vicente, and M. C. Romero
 2010 "Orientation preference and horizontal disparity sensitivity in the monkey visual cortex", *Ophthalmic and Physiological Optics*, 30, 6, pp. 824-833, DOI: [10.1111/j.1475-1313.2010.00781.x](https://doi.org/10.1111/j.1475-1313.2010.00781.x).
- Göppert-Mayer, M.
 1931 "Über Elementarakte mit zwei Quantensprüngen", *Annalen der Physik*, 401, 3, pp. 273-294, DOI: [10.1002/andp.19314010303](https://doi.org/10.1002/andp.19314010303).
- Gordon, J. A. and M. P. Stryker
 1996 "Experience-dependent plasticity of binocular responses in the primary visual cortex of the mouse." *Journal of Neuroscience*, 16, 10, pp. 3274-86, DOI: [10.1523/JNEUROSCI.1632-96.1996](https://doi.org/10.1523/JNEUROSCI.1632-96.1996).
- Gradinaru, V., F. Zhang, C. Ramakrishnan, J. Mattis, R. Prakash, I. Diester, I. Goshen, K. R. Thompson, and K. Deisseroth
 2010 "Molecular and cellular approaches for diversifying and extending optogenetics", *Cell*, 141, 1, pp. 154-165, DOI: [10.1016/j.cell.2010.02.037](https://doi.org/10.1016/j.cell.2010.02.037).
- Graf, A. B. A., A. Kohn, M. Jazayeri, and J. A. Movshon
 2011 "Decoding the activity of neuronal populations in macaque primary visual cortex." *Nature Neuroscience*, 14, 2, pp. 239-245, DOI: [10.1038/nn.2733](https://doi.org/10.1038/nn.2733).
- Grama, A. and F. Engert
 2012 "Direction selectivity in the larval zebrafish tectum is mediated by asymmetric inhibition", *Frontiers in Neural Circuits*, 6, September, p. 59, DOI: [10.3389/fncir.2012.00059](https://doi.org/10.3389/fncir.2012.00059).
- Grienberger, C., X. Chen, and A. Konnerth
 2014 "Dendritic function in vivo", *Trends in Neurosciences*, 38, 1, pp. 45-54, DOI: [10.1016/j.tins.2014.11.002](https://doi.org/10.1016/j.tins.2014.11.002).
- Grienberger, C. and A. Konnerth
 2012 "Imaging Calcium in Neurons", *Neuron*, 73, 5, pp. 862-885, DOI: [10.1016/j.neuron.2012.02.011](https://doi.org/10.1016/j.neuron.2012.02.011).
- Grieve, K. L.
 2005 "Binocular visual responses in cells of the rat dLGN", *Journal of Physiology*, 566, 1, pp. 119-124, DOI: [10.1113/jphysiol.2005.090878](https://doi.org/10.1113/jphysiol.2005.090878).

- Grothe, B.
2018 "How the barn owl computes auditory space", *Trends in Neurosciences*, 41, 3, pp. 115-117, DOI: [10.1016/j.tins.2018.01.004](https://doi.org/10.1016/j.tins.2018.01.004).
- Grubb, M. S. and I. D. Thompson
2003 "Quantitative characterization of visual response properties in the mouse dorsal lateral geniculate nucleus", *Journal of Neurophysiology*, 90, 6, pp. 3594-3607, DOI: [10.1152/jn.00699.2003](https://doi.org/10.1152/jn.00699.2003).
- Gu, Y. and J. Cang
2016 "Binocular matching of thalamocortical and intracortical circuits in the mouse visual cortex", *eLife*, 5, pp. 1-14, DOI: [10.7554/eLife.22032](https://doi.org/10.7554/eLife.22032).
- Guido, W.
2018 "Development, form, and function of mouse visual thalamus." *Journal of Neurophysiology*, DOI: [10.1152/jn.00651.2017](https://doi.org/10.1152/jn.00651.2017).
- Guo, K., P. J. Benson, and C. Blakemore
2004 "Pattern motion is present in V1 of awake but not anaesthetized monkeys", *European Journal of Neuroscience*, 19, 4, pp. 1055-1066, DOI: [10.1111/j.1460-9568.2004.03212.x](https://doi.org/10.1111/j.1460-9568.2004.03212.x).
- Haefner, R. M. and B. G. Cumming
2008 "Adaptation to natural binocular disparities in primate V1 explained by a generalized energy model", *Neuron*, 57, 1, pp. 147-158, DOI: [10.1016/j.neuron.2007.10.042](https://doi.org/10.1016/j.neuron.2007.10.042).
- Hagihara, K. M., T. Murakami, T. Yoshida, Y. Tagawa, and K. Ohki
2015 "Neuronal activity is not required for the initial formation and maturation of visual selectivity", *Nature Neuroscience*, November, pp. 1-12, DOI: [10.1038/nn.4155](https://doi.org/10.1038/nn.4155).
- Haider, B., M. Häusser, and M. Carandini
2013 "Inhibition dominates sensory responses in the awake cortex." *Nature*, 493, 7430, pp. 97-100, DOI: [10.1038/nature11665](https://doi.org/10.1038/nature11665).
- Han, W., L. A. Tellez, M. J. Rangel, S. C. Motta, X. Zhang, I. O. Perez, N. S. Canteras, S. J. Shammah-Lagnado, A. N. van den Pol, and I. E. de Araujo
2017 "Integrated control of predatory hunting by the central nucleus of the amygdala", *Cell*, 168, 1-2, 311-324.e18, DOI: [10.1016/j.cell.2016.12.027](https://doi.org/10.1016/j.cell.2016.12.027).
- Han, Y., J. M. Kebschull, R. A. A. Campbell, D. Cowan, F. Imhof, A. M. Zador, and T. D. Mrsic-Flogel
2018 "The logic of single-cell projections from visual cortex", *Nature*, 556, 7699, pp. 51-56, DOI: [10.1038/nature26159](https://doi.org/10.1038/nature26159).
- Harris, K. D. and T. D. Mrsic-Flogel
2013 "Cortical connectivity and sensory coding", *Nature*, 503, 7474, pp. 51-8, DOI: [10.1038/nature12654](https://doi.org/10.1038/nature12654).
- Harris, K. D. and G. M. G. Shepherd
2015 "The neocortical circuit: themes and variations", *Nature Neuroscience*, 18, 2, pp. 170-181, DOI: [10.1038/nn.3917](https://doi.org/10.1038/nn.3917).
- Harvey, C. D., P. Coen, and D. W. Tank
2012 "Choice-specific sequences in parietal cortex during a virtual-navigation decision task", *Nature*, 484, 7392, pp. 62-68, DOI: [10.1038/nature10918](https://doi.org/10.1038/nature10918).
- Hassenstein, B. and W. Reichardt
1956 "Systemtheoretische Analyse der Zeit-, Reihenfolgen- und Vorzeichenauswertung bei der Bewegungsperzeption des Rüsselkäfers *Chlorophanus*", *Z. Naturforschg.* 11 b, pp. 513-524, DOI: doi.org/10.1515/znb-1956-9-1004.

- Hei, X., C. R. Stoelzel, J. Zhuang, Y. Bereshpolova, J. M. Huff, J.-M. Alonso, and H. A. Swadlow
 2014 "Directional selective neurons in the awake LGN: response properties and modulation by brain state", *Journal of Neurophysiology*, 112, 2, pp. 362-373, DOI: [10.1152/jn.00121.2014](https://doi.org/10.1152/jn.00121.2014).
- Helmchen, F. and W. Denk
 2005 "Deep tissue two-photon microscopy", *Nature Methods*, 2, 12, pp. 932-940, DOI: [10.1038/nmeth818](https://doi.org/10.1038/nmeth818), arXiv: [NIHMS150003](https://arxiv.org/abs/NIHMS150003).
- Hendel, T., M. Mank, B. Schnell, O. Griesbeck, A. Borst, and D. F. Reiff
 2008 "Fluorescence changes of genetic calcium indicators and OGB-1 correlated with neural activity and calcium in vivo and in vitro", *Journal of Neuroscience*, 28, 29, pp. 7399-7411, DOI: [10.1523/JNEUROSCI.1038-08.2008](https://doi.org/10.1523/JNEUROSCI.1038-08.2008).
- Hillier, D., M. Fiscella, A. Drinnenberg, S. Trenholm, S. B. Rompani, Z. Raics, G. Katona, J. Juettner, A. Hierlemann, B. Rozsa, and B. Roska
 2017 "Causal evidence for retina-dependent and -independent visual motion computations in mouse cortex", *Nature Neuroscience*, 20, 7, pp. 960-968, DOI: [10.1038/nn.4566](https://doi.org/10.1038/nn.4566).
- Hinkle, D. A. and C. E. Connor
 2005 "Quantitative characterization of disparity tuning in ventral pathway area V4", *Journal of Neurophysiology*, 94, 4, pp. 2726-2737, DOI: [10.1152/jn.00341.2005](https://doi.org/10.1152/jn.00341.2005).
- Hochman, E. R.
 2018 "Vision therapy for an adult with surgically removed congenital cataract", *Optometry and Vision Science*, 6, 1, pp. 19-24.
- Hoffman, D. D. and W. A. Richards
 1984 "Parts of recognition", *Cognition*, 18, 1-3, pp. 65-96, DOI: [10.1016/0010-0277\(84\)90022-2](https://doi.org/10.1016/0010-0277(84)90022-2).
- Holtmaat, A., T. Bonhoeffer, D. K. Chow, J. Chuckowree, V. De Paola, S. B. Hofer, M. Hübener, T. Keck, G. Knott, W. C. A. Lee, R. Mostany, T. D. Mrsic-Flogel, E. Nedivi, C. Portera-Cailliau, K. Svoboda, J. T. Trachtenberg, and L. Wilbrecht
 2009 "Long-term, high-resolution imaging in the mouse neocortex through a chronic cranial window", *Nature Protocols*, 4, 8, pp. 1128-1144, DOI: [10.1038/nprot.2009.89](https://doi.org/10.1038/nprot.2009.89).
- Howard, I. P. and B. J. Rogers
 1995 *Binocular Vision and Stereopsis*, Oxford University Press, New York, pp. 1-751.
- Howarth, M., L. Walmsley, and T. M. Brown
 2014 "Binocular integration in the mouse lateral geniculate nuclei", *Current Biology*, 24, 11, pp. 1241-1247, DOI: [10.1016/j.cub.2014.04.014](https://doi.org/10.1016/j.cub.2014.04.014).
- Hoy, J. L. and C. M. Niell
 2015 "Layer-specific refinement of visual cortex function after eye opening in the awake mouse", *Journal of Neuroscience*, 35, 8, pp. 3370-3383, DOI: [10.1523/JNEUROSCI.3174-14.2015](https://doi.org/10.1523/JNEUROSCI.3174-14.2015).
- Hoy, J. L., I. Yavorska, M. Wehr, and C. M. Niell
 2016 "Vision drives accurate approach behavior during prey capture in laboratory mice", *Current Biology*, 26, 22, pp. 3046-3052, DOI: [10.1016/j.cub.2016.09.009](https://doi.org/10.1016/j.cub.2016.09.009).

- Hubel, D. H.
 1959 "Single unit activity in striate cortex of unrestrained cats", *Journal of Physiology*, 147, 2, pp. 226-238, DOI: [10.1113/jphysiol.1959.sp006238](https://doi.org/10.1113/jphysiol.1959.sp006238).
- Hubel, D. H. and T. N. Wiesel
 1968 "Receptive fields and functional architecture of monkey striate cortex", *Journal of Physiology*, 195, pp. 215-243, DOI: [papers://47831562-1F78-4B52-B52E-78BF7F97A700/Paper/p352](https://doi.org/papers://47831562-1F78-4B52-B52E-78BF7F97A700/Paper/p352).
- Hubel, D. H. and T. N. Wiesel
 1969 "Anatomical demonstration of columns in the monkey striate cortex", *Nature*, 221, 5182, pp. 747-750, DOI: [10.1038/221747a0](https://doi.org/10.1038/221747a0).
 1977 "Functional architecture of macaque monkey visual cortex", *Proc. R. Soc. Lond. B*, 198, July, pp. 1-59, DOI: [10.1098/rspb.1977.0085](https://doi.org/10.1098/rspb.1977.0085).
- Hubel, D. H. and T. N. Wiesel
 1959 "Receptive fields of single neurones in the cat's striate cortex", *Journal of Physiology*, 148, pp. 574-591, DOI: [10.1113/jphysiol.2009.174151](https://doi.org/10.1113/jphysiol.2009.174151).
- Hubel, D. H., T. N. Wiesel, E. M. Yeagle, R. Lafer-Sousa, and B. R. Conway
 2013 "Binocular stereoscopy in visual areas V-2, V-3, and V-3A of the macaque monkey." *Cerebral Cortex*, April, pp. 959-971, DOI: [10.1093/cercor/bht288](https://doi.org/10.1093/cercor/bht288).
- Hubel, D. and T. Wiesel
 1962 "Receptive fields, binocular interaction and functional architecture in the cat's visual cortex", *Journal of Physiology*, 160, pp. 106-154, DOI: doi.org/10.1113/jphysiol.1962.sp006837.
- Hübener, M.
 2003 "Mouse visual cortex", *Current Opinion in Neurobiology*, 13, 4, pp. 413-420, DOI: [10.1016/S0959-4388\(03\)00102-8](https://doi.org/10.1016/S0959-4388(03)00102-8).
- Hübener, M. and J. Bolz
 1988 "Morphology of identified projection neurons in layer 5 of rat visual cortex", *Neuroscience Letters*, 94, 1-2, pp. 76-81, DOI: [10.1016/0304-3940\(88\)90273-X](https://doi.org/10.1016/0304-3940(88)90273-X).
- Huberman, A. D., W. Wei, J. Elstrott, B. K. Stafford, M. B. Feller, and B. a. Barres
 2009 "Genetic identification of an On-Off direction-selective retinal ganglion cell subtype reveals a layer-specific subcortical map of posterior motion", *Neuron*, 62, 3, pp. 327-334, DOI: [10.1016/j.neuron.2009.04.014](https://doi.org/10.1016/j.neuron.2009.04.014).
- Huberman, A. D. and C. M. Niell
 2011 "What can mice tell us about how vision works?", *Trends in Neurosciences*, 34, 9, pp. 464-473, DOI: [10.1016/j.tins.2011.07.002](https://doi.org/10.1016/j.tins.2011.07.002).
- Hughes, A.
 1971 "Topographical relationships between the anatomy and physiology of the rabbit visual system", *Documenta Ophthalmologica*, 30, 1, pp. 33-159, DOI: [10.1007/BF00142518](https://doi.org/10.1007/BF00142518).
- Huh, C. Y. L., J. P. Peach, C. Bennett, R. M. Vega, and S. Hestrin
 2018 "Feature-specific organization of feedback pathways in mouse visual cortex", *Current Biology*, 28, 1, pp. 1-7, DOI: [10.1016/j.cub.2017.11.056](https://doi.org/10.1016/j.cub.2017.11.056).
- Husson, T. R., A. K. Mallik, J. X. Zhang, and N. P. Issa
 2007 "Functional imaging of primary visual cortex using flavoprotein autofluorescence", *Journal of Neuroscience*, 27, 32, pp. 8665-8675, DOI: [10.1523/JNEUROSCI.2156-07.2007](https://doi.org/10.1523/JNEUROSCI.2156-07.2007).

- Iacaruso, M. F., I. T. Gasler, and S. B. Hofer
 2017 "Synaptic organization of visual space in primary visual cortex", *Nature*, 547, 7664, pp. 449-452, DOI: [10.1038/nature23019](https://doi.org/10.1038/nature23019).
- Ibrahim, L. and E. A. Wright
 1975 "The growth of rats and mice vibrissae under normal and some abnormal conditions." *Journal of embryology and experimental morphology*, 33, 4, pp. 831-44.
- Ibrahim, L. A., L. Mesik, X.-y. Ji, B. Zingg, L. I. Zhang, L. A. Ibrahim, L. Mesik, X.-y. Ji, Q. Fang, H.-f. Li, Y.-t. Li, B. Zingg, and L. I. Zhang
 2016 "Cross-modality sharpening of visual cortical processing through layer-1-mediated inhibition and disinhibition", *Neuron*, 89, 5, pp. 1-15, DOI: [10.1016/j.neuron.2016.01.027](https://doi.org/10.1016/j.neuron.2016.01.027).
- Isaacson, J. S. and M. Scanziani
 2011 "How inhibition shapes cortical activity." *Neuron*, 72, 2, pp. 231-43, DOI: [10.1016/j.neuron.2011.09.027](https://doi.org/10.1016/j.neuron.2011.09.027).
- Iurilli, G. and S. R. Datta
 2017 "Population coding in an innately relevant olfactory area", *Neuron*, 93, 5, pp. 1-18, DOI: [10.1016/j.neuron.2017.02.010](https://doi.org/10.1016/j.neuron.2017.02.010).
- Jaepel, J., M. Hübener, T. Bonhoeffer, and T. Rose
 2017 "Lateral geniculate neurons projecting to primary visual cortex show ocular dominance plasticity in adult mice", *Nature neuroscience*, 20, 12, pp. 1708-1714, DOI: [10.1038/s41593-017-0021-0](https://doi.org/10.1038/s41593-017-0021-0).
- Jeffery, G.
 2001 "Architecture of the optic chiasm and the mechanisms that sculpt its development", *Physiological Reviews*, 81, 4, pp. 1393-414, DOI: [10.1152/physrev.2001.81.4.1393](https://doi.org/10.1152/physrev.2001.81.4.1393).
- Jeon, C. J., E. Strettoi, and R. H. Masland
 1998 "The major cell populations of the mouse retina", *Journal of Neuroscience*, 18, 21, pp. 8936-8946, DOI: doi.org/10.1523/JNEUROSCI.18-21-08936.1998.
- Ji, W., R. Gămănuț, P. Bista, R. D. D'Souza, Q. Wang, and A. Burkhalter
 2015 "Modularity in the organization of mouse primary visual cortex", *Neuron*, 87, 3, pp. 632-643, DOI: [10.1016/j.neuron.2015.07.004](https://doi.org/10.1016/j.neuron.2015.07.004).
- Ji, X. Y., B. Zingg, L. Mesik, Z. Xiao, L. I. Zhang, and H. W. Tao
 2016 "Thalamocortical innervation pattern in mouse auditory and visual cortex: Laminar and cell-type specificity", *Cerebral Cortex*, 26, 6, pp. 2612-2625, DOI: [10.1093/cercor/bhv099](https://doi.org/10.1093/cercor/bhv099).
- Jiang, X., S. Shen, C. R. Cadwell, P. Berens, F. Sinz, A. S. Ecker, S. Patel, and A. S. Tolias
 2015 "Principles of connectivity among morphologically defined cell types in adult neocortex", *Science*, 350, 6264, aac9462-aac9462, DOI: [10.1126/science.aac9462](https://doi.org/10.1126/science.aac9462).
- Jimenez, L. O., E. Tring, J. T. Trachtenberg, and D. L. Ringach
 2017 "Untangling cortical maps in mouse primary visual cortex", *bioRxiv*, DOI: doi.org/10.1101/102079.
- Jin, J., Y. Wang, H. A. Swadlow, and J. M. Alonso
 2011 "Population receptive fields of on and off thalamic inputs to an orientation column in visual cortex", *Nature Neuroscience*, 14, 2, pp. 232-240, DOI: [10.1038/nn.2729](https://doi.org/10.1038/nn.2729).

- Jones, J. P. and L. A. Palmer
 1987 "The two-dimensional spectral structure of simple receptive fields in cat striate cortex", *Journal of Neurophysiology*, 58, 6, pp. 1187-1211, DOI: [10.1152/jn.1987.58.6.1212](https://doi.org/10.1152/jn.1987.58.6.1212).
- Juavinett, A. L. and E. M. Callaway
 2015 "Pattern and component motion responses in mouse visual cortical areas", *Current Biology*, 25, 13, pp. 1759-1764, DOI: [10.1016/j.cub.2015.05.028](https://doi.org/10.1016/j.cub.2015.05.028).
- Juavinett, A. L., J. C. Erlich, and A. K. Churchland
 2018 "Decision-making behaviors: weighing ethology, complexity, and sensorimotor compatibility", *Current Opinion in Neurobiology*, 49, pp. 42-50, DOI: [10.1016/j.conb.2017.11.001](https://doi.org/10.1016/j.conb.2017.11.001).
- Juavinett, A. L., I. Nauhaus, M. E. Garrett, and E. M. Callaway
 2016 "Automated identification of mouse visual areas with intrinsic signal imaging", *Nature Protocols*, 12, 1, pp. 32-43, DOI: [10.1038/nprot.2016.158](https://doi.org/10.1038/nprot.2016.158).
- Julesz, B.
 1960 "Binocular depth perception of computer-generated patterns", *Bell System Technical Journal*, 39, 5, pp. 1125-1162, DOI: [10.1002/j.1538-7305.1960.tb03954.x](https://doi.org/10.1002/j.1538-7305.1960.tb03954.x).
 1971 *Foundations of cyclopean perception*, p. 406, DOI: [10.1097/OPX.0b013e318155ab62](https://doi.org/10.1097/OPX.0b013e318155ab62).
- Jun, J. J., N. A. Steinmetz, J. H. Siegle, D. J. Denman, M. Bauza, B. Barbarits, A. K. Lee, C. A. Anastassiou, A. Andrei, Ç. Aydın, M. Barbic, T. J. Blanche, V. Bonin, J. Couto, B. Dutta, S. L. Gratiy, D. A. Gutnisky, M. Häusser, B. Karsh, P. Ledochowitsch, C. M. Lopez, C. Mitelut, S. Musa, M. Okun, M. Pachitariu, J. Putzeys, P. D. Rich, C. Rossant, W.-l. Sun, K. Svoboda, M. Carandini, K. D. Harris, C. Koch, J. O'Keefe, and T. D. Harris
 2017 "Fully integrated silicon probes for high-density recording of neural activity", *Nature*, 551, 7679, pp. 232-236, DOI: [10.1038/nature24636](https://doi.org/10.1038/nature24636).
- Kalatsky, V. a. and M. P. Stryker
 2003 "New paradigm for optical imaging: temporally encoded maps of intrinsic signal." *Neuron*, 38, 4, pp. 529-45, DOI: [doi.org/10.1016/S0896-6273\(03\)00286-1](https://doi.org/10.1016/S0896-6273(03)00286-1).
- Kameyama, K., K. Sohya, T. Ebina, A. Fukuda, Y. Yanagawa, and T. Tsumoto
 2010 "Difference in binocularity and ocular dominance plasticity between GABAergic and excitatory cortical neurons." *Journal of Neuroscience*, 30, 4, pp. 1551-1559, DOI: [10.1523/JNEUROSCI.5025-09.2010](https://doi.org/10.1523/JNEUROSCI.5025-09.2010).
- Kandel, E. R., J. H. Schwartz, and T. M. Jessell
 2013 *Principles of Neural Science*, vol. 4, p. 1414, DOI: [10.1036/0838577016](https://doi.org/10.1036/0838577016).
- Kara, P. and J. D. Boyd
 2009 "A micro-architecture for binocular disparity and ocular dominance in visual cortex." *Nature*, 458, 7238, pp. 627-631, DOI: [10.1167/7.15.21](https://doi.org/10.1167/7.15.21).
- Kaschube, M.
 2014 "Neural maps versus salt-and-pepper organization in visual cortex", *Current Opinion in Neurobiology*, 24C, pp. 95-102, DOI: [10.1016/j.conb.2013.08.017](https://doi.org/10.1016/j.conb.2013.08.017).
- Kassraian-Fard, P., C. Matthis, J. H. Balsters, M. Maathuis, and N. Wenderoth
 2016 "Promises, pitfalls, and basic guidelines for applying machine learning classifiers to psychiatric imaging data, with autism as an example", *Frontiers in Psychiatry*, 7, December, p. 177, DOI: [10.3389/FPSYT.2016.00177](https://doi.org/10.3389/FPSYT.2016.00177).

- Kato, D., M. Baba, K. S. Sasaki, and I. Ohzawa
 2016 "Effects of generalized pooling on binocular disparity selectivity of neurons in the early visual cortex", *Philosophical Transactions of the Royal Society of London B*, 371, 1697, DOI: [10.1098/rstb.2015.0266](https://doi.org/10.1098/rstb.2015.0266).
- Kätzel, D., B. V. Zemelman, C. Buetfering, M. Wölfel, and G. Miesenböck
 2011 "The columnar and laminar organization of inhibitory connections to neocortical excitatory cells", *Nature Neuroscience*, 14, 1, pp. 100-109, DOI: [10.1038/nn.2687](https://doi.org/10.1038/nn.2687).
- Kaufman, L. and J. H. Kaufman
 2000 "Explaining the moon illusion", *Proceedings of the National Academy of Sciences*, 97, 1, pp. 500-505, DOI: [10.1073/pnas.97.1.500](https://doi.org/10.1073/pnas.97.1.500).
- Kay, J. N., I. De la Huerta, I.-J. Kim, Y. Zhang, M. Yamagata, M. W. Chu, M. Meister, and J. R. Sanes
 2011 "Retinal ganglion cells with distinct directional preferences differ in molecular identity, structure, and central projections." *Journal of Neuroscience*, 31, 21, pp. 7753-62, DOI: [10.1523/JNEUROSCI.0907-11.2011](https://doi.org/10.1523/JNEUROSCI.0907-11.2011).
- Keller, G. B., T. Bonhoeffer, and M. Hübener
 2012 "Sensorimotor mismatch signals in primary visual cortex of the behaving mouse", *Neuron*, 74, 5, pp. 809-815, DOI: [10.1016/j.neuron.2012.03.040](https://doi.org/10.1016/j.neuron.2012.03.040).
- Kerlin, A. M., M. L. Andermann, V. K. Berezovskii, and R. C. Reid
 2010 "Broadly tuned response properties of diverse inhibitory neuron subtypes in mouse visual cortex", *Neuron*, 67, 5, pp. 858-871, DOI: [10.1016/j.neuron.2010.08.002](https://doi.org/10.1016/j.neuron.2010.08.002).
- Khan, A. G., J. Poort, A. Chadwick, A. Blot, M. Sahani, T. D. Mrsic-Flogel, and S. B. Hofer
 2018 "Distinct learning-induced changes in stimulus selectivity and interactions of GABAergic interneuron classes in visual cortex", *Nature Neuroscience*, 21, 6, pp. 851-859, DOI: [10.1038/s41593-018-0143-z](https://doi.org/10.1038/s41593-018-0143-z).
- Kim, C. K., A. Adhikari, and K. Deisseroth
 2017 "Integration of optogenetics with complementary methodologies in systems neuroscience", *Nature Reviews Neuroscience*, 18, 4, pp. 222-235, DOI: [10.1038/nrn.2017.15](https://doi.org/10.1038/nrn.2017.15), arXiv: [15334406](https://arxiv.org/abs/15334406).
- Klapoetke, N. C., Y. Murata, S. S. Kim, S. R. Pulver, A. Birdsey-Benson, Y. K. Cho, T. K. Morimoto, A. S. Chuong, E. J. Carpenter, Z. Tian, J. Wang, Y. Xie, Z. Yan, Y. Zhang, B. Y. Chow, B. Surek, M. Melkonian, V. Jayaraman, M. Constantine-Paton, G. K.-S. Wong, and E. S. Boyden
 2014 "Independent optical excitation of distinct neural populations." *Nature Methods*, 11, 3, pp. 338-46, DOI: [10.1038/nmeth.2836](https://doi.org/10.1038/nmeth.2836).
- Kleiner, M.
 2010 "Visual stimulus timing precision in Psychtoolbox-3: Tests, pitfalls and solutions", *Perception 39 ECVF Abstract Supplement*, p. 189, DOI: [10.1068/v100546](https://doi.org/10.1068/v100546).
- Kleiner, M., D. H. Brainard, D. G. Pelli, C. Broussard, T. Wolf, and D. Niehorster
 2007 "What's new in Psychtoolbox-3?", *Perception*, 36, S14, DOI: [10.1068/v070821](https://doi.org/10.1068/v070821).
- Knudsen, E. I. and P. F. Knudsen
 1985 "Vision guides the adjustment of auditory localization in young barn owls." *Science*, 230, 4725, pp. 545-548, DOI: [10.1126/science.4048948](https://doi.org/10.1126/science.4048948).

- Knudsen, E. I.
1982 "Auditory and visual maps of space in the optic tectum of the owl", *Journal of Neuroscience*, 2, 9, pp. 1177-1194, DOI: [10.1177/0956797610380696](https://doi.org/10.1177/0956797610380696).
- Knudsen, E. I.
1983 "Early auditory experience aligns the auditory map of space in the optic tectum of the barn owl." *Science*, 222, 4626, pp. 939-942, DOI: [10.1126/science.6635667](https://doi.org/10.1126/science.6635667).
2002 "Instructed learning in the auditory localization pathway of the barn owl", *Nature*, 417, 6886, pp. 322-328, DOI: [10.1038/417322a](https://doi.org/10.1038/417322a).
- Knudsen, E. I. and M. S. Brainard
1991 "Visual instruction of the neural map of auditory space in the developing optic tectum", *Science*, 253, 5015, pp. 85-87, DOI: [10.1126/science.2063209](https://doi.org/10.1126/science.2063209).
- Ko, H., S. B. Hofer, B. Pichler, K. a. Buchanan, P. J. Sjöström, and T. D. Mrsic-Flogel
2011 "Functional specificity of local synaptic connections in neocortical networks." *Nature*, 473, 7345, pp. 87-91, DOI: [10.1038/nature09880](https://doi.org/10.1038/nature09880).
- Koch, C. and T. Poggio
1987 "Synaptic Function", in *Biophysics of computational systems: neurons, synapses and membranes*, ed. by G. M. Edelman, W. E. Gall, and W. M. Cowan, Wiley, New York, pp. 637-697.
- Kohn, A., R. Coen-Cagli, I. Kanitscheider, and A. Pouget
2016 "Correlations and neuronal population information", *Annual Review of Neuroscience*, 39, April, pp. 237-256, DOI: [10.1146/annurev-neuro-070815-013851](https://doi.org/10.1146/annurev-neuro-070815-013851).
- Kondo, S. and K. Ohki
2015 "Laminar differences in the orientation selectivity of geniculate afferents in mouse primary visual cortex", *Nature Neuroscience*, December, pp. 1-6, DOI: [10.1038/nn.4215](https://doi.org/10.1038/nn.4215).
- Kondo, S., T. Yoshida, and K. Ohki
2016 "Mixed functional microarchitectures for orientation selectivity in the mouse primary visual cortex." *Nature Communications*, 7, p. 13210, DOI: [10.1038/ncomms13210](https://doi.org/10.1038/ncomms13210).
- Kravitz, D. J., K. S. Saleem, C. I. Baker, and M. Mishkin
2011 "A new neural framework for visuospatial processing", *Nature Reviews Neuroscience*, 12, 4, pp. 217-230, DOI: [10.1038/nrn3008](https://doi.org/10.1038/nrn3008), arXiv: [NIHMS150003](https://arxiv.org/abs/1505.00003).
- Kreile, A. K., T. Bonhoeffer, and M. Hübener
2011 "Altered visual experience induces instructive changes of orientation preference in mouse visual cortex", *Journal of Neuroscience*, 31, 39, pp. 13911-13920, DOI: [10.1523/JNEUROSCI.2143-11.2011](https://doi.org/10.1523/JNEUROSCI.2143-11.2011).
- Kremkow, J., J. Jin, Y. Wang, and J. M. Alonso
2016 "Principles underlying sensory map topography in primary visual cortex", *Nature*, 533, 7601, pp. 52-57, DOI: [10.1038/nature17936](https://doi.org/10.1038/nature17936).
- Krug, K.
2004 "Comparing perceptual signals of single V5/MT neurons in two binocular depth tasks", *Journal of Neurophysiology*, 92, 3, pp. 1586-1596, DOI: [10.1152/jn.00851.2003](https://doi.org/10.1152/jn.00851.2003).

- Krug, K., T. Curnow, and A. Parker
 2016 "Defining the V5/MT neuronal pool for perceptual decisions in a visual stereo-motion task", *Philosophical Transactions of the Royal Society of London B*, 371, 1697, DOI: [10.1098/rstb.2015.0260](https://doi.org/10.1098/rstb.2015.0260).
- Krug, K. and A. J. Parker
 2011 "Neurons in dorsal visual area V5/MT signal relative disparity", *Journal of Neuroscience*, 31, 49, pp. 17892-17904, DOI: [10.1523/JNEUROSCI.2658-11.2011](https://doi.org/10.1523/JNEUROSCI.2658-11.2011).
- Krug, K., N. Cicmil, A. J. Parker, and B. G. Cumming
 2013 "A causal role for V5/MT neurons coding motion-disparity conjunctions in resolving perceptual ambiguity", *Current Biology*, 23, 15, pp. 1454-1459, DOI: [10.1016/j.cub.2013.06.023](https://doi.org/10.1016/j.cub.2013.06.023).
- Langford, D. J., S. E. Crager, Z. Shehzad, S. B. Smith, S. G. Sotocinal, J. S. Levenstadt, M. L. Chanda, D. J. Levitin, and J. S. Mogil
 2006 "Social modulation of pain as evidence for empathy in mice." *Science*, 312, 5782, pp. 1967-70, DOI: [10.1126/science.1128322](https://doi.org/10.1126/science.1128322).
- Laramée, M.-E. and D. Boire
 2014 "Visual cortical areas of the mouse: comparison of parcellation and network structure with primates." *Frontiers in Neural Circuits*, 8, January, p. 149, DOI: [10.3389/fncir.2014.00149](https://doi.org/10.3389/fncir.2014.00149).
- Larsson, M. L.
 2015 "Binocular vision, the optic chiasm, and their associations with vertebrate motor behavior", *Frontiers in Ecology and Evolution*, 3, July, pp. 1-12, DOI: [10.3389/fevo.2015.00089](https://doi.org/10.3389/fevo.2015.00089).
- Leamey, C. A., S. Merlin, P. Lattouf, A. Sawatari, X. Zhou, N. Demel, K. A. Glending, T. Oohashi, M. Sur, and R. Fässler
 2007 "Ten_m3 regulates eye-specific patterning in the mammalian visual pathway and is required for binocular vision", *PLoS Biology*, 5, 9, pp. 2077-2092, DOI: [10.1371/journal.pbio.0050241](https://doi.org/10.1371/journal.pbio.0050241).
- Lee, J. and A. L. Barth
 2017 "Constructing the external world", *Neuron*, 94, 6, pp. 1048-1050, DOI: [10.1016/j.neuron.2017.06.006](https://doi.org/10.1016/j.neuron.2017.06.006).
- Lee, K.-S., X. Huang, and D. Fitzpatrick
 2016 "Topology of ON and OFF inputs in visual cortex enables an invariant columnar architecture", *Nature*, 533, 7601, pp. 90-94, DOI: [10.1038/nature17941](https://doi.org/10.1038/nature17941).
- Lee, S.-H., A. C. Kwan, S. Zhang, V. Phoumthippavong, J. G. Flannery, S. C. Masmanidis, H. Taniguchi, Z. J. Huang, F. Zhang, E. S. Boyden, K. Deisseroth, and Y. Dan
 2012 "Activation of specific interneurons improves V1 feature selectivity and visual perception." *Nature*, 488, 7411, pp. 379-83, DOI: [10.1038/nature11312](https://doi.org/10.1038/nature11312).
- Leinweber, M., P. Zmarz, P. Buchmann, P. Argast, M. Hübener, T. Bonhoeffer, and G. B. Keller
 2014 "Two-photon calcium imaging in mice navigating a virtual reality environment", *Journal of Visualized Experiments*, 84, pp. 1-6, DOI: [10.3791/50885](https://doi.org/10.3791/50885).
- LeVay, S. and T. Voigt
 1988 "Ocular dominance and disparity coding in cat visual cortex", *Visual Neuroscience*, 1, 4, pp. 395-414, DOI: [10.1017/S0952523800004168](https://doi.org/10.1017/S0952523800004168).

- Levelt, C. N. and M. Hübener
 2012 "Critical-period plasticity in the visual cortex." *Annual Review of Neuroscience*, 35, March, pp. 309-30, DOI: [10.1146/annurev-neuro-061010-113813](https://doi.org/10.1146/annurev-neuro-061010-113813).
- Li, L., X. Feng, Z. Zhou, H. Zhang, Q. Shi, Z. Lei, P. Shen, Q. Yang, B. Zhao, S. Chen, L. Li, Y. Zhang, P. Wen, Z. Lu, X. Li, F. Xu, and L. Wang
 2018 "Stress accelerates defensive responses to looming in mice and involves a locus coeruleus-superior colliculus projection", *Current Biology*, 28, 6, 859-870.e5, DOI: [10.1016/j.cub.2018.02.005](https://doi.org/10.1016/j.cub.2018.02.005).
- Li, Y.-t., Q. Fang, L. I. Zhang, and H. W. Tao
 2017 "Spatial asymmetry and short-term suppression underlie direction selectivity of synaptic excitation in the mouse visual cortex", *Cerebral Cortex*, March, pp. 1-12, DOI: [10.1093/cercor/bhx111](https://doi.org/10.1093/cercor/bhx111).
- Li, Y.-T., B.-H. Liu, X.-L. Chou, L. I. Zhang, and H. W. Tao
 2015 "Strengthening of direction selectivity by broadly tuned and spatiotemporally slightly offset inhibition in mouse visual cortex", *Cerebral Cortex*, 25, 9, pp. 2466-2477, DOI: [10.1093/cercor/bhu049](https://doi.org/10.1093/cercor/bhu049).
- Liang, L., A. Fratzl, G. Goldey, R. N. Ramesh, A. U. Sugden, J. L. Morgan, C. Chen, and M. L. Andermann
 2018 "A fine-scale functional logic to convergence from retina to thalamus", *Cell*, 173, 6, 1343.e1-1343.e24, DOI: [10.1016/j.cell.2018.04.041](https://doi.org/10.1016/j.cell.2018.04.041).
- Liebscher, S., G. B. Keller, P. M. Goltstein, T. Bonhoeffer, and M. Hübener
 2016 "Selective persistence of sensorimotor mismatch signals in visual cortex of behaving alzheimer's disease mice", *Current Biology*, 26, 7, pp. 956-964, DOI: [10.1016/j.cub.2016.01.070](https://doi.org/10.1016/j.cub.2016.01.070).
- Lien, A. D. and M. Scanziani
 2018 "Cortical direction selectivity emerges at convergence of thalamic synapses", *Nature*, 558, 7708, pp. 80-86, DOI: [10.1038/s41586-018-0148-5](https://doi.org/10.1038/s41586-018-0148-5).
- Lin, M. Z. and M. J. Schnitzer
 2016 "Genetically encoded indicators of neuronal activity", *Nature Neuroscience*, 19, 9, pp. 1142-1153, DOI: [10.1038/nn.4359](https://doi.org/10.1038/nn.4359).
- Liu, B.-h., P. Li, Y. J. Sun, Y.-t. Li, L. I. Zhang, and H. W. Tao
 2010 "Intervening inhibition underlies simple-cell receptive field structure in visual cortex." *Nature Neuroscience*, 13, 1, pp. 89-96, DOI: [10.1038/nn.2443](https://doi.org/10.1038/nn.2443).
- Livingstone, M. S.
 1998 "Mechanisms of direction selectivity in macaque V1", *Neuron*, 20, 3, pp. 509-526, DOI: [10.1016/S0896-6273\(00\)80991-5](https://doi.org/10.1016/S0896-6273(00)80991-5).
- London, M. and M. Häusser
 2005 "Dendritic computation", *Annual Review of Neuroscience*, 28, 1, pp. 503-532, DOI: [10.1146/annurev.neuro.28.061604.135703](https://doi.org/10.1146/annurev.neuro.28.061604.135703).
- Longordo, F., M.-S. To, K. Ikeda, and G. J. Stuart
 2013 "Sublinear integration underlies binocular processing in primary visual cortex", *Nature Neuroscience*, 16, 6, pp. 714-23, DOI: [10.1038/nn.3394](https://doi.org/10.1038/nn.3394).
- Luo, L., E. M. Callaway, and K. Svoboda
 2018 "Genetic dissection of neural circuits: A decade of progress", *Neuron*, 98, 2, pp. 256-281, DOI: [10.1016/j.neuron.2018.03.040](https://doi.org/10.1016/j.neuron.2018.03.040).

- Lütcke, H., F. Gerhard, F. Zenke, W. Gerstner, and F. Helmchen
 2013 "Inference of neuronal network spike dynamics and topology from calcium imaging data." *Frontiers in Neural Circuits*, 7, p. 201, DOI: [10.3389/fncir.2013.00201](https://doi.org/10.3389/fncir.2013.00201).
- Maex, R. and G. a. Orban
 1996 "Model circuit of spiking neurons generating directional selectivity in simple cells", *Journal of Neurophysiology*, 75, 4, pp. 1515-1545, DOI: [10.1152/jn.1996.75.4.1515](https://doi.org/10.1152/jn.1996.75.4.1515).
- Manookin, M. B., S. S. Patterson, and C. M. Linehan
 2018 "Neural mechanisms mediating motion sensitivity in parasol ganglion cells of the primate retina", *Neuron*, pp. 1-14, DOI: [10.1016/j.neuron.2018.02.006](https://doi.org/10.1016/j.neuron.2018.02.006).
- Mantini, D., U. Hasson, V. Betti, M. G. Perrucci, G. L. Romani, M. Corbetta, G. A. Orban, and W. Vanduffel
 2012 "Interspecies activity correlations reveal functional correspondence between monkey and human brain areas", *Nature Methods*, 9, 3, pp. 277-282, DOI: [10.1038/nmeth.1868](https://doi.org/10.1038/nmeth.1868).
- Marcos, A. S. and C. D. Harvey
 2016 "History-dependent variability in population dynamics during evidence accumulation in cortex", *Nature Neuroscience*, 19, 12, pp. 1672-1680, DOI: [10.1038/nn.4403](https://doi.org/10.1038/nn.4403).
- Mardinly, A. R., I. A. Oldenburg, N. C. Pégard, S. Sridharan, E. H. Lyall, K. Chesnov, S. G. Brohawn, L. Waller, and H. Adesnik
 2018 "Precise multimodal optical control of neural ensemble activity", *Nature Neuroscience*, 21, 6, pp. 881-893, DOI: [10.1038/s41593-018-0139-8](https://doi.org/10.1038/s41593-018-0139-8).
- Marques, T., M. T. Summers, G. Fioreze, M. Fridman, R. F. Dias, M. B. Feller, and L. Petreanu
 2018 "A role for mouse primary visual cortex in motion perception", *Current Biology*, 28, 11, 1703-1713.e6, DOI: [10.1016/j.cub.2018.04.012](https://doi.org/10.1016/j.cub.2018.04.012).
- Marshel, J. H., M. E. Garrett, I. Nauhaus, and E. M. Callaway
 2011 "Functional specialization of seven mouse visual cortical areas", *Neuron*, 72, 6, pp. 1040-54, DOI: [10.1016/j.neuron.2011.12.004](https://doi.org/10.1016/j.neuron.2011.12.004).
- Marshel, J. H., A. P. Kaye, I. Nauhaus, and E. M. Callaway
 2012 "Anterior-posterior direction opponency in the superficial mouse lateral geniculate nucleus." *Neuron*, 76, 4, pp. 713-20, DOI: [10.1016/j.neuron.2012.09.021](https://doi.org/10.1016/j.neuron.2012.09.021).
- Maruoka, H., N. Nakagawa, S. Tsuruno, S. Sakai, T. Yoneda, and T. Hosoya
 2017 "Lattice system of functionally distinct cell types in the neocortex - Suppl", *Science*, 358, 6363, pp. 610-615, DOI: [10.1126/science.aam6125](https://doi.org/10.1126/science.aam6125).
- Matsui, T. and K. Ohki
 2013 "Target dependence of orientation and direction selectivity of corticocortical projection neurons in the mouse V1." *Frontiers in Neural Circuits*, 7, September, p. 143, DOI: [10.3389/fncir.2013.00143](https://doi.org/10.3389/fncir.2013.00143).
- Maunsell, J. H. R. and W. T. Newsome
 1987 "Visual processing in monkey extrastriate cortex." *Annual Review of Neuroscience*, 10, pp. 363-401, DOI: [10.1146/annurev.neuro.10.1.363](https://doi.org/10.1146/annurev.neuro.10.1.363).

- Maunsell, J. H. R. and D. C. Van Essen
 1983 "Functional properties of neurons in middle temporal visual area of the macaque monkey. I. Selectivity for stimulus direction, speed, and orientation", *Journal of Neurophysiology*, 49, 5, pp. 1127-1147, DOI: [10.1016/j.aqpro.2013.07.003](https://doi.org/10.1016/j.aqpro.2013.07.003).
- Mauss, A. S., A. Vlasits, A. Borst, and M. Feller
 2017 "Visual circuits for direction selectivity", *Annual Review of Neuroscience*, 40, 1, pp. 211-230, DOI: [10.1146/annurev-neuro-072116-031335](https://doi.org/10.1146/annurev-neuro-072116-031335).
- Mayhew, J. E., S. Askew, Y. Zheng, J. Porrill, G. W. Westby, P. Redgrave, D. M. Rector, and R. M. Harper
 1996 "Cerebral vasomotion: A 0.1-Hz oscillation in reflected light imaging of neural activity", *NeuroImage*, DOI: [10.1006/nimg.1996.0069](https://doi.org/10.1006/nimg.1996.0069).
- Mazurek, M., M. Kager, and S. D. Van Hooser
 2014 "Robust quantification of orientation selectivity and direction selectivity", *Frontiers in Neural Circuits*, 8, August, pp. 1-17, DOI: [10.3389/fncir.2014.00092](https://doi.org/10.3389/fncir.2014.00092).
- Mazziotti, R., L. Baroncelli, N. Ceglia, G. Chelini, G. D. Sala, C. Magnan, D. Napoli, E. Putignano, D. Silingardi, J. Tola, P. Tognini, J. S. C. Arthur, P. Baldi, and T. Pizzorusso
 2017 "Mir-132/212 is required for maturation of binocular matching of orientation preference and depth perception", *Nature Communications*, 8, May, p. 15488, DOI: [10.1038/ncomms15488](https://doi.org/10.1038/ncomms15488).
- Mechler, F. and D. L. Ringach
 2002 "On the classification of simple and complex cells", *Vision Research*, 42, 8, pp. 1017-1033, DOI: [10.1016/S0042-6989\(02\)00025-1](https://doi.org/10.1016/S0042-6989(02)00025-1).
- Meister, M. and D. Cox
 2013 "Rats maintain a binocular field centered on the horizon." *F1000Research*, 2, p. 176, DOI: [10.12688/f1000research.2-176.v1](https://doi.org/10.12688/f1000research.2-176.v1).
- Mel, B. W., D. L. Ruderman, and K. A. Archie
 1998a *Advances in Neural Information Processing Systems*, ed. by M. I. Jordan, M. J. Kearns, and S. A. Solla, MIT Press, Cambridge, Massachusetts, pp. 208-214.
 1998b "Translation-invariant orientation tuning in visual "complex" cells could derive from intradendritic computations." *Journal of Neuroscience*, 18, 11, pp. 4325-4334, DOI: [10.1098/rspb.1986.0060](https://doi.org/10.1098/rspb.1986.0060).
- Meyer, A. F., J. Poort, J. O'Keefe, M. Sahani, and J. F. Linden
 2018 "An ultralight head-mounted camera system integrates detailed behavioral monitoring with multichannel electrophysiology in freely moving mice", *bioRxiv*, pp. 1-37, DOI: doi.org/10.1101/294397.
- Meyers, E. and G. Kreiman
 2012 "Tutorial on pattern classification in cell recording", *Visual Population Codes, ML*, pp. 517-538.
- Miller, K. D.
 2016 "Canonical computations of cerebral cortex", *Current Opinion in Neurobiology*, 37, pp. 75-84, DOI: [10.1016/j.conb.2016.01.008](https://doi.org/10.1016/j.conb.2016.01.008).
- Minini, L., A. J. Parker, and H. Bridge
 2010 "Neural modulation by binocular disparity greatest in human dorsal visual stream", *Journal of Neurophysiology*, 104, 1, pp. 169-178, DOI: [10.1152/jn.00790.2009](https://doi.org/10.1152/jn.00790.2009).

- Mizuno, H., T. Hirano, and Y. Tagawa
 2007 "Evidence for activity-dependent cortical wiring: Formation of interhemispheric connections in neonatal mouse visual cortex requires projection neuron activity", *Journal of Neuroscience*, 27, 25, pp. 6760-6770, DOI: [10.1523/JNEUROSCI.1215-07.2007](https://doi.org/10.1523/JNEUROSCI.1215-07.2007).
- Monavarfeshani, A., U. Sabbagh, and M. A. Fox
 2017 "Not a one-trick pony: Diverse connectivity and functions of the rodent lateral geniculate complex", *Visual Neuroscience*, 34, 2017, E012, DOI: [10.1017/S0952523817000098](https://doi.org/10.1017/S0952523817000098).
- Montijn, J. S., M. Vinck, and C. M. a. Pennartz
 2014 "Population coding in mouse visual cortex: response reliability and dissociability of stimulus tuning and noise correlation." *Frontiers in Computational Neuroscience*, 8, June, p. 58, DOI: [10.3389/fncom.2014.00058](https://doi.org/10.3389/fncom.2014.00058).
- Morin, L. P. and K. M. Studholme
 2014 "Retinofugal projections in the mouse", *Journal of Comparative Neurology*, 522, 16, pp. 3733-3753, DOI: [10.1002/cne.23635](https://doi.org/10.1002/cne.23635).
- Morris, R. G., P. Garrud, J. N. Rawlins, and J. O'Keefe
 1982 "Place navigation impaired in rats with hippocampal lesions", *Nature*, 297, 5868, pp. 681-683, DOI: [10.1038/297681a0](https://doi.org/10.1038/297681a0).
- Mrsic-Flogel, T. D., S. B. Hofer, K. Ohki, R. C. Reid, T. Bonhoeffer, and M. Hübener
 2007 "Homeostatic regulation of eye-specific responses in visual cortex during ocular dominance plasticity", *Neuron*, 54, 6, pp. 961-972, DOI: [10.1016/j.neuron.2007.05.028](https://doi.org/10.1016/j.neuron.2007.05.028).
- Mrsic-Flogel, T. D., M. Hübener, and T. Bonhoeffer
 2003 "Brain mapping: New wave optical imaging", *Current Biology*, 13, 19, pp. 778-780, DOI: [10.1016/j.cub.2003.09.022](https://doi.org/10.1016/j.cub.2003.09.022).
- Murakami, T., T. Matsui, and K. Ohki
 2017 "Functional segregation and development of mouse higher visual areas", *Journal of Neuroscience*, 37, 39, pp. 9424-9437, DOI: [10.1523/JNEUROSCI.0731-17.2017](https://doi.org/10.1523/JNEUROSCI.0731-17.2017).
- Murakami, T., T. Yoshida, T. Matsui, and K. Ohki
 2015 "Wide-field Ca²⁺ imaging reveals visually evoked activity in the retrosplenial area", *Frontiers in Molecular Neuroscience*, 08, June, pp. 1-12, DOI: [10.3389/fnmol.2015.00020](https://doi.org/10.3389/fnmol.2015.00020).
- Nasr, S. and R. B. H. Tootell
 2016 "Visual field biases for near and far stimuli in disparity selective columns in human visual cortex", *NeuroImage*, September, DOI: [10.1016/j.neuroimage.2016.09.012](https://doi.org/10.1016/j.neuroimage.2016.09.012).
- Nassi, J. J. and E. M. Callaway
 2009 "Parallel processing strategies of the primate visual system", *Nature Reviews Neuroscience*, 10, 5, pp. 360-372, DOI: [10.1038/nrn2619](https://doi.org/10.1038/nrn2619), arXiv: [NIHMS 150003](https://arxiv.org/abs/150003).
- Neri, P., H. Bridge, and D. J. Heeger
 2004 "Stereoscopic processing of absolute and relative disparity in human visual cortex", *Journal of Neurophysiology*, 92, 3, pp. 1880-1891, DOI: [10.1152/jn.01042.2003](https://doi.org/10.1152/jn.01042.2003).
- Neri, P., A. J. Parker, and C. Blakemore
 1999 "Probing the human stereoscopic system with reverse correlation", *Nature*, 401, 6754, pp. 695-698, DOI: [10.1038/44409](https://doi.org/10.1038/44409).

- Nguyen, J., T. Marques, G. Fioreze, and L. Petreanu
 2018 "The functional organization of cortical feedback inputs to primary visual cortex", *Nature Neuroscience*, DOI: [10.1038/s41593-018-0135-z](https://doi.org/10.1038/s41593-018-0135-z).
- Niell, C.
 2015 "Cell types, circuits, and receptive fields in the mouse visual cortex", *Annual Review of Neuroscience*, 38, 1, pp. 413-31, DOI: [10.1146/annurev-neuro-071714-033807](https://doi.org/10.1146/annurev-neuro-071714-033807).
- Niell, C. M.
 2011 "Exploring the next frontier of mouse vision." *Neuron*, 72, 6, pp. 889-92, DOI: [10.1016/j.neuron.2011.12.011](https://doi.org/10.1016/j.neuron.2011.12.011).
- Niell, C. M. and S. J. Smith
 2005 "Functional imaging reveals rapid development of visual response properties in the zebrafish tectum", *Neuron*, 45, 6, pp. 941-951, DOI: [10.1016/j.neuron.2005.01.047](https://doi.org/10.1016/j.neuron.2005.01.047).
- Niell, C. M. and M. P. Stryker
 2010 "Modulation of visual responses by behavioral state in mouse visual cortex", *Neuron*, 65, 4, pp. 472-479, DOI: [10.1016/j.neuron.2010.01.033](https://doi.org/10.1016/j.neuron.2010.01.033).
- Niell, C. M. and M. P. Stryker
 2008 "Highly selective receptive fields in mouse visual cortex." *Journal of Neuroscience*, 28, 30, pp. 7520-7536, DOI: [10.1523/JNEUROSCI.0623-08.2008](https://doi.org/10.1523/JNEUROSCI.0623-08.2008).
- Nienborg, H., H. Bridge, A. J. Parker, and B. G. Cumming
 2004 "Receptive field size in V1 neurons limits acuity for perceiving disparity modulation", *Journal of Neuroscience*, 24, 9, pp. 2065-76, DOI: [10.1523/JNEUROSCI.3887-03.2004](https://doi.org/10.1523/JNEUROSCI.3887-03.2004).
- Nikara, T., P. O. Bishop, and J. D. Pettigrew
 1968 "Analysis of retinal correspondence by studying receptive fields of binocular single units in cat striate cortex", *Experimental Brain Research*, 6, pp. 353-372, DOI: doi.org/10.1007/BF00233184.
- Nityananda, V. and Read
 2017 "Stereopsis in animals: evolution, function and mechanisms", *Journal of Experimental Biology*, 220, pp. 2502-2512, DOI: [10.1242/jeb.143883](https://doi.org/10.1242/jeb.143883).
- Nityananda, V., G. Tarawneh, S. Henriksen, D. Umeton, A. Simmons, and J. C. Read
 2018 "A novel form of stereo vision in the praying mantis", *Current Biology*, 28, 4, 588-593.e4, DOI: [10.1016/j.cub.2018.01.012](https://doi.org/10.1016/j.cub.2018.01.012).
- Nityananda, V., G. Tarawneh, R. Rosner, J. Nicolas, S. Crichton, and J. Read
 2016 "Insect stereopsis demonstrated using a 3D insect cinema." *Scientific Reports*, 6, p. 18718, DOI: [10.1038/srep18718](https://doi.org/10.1038/srep18718).
- Norcia, A. M., H. E. Gerhard, and W. J. Meredith
 2017 "Development of relative disparity sensitivity in human visual cortex", *Journal of Neuroscience*, 37, 23, pp. 5608-5619, DOI: [10.1523/JNEUROSCI.3570-16.2017](https://doi.org/10.1523/JNEUROSCI.3570-16.2017).
- O'Connor, D. H., N. G. Clack, D. Huber, T. Komiyama, E. W. Myers, and K. Svoboda
 2010 "Vibrissa-based object localization in head-fixed mice", *Journal of Neuroscience*, 30, 5, pp. 1947-1967, DOI: [10.1523/JNEUROSCI.3762-09.2010](https://doi.org/10.1523/JNEUROSCI.3762-09.2010).
- O'Herron, P., J. Woodward, and P. Kara
 2018 "The influence of cortical depth on neuronal responses in mouse visual cortex", *bioRxiv*, DOI: [10.1101/241661](https://doi.org/10.1101/241661).

- O'Leary, D. D., N. L. Ruff, and R. H. Dyck
 1994 "Development, critical period plasticity, and adult reorganizations of mammalian somatosensory systems", *Current Opinion in Neurobiology*, 4, 4, pp. 535-544, DOI: [10.1016/0959-4388\(94\)90054-X](https://doi.org/10.1016/0959-4388(94)90054-X).
- Ohki, K., S. Chung, P. Kara, M. Hübener, T. Bonhoeffer, and R. C. Reid
 2006 "Highly ordered arrangement of single neurons in orientation pinwheels", *Nature*, 442, 7105, pp. 925-928, DOI: [10.1038/nature05019](https://doi.org/10.1038/nature05019).
- Ohki, K. and R. C. Reid
 2007 "Specificity and randomness in the visual cortex", *Current Opinion in Neurobiology*, 17, 4, pp. 401-407, DOI: [10.1016/j.conb.2007.07.007](https://doi.org/10.1016/j.conb.2007.07.007), arXiv: [NIHMS150003](https://arxiv.org/abs/NIHMS150003).
- Ohzawa, I. and R. D. Freeman
 1986 "The binocular organization of simple cells in the cat's visual cortex." *Journal of Neurophysiology*, 56, 1, pp. 221-242, DOI: [10.1152/jn.1986.56.1.221](https://doi.org/10.1152/jn.1986.56.1.221).
- Olcese, U., G. Iurilli, and P. Medini
 2013 "Cellular and synaptic architecture of multisensory integration in the mouse neocortex", *Neuron*, 79, 3, pp. 579-593, DOI: [10.1016/j.neuron.2013.06.010](https://doi.org/10.1016/j.neuron.2013.06.010).
- Ooi, T. L., B. Wu, and Z. J. He
 2001 "Distance determined by the angular declination below the horizon", *Nature*, 414, 6860, pp. 197-200, DOI: [10.1038/35102562](https://doi.org/10.1038/35102562).
- Orban, G. A.
 2008 "Higher order visual processing in macaque extrastriate cortex", *Physiological Reviews*, 88, pp. 59-89, DOI: [10.1152/physrev.00008.2007](https://doi.org/10.1152/physrev.00008.2007).
- Oyster, C. W. and H. B. Barlow
 1967 "Direction-selective units in rabbit retina: distribution of preferred directions." *Science*, 155, 764, pp. 841-842, DOI: [10.1126/science.155.3764.841](https://doi.org/10.1126/science.155.3764.841).
- Packwood, J. and B. Gordon
 1975 "Stereopsis in normal domestic cat, Siamese cat, and cat raised with alternating monocular occlusion." *Journal of Neurophysiology*, 38, 6, pp. 1485-99, DOI: [10.1152/jn.1975.38.6.1485](https://doi.org/10.1152/jn.1975.38.6.1485).
- Pammer, L., D. H. O'Connor, S. A. Hires, N. G. Clack, D. Huber, E. W. Myers, and K. Svoboda
 2013 "The mechanical variables underlying object localization along the axis of the whisker", *Journal of Neuroscience*, 33, 16, pp. 6726-6741, DOI: [10.1523/JNEUROSCI.4316-12.2013](https://doi.org/10.1523/JNEUROSCI.4316-12.2013).
- Park, S.-G., Y.-C. Jeong, D. D.-G. Kim, M.-H. Lee, A. Shin, G. Park, J. Ryoo, J. Hong, S. Bae, C.-H. Kim, P.-S. Lee, and D. D.-G. Kim
 2018 "Medial preoptic circuit induces hunting-like actions to target objects and prey", *Nature Neuroscience*, 21, 3, pp. 364-372, DOI: [10.1038/s41593-018-0072-x](https://doi.org/10.1038/s41593-018-0072-x).
- Parker, A. J.
 2016 "Vision in our three-dimensional world", *Philosophical Transactions of the Royal Society of London B*, 371, p. 20150251, DOI: [10.1098/rstb.2015.0251](https://doi.org/10.1098/rstb.2015.0251).
- Parker, A. J.
 2007 "Binocular depth perception and the cerebral cortex", *Nature Reviews Neuroscience*, 8, 5, pp. 379-91, DOI: [10.1038/nrn2131](https://doi.org/10.1038/nrn2131).

- Parker, A., J. Smith, and K. Krug
 2016 "Neural architectures for stereo vision", *Philosophical Transactions of the Royal Society of London B*, 371, 1697, pp. 1125-1162, DOI: [10.1098/rstb.2015.0261](https://doi.org/10.1098/rstb.2015.0261).
- Patten, M. L. and A. P. Murphy
 2012 "Relative disparity processing in the dorsal visual pathway", *Journal of Neuroscience*, 32, 16, pp. 5353-5355, DOI: [10.1523/JNEUROSCI.0588-12.2012](https://doi.org/10.1523/JNEUROSCI.0588-12.2012).
- Pelli, D. G.
 1997 "The VideoToolbox software for visual psychophysics: Transforming numbers into movies", *Spatial Vision*, 10, 4, pp. 437-442, DOI: [10.1163/156856897X00366](https://doi.org/10.1163/156856897X00366).
- Peña, J. L. and W. M. DeBello
 2010 "Auditory processing, plasticity, and learning in the barn owl", *ILAR Journal*, 51, 4, pp. 338-352, DOI: [10.1093/ilar.51.4.338](https://doi.org/10.1093/ilar.51.4.338).
- Perry, V. H. and A. Cowey
 1984 "Retinal ganglion cells that project to the superior colliculus and pretectum in the macaque monkey", *Neuroscience*, 12, 4, pp. 1125-1137, DOI: [10.1016/0306-4522\(84\)90007-1](https://doi.org/10.1016/0306-4522(84)90007-1).
- Peterson, M. R., B. Li, and R. D. Freeman
 2004 "The derivation of direction selectivity in the striate cortex." *Journal of Neuroscience*, 24, 14, pp. 3583-91, DOI: [10.1523/JNEUROSCI.5398-03.2004](https://doi.org/10.1523/JNEUROSCI.5398-03.2004).
- Peticolas, W. L., J. P. Goldsborough, and K. E. Rieckhoff
 1963 "Double photon excitation in organic crystals", *Physical Review Letters*, 10, 2, pp. 43-45, DOI: [10.1103/PhysRevLett.10.43](https://doi.org/10.1103/PhysRevLett.10.43).
- Pettigrew, J. D., T. Nikara, and P. O. Bishop
 1968 "Binocular interaction on single units in cat striate cortex: Simultaneous stimulation by single moving slit with receptive fields in correspondence", *Experimental Brain Research*, 6, 4, pp. 391-410, DOI: [10.1007/BF00233186](https://doi.org/10.1007/BF00233186).
- Pietrasanta, M., L. Restani, and M. Caleo
 2012 "The corpus callosum and the visual cortex: Plasticity is a game for two", *Neural Plasticity*, 2012, DOI: [10.1155/2012/838672](https://doi.org/10.1155/2012/838672).
- Piscopo, D. M., R. N. El-Danaf, a. D. Huberman, and C. M. Niell
 2013 "Diverse visual features encoded in mouse lateral geniculate nucleus", *Journal of Neuroscience*, 33, 11, pp. 4642-4656, DOI: [10.1523/JNEUROSCI.5187-12.2013](https://doi.org/10.1523/JNEUROSCI.5187-12.2013).
- Pluta, S. R., E. H. Lyall, G. I. Telian, E. Ryapolova-Webb, and H. Adesnik
 2017 "Surround integration organizes a spatial map during active sensation", *Neuron*, 94, 6, 1220-1233.e5, DOI: [10.1016/j.neuron.2017.04.026](https://doi.org/10.1016/j.neuron.2017.04.026).
- Poggio, G. F., F. Gonzalez, and F. Krause
 1988 "Stereoscopic mechanisms in monkey visual cortex: binocular correlation and disparity selectivity." *Journal of Neuroscience*, 8, 12, pp. 4531-4550, DOI: doi.org/10.1523/JNEUROSCI.08-12-04531.1988.
- Poggio, G. F. and B. Fischer
 1977 "Binocular interaction and depth sensitivity in striate and prestriate cortex of behaving rhesus monkey", *Journal of Neurophysiology*, 40, 6, pp. 1392-1405.

- Poggio, G. F.
 1995 "Mechanisms of stereopsis in monkey visual cortex", *Cerebral Cortex*, 5, 9, pp. 1689-1699, DOI: [10.1017/CB09781107415324.004](https://doi.org/10.1017/CB09781107415324.004).
- Poggio, G. F., B. C. Motter, S. Squatrito, and Y. Trotter
 1985 "Responses of neurons in visual cortex (V1 and V2) of the alert macaque to dynamic random-dot stereograms", *Vision Research*, 25, 3, pp. 397-406, DOI: [10.1016/0042-6989\(85\)90065-3](https://doi.org/10.1016/0042-6989(85)90065-3).
- Priebe, N. J. and D. Ferster
 2005 "Direction selectivity of excitation and inhibition in simple cells of the cat primary visual cortex." *Neuron*, 45, 1, pp. 133-145, DOI: [10.1016/j.neuron.2004.12.024](https://doi.org/10.1016/j.neuron.2004.12.024).
 2008 "Inhibition, spike threshold, and stimulus selectivity in primary visual cortex." *Neuron*, 57, 4, pp. 482-97, DOI: [10.1016/j.neuron.2008.02.005](https://doi.org/10.1016/j.neuron.2008.02.005).
 2012 "Mechanisms of neuronal computation in mammalian visual cortex", *Neuron*, 75, 2, pp. 194-208, DOI: [10.1016/j.neuron.2012.06.011](https://doi.org/10.1016/j.neuron.2012.06.011).
- Prince, S. J. D., B. G. Cumming, and A. J. Parker
 2002a "Range and mechanism of encoding of horizontal disparity in macaque V1", *Journal of Neurophysiology*, 87, 1, pp. 209-221, DOI: [10.1152/jn.00466.2000](https://doi.org/10.1152/jn.00466.2000).
- Prince, S., A. D. Pointon, B. G. Cumming, and A. J. Parker
 2002b "Quantitative analysis of the responses of V1 neurons to horizontal disparity in dynamic random-dot stereograms", *Journal of Neurophysiology*, 87, 1, pp. 191-208, DOI: [10.1152/jn.00465.2000](https://doi.org/10.1152/jn.00465.2000).
- Ptito, M., F. Lepore, and J. P. Guillemot
 1991 "Stereopsis in the cat: Behavioral demonstration and underlying mechanisms", *Neuropsychologia*, 29, 6, pp. 443-464, DOI: [10.1016/0028-3932\(91\)90004-R](https://doi.org/10.1016/0028-3932(91)90004-R).
- Pushchin, I. I.
 2013 "Retinal ganglion cells of the accessory optic system: A review", *Journal of Integrative Neuroscience*, 12, 01, pp. 145-162, DOI: [10.1142/S0219635213300011](https://doi.org/10.1142/S0219635213300011).
- Qian, N.
 1997 "Binocular disparity and the perception of depth", *Neuron*, 18, 3, pp. 359-368, DOI: [10.1016/S0896-6273\(00\)81238-6](https://doi.org/10.1016/S0896-6273(00)81238-6).
- Ramdyia, P. and F. Engert
 2008 "Emergence of binocular functional properties in a monocular neural circuit." *Nature Neuroscience*, 11, 9, pp. 1083-90, DOI: [10.1038/nn.2166](https://doi.org/10.1038/nn.2166).
- Rapaport, D. H. and J. Stone
 1984 "The area centralis of the retina in the cat and other mammals: Focal point for function and development of the visual system", *Neuroscience*, 11, 2, pp. 289-301, DOI: [10.1016/0306-4522\(84\)90024-1](https://doi.org/10.1016/0306-4522(84)90024-1).
- Ray, T. a. and J. N. Kay
 2015 "Following directions from the retina to the brain", *Neuron*, 86, 4, pp. 855-857, DOI: [10.1016/j.neuron.2015.05.017](https://doi.org/10.1016/j.neuron.2015.05.017).
- Read, J. C. A. and B. G. Cumming
 2007 "Sensors for impossible stimuli may solve the stereo correspondence problem." *Nature neuroscience*, 10, 10, pp. 1322-1328, DOI: [10.1038/nn1951](https://doi.org/10.1038/nn1951).

- Read, J. C. a.
 2015 "What is stereoscopic vision good for?", *Proc. SPIE*, 9391, Stereoscopic Displays and Applications XXVI, 93910N, DOI: [10.1117/12.2184988](https://doi.org/10.1117/12.2184988).
- Read, J. C. A. and B. G. Cumming
 2003 "Ocular dominance predicts neither strength nor class of disparity selectivity with random-dot stimuli in primate V1", *Journal of Neurophysiology*, 91, 3, pp. 1271-1281, DOI: [10.1152/jn.00588.2003](https://doi.org/10.1152/jn.00588.2003).
- Read, J. C. and B. G. Cumming
 2017 "Visual perception: Neural networks for stereopsis", *Current Biology*, 27, 12, R594-R596, DOI: [10.1016/j.cub.2017.05.013](https://doi.org/10.1016/j.cub.2017.05.013).
- Reid, R. C., R. E. Soodak, and R. M. Shapley
 1987 "Linear mechanisms of directional selectivity in simple cells of cat striate cortex." *Proceedings of the National Academy of Sciences*, 84, 23, pp. 8740-4, DOI: doi.org/10.1073/pnas.84.23.8740.
 1991 "Directional selectivity and spatiotemporal structure of receptive fields of simple cells in cat striate cortex." *Journal of Neurophysiology*, 66, 2, pp. 505-529, DOI: [10.1152/jn.1991.66.2.505](https://doi.org/10.1152/jn.1991.66.2.505).
- Reid, R. C. and J.-M. Alonso
 1995 "Specificity of monosynaptic connections from thalamus to visual cortex", *Nature*, 378, 6554, pp. 281-284, DOI: [10.1038/378281a0](https://doi.org/10.1038/378281a0).
- Reinhold, K., A. D. Lien, and M. Scanziani
 2015 "Distinct recurrent versus afferent dynamics in cortical visual processing", *Nature Neuroscience*, 18, 12, DOI: [10.1038/nn.4153](https://doi.org/10.1038/nn.4153).
- Restani, L., C. Cerri, M. Pietrasanta, L. Gianfranceschi, L. Maffei, and M. Caleo
 2009 "Functional masking of deprived eye responses by callosal input during ocular dominance plasticity", *Neuron*, 64, 5, pp. 707-718, DOI: [10.1016/j.neuron.2009.10.019](https://doi.org/10.1016/j.neuron.2009.10.019).
- Richards, W.
 1970 "Stereopsis and stereoblindness", *Experimental Brain Research*, 10, 4, pp. 380-388, DOI: [10.1007/BF02324765](https://doi.org/10.1007/BF02324765).
- Ringach, D. L., M. J. Hawken, and R. Shapley
 1997 "Dynamics of orientation tuning in macaque primary visual cortex", *Nature*, 387, 6630, pp. 281-284, DOI: [10.1038/387281a0](https://doi.org/10.1038/387281a0).
- Ringach, D. L., P. J. Mineault, E. Tring, N. D. Olivas, P. Garcia-Junco-Clemente, and J. T. Trachtenberg
 2016 "Spatial clustering of tuning in mouse primary visual cortex", *Nature Communications*, 7, p. 12270, DOI: [10.1038/ncomms12270](https://doi.org/10.1038/ncomms12270).
- Ringach, D. L., R. M. Shapley, and M. J. Hawken
 2002 "Orientation selectivity in macaque V1: diversity and laminar dependence." *Journal of Neuroscience*, 22, 13, pp. 5639-5651, DOI: doi.org/10.1523/JNEUROSCI.22-13-05639.2002.
- Rivlin-Etzion, M., K. Zhou, W. Wei, J. Elstrott, P. L. Nguyen, B. a. Barres, A. D. Huberman, and M. B. Feller
 2011 "Transgenic mice reveal unexpected diversity of on-off direction-selective retinal ganglion cell subtypes and brain structures involved in motion processing." *Journal of Neuroscience*, 31, 24, pp. 8760-9, DOI: [10.1523/JNEUROSCI.0564-11.2011](https://doi.org/10.1523/JNEUROSCI.0564-11.2011).

- Rizzolatti, G., M. Gentilucci, R. M. Camarda, V. Gallese, G. Luppino, M. Matelli, and L. Fogassi
 1990 "Neurons related to reaching-grasping arm movements in the rostral part of area 6 (area 6a β)", *Experimental Brain Research*, 82, 2, pp. 337-350, DOI: [10.1007/BF00231253](https://doi.org/10.1007/BF00231253).
- Robinson, L., H. Bridge, and G. Riedel
 2001 "Visual discrimination learning in the water maze: a novel test for visual acuity", *Behavioural Brain Research*, 119, 1, pp. 77-84, DOI: [S0166-4328\(00\)00334-X](https://doi.org/10.1016/S0166-4328(00)00334-X)[pii].
- Rocheffort, N. L., M. Narushima, C. Grienberger, N. Marandi, D. N. Hill, and A. Konnerth
 2011 "Development of direction selectivity in mouse cortical neurons." *Neuron*, 71, 3, pp. 425-432, DOI: [10.1016/j.neuron.2011.06.013](https://doi.org/10.1016/j.neuron.2011.06.013).
- Roe, A. W., A. J. Parker, R. T. Born, and G. C. DeAngelis
 2007 "Disparity channels in early vision", *Journal of Neuroscience*, 27, 44, pp. 11820-11831, DOI: [10.1523/JNEUROSCI.4164-07.2007](https://doi.org/10.1523/JNEUROSCI.4164-07.2007).
- Román Rosón, M., Y. Bauer, P. Berens, T. Euler, and L. Busse
 2018 "Mouse dLGN receives input from a diverse population of retinal ganglion cells with limited convergence", *bioRxiv*, DOI: <http://dx.doi.org/10.1101/322164>.
- Rompani, S. B., F. E. Mullner, A. Wanner, C. Zhang, C. N. Roth, K. Yonehara, and B. Roska
 2017 "Different modes of visual integration in the lateral geniculate nucleus revealed by single-cell-initiated transsynaptic tracing", *Neuron*, pp. 767-776, DOI: [10.1016/j.neuron.2017.01.028](https://doi.org/10.1016/j.neuron.2017.01.028).
- Rose, M.
 1929 "Cytoarchitektonischer atlas der großhirnrinde der maus", *J. Psychol. Neurol.* 40, pp. 1-51.
- Rose, T., P. M. Goltstein, R. Portugues, and O. Griesbeck
 2014 "Putting a finishing touch on GECIs", *Frontiers in Molecular Neuroscience*, 7, November, pp. 1-15, DOI: [10.3389/fnmol.2014.00088](https://doi.org/10.3389/fnmol.2014.00088).
- Rose, T., J. Jaepel, M. Hübener, and T. Bonhoeffer
 2016 "Cell-specific restoration of stimulus preference after monocular deprivation in the visual cortex", *Science*, 352, 6291, pp. 1319-1322, DOI: [10.1126/science.aad3358](https://doi.org/10.1126/science.aad3358).
- Roska, B. and M. Meister
 2014 *The retina dissects the visual scene into distinct features*, ed. by J. S. Werner and L. M. Chalupa, Cambridge, MA: MIT Press, pp. 163-182.
- Rossel, S.
 1983 "Binocular stereopsis in an insect", *Nature*, 302, 5911, pp. 821-822, DOI: [10.1038/302821a0](https://doi.org/10.1038/302821a0).
- Roth, M. M., J. C. Dahmen, D. R. Muir, F. Imhof, F. J. Martini, and S. B. Hofer
 2015 "Thalamus conveys diverse contextual information to layer 1 of visual cortex", *Nature Neuroscience*, 19, 148.26, p. 148, DOI: [10.1038/nn.4197](https://doi.org/10.1038/nn.4197).
- Roth, M. M., F. Helmchen, and B. M. Kampa
 2012 "Distinct functional properties of primary and posteromedial visual area of mouse neocortex." *Journal of Neuroscience*, 32, 28, pp. 9716-26, DOI: [10.1523/JNEUROSCI.0110-12.2012](https://doi.org/10.1523/JNEUROSCI.0110-12.2012).

- Sabbah, S., J. A. Gemmer, A. Bhatia-Lin, G. Manoff, G. Castro, J. K. Siegel, N. Jeffery, and D. M. Berson
2017 "A retinal code for motion along the gravitational and body axes", *Nature*, DOI: [10.1038/nature22818](https://doi.org/10.1038/nature22818).
- Sajovic, P. and C. Levinthal
1982 "Visual cells of zebrafish optic tectum: Mapping with small spots", *Neuroscience*, 7, 10, pp. 2407-2426, DOI: [10.1016/0306-4522\(82\)90204-4](https://doi.org/10.1016/0306-4522(82)90204-4).
- Sakatani, T. and T. Isa
2007 "Quantitative analysis of spontaneous saccade-like rapid eye movements in C57BL/6 mice", *Neuroscience Research*, 58, 3, pp. 324-331, DOI: [10.1016/j.neures.2007.04.003](https://doi.org/10.1016/j.neures.2007.04.003).
- Saleem, A. B., A. Ayaz, K. J. Jeffery, K. D. Harris, and M. Carandini
2013 "Integration of visual motion and locomotion in mouse visual cortex." *Nature Neuroscience*, 16, 12, pp. 1864-1869, DOI: [10.1038/nn.3567](https://doi.org/10.1038/nn.3567).
- Samonds, J. M., B. R. Potetz, and T. S. Lee
2012 "Relative luminance and binocular disparity preferences are correlated in macaque primary visual cortex, matching natural scene statistics", *Proceedings of the National Academy of Sciences*, 109, 16, pp. 6313-6318, DOI: [10.1073/pnas.1200125109](https://doi.org/10.1073/pnas.1200125109).
- Sanada, T. M. and G. C. DeAngelis
2014 "Neural representation of motion-in-depth in area MT", *Journal of Neuroscience*, 34, 47, pp. 15508-21, DOI: [10.1523/JNEUROSCI.1072-14.2014](https://doi.org/10.1523/JNEUROSCI.1072-14.2014).
- Sanes, J. R. and R. H. Masland
2014 "The types of retinal ganglion cells: current status and implications for neuronal classification", *Annual Review of Neuroscience*, 38, 1, p. 150421150146009, DOI: [10.1146/annurev-neuro-071714-034120](https://doi.org/10.1146/annurev-neuro-071714-034120).
- Sarnaik, R., B.-S. Wang, and J. Cang
2014 "Experience-dependent and independent binocular correspondence of receptive field subregions in mouse visual cortex." *Cerebral Cortex*, 24, 6, pp. 1658-70, DOI: [10.1093/cercor/bht027](https://doi.org/10.1093/cercor/bht027).
- Saul, A. B., P. L. Carras, and A. L. Humphrey
2005 "Temporal properties of inputs to direction-selective neurons in monkey V1." *Journal of Neurophysiology*, 94, 1, pp. 282-94, DOI: [10.1152/jn.00868.2004](https://doi.org/10.1152/jn.00868.2004).
- Saul, A. B. and A. L. Humphrey
1992 "Evidence of input from lagged cells in the lateral geniculate nucleus to simple cells in cortical area 17 of the cat", *Journal of Neurophysiology*, 68, 4, pp. 1190-1208, DOI: [10.1152/jn.1992.68.4.1190](https://doi.org/10.1152/jn.1992.68.4.1190).
- Scholl, B. K., J. Burge, and N. J. Priebe
2013a "Binocular integration and disparity selectivity in mouse primary visual cortex", *Journal of Neurophysiology*, 109, 12, pp. 3013-3024, DOI: [10.1093/cercor/bht027](https://doi.org/10.1093/cercor/bht027).
- Scholl, B. K., J. J. Pattadkal, G. A. Dilly, N. J. Priebe, and B. V. Zemelman
2015 "Local integration accounts for weak selectivity of mouse neocortical parvalbumin interneurons", *Neuron*, 87, 2, pp. 424-436, DOI: [10.1016/j.neuron.2015.06.030](https://doi.org/10.1016/j.neuron.2015.06.030).
- Scholl, B. K., J. J. Pattadkal, and N. J. Priebe
2017a "Binocular disparity selectivity weakened after monocular deprivation in mouse V1", *Journal of Neuroscience*, 37, 27, pp. 6517-6526, DOI: [10.1523/JNEUROSCI.1193-16.2017](https://doi.org/10.1523/JNEUROSCI.1193-16.2017).

- Scholl, B. K., J. J. Pattadkal, A. Rowe, and N. J. Priebe
 2017b "Functional characterization and spatial clustering of visual cortical neurons in the predatory grasshopper mouse *Onychomys arenicola*", *Journal of Neurophysiology*, 117, 3, pp. 910-918, DOI: [10.1152/jn.00779.2016](https://doi.org/10.1152/jn.00779.2016).
- Scholl, B. K., A. Y. Y. Tan, J. Corey, and N. J. Priebe
 2013b "Emergence of orientation selectivity in the mammalian visual pathway", *Journal of Neuroscience*, 33, 26, pp. 10616-10624, DOI: [10.1523/JNEUROSCI.0404-13.2013](https://doi.org/10.1523/JNEUROSCI.0404-13.2013).
- Schuett, S., T. Bonhoeffer, and M. Hübener
 2002 "Mapping retinotopic structure in mouse visual cortex with optical imaging." *Journal of Neuroscience*, 22, 15, pp. 6549-6559, DOI: [20026635](https://doi.org/20026635).
- Schulz, D. P. a., M. Sahani, and M. Carandini
 2015 "Five key factors determining pairwise correlations in visual cortex", *Journal of Neurophysiology*, May 2015, jn.00094.2015, DOI: [10.1152/jn.00094.2015](https://doi.org/10.1152/jn.00094.2015).
- Seabrook, T. A., T. J. Burbridge, M. C. Crair, and A. D. Huberman
 2017 "Architecture, function, and assembly of the mouse visual system", *Annual Review of Neuroscience*, 40, 1, pp. 499-538, DOI: [10.1146/annurev-neuro-071714-033842](https://doi.org/10.1146/annurev-neuro-071714-033842).
- Sereno, M. I. and R. B. Tootell
 2005 "From monkeys to humans: What do we now know about brain homologies?", *Current Opinion in Neurobiology*, 15, 2, pp. 135-144, DOI: [10.1016/j.conb.2005.03.014](https://doi.org/10.1016/j.conb.2005.03.014).
- Shadlen, M. and T. Carney
 1986 "Mechanisms of human motion perception revealed by a new cyclopean illusion." *Science*, 232, 4746, pp. 95-7, DOI: doi.org/10.1126/science.3952502.
- Shang, C., Z. Liu, Z. Chen, Y. Shi, Q. Wang, S. Liu, D. Li, and P. Cao
 2015 "A parvalbumin-positive excitatory visual pathway to trigger fear responses in mice", *Science*, 348, 6242, pp. 6-11, DOI: [10.1126/science.aaa8694](https://doi.org/10.1126/science.aaa8694).
- Shatz, C. J. and M. P. Stryker
 1978 "Ocular dominance in layer IV of the cat's visual cortex and the effects of monocular deprivation." *Journal of Physiology*, 281, 1, pp. 267-283, DOI: [10.1113/jphysiol.1978.sp012421](https://doi.org/10.1113/jphysiol.1978.sp012421).
- Shatz, C. J., S. Lindstrom, and T. N. Wiesel
 1977 "The distribution of afferents representing the right and left eyes in the cat's visual cortex", *Brain Research*, 131, pp. 103-116, DOI: [doi.org/10.1016/0006-8993\(77\)90031-2](https://doi.org/10.1016/0006-8993(77)90031-2).
- Sherman, S. M.
 2016 "Thalamus plays a central role in ongoing cortical functioning", *Nature Neuroscience*, 19, 4, pp. 533-541, DOI: [10.1038/nn.4269](https://doi.org/10.1038/nn.4269).
- Shi, X., J. Barchini, H. A. Ledesma, D. Koren, Y. Jin, X. Liu, W. Wei, and J. Cang
 2017 "Retinal origin of direction selectivity in the superior colliculus", *Nature Neuroscience*, August 2016, pp. 1-12, DOI: [10.1038/nn.4498](https://doi.org/10.1038/nn.4498).
- Shimojo, S., Y. Kamitani, and S. Nishida
 2001 "Afterimage of perceptually filled-in surface", *Science*, 293, 5535, pp. 1677-80, DOI: [10.1126/science.1060161](https://doi.org/10.1126/science.1060161).

- Shinkman, P. G. and C. J. Bruce
 1977 "Binocular differences in cortical receptive fields of kittens after rotationally disparate binocular experience." *Science*, 197, 4300, pp. 285-287, DOI: [10.1126/science.877554](https://doi.org/10.1126/science.877554).
- Shou, T., A. G. Leventhal, K. G. Thompson, and Y. Zhou
 1995 "Direction biases of X and Y type retinal ganglion cells in the cat", *Journal of Neurophysiology*, 73, 4, pp. 1414-1421, DOI: <https://doi.org/10.1152/jn.1995.73.4.1414>.
- Simpson, J. I.
 1984 "The accessory optic system", *Annual Review of Neuroscience*, 7, pp. 13-41, DOI: [10.1146/annurev.ne.07.030184.000305](https://doi.org/10.1146/annurev.ne.07.030184.000305).
- Smith, E. L., Y. M. Chino, J. Ni, W. H. Ridder, and M. L. Crawford
 1997 "Binocular spatial phase tuning characteristics of neurons in the macaque striate cortex." *Journal of Neurophysiology*, 78, 1, pp. 351-365, DOI: doi.org/10.1152/jn.1997.78.1.351.
- Smith, I. T., L. B. Townsend, R. Huh, H. Zhu, and S. L. Smith
 2017 "Stream-dependent development of higher visual cortical areas", *Nature Neuroscience*, August 2016, pp. 1-11, DOI: [10.1038/nn.4469](https://doi.org/10.1038/nn.4469).
- Smith, S. L. and M. Häusser
 2010 "Parallel processing of visual space by neighboring neurons in mouse visual cortex." *Nature Neuroscience*, 13, 9, pp. 1144-9, DOI: [10.1038/nn.2620](https://doi.org/10.1038/nn.2620).
- Sofroniew, N. J., J. D. Cohen, A. K. Lee, and K. Svoboda
 2014 "Natural whisker-guided behavior by head-fixed mice in tactile virtual reality", *Journal of Neuroscience*, 34, 29, pp. 9537-9550, DOI: [10.1523/JNEUROSCI.0712-14.2014](https://doi.org/10.1523/JNEUROSCI.0712-14.2014).
- Sofroniew, N. J. and K. Svoboda
 2015 "Whisking", *Current Biology*, 25, 4, R137-R140, DOI: [10.1016/j.cub.2015.01.008](https://doi.org/10.1016/j.cub.2015.01.008).
- Sofroniew, N. J., D. Flickinger, J. King, and K. Svoboda
 2016 "A large field of view two-photon mesoscope with subcellular resolution for in vivo imaging", *eLife*, 5, pp. 1-20, DOI: [10.7554/eLife.14472](https://doi.org/10.7554/eLife.14472).
- Sprague, W. W., E. A. Cooper, I. Tasic, and M. S. Banks
 2015 "Stereopsis is adaptive for the natural environment", *Science Advances*, 1, 4, e1400254-e1400254, DOI: [10.1126/sciadv.1400254](https://doi.org/10.1126/sciadv.1400254).
- Sterratt, D. C., D. Lyngholm, D. J. Willshaw, and I. D. Thompson
 2013 "Standard anatomical and visual space for the mouse retina: computational reconstruction and transformation of flattened retinæ with the Retistruct package." *PLoS Computational Biology*, 9, 2, ed. by H. Lapp, e1002921, DOI: [10.1371/journal.pcbi.1002921](https://doi.org/10.1371/journal.pcbi.1002921).
- Stirman, J. N., L. B. Townsend, and S. L. Smith
 2016 "A touchscreen based global motion perception task for mice", *Vision Research*, 127, pp. 74-83, DOI: [10.1016/j.visres.2016.07.006](https://doi.org/10.1016/j.visres.2016.07.006).
- Stuart, G. J. and N. Spruston
 2015 "Dendritic integration: 60 years of progress", *Nature Neuroscience*, 18, 12, pp. 1713-1721, DOI: [10.1038/nn.4157](https://doi.org/10.1038/nn.4157).

- Suarez, H., C. Koch, and R. Douglas
 1995 "Modeling direction selectivity of simple cells in striate visual cortex within the framework of the canonical microcircuit", *Journal of Neuroscience*, 15, 10, pp. 6700-19, DOI: doi.org/10.1523/JNEUROSCI.15-10-06700.1995.
- Sugawara, E. and H. Nikaido
 2014 "Properties of AdeABC and AdeIJK efflux systems of *Acinetobacter baumannii* compared with those of the AcrAB-TolC system of *Escherichia coli*." *Antimicrobial agents and chemotherapy*, 58, 12, pp. 7250-7, DOI: [10.1128/AAC.03728-14](https://doi.org/10.1128/AAC.03728-14).
- Sun, L. O. O., C. M. M. Brady, H. Cahill, T. Al-Khindi, H. Sakuta, O. S. S. Dhande, M. Noda, A. D. D. Huberman, J. Nathans, and A. L. L. Kolodkin
 2015 "Functional assembly of accessory optic system circuitry critical for compensatory eye movements", *Neuron*, 86, 4, pp. 971-984, DOI: [10.1016/j.neuron.2015.03.064](https://doi.org/10.1016/j.neuron.2015.03.064).
- Sun, W., Z. Tan, B. D. Mensh, and N. Ji
 2016 "Thalamus provides layer 4 of primary visual cortex with orientation- and direction-tuned inputs", *Nature Neuroscience*, 1, December, DOI: [10.1038/nn.4196](https://doi.org/10.1038/nn.4196).
- Tanabe, S., T. Doi, K. Umeda, and I. Fujita
 2005 "Disparity-tuning characteristics of neuronal responses to dynamic random-dot stereograms in macaque visual area V4", *Journal of Neurophysiology*, 94, 4, pp. 2683-2699, DOI: [10.1152/jn.00319.2005](https://doi.org/10.1152/jn.00319.2005).
- Theis, L., P. Berens, E. Froudarakis, T. Euler, and A. S. Tolias
 2016 "Benchmarking spike rate inference in population calcium imaging", *Neuron*, 90, pp. 471-482, DOI: [10.1016/j.neuron.2016.04.014](https://doi.org/10.1016/j.neuron.2016.04.014).
- Thomas, O. M., B. G. Cumming, and a. J. Parker
 2002 "A specialization for relative disparity in V2." *Nature Neuroscience*, 5, 5, pp. 472-478, DOI: [10.1038/nn837](https://doi.org/10.1038/nn837).
- Tian, L., S. A. Hires, and L. L. Looger
 2012 "Imaging neuronal activity with genetically encoded calcium indicators." *Cold Spring Harbor Protocols*, 7, 6, pp. 647-656, DOI: [10.1101/pdb.top069609](https://doi.org/10.1101/pdb.top069609).
- Timney, B. and K. Keil
 1999 "Local and global stereopsis in the horse", *Vision Research*, 39, 10, pp. 1861-1867, DOI: [10.1016/S0042-6989\(98\)00276-4](https://doi.org/10.1016/S0042-6989(98)00276-4).
- Tkatchenko, T. V., Y. Shen, and A. V. Tkatchenko
 2010 "Analysis of postnatal eye development in the mouse with high-resolution small animal magnetic resonance imaging." *Investigative Ophthalmology and Visual Science*, 51, 1, pp. 21-7, DOI: [10.1167/iovs.08-2767](https://doi.org/10.1167/iovs.08-2767).
- Tohmi, M., R. Meguro, H. Tsukano, R. Hishida, and K. Shibuki
 2014 "The extrageniculate visual pathway generates distinct response properties in the higher visual areas of mice." *Current Biology*, 24, 6, pp. 587-97, DOI: [10.1016/j.cub.2014.01.061](https://doi.org/10.1016/j.cub.2014.01.061).
- Tohmi, M., K. Takahashi, Y. Kubota, R. Hishida, and K. Shibuki
 2009 "Transcranial flavoprotein fluorescence imaging of mouse cortical activity and plasticity", *Journal of Neurochemistry*, 109, SUPPL. 1, pp. 3-9, DOI: [10.1111/j.1471-4159.2009.05926.x](https://doi.org/10.1111/j.1471-4159.2009.05926.x).

- Torre, V. and T. Poggio
 1978 "A synaptic mechanism possibly underlying directional selectivity to motion", *Proceedings of the Royal Society of London - Biological Sciences*, 202, 1148, pp. 409-416, DOI: [10.1098/rspb.1978.0075](https://doi.org/10.1098/rspb.1978.0075).
- Tran-Van-Minh, A., R. D. Cazé, T. Abrahamsson, L. Cathala, B. S. Gutkin, and D. A. DiGregorio
 2015 "Contribution of sublinear and supralinear dendritic integration to neuronal computations", *Frontiers in Cellular Neuroscience*, 9, March, pp. 1-15, DOI: [10.3389/fncel.2015.00067](https://doi.org/10.3389/fncel.2015.00067).
- Tremblay, R., S. Lee, and B. Rudy
 2016 "GABAergic interneurons in the neocortex: From cellular properties to circuits", *Neuron*, 91, 2, pp. 260-292, DOI: [10.1016/j.neuron.2016.06.033](https://doi.org/10.1016/j.neuron.2016.06.033).
- Tsao, D. Y., B. R. Conway, and M. S. Livingstone
 2003 "Receptive fields of disparity-tuned simple cells in macaque V1", *Neuron*, 38, 1, pp. 103-114, DOI: [10.1016/S0896-6273\(03\)00150-8](https://doi.org/10.1016/S0896-6273(03)00150-8).
- Turrigiano, G.
 2011 "Too many cooks? Intrinsic and synaptic homeostatic mechanisms in cortical circuit refinement", *Annual Review of Neuroscience*, 34, 1, pp. 89-103, DOI: [10.1146/annurev-neuro-060909-153238](https://doi.org/10.1146/annurev-neuro-060909-153238).
 2017 "The dialectic of hebb and homeostasis", *Philosophical Transactions of the Royal Society of London B*, 372, 1715, pp. 4-6, DOI: [10.1098/rstb.2016.0258](https://doi.org/10.1098/rstb.2016.0258).
- Tyler, C. W.
 1974 "Depth perception in disparity gratings", *Nature*, 251, 5471, pp. 140-142, DOI: [10.1038/251140a0](https://doi.org/10.1038/251140a0).
- Ungerleider, L. G. and M. Mishkin
 1982 "Two cortical visual systems", in *Analysis of Visual Behavior*, DOI: [10.2139/ssrn.1353746](https://doi.org/10.2139/ssrn.1353746).
- Usrey, W. M. and H. J. Alitto
 2015 "Visual functions of the thalamus", *Annual Review of Vision Science*, 1, 1, pp. 351-371, DOI: [10.1146/annurev-vision-082114-035920](https://doi.org/10.1146/annurev-vision-082114-035920).
- Vaiceliunaite, A., S. Eriskien, F. Franzen, S. Katzner, and L. Busse
 2013 "Spatial integration in mouse primary visual cortex", *Journal of Neurophysiology*, 110, 4, pp. 964-972, DOI: [10.1152/jn.00138.2013](https://doi.org/10.1152/jn.00138.2013).
- Vale, R., D. A. Evans, and T. Branco
 2017 "Rapid spatial learning controls instinctive defensive behavior in mice", *Current Biology*, 27, 9, pp. 1342-1349, DOI: [10.1016/j.cub.2017.03.031](https://doi.org/10.1016/j.cub.2017.03.031).
- Van den Bergh, G., B. Zhang, L. Arckens, and Y. M. Chino
 2010 "Receptive-field properties of V1 and V2 neurons in mice and macaque monkeys." *Journal of Comparative Neurology*, 518, 11, pp. 2051-70, DOI: [10.1002/cne.22321](https://doi.org/10.1002/cne.22321).
- Van der Willigen, R. F.
 2011 "Owls see in stereo much like humans do", *Journal of Vision*, 11, 7, pp. 1-27, DOI: [10.1167/11.7.10.Introduction](https://doi.org/10.1167/11.7.10.Introduction).
- Vaney, D. I., B. Sivyver, and W. R. Taylor
 2012 "Direction selectivity in the retina: symmetry and asymmetry in structure and function." *Nature Reviews Neuroscience*, 13, 3, pp. 194-208, DOI: [10.1038/nrn3165](https://doi.org/10.1038/nrn3165).

- Vélez-Fort, M., C. V. Rousseau, C. J. Niedworok, I. R. Wickersham, E. A. Rancz, A. P. Brown, M. Strom, and T. W. Margrie
 2014 "The stimulus selectivity and connectivity of layer six principal cells reveals cortical microcircuits underlying visual processing", *Neuron*, 83, 6, pp. 1431-1443, DOI: [10.1016/j.neuron.2014.08.001](https://doi.org/10.1016/j.neuron.2014.08.001).
- Verhoef, B.-E., R. Vogels, and P. Janssen
 2016 "Binocular depth processing in the ventral visual pathway", *Philosophical Transactions of the Royal Society of London B*, 371, 1697, p. 20150259, DOI: [10.1098/rstb.2015.0259](https://doi.org/10.1098/rstb.2015.0259).
- Vickery, R. M. and J. W. Morley
 1999 "Binocular phase interactions in area 21a of the cat", *Journal of Physiology*, 514, 2, pp. 541-549, DOI: [10.1111/j.1469-7793.1999.541ae.x](https://doi.org/10.1111/j.1469-7793.1999.541ae.x).
- Volland, S., J. Esteve-Rudd, J. Hoo, C. Yee, and D. S. Williams
 2015 "A comparison of some organizational characteristics of the mouse central retina and the human macula", *PLoS ONE*, 10, 4, pp. 1-13, DOI: [10.1371/journal.pone.0125631](https://doi.org/10.1371/journal.pone.0125631).
- Vora, S. R., E. D. Camci, and T. C. Cox
 2016 "Postnatal ontogeny of the cranial base and craniofacial skeleton in male C57BL/6J mice: A reference standard for quantitative analysis", *Frontiers in Physiology*, 6, JAN, pp. 1-14, DOI: [10.3389/fphys.2015.00417](https://doi.org/10.3389/fphys.2015.00417).
- Wager, T. D. and T. Yarkoni
 2012 "Establishing homology between monkey and human brains", *Nature Methods*, 9, 3, pp. 237-238, DOI: [10.1038/nmeth.1869](https://doi.org/10.1038/nmeth.1869).
- Wagner, H. and B. Frost
 1993 "Disparity-sensitive cells in the owl have a characteristic disparity", *Nature*, 364, pp. 210-211, DOI: doi.org/10.1038/364796a0.
- Wagor, E., N. J. Mangini, and A. L. Pearlman
 1980 "Retinotopic organization of striate and extrastriate visual cortex in the mouse", *Journal of Comparative Neurology*, 193, 1, pp. 187-202, DOI: [10.1002/cne.901930113](https://doi.org/10.1002/cne.901930113).
- Wallace, D. J., D. S. Greenberg, J. Sawinski, S. Rulla, G. Notaro, and J. N. D. Kerr
 2013 "Rats maintain an overhead binocular field at the expense of constant fusion", *Nature*, 498, 7452, pp. 65-69, DOI: [10.1038/nature12153](https://doi.org/10.1038/nature12153).
- Wallach, H. and A. O'Leary
 1982 "Slope of regard as a distance cue", *Perception & Psychophysics*, 31, 2, pp. 145-148, DOI: [10.3758/BF03206214](https://doi.org/10.3758/BF03206214).
- Wang, B. S., R. Sarnaik, and J. Cang
 2010 "Critical period plasticity matches binocular orientation preference in the visual cortex", *Neuron*, 65, 2, pp. 246-256, DOI: [10.1016/j.neuron.2010.01.002](https://doi.org/10.1016/j.neuron.2010.01.002).
- Wang, L., M. Liu, M. A. Segreaves, and J. Cang
 2015 "Visual experience is required for the development of eye movement maps in the mouse superior colliculus", *Journal of Neuroscience*, 35, 35, pp. 12281-12286, DOI: [10.1523/JNEUROSCI.0117-15.2015](https://doi.org/10.1523/JNEUROSCI.0117-15.2015).
- Wang, Q. and A. Burkhalter
 2013 "Stream-related preferences of inputs to the superior colliculus from areas of dorsal and ventral streams of mouse visual cortex", *Journal of Neuroscience*, 33, 4, pp. 1696-1705, DOI: [10.1523/JNEUROSCI.3067-12.2013](https://doi.org/10.1523/JNEUROSCI.3067-12.2013).

- Wang, Q., E. Gao, and A. Burkhalter
 2011 "Gateways of ventral and dorsal streams in mouse visual cortex", *Journal of Neuroscience*, 31, 5, pp. 1905-1918, DOI: [10.1523/JNEUROSCI.3488-10.2011](https://doi.org/10.1523/JNEUROSCI.3488-10.2011).
- Wang, Q., O. Sporns, and A. Burkhalter
 2012 "Network analysis of corticocortical connections reveals ventral and dorsal processing streams in mouse visual cortex", *Journal of Neuroscience*, 32, 13, pp. 4386-4399, DOI: [10.1523/JNEUROSCI.6063-11.2012](https://doi.org/10.1523/JNEUROSCI.6063-11.2012).
- Wang, Q. and A. Burkhalter
 2007 "Area map of mouse visual cortex", *Journal of Comparative Neurology*, 502, 3, pp. 339-357, DOI: [10.1002/cne.21286](https://doi.org/10.1002/cne.21286), arXiv: [NIHMS150003](https://arxiv.org/abs/NIHMS150003).
- Wang, Q., E. Gao, and A. Burkhalter
 2007 "In vivo transcranial imaging of connections in mouse visual cortex." *Journal of Neuroscience Methods*, 159, 2, pp. 268-76, DOI: [10.1016/j.jneumeth.2006.07.024](https://doi.org/10.1016/j.jneumeth.2006.07.024).
- Watanabe, M., H. Tanaka, T. Uka, and I. Fujita
 2002 "Disparity-selective neurons in area V4 of macaque monkeys." *Journal of Neurophysiology*, 87, 4, pp. 1960-1973, DOI: [10.1152/jn.00780.2000](https://doi.org/10.1152/jn.00780.2000).
- Waugh, K. T.
 1910 "The rôle of vision in the mental life of the mouse", *Journal of Comparative Neurology and Psychology*, 20, 6, pp. 549-599, DOI: [10.1002/cne.920200602](https://doi.org/10.1002/cne.920200602).
- Wei, W., A. M. Hamby, K. Zhou, and M. B. Feller
 2011 "Development of asymmetric inhibition underlying direction selectivity in the retina." *Nature*, 469, 7330, pp. 402-6, DOI: [10.1038/nature09600](https://doi.org/10.1038/nature09600), arXiv: [NIHMS150003](https://arxiv.org/abs/NIHMS150003).
- Weigand, M., F. Sartori, and H. Cuntz
 2017 "Universal transition from unstructured to structured neural maps", *Proceedings of the National Academy of Sciences*, p. 201616163, DOI: [10.1073/pnas.1616163114](https://doi.org/10.1073/pnas.1616163114).
- Weiler, S., J. Bauer, M. Hübener, T. Bonhoeffer, T. Rose, and V. Scheuss
 2018 "High-yield in vitro recordings from neurons functionally characterized in vivo", *Nature Protocols*, 13, 6, pp. 1275-1293, DOI: [10.1038/nprot.2018.026](https://doi.org/10.1038/nprot.2018.026).
- Wekselblatt, J. B., E. D. Flister, D. M. Piscopo, and C. M. Niell
 2016 "Large-scale imaging of cortical dynamics during sensory perception and behavior", *Journal of Neurophysiology*, February, jn.01056.2015, DOI: [10.1152/jn.01056.2015](https://doi.org/10.1152/jn.01056.2015).
- Welchman, A. E.
 2016 "The human brain in depth: How we see in 3D", *Annual Review of Vision Science*, 2, 1, pp. 345-376, DOI: [10.1146/annurev-vision-111815-114605](https://doi.org/10.1146/annurev-vision-111815-114605).
- Wertz, A., S. Trenholm, K. Yonehara, D. Hillier, Z. Raics, M. Leinweber, G. Szalay, A. Ghanem, G. Keller, B. Rózsa, K. K. Conzelmann, and B. Roska
 2015 "Single-cell-initiated monosynaptic tracing reveals layer-specific cortical network modules", *Science*, 349, 6243, pp. 70-74, DOI: [10.1126/science.aab1687](https://doi.org/10.1126/science.aab1687).
- Westheimer, G.
 2009 "The third dimension in the primary visual cortex." *Journal of Physiology*, 587, Pt 12, pp. 2807-2816, DOI: [10.1113/jphysiol.2009.170175](https://doi.org/10.1113/jphysiol.2009.170175).

- Wheatstone, C.
 1838 "XVIII. Contributions to the physiology of vision. —Part the first. On some remarkable, and hitherto unobserved, phenomena of binocular vision", *Philosophical Transactions of the Royal Society of London*, 128, 0, pp. 371-394, DOI: [10.1098/rstl.1838.0019](https://doi.org/10.1098/rstl.1838.0019).
- White, L. E., W. H. Bosking, S. M. Williams, and D. Fitzpatrick
 1999 "Maps of central visual space in ferret V1 and V2 lack matching inputs from the two eyes." *Journal of Neuroscience*, 19, 16, pp. 7089-7099, DOI: [20024066](https://doi.org/10.1523/JNEUROSCI.2406-99.2000).
- Wiesel, T. N., D. H. Hubel, and D. M. K. Lam
 1974 "Autoradiographic demonstration of ocular dominance columns in monkey striate cortex by means of transneuronal transport", *Brain Research*, 79, pp. 273-279, DOI: [doi.org/10.1016/0006-8993\(74\)90416-8](https://doi.org/10.1016/0006-8993(74)90416-8).
- Wilson, D. E., B. Scholl, and D. Fitzpatrick
 2018a "Differential tuning of excitation and inhibition shapes direction selectivity in ferret visual cortex", *Nature*, 560, 7716, pp. 97-101, DOI: [10.1038/s41586-018-0354-1](https://doi.org/10.1038/s41586-018-0354-1).
- Wilson, J. J., N. Alexandre, C. Trentin, and M. Tripodi
 2018b "Three-dimensional representation of motor space in the mouse superior colliculus", *Current Biology*, 28, pp. 1-12, DOI: [10.1016/j.cub.2018.04.021](https://doi.org/10.1016/j.cub.2018.04.021).
- Wilson, N. R., C. a. Runyan, F. L. Wang, and M. Sur
 2012 "Division and subtraction by distinct cortical inhibitory networks in vivo." *Nature*, 488, 7411, pp. 343-8, DOI: [10.1038/nature11347](https://doi.org/10.1038/nature11347).
- Wilt, B. A., L. D. Burns, E. T. Wei Ho, K. K. Ghosh, E. A. Mukamel, and M. J. Schnitzer
 2009 "Advances in light microscopy for neuroscience", *Annual Review of Neuroscience*, 32, 1, pp. 435-506, DOI: [10.1146/annurev.neuro.051508.135540](https://doi.org/10.1146/annurev.neuro.051508.135540).
- Wong, a. a. and R. E. Brown
 2006 "Visual detection, pattern discrimination and visual acuity in 14 strains of mice", *Genes, Brain and Behavior*, 5, 5, pp. 389-403, DOI: [10.1111/j.1601-183X.2005.00173.x](https://doi.org/10.1111/j.1601-183X.2005.00173.x).
- Yang, W. and R. Yuste
 2017 "In vivo imaging of neural activity", *Nature Methods*, 14, 4, pp. 349-359, DOI: [10.1038/nmeth.4230](https://doi.org/10.1038/nmeth.4230).
- Yang, Z. and D. Purves
 2003 "A statistical explanation of visual space", *Nature Neuroscience*, 6, 6, pp. 632-640, DOI: [10.1038/nn1059](https://doi.org/10.1038/nn1059).
- Yilmaz, M. and M. Meister
 2013 "Rapid innate defensive responses of mice to looming visual stimuli", *Current Biology*, 23, 20, pp. 2011-2015, DOI: [10.1016/j.cub.2013.08.015](https://doi.org/10.1016/j.cub.2013.08.015).
- Yonehara, K., K. Balint, M. Noda, G. Nagel, E. Bamberg, and B. Roska
 2011 "Spatially asymmetric reorganization of inhibition establishes a motion-sensitive circuit", *Nature*, 469, 7330, pp. 407-410, DOI: [10.1038/nature09711](https://doi.org/10.1038/nature09711).

- Yonehara, K., M. Fiscella, A. Drinnenberg, F. Esposti, S. Trenholm, J. Krol, F. Franke, B. G. Scherf, A. Kusnyerik, J. Müller, A. Szabo, J. Jüttner, F. Cordoba, A. P. Reddy, J. Németh, Z. Z. Nagy, F. Munier, A. Hierlemann, and B. Roska
2016 "Congenital nystagmus gene FRMD7 is necessary for establishing a neuronal circuit asymmetry for direction selectivity", *Neuron*, 89, 1, pp. 177-193, DOI: [10.1016/j.neuron.2015.11.032](https://doi.org/10.1016/j.neuron.2015.11.032).
- Yoshida, K., D. Watanabe, H. Ishikane, M. Tachibana, I. Pastan, and S. Nakanishi
2001 "A key role of starburst amacrine cells in originating retinal directional selectivity and optokinetic eye movement." *Neuron*, 30, 3, pp. 771-80, DOI: [doi.org/10.1016/S0896-6273\(01\)00316-6](https://doi.org/10.1016/S0896-6273(01)00316-6).
- Yoshitake, K., H. Tsukano, M. Tohmi, S. Komagata, R. Hishida, T. Yagi, and K. Shibuki
2013 "Visual map shifts based on whisker-guided cues in the young mouse visual cortex", *Cell Reports*, 5, 5, pp. 1365-1374, DOI: [10.1016/j.celrep.2013.11.006](https://doi.org/10.1016/j.celrep.2013.11.006).
- Yu, Y., R. Hira, J. N. Stirman, W. Yu, I. T. Smith, and S. L. Smith
2017 "Mice use robust and common strategies to discriminate natural scenes", *Scientific Reports*, pp. 1-36, DOI: <https://doi.org/10.1101/156653>, arXiv: [/doi.org/10.1101/156653](https://doi.org/10.1101/156653) [https:].
- Zariwala, H. a., L. Madisen, K. F. Ahrens, A. Bernard, E. S. Lein, A. R. Jones, and H. Zeng
2011 "Visual tuning properties of genetically identified layer 2/3 neuronal types in the primary visual cortex of Cre-transgenic mice", *Frontiers in Systems Neuroscience*, 4, January, p. 16, DOI: [10.3389/fnsys.2010.00162](https://doi.org/10.3389/fnsys.2010.00162).
- Zeater, N., S. K. Cheong, S. G. Solomon, B. Dreher, and P. R. Martin
2015 "Binocular visual responses in the primate lateral geniculate nucleus", *Current Biology*, 25, 24, pp. 3190-3195, DOI: [10.1016/j.cub.2015.10.033](https://doi.org/10.1016/j.cub.2015.10.033).
- Zeng, H. and J. R. Sanes
2017 "Neuronal cell-type classification: Challenges, opportunities and the path forward", *Nature Reviews Neuroscience*, 18, 9, pp. 530-546, DOI: [10.1038/nrn.2017.85](https://doi.org/10.1038/nrn.2017.85).
- Zhang, S., M. Xu, T. Kamigaki, J. P. Hoang Do, W.-C. Chang, S. Jenvay, K. Miyamichi, L. Luo, and Y. Dan
2014 "Long-range and local circuits for top-down modulation of visual cortex processing", *Science*, 345, 6197, pp. 660-665, DOI: [10.1126/science.1254126](https://doi.org/10.1126/science.1254126).
- Zhao, X., H. Chen, X. Liu, and J. Cang
2013 "Orientation-selective responses in the mouse lateral geniculate nucleus", *Journal of Neuroscience*, 33, 31, pp. 12751-12763, DOI: [10.1523/JNEUROSCI.0095-13.2013](https://doi.org/10.1523/JNEUROSCI.0095-13.2013).
- Zhuang, J., L. Ng, D. Williams, M. Valley, Y. Li, M. Garrett, and J. Waters
2017 "An extended retinotopic map of mouse cortex", *eLife*, 6, pp. 1-29, DOI: [10.7554/eLife.18372](https://doi.org/10.7554/eLife.18372).
- Zihl, J. and C. A. Heywood
2015 "The contribution of LM to the neuroscience of movement vision", *Frontiers in Integrative Neuroscience*, 9, February, pp. 1-13, DOI: [10.3389/fnint.2015.00006](https://doi.org/10.3389/fnint.2015.00006).
- Zoccolan, D.
2015 "Invariant visual object recognition and shape processing in rats", *Behavioural Brain Research*, 285, pp. 10-33, DOI: [10.1016/j.bbr.2014.12.053](https://doi.org/10.1016/j.bbr.2014.12.053).

CURRICULUM VITAE

Alessandro La Chioma

Address: Am Klopferspitz 18
 Max Planck Institute of Neurobiology
 82152 – Martinsried, Germany
 ☎ (+49) 1522 5975063
 ✉ lachioma@neuro.mpg.de
 💬 Skype: [lachioma](#)
 🌐 Twitter [@ale_lach](#)

Higher Education

- Jan 2013 – now **PhD student**
 International Max Planck Research School for Molecular Life Sciences (IMPRS-LS)
 Boehringer Ingelheim Fonds PhD fellowship
 Department of Synapses – Circuits – Plasticity, Prof. Tobias Bonhoeffer
 Max Planck Institute of Neurobiology, Martinsried (Germany)
 Supervisors: Prof. Mark Hübener, Prof. Tobias Bonhoeffer
- Jan – Sep 2012 **Master's thesis research project**
 Lab of Dynamic Organization & Function of Synapses, Dr. Daniel Choquet,
 Interdisciplinary Institute for Neuroscience IINS, Bordeaux (France)
 Supervisors: Dr. Françoise Coussen, Dr. Daniel Choquet
 Topic: AMPAR trafficking with super-resolution imaging and endocytosis assays
- Sep 2010 –
 Sep 2012 **Master of Science in Biology applied to biomedicine - curriculum *Neurobiology***
 Scuola Normale Superiore of Pisa and University of Pisa (Italy)
 GPA: 29.4 out of 30; final grade: 110/110 cum Laude
- Oct 2007 –
 Jul 2010 **Bachelor of Science in Biological and Molecular Sciences**
 Scuola Normale Superiore of Pisa (merit scholarship) and University of Pisa (Italy)
 GPA: 29.6 out of 30; final grade: 110/110 cum Laude
 BSc thesis research project in Prof. Gian Michele Ratto group

Fellowships and Scientific Awards

- 2016 2nd best poster at IMPRS (PhD program) symposium
 2015 1st best poster at IMPRS (PhD program) symposium
 2014 – 2015 Boehringer Ingelheim Fonds PhD fellowship (BIF)
 ~15 fellowships awarded at selection round, <10% acceptance rate
 2015 Selected for Cold Spring Harbor Laboratory course: Imaging Structure & Function in the Nervous System
 2012 Selected for the International Max Planck Research School for Molecular Life Sciences (IMPRS-LS)
 ~30 students admitted per year in this PhD program, <5% acceptance rate
 2007 – 2012 5-year scholarship by Scuola Normale Superiore of Pisa
 30 students admitted per year in the Faculty of Sciences, <5% acceptance rate
 2011 Selected for the International Biology Undergraduate Summer School 2011 at ETH Zürich (BUSS 2011)
 Research project of 2 months in the lab of Helge Ewers lab
 2006 Selected for "Gran Sasso - Princeton Physics Summer School" at Princeton University

Methods and Specialized Techniques

Imaging	<i>In vivo</i> two-photon calcium imaging in the mouse neocortex (in anesthetized and awake animals) two-photon custom set-up building and maintenance virus injections and cranial window implantation in the mouse for chronic imaging <i>in vivo</i> imaging of intrinsic optical signals
Data analysis	Image processing; single-cell and population analysis of neuronal fluorescence signals; decoding analysis (SVM, Bayesian)
Programming	Advanced knowledge of MATLAB programming (including image analysis, data acquisition and psychophysics toolboxes); basic knowledge of Python programming

Further Training and Workshops

- Cold Spring Harbor Laboratory course: **Imaging Structure & Function in the Nervous System** (3-week course):
 - Participation as Technical Assistant (2018)
 - Participation as Student (2015)
- Scientific programming with Python (4-day workshop, 2017)
- Machine Learning Summer School by PRONIA (4-day workshop, 2017)
- Scientific communication (5-day workshop, Cold Spring Harbor Laboratory)

Meetings and Conferences

- 2018 **La Chioma, A.**, Bonhoeffer, T., Hübener, M. Distinct representations of binocular disparities across areas of mouse visual cortex. *FENS Forum, Berlin, Germany, 2018*
- 2017 IMPRS (PhD program) symposium talk:
La Chioma, A., Binocular disparity selectivity across areas of mouse visual cortex
- 2017 **La Chioma, A.**, Bonhoeffer, T., Hübener, M. Binocular integration and disparity sensitivity in mouse visual cortex. *Society for Neuroscience, Washington, DC, 2017*
- 2017 **La Chioma, A.**, Bonhoeffer, T., Hübener, M. Binocular integration and disparity sensitivity in mouse visual cortex. *German Neuroscience Society (NWG), Göttingen, Germany, 2017*
- 2016 IMPRS (PhD program) symposium, poster (2nd best poster award):
La Chioma, A., Bonhoeffer, T., Hübener, M. Generation of direction selectivity in mouse visual cortex
- 2015 IMPRS (PhD program) symposium, poster (1st best poster award):
La Chioma, A., Bonhoeffer, T., Hübener, M. Generation of direction selectivity in mouse visual cortex

Work-related Responsibilities

- 2013 – now Organizer of weekly departmental meetings in PhD host lab
- 2015 Co-organizer of department retreat
- 2014, 2016 Co-organizer of Open Day of Max Planck Institute of Neurobiology
- 2014 Co-organizer of 7th Interact PhD symposium <interact>, Munich

Extracurricular Activities and Hobbies

- Regular runner, half-marathons; soccer goalkeeper
- Nature and landscape photography, macrophotography

ACKNOWLEDGEMENTS

I would like to express my gratitude to Mark Hübener for guiding me throughout my PhD. I deeply appreciated his mentorship, in both supporting and challenging me, while allowing me ample space to develop and follow my own ideas. His office has always been open for extended discussions on data and experiments as well as for advice on my future career. I am also especially grateful to him for very carefully reading this thesis and greatly contributing to it with invaluable insights and suggestions.

I am thankful to Tobias Bonhoeffer for giving me the freedom to pursue my own direction of research and for honest advice and support for my future career.

I am grateful to my thesis advisory committee – Mark, Tobias, David Fitzpatrick and Moritz Helmstaedter – for fruitful discussions and input regarding my projects throughout my time here.

Special thanks go to my PhD brother Simon Weiler, with whom I shared plenty of memorable moments in and outside the lab, through the many joyful and some less joyful times of our journey. Without him, life would have been much harder.

I thank Pieter Goltstein for sharing some of his MATLAB code, including the Multiple ROI Predator and the Retinotopic Mapper. Also thanks to Tobias Rose for sharing the great “double construct” which made imaging far easier. I thank Max Sperling for his often-crucial help with hardware and software for image acquisition.

I thank all members of the lab for the many scientific and non-scientific moments, for all discussions, coffee breaks, barbecues, evenings out, parties, for stopping by the office whenever they needed five minutes of entertainment. They have always created a fun and supportive atmosphere, making the lab a second (or first) home for me. Many thanks to the volunteers of the needle threading task (Fig. 1.9): Simon Weiler, Martin Fernholz, Isa-Maria Gross, David Laubender, Mark Hübener. I thank all friends and colleagues who made both the Max Planck Institute of Neurobiology and Munich such great places to live in.

I am grateful to the Boehringer Ingelheim Fonds, for financial support, for unique retreats and for the privilege of meeting many great people. I thank the International Max Planck Research School for Life Sciences, for financial and non-financial support, for providing many opportunities for training.

Finally, my deepest gratitude goes to my family, who has always believed in me with unconditional support and for giving me the freedom to pursue my goals, even though this meant to be far from them. I thank with all my heart my partner Rossella, the person I can always count on, for her extraordinary support these past years, tolerating the distance and my overly busy work schedule.

Danke für alles!

EIDESSTATTLICHE ERKLÄRUNG

Ich versichere hiermit an Eides statt, dass die vorgelegte Dissertation von mir selbständig und ohne unerlaubte Hilfe angefertigt ist.

München, 17.7.2018

Alessandro La Chioma

ERKLÄRUNG

Hiermit erkläre ich,

dass die Dissertation nicht ganz oder in wesentlichen Teilen einer anderen Prüfungskommission vorgelegt worden ist.

dass ich mich anderweitig einer Doktorprüfung ohne Erfolg nicht unterzogen habe.

München, 17.7.2018

Alessandro La Chioma